Non-invasive measurement techniques to monitor acoustic cavitation activity

Kornpatsitt Promasa

Submitted in May 2014
for the degree of Doctor of Philosophy

Centre for Ultrasonic Engineering
Department of Electronic and Electrical Engineering
University of Strathclyde
204 George Street, Glasgow,
G1 1XW, Scotland, UK

For all those who gave everything to allow others the opportunity to

follow their own choices in life.

List of Contents

Chapter 7 Conclusions and Future work

List of Figures

List of Tables

List of Symbols

Symbol	Definition	unit
R_{Max}	maximum size of bubbles	
R_0	bubble equilibrium radius	
P_i	pressure within the bubble	$Pa\ or Nm^{-2}$
P_L	liquid pressure at bubble wall	$Pa\ or Nm^{-2}$
P_o	hydrostatic pressure in the body of liquid	$Pa\ or Nm^{-2}$
P_σ	surface tension pressure	$Pa\ or Nm^{-2}$
$P_L(R)$	liquid pressure outside the bubble wall	$Pa\ or Nm^{-2}$
$P_\infty(t)$	acoustic pressure in the liquid medium	$Pa\ or Nm^{-2}$
R	bubble radius	
$\dot{R}$	first-order time derivatives of the bubble radius	
$\ddot{R}$	second-order time derivatives of the bubble radius	
σ	surface-tension constant	
μ_c	coefficient of the liquid viscosity	
ρ	density of liquid medium	kgm^{-3}
$P()$	gas pressure	$Pa\ or Nm^{-2}$
$P_T(R)$	pressure of total mass content in bubble at a given radius	
P_m	ambient pressure over the collapse period	$Pa\ or Nm^{-2}$
γ	specific heat ratio of the gas within the bubble	
T_{max}	maximum temperature within a collapsing bubble	$Pa\ or Nm^{-2}$
P_{max}	maximum pressure within a collapsing bubble	$Pa\ or Nm^{-2}$
To	temperature in the bubble	
Ω_b^{scat}	acoustic scatter cross section	
B_{tot}	damping of bubbles	
ω_0	radian frequency of bubble resonance	
ω_1	insonating frequency	Hz
f_0	fundamental frequency	Hz
$u(z,t)$	longitudinal wave	
A	amplitude	
ω	angular frequency	
φ	phase angle	
c	velocity of wave	ms^{-1}
f	wave frequency	Hz
t	time	s
n	reflective index of medium	
ϵ_r	relative permittivity of medium	
μ_{op}	piezo-optical coefficient	
δn	variation in the ambient refractive index	
δp	variation in the ambient pressure	
$n(r)$	reflective index obtained from the relative phase delay	
n_0	ambient reflective index of the medium	
$n_p(r)$	reflective index in plane wave	
n_1	maximum change in reflective index	
δ_φ	phase difference	

φ_0	reference phase	
φ_{Ref}	reflected phase	
A_0	amplitude of referent signal	
A_{ref}	amplitude of reflected signal	
A_l	amplitude of optical source	
φ_i	phase shift in optical path *i*	
λ	wavelength	m
A_{tot}	total amplitude of laser beam	
I_L	detected light intensity	
I	light intensity	
D	displacement of object	
$D(t)$	displacement at a given time	
f_D	doppler frequency induced by a moving object	
f_B	offset frequency	Hz
f_{out}	modulation frequency	Hz
L	optical path *L*	
$\delta_p(t)$	change in ambient pressure	
$\emptyset_c$	constant phase	
$p(x,t)$	sound pressure in x-direction	Pa
u	piezo optical co-efficient	
$\varphi_u(t)$	change in ambient pressure by piezo optical co-efficient	
$\varphi_u(x)$	optical phase change induced in the x- direction	
$P_\theta(t)$	projection of x-y plane	
$f(x,y)$	two dimensional function of projection	
$F(H,G)$	2D Fourier transform	
W	pie-shaped wedge of the object's Fourier transform	
K	weighting angles	
BIE	broadband integrated energy	V^2/Hz
$v(f)$	amplitude of acoustic spectrum	V
m	integer	
p	integer	
k_t	electromechnical coupling factor	
f_m	resonance frequency	Hz
f_n	anti-resonance frequency	Hz
AR	aspect ratio	
w	pillar width	m
h	height	m
v	velocity factor	ms^{-1}
Z	impedance	MRayls
$S_{Tx}(\omega)$	transmission sensitivity	$P_a V^{-1}$
$\hat{P}_{out}(\omega)$	average output pressure	Pa
$\hat{V}_{in}(\omega)$	complex input voltage of transducer	V
$S_{Rx}(\omega)$	reception sensitivity	$V.P_a^{-1}$
$\hat{P}_{in}(\omega)$	complex pressure on transducer	Pa
$\hat{V}_{out}(\omega)$	complex output voltage generated by complex pressure	V
Z_m	matching impedance	MRayls
Z_1	acoustic impedance of first medium	MRayls

Z_2	acoustic impedance of second medium	MRayls
Q	Q-factor	
f_c	central frequency of transducer	Hz
BW	bandwidth of transducer	Hz
f_s	sub-harmonic frequency	Hz
f_h	harmonic frequency	Hz

Acknowledgements

Firstly, I would like to sincerely thank my long-suffering supervisors, Dr. Anthony Gachagan and Dr S. Gareth Pierce, who have provided the invaluable guidance, technical knowledge and grammatical superiority throughout this project. This thesis would not have been possible without their support.

I also wish to thank colleagues in Centre for Ultrasonic Engineering (CUE) especially, Chuangnan Wang, Tapiwa Matasa, Elaine Mackie, Syamsul Bahrin, David Mackie and the others for their good friendships and assistance. My sincere thanks are due to staffs in Centre for Ultrasonic Engineering (CUE) for their good friendships and their excellent support. I would like to thank Tommy McCunnie, Grant Smillie and their team for their manufacturing skill and expertise and for developing transducers.

I would like to thank to the Royal Thai Government, Ministry of Sciences and Technology of Thailand and National Institute of Metrology Thailand (NIMT) for awarding me this scholarship. I also wish to extend my warmest thank to Thai friends in Glasgow (UK) for their friendly and cheerful, assistance and sharing happiness and distress.

Finally, I want to thank my family and Rojana Sutjarit for their love, enduring patience, support and encouragement through my study in UK.

Abstract

High power ultrasound has been used in a number of biomedical and industrial applications. In particular, such systems, when used in chemical processing, modify the course of a chemical reaction. The use of high power ultrasound induces cavitation in the load medium, which then leads to certain mechanical and chemical effects. These effects can cause damage to objects, increase local temperatures and can accelerate chemical reactions. Thus, in order to evaluate an efficient ultrasonic system and to quantify the cavitation activity, it is necessary to measure the cavitation in the reaction under the influence of a high power ultrasonic field. Conventional hydrophone techniques and sensor technologies are not suitable for this type of measurement because the sensor can be damaged and change the acoustic field in the presence of cavitation generated by the high power ultrasound.

This Thesis describes the development of a non-invasive technique used to monitor acoustic cavitation activity within a reactor vessel. Both Laser Doppler Velocimetry (LDV) and broadband ultrasonic transducer approaches are considered as potential measurement techniques to measure the acoustic emission (AE) signals associated with a cavitating field. The LDV approach uses laser detection to provide information about cavitation intensity and distribution occurring within a reactor vessel. Next, finite element analysis (FEA) is used to provide a simulation platform to investigate the detection of AE sources from within the reactor vessel. This provides the necessary information to support the design of a broadband transducer appropriate for detection of cavitation generated AE. FEA is then used to design a piezoelectric ceramic composite transducer to develop a non-invasive transducer measurement system. In both approaches, a broadband integrated energy (BIE) approach is used to determine the intensity of the cavitation activity. This technique has been evaluated in different frequency ranges and at various power levels. Interestingly, the BIE in the frequency ranges of 1-5MHz was shown to be sufficient in monitoring the cavitation. Overall, the results reveal that both non-invasive techniques can be used to monitor cavitation activity. Although, neither approach provided adequate spatial resolution to accurately map the cavitation field. These techniques are most appropriate to use when the region of cavitation activity in the

reactor vessel is known and the external, non-invasive technique can be targeted at this known position to provide information on the regional cavitation intensity.

CHAPTER 1

INTRODUCTION

1.1 Introduction

High power ultrasound has been used in a wide variety of application areas including ultrasound cleaning [1], industrial processes [2] and medicine [3], all of which require high intensity ultrasound and high power fields. When a high intensity ultrasonic wave is applied to and propagates through a target load, high pressure and temperatures can be created. The application of high power ultrasound in a liquid medium can produce acoustic cavitation when certain conditions are met [4]. The phenomenon causes the formation and collapse of microbubbles and can produce high localized pressure in the order of hundreds of atmospheres as well as high temperatures in the order of thousands of degrees Kelvin. The inertial cavitation produces extreme conditions, which are believed to be responsible for sonochemistry [5], cleaning [1] and erosive effects [6].

Acoustic cavitation describes the phenomenon of the formation, growth and violent collapse of bubbles under an ultrasonic field [7]. The bubble collapse produces high

energy densities and can initiate mechanical and chemical effects. The mechanism of cavitation has the potential to play a key role in cleaning, enhancing chemical reactions and causing the degradation of a delicate object, such as the damage inflicted upon a hydrophone during cavitation measurements and thin aluminium foil during high power testing. The characterisation of cavitation activity is the key to process optimisation and the scale-up of many ultrasonic applications. Thus, understanding the mechanism of cavitation will allow for process optimization and avoids damage to an object or detection sensor located within the high power ultrasound field. Hence, monitoring acoustic cavitation activity would be necessary for system optimization and safety reasons.

Acoustic cavitation occurs within a high power ultrasonic system. Measuring cavitation is challenging due to the unpredictability of cavitation occurrence, as well as the lack of a suitable sensor and the potentially hostile and erosive nature of the environment. Moreover, high power ultrasonic fields are the result of complex multidisciplinary problems which lead to occurrences such as cavitation and bubble jets [4]. Therefore, acoustic cavitation is difficult to measure, to control, to predict, and to scale up. The techniques that have been applied to determine cavitation on a localised basis involve measuring cavitation effects, such as sonoluminescence, and the erosion of aluminium foil. These approaches can predict high-intensity locations where cavitation is most likely to occur. However, all of these approaches offer poor resolution and are inefficient techniques with which to quantify the amount of cavitation activity. Cavitation detection and monitoring can be achieved by the application of sensors such as hydrophones [8], the NPL cavitation sensor [9] and a fibre optic sensor [8]. Conventional measurements require the insertion of a sensor into an acoustic field. The presence of a sensor in the liquid medium causes perturbation to the acoustic field. Moreover, the sensor may also be subjected to bandwidth and sensitivity issues and may sustain damage from the cavitation and extreme conditions during the measurement process. Hence, the removal of the sensor from the high power ultrasonic field leads to the avoidance of sensor damage and disruption of the acoustic field. The creation of a non-invasive monitoring

system with wide bandwidth and high sensitivity would enable the monitoring of acoustic cavitation without damaging the sensor and disturbing the sound field. Cavitation activity can therefore be monitored using the acoustic emission technique.

Acoustic emission has the potential to monitor acoustic cavitation. It is known that bubbles act as secondary acoustic sources. The oscillation and collapse of bubbles can generate acoustic emissions [4],[9] and the acoustic signals emitted by cavitation have been studied [8],[9],[10]. The emission signal contains a substantial amount of information related to the dynamics of the cavitation process. The acoustic emission from cavitating bubbles is analysed in terms of the spectrum of the sound pressure signal that provides information about bubble oscillations and inertial cavitation. The acoustic emission signal generated by cavitating bubbles can be detected by sensors such as hydrophones. The cavitation can be characterized by the appearance of subharmonics, ultraharmonics and the broadband signal of the acoustic spectrum in a high frequency signal. It is believed that the harmonics of the acoustic driving frequency, including sub-and ultra-harmonics, result in the nonlinear motion of the bubble oscillation and bubble collapse. The frequency components of acoustic emission are caused by the cavitation activity which is dependent upon sound intensity. The broadband signal produced in a high frequency signal can be used to determine the energy associated with the occurrence of inertial bubble collapse using the broadband integrated energy (BIE) approach [9],[10]. The intensity of cavitation obtained from a broadband acoustic signal can be used to inform system optimization and safety issues.

This Thesis addresses the implementation of a non-invasive measurement technique to monitoring acoustic cavitation, using both an optical measurement method and a broadband transducer approach. The proposed techniques avoid the problems of sensor damage and the disturbance of the acoustic field. Acoustic cavitation is monitored through the acoustic emission technique. This technique also has the potential to evaluate the strength of cavitation activity. The intensity of the cavitation

activity can be calculated by broadband integrated energy (BIE) in the acoustic emission spectrum. Both measurement systems, the optical measurement technique and the manufactured broadband piezocomposite transducer, are presented as non-invasive approaches to monitoring acoustic cavitation produced within a reactor vessel.

1.2 Aim and Contributions of this Thesis

1.2.1 Aims of this Thesis

- Implementation of a non-invasive measurement system through which acoustic cavitation activity can be monitored. This will comprise evaluation into the application of both optical and ultrasonic techniques to measure the acoustic emission signals produced as a direct result of a cavitating field.

- To undertake an experimental programme to investigate the performance of Laser Doppler Velocimetry (LDV) to measure acoustic emission from a cavitating field.

- To develop finite element simulations to understand the relationship between acoustic emission events, associated with cavitation, and the resulting complex wave propagation through the reactor vessel wall. Importantly, this simulation work will be used to obtain information necessary for the design specifications of a bespoke ultrasonic transducer which will be used to monitor acoustic cavitation.

- To use finite element modelling to design an appropriate ultrasonic transducer for use as a probe for monitoring acoustic cavitation.

- The performance of this device will be experimentally evaluated for detection of acoustic emission signals caused by cavitation events, when attached to the external wall of the reactor vessel.

1.2.2 Contributions to the Knowledge of the Field of Ultrasonics and Acoustic Cavitation Monitoring.

The major achievement of this Thesis and its contribution to the field of ultrasound and cavitation monitoring are as follows;

- A non-invasive measurement technique, using an optical approach based on Laser Doppler Velocimetry (LDV), is developed to monitor acoustic cavitation within a reactor vessel. The implemented experiment approach is described The characteristic signatures of acoustic emission are the fundamental frequencies of both sub-and ultra-harmonics, and broadband noise produced in the high frequency ranges of an acoustic emission signal associated with cavitation, all of which have been identified in the acquired LDV measurements.

- Broadband integrated energy (BIE) is used to evaluate the intensity of cavitation produced by a 40kHz Tonpilz transducer. The cavitation intensity is considered through analysis of the acoustic emission spectrum within the frequency ranges of 1MHz to 5MHz.

- A detailed analysis across the 1-5MHz frequency range indicates that using a reduced frequency range between 1-3MHz is sufficient for measuring the extent of cavitation.

- An experimental approach combining LDV and tomography is shown to measure the acoustic field within a Perspex walled vessel. A scan of the field distribution displays ‘hot-spot’ and ‘cold-spot’ regions associated with high and low cavitation areas.

- Finite element (FE) modelling is used to simulate the cavitation event within the reactor vessel. The model is used to predict frequency content of the signal received by a transducer located on the outer wall of a reactor vessel. A linear chirp signal, between 1-7MHz, is employed as an excitation function in the model to simulate the acoustic emission generated by a collapsing bubble. The model investigates the position of the reception point on the vessel wall,

acoustic pressure, the wall material and the number of sound sources. The information gathered from the FE simulation has been used as the basis for designing the ultrasonic transducer with which acoustic cavitation will be monitored.

- A piezocomposite transducer has been designed, and fabricated, to operate at the desired resonant frequency of 2MHz, with a bandwidth characteristic of 1-3MHz. Moreover, the device includes low acoustic impedance matching to operate into a Perspex walled vessel.

- An experimental evaluation of the broadband (1-3MHz) piezocomposite transducer confirms that cavitation within a reactor vessel can be monitored when this device is mounted onto the external wall of the vessel.

1.2.3 Publications to Date Arising as a result of this Thesis

Conference Publications

- Kornpatsitt Promasa, Anthony Gachagan and S. Gareth Pierce "Non-invasive optical technique to map acoustic cavitation activity" 8th International Symposium on Cavitation, 13th-16th August 2012, Singapore, pp 88-92.

Presentations

- Kornpatsitt Promasa, Anthony Gachagan and S. Gareth Pierce "Measurement of acoustic cavitation" Faculty of Engineering, Research Presentation Day 2011, University of Strathclyde, Glasgow, 18th January 2011.

- Kornpatsitt Promasa, Anthony Gachagan and S. Gareth Pierce "Overview of acoustic cavitation measurement" Ultrasonic Industry Association, University of Glasgow, 23-25 th May 2011.

- Kornpatsitt Promasa, Anthony Gachagan and S. Gareth Pierce "Non-invasive optical technique to Map Acoustic cavitation activity" Faculty of Engineering, Research Presentation Day 2012, University of Strathclyde, Glasgow, 2rd May 2012.

1.3 Overview of Thesis

Chapter2: High power ultrasound: Application, Cavitation and Detection

This Chapter presents an overview of the common applications of high power ultrasound, which have the potential to produce cavitation. Next, acoustic cavitation and cavitation effects are described and the measurement techniques available for detecting cavitation are reviewed. Furthermore, a critique of the measurement techniques helps to assess their suitability for monitoring cavitation activity. Subsequently, a review of the acoustic sensor used in the cavitation investigation is also provided. From this review, the acoustic emission method is considered to be a suitable technique for the development of a non-invasive measurement system with which to monitor cavitation activity.

Chapter3: Development of a non-invasive optical measurement technique to monitor acoustic cavitation

This Chapter describes a theoretical and experimental investigation into the use of Laser Doppler Velocimetry (LDV), based on acoustic emission, for monitoring acoustic cavitation. Firstly, the application of a non-invasive optical measurement technique for monitoring acoustic cavitation, based on an acousto-optic approach is described. Next, the cavitation activity is determined using the broadband integrated energy (BIE) approach, which calculates the power of the acoustic spectrum, in the frequency range of 1MHz to 5MHz, [10] produced by a 40kHz ultrasonic Tonpilz transducer. A scanning algorithm is then used to identify 'cold spots' and 'hot spots' associated with low and high cavitation regions occurring in the reactor vessel is developed and implemented. Finally, an aluminium foil erosion test indicating the cavitation areas through the erosion of aluminium foil is implemented to verify the cavitating region of the optical measurement approach.

Chapter4: Modelling the effects of the reactor vessel

This Chapter describes the process of modelling the cavitation event within the reactor vessel. The finite element (FE) model is used to analyse the complicated interactions between sound wave propagation and the reactor vessel. The development of the reactor vessel using a two dimensional FE model is presented and a linear chirp signal of 1-7MHz, correlated with sources of cavitation, is employed as an excitation function used in the model. The relationship between acoustic wave propagation caused by the cavitation event and the wall of the vessel in the FE environment is simulated. The overall model is used to predict the acoustic emission signal responses in different situations such as the varying reception positions, pressure, wall thickness and wall materials. Next, the analysis of the bandwidth of the acoustic emission signal is described so that the transducer's bandwidth is suited to monitoring acoustic cavitation. The modelling results will provide the basis of the design specifications for the development of a non-invasive measurement system with which to monitor acoustic cavitation.

Chapter5: Broadband non-invasive piezoelectric composite probe: Design and Characterisation

This Chapter describes the design and development of the wideband piezocomposite transducer. Initially, a background of piezocomposite transducer technology is provided to the reader to explain the advantages of this technology. Then, finite element analysis, PZFlex, is employed in the design of a piezocomposite transducer to operate with a resonance frequency of 2MHz. The finite element analysis is used to evaluate reception characteristics over the complete volume fraction range to evaluate designs providing the maximum efficiency. Next, the analysis of several parameters in the transducer design, such as the electromechanical coupling coefficient and resonance frequency are also presented. Finally, a characterisation method is implemented in order to evaluate the performance of the designed piezocomposite transducer.

Chapter6: Development of a broadband non-invasive transducer monitoring system to monitor acoustic cavitation

This Chapter presents the implementation of a non-invasive measurement system using the wideband piezocomposite transducer to monitor acoustic cavitation. Initially, the finite element model is used to predict the ability of the designed piezocomposite transducer to detect acoustic emission signals. Subsequently, the fabrication of this transducer is described. The piezocomposite transducer is attached to the external wall of the reactor vessel to detect the acoustic emission signal produced by high power ultrasound and the ensuing cavitation events within the vessel. The experimental results illustrate that the detected acoustic emission signal and the cavitation intensity, determined by the BIE approach, increases with the power input. Subsequently, through monitoring the cavitation at various locations on the reactor vessel wall it is possible to identify high and low cavitation regions within the reactor vessel.

Chapter7: Conclusions and Future work

This Thesis ends with a review of the important conclusions within all previous Chapters and summarizes the main findings of this research work. Finally, the Chapter presents suggestions for extending the knowledge of applications and future work in this field.

CHAPTER 2

High Power Ultrasound: Application, Cavitation and Detection of Cavitation

2.1 Introduction

Ultrasound is defined as a form of mechanical energy generated by sound pressure waves, whose frequencies are beyond 20kHz [11],and has been employed in various applications. The first applications of ultrasonic waves, such as the production of sound in water used to detect submarines, began during the First World War [12]. Thereafter, innovative work in both wave propagation theory and the first ultrasound transducer were developed by Professor Paul Langevin [12]. Further developments enabled ultrasonic waves to be employed in ultrasonic flow detection for measuring flow in materials [13]. Additional applications followed with ultrasonic waves utilised in a sound navigation and ranging (SONAR) [14], Non-Destructive Testing

(NDT) [15], biomedical diagnosis [16] and in the treatment of diseases and surgery to remove malignant tissues [16].

The use of ultrasonics can be classified into two main groups. The first group involves the application of low power ultrasonics, which operates at frequencies above 100kHz and characteristically has an ultrasound intensity of below 1W/cm^2. As such, these applications are typically in the linear regime and cover areas such as communication, non-detective testing and medical imaging. The second group of ultrasonic applications engages with high power ultrasound. This high power ultrasound forms the most significant part of the ultrasound field with regards to studying cavitation. The application of high power ultrasound deals with an ultrasonic intensity power higher than 1W/cm^2 and normally operates at frequencies below 100kHz [17]. The various applications of high power ultrasound are described in Section 2.3.

High power ultrasound applications involve high intensity or high power leading to the generation of a cavitation field [8]. The application of high power ultrasound can induce permanent physical changes in a target object or regions in a liquid medium. This involves the utilization of cavitation, which will be discussed in Section 2.2, to produce specific desired effects. Moreover, high power ultrasound is used in medical applications such as high intensity focused ultrasound (HIFU). This application involves the frequency range of 1-5MHz, with high power intensity ultrasound generated at a controlled focal point to target cancerous regions, for example [18].

Cavitation produced by high power ultrasound applications can lead to object damage [6] as well as several other effects [5]. Therefore, the measurement of the high power field is important for safety purposes and efficiency reasons. However, there are very few reliable measurement methods available to monitor cavitation in a high power ultrasound field. In particular, damage can be sustained by a detection

probe located within the liquid load medium. Hence, the development of methods for monitoring cavitation requires an approach which is durable enough to withstand the effects of acoustic cavitation in a high power ultrasound field. The currently available detection methods and detecting devices are reviewed in Section 2.4 and 2.5, respectively. Overall, this Chapter shows an increasing demand for knowledge of high power ultrasonic fields within these environments. Therefore, it is important to understand the current body of knowledge associated with high power fields, cavitation and measurement techniques.

This Chapter presents a review of high power ultrasound, acoustic cavitation and detection methods. High power ultrasound is used in a number of diverse application areas such as sonochemistry, cleaning, and medicine. Importantly, the application of high power ultrasound in a fluid medium that can produce acoustic cavitation is reviewed. Finally, a contemporary measurement method for monitoring acoustic cavitation is noted, and the detection devices, which are available for monitoring cavitation, will be introduced as a means of developing a new cavitation measurement system.

2.2 Acoustic Cavitation

Acoustic cavitation is a result of bubble activity caused by high power ultrasound in a liquid medium. It is also well known as the process of formation, growth and subsequent collapse of acoustic bubbles [7],[19],[20],[21],[22]. This leads to mechanical and chemical phenomena. There are many activities that can influence the occurrence of cavitation such as flow, compression and decompression of the acoustic wave, and boiling. The generation of cavitation can provide advantages as well as disadvantages, depending upon its application.

This Section introduces cavitation and the influence the propagating ultrasound wave has on bubble activity in a high power ultrasound field. In addition, the cavitation threshold is split into two categories, stable and inertial. Any cavitation occurring with the application of high power ultrasound is briefly reviewed in order to understand the behaviour of acoustic cavitation. For more extensive analysis of acoustic cavitation, cavitation effects and applications, the reader is referred to Leighton's book [4].

2.2.1 Introduction

Acoustic cavitation and bubbles are induced by high power ultrasound waves propagating within a liquid medium. The cavitation bubbles will first oscillate because of the high power ultrasound and the bubbles are stimulated by a negative cycle of sound waves, before they subsequently collapse and produce a shock-wave. A theory of oscillating, growing bubbles and bubble motion is suggested by Noltingk *et al*. [23]. As the acoustic excitation is increased, the bubble motion is more oscillatory and becomes increasingly violent and nonlinear. It is at this point that bubble creation increases rapidly with bubbles exceeding a maximum size, causing their violent collapse. The process of the expansion and rapid collapse of the bubbles gives rise to the initiation of inertial cavitation. A schematic diagram of the cavitation inception process is depicted in Figure 2.1.

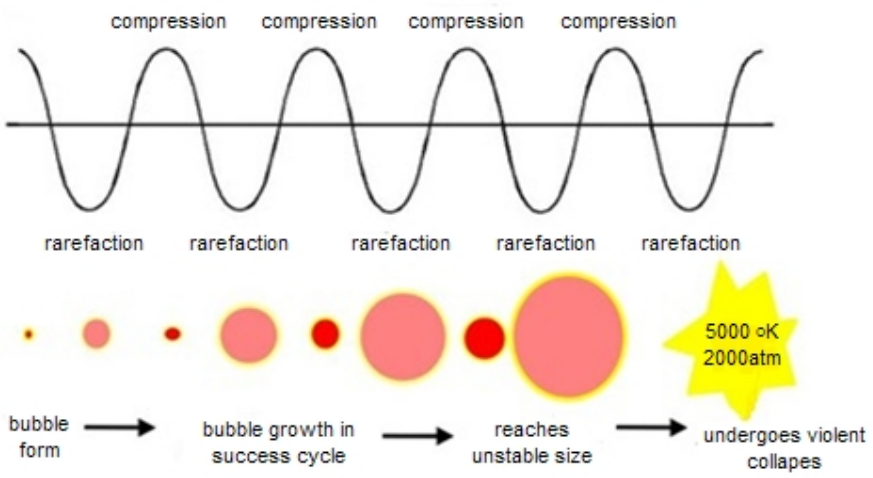

Figure 2.1 The schematic illustration of the expansion and collapse of bubbles [24].

The amount of bubble expansion is crucial to the cavitation system as there are two separate evolutionary parts which are dependent on this. Stable cavitation describes the expansion of gas bubbles under equilibrium conditions. Inertial cavitation is described as the process of oscillation and collapse of bubbles. During the collapse process, a bubble is capable of causing high pressure in the liquid medium, which in turn causes high fluid velocity and the micro-jetting phenomena. This creates the cavitation effect which produces high local temperatures, approaching 5,000^{o}K, and extremely high pressure up to 2,000atm in a liquid medium [24]. Cavitation bubbles grow due to the negative cycle of the propagating high power sound waves and undergo several rapid expansions to reach a maximum radius before collapsing. The maximum size of bubble, R_{Max}, which is attained from the transient effect is defined [21] by;

$$R_{Max} = 2.3\, R_0 \qquad 2.1$$

Where R_0 = bubble equilibrium radius

Inertial cavitation is described as the expansion of the gas bubble radius reaching approximately twice its original size in relatively few cycles. Apfel predicts that a bubble radius may reach 2.3 times the equilibrium radius during inertial cavitations [21], which is a larger size than during stable cavitation, and then collapses. This final stage produces violent bubble collapse with radial velocities approaching the velocity of sound and causes both the chemical and physical effects [25]. The cavitation effect can be responsible for damage to soft tissues such as biological cells [26]. The mechanical effects can cause damage to objects during cleaning. Moreover, the cavitation effects caused are dependent upon the intensity of the occurring cavitation. Comprehensive studies of the cavitation phenomenon enable an understanding of its use in a variety of application areas.

Early research of acoustic cavitation was mainly centred on inertial cavitation because of its spectacular, disruptive effects. The application of cavitation caused effects such as erosion, as well as many other chemical and biological effects. When cavitation begins in a liquid medium, the properties of the liquid medium are changed. Thereafter, the cavitation changes from stable to inertial, the resonant bubbles may become very active, displaying strong micro-bubble streaming. The concentration of energy in inertial cavitation results from bubble collapse. Nevertheless, applications of high power ultrasound are developed through both stable and inertial cavitation.

2.2.2 Cavitation threshold

Cavitation bubbles are a result of the excitation of high power ultrasound of sufficient intensity passing through a liquid medium. The oscillation and collapse of the bubbles within the high pressure field produce acoustic cavitation. As bubbles develop in the liquid medium, the acoustic cavitation relates to two categories of cavitational stages; stable and inertial cavitation thresholds. It is difficult to identify stable and inertial cavitation in practice due to inappropriate measurement methods.

Many papers exist in which attempts to define the boundaries between the stable and inertial thresholds have been made. Apfel *et al*. provided the boundary of the cavitation thresholds with a series of cavitation prediction charts [21]. The cavitation prediction graphs are determined under specific boundary conditions of acoustic pressure, frequency and bubble radius. However, these parameters are difficult to measure in practice. As a result, it has been suggested that a numerical simulation would be the simplest method of evaluating the cavitaton threshold. Moreover, Apfel *et al.* proposed a simulation model to predict stable and inertial cavitation threshold intensities. The resultant graph of this mathematical simulation is shown in Figure 2.2 [27]. The source of a cavitation threshold is determined under the primary parameters of the acoustic pressure amplitude, frequency and the size of the bubble nucleus. The threshold transition graph provides a boundary condition between the inertial and stable cavitation. The threshold transition curve of Apfel *et al.* provides the approximation value of the peak negative pressure amplitude required to cause a bubble to undergo inertial cavitation. The alteration from stable cavitation to inertial cavitation can be determined under specific bubble radius and frequency conditions. For example, if the initial bubble radius is 0.3μm and an operating frequency of 5MHz is used, then the cavitation threshold is predicted to be at 0.58MPa of peak negative pressure.

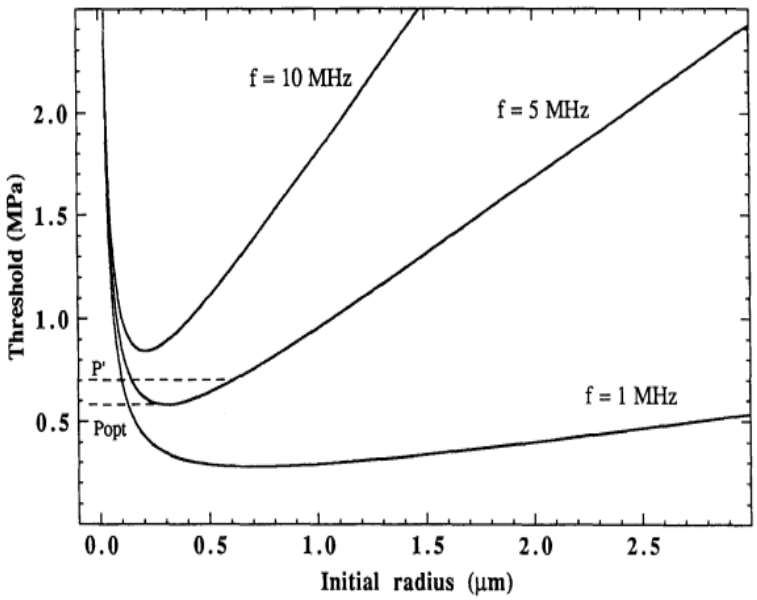

Figure 2.2 The cavitation transition threshold in water as a function of initial nucleus radius for three frequencies of insonification: 1, 5, and 10MHz [27].

Thompson assumed that the effects of ultrasound were attributed to an activity of the stable or inertial cavitation event. It is believed that these effects are related to the bubble dynamic phenomenon [28] and can be related to the acoustic pressure associated with the cavitation threshold.

2.2.2.1 Stable cavitation

Stable cavitation can be described as the formation of bubbles which oscillate in an equilibrium radius without collapsing. Under these circumstances, bubble growth involves a stable cavity. The bubbles are forced into nonlinear pulsation and become violent. The radius of the bubbles expands as they are under the influence of a negative pulse cycle. The bubbles contract during a positive pulse cycle. This process, under the intense pressure field, causes forces to build inside the bubbles. The growth rate of a bubble corresponds to the rate of contraction during the compression phase, but will not exceed the equilibrium radius.

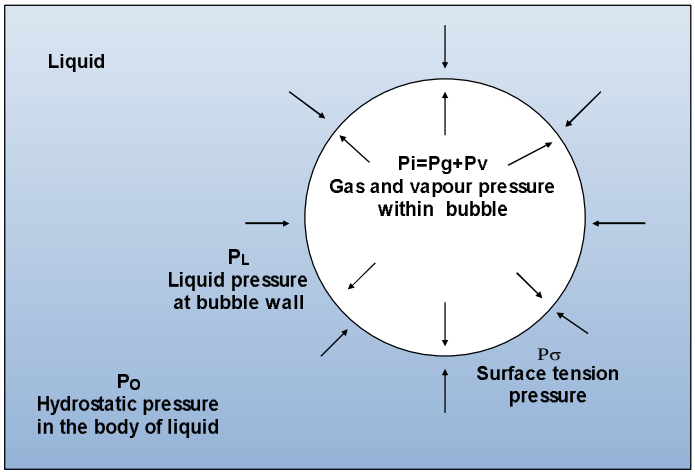

Figure 2.3 The pressure condition of a single bubble under stable conditions.

Stable cavitation is dependent upon the static equilibrium pressure of the bubble. In the stable stage, the pressure within the bubble, P_i, is greater than the pressure in the liquid, P_L. The force within a bubble, generated to balance the surface tension, P_σ , is greater than that in the surrounding body of liquid, P_o. Figure 2.3 illustrates the pressure acting on the stable bubble and when P_L is decreased but remains positive, the bubble will expand, but remains at equilibrium. Importantly, the bubble wall will remain intact throughout.

In the stable caviation stage, the equation of the wall motion for a stable bubble [28] is presented as;

$$R\ddot{R} + \frac{3}{2}\dot{R}^2 = \frac{1}{\rho}[P_L(R) - P_\infty(t)] \qquad 2.2$$

Where ρ is the density of liquid medium, $\dot{R}$ and $\ddot{R}$ are the first-and second-order time derivatives of the bubble radius, R, respectively. $P_\infty(t)$ is the acoustic pressure in the liquid medium, and $P_L(R)$ is the liquid pressure outside the bubble wall. The surface tension pressure of the outer bubble wall [28] is given as;

$$P_L(R) = P_T(R) - \frac{4\mu_c \dot{R}}{R} - \frac{2\sigma}{R} \qquad 2.3$$

where σ is the surface-tension constant and μ_c is the coefficient of the liquid viscosity. $P_T(R)$ is the pressure of total mass content in the bubble at a given radius. Equations 2.2 and 2.3 are based on the assumption that the liquid density (ρ) is constant and will calculate the bubble radius at its equilibrium stage.

As mentioned, during bubble oscillation near resonance size, it is assumed that the violent pulsations of a gas bubble can cause damaging effects to a biological system [29]. The effects of the stable cavitation result from the presence of acoustic streaming and are of sufficient magnitude to cause biological damage. The calculation of shear force amplitudes produced by acoustic streaming, to estimate the influence of any biological effect, is proposed by Lawn *et al.* [30]. Also mentioned is the degradation of mammalian tissue caused by cavitation with a high spatial peak in the intensity of the ultrasound wave [31].

2.2.2.2 Inertial cavitation

Transient or inertial cavitation describes the phenomenon by which cavitation bubbles rapidly grow and subsequently collapse in a liquid medium. The physical process of the inertial threshold can be described as follows. A gas bubble in a medium is greatly expanded when pressure decreases rapidly. The pressure inside the bubble increases one-half cycle later, causing the bubble to collapse and disappear. During a very large pressure swing, the gas bubble radius increases suddenly, reaching a peak, after which the gas bubble can no longer maintain its equilibrium and subsequently collapses. The theory of the inertial cavitation stage, provided by Nappirus [32], is described as;

$$R\ddot{R} + \frac{3}{2}\dot{R}^2 = \frac{1}{\rho}\left[P\left(\frac{R_{max}}{R}\right)^{3\gamma} - P_m\right] \qquad 2.4$$

Where P refers to the gas pressure in the bubble at the maximum radius, R_{max} is the maximum size of the bubble before collapse, P_m is ambient pressure over the collapse period under maximum pressure amplitude and hydrostatic pressure, γ is the specific heat ratio of the gas within the bubble.

During the stages of the inertial threshold, the energy of collapsing bubbles will increase and then be released into the load medium. The collapse of a gas bubble is typically violent, which gives rise to high local temperatures and high pressure conditions causing object damage and the effects of cavitation. The maximum temperature (T_{max}) and pressure (P_{max}) obtained within a collapsing bubble were provided by Thompson *et al.* [28], and are described as;

$$T_{max} = T_o \left[\frac{P_m(\gamma-1)}{P}\right] \quad 2.5$$

$$P_{max} = P \left[\frac{P_m(\gamma-1)}{P}\right]^{\gamma/(\gamma-1)} \quad 2.6$$

Cavitation is related to bubble dynamics in the load medium and can determine the pressure and velocity fields in a liquid medium related to the motion of the bubble wall. The generating bubble contains unknown gas pressure. When a bubble oscillates and reaches its resonance size whilst failing to maintain an equilibrium radius, high shearing forces may be released into the surrounding area. The cavitation process may give rise to acoustic streaming and subsequently bubble collapse, producing high local temperatures and high pressure in the liquid medium [33]. The intensity of the cavitation corresponds to the energy stored in the liquid medium, and depends on initial bubble size, the stored acoustic pressure and driving ultrasonic frequency [34]. The occurring inertial cavitation effects can be exploited for use in chemical reactions or processes [28] and can cause damage to objects [6].

2.3 High power ultrasound applications

High power ultrasonic fields are used in a broad range of applications which can be divided into three categories: power ultrasound, sonochemistry and medical applications. The application of cavitation in each area is dependent on the system operation, as well as the frequencies and levels of acoustic pressure involved. This section is concerned only with high power applications which may produce acoustic cavitation. The propagation of the high power ultrasound wave leads to the non-linearity of acoustic fields and can cause cavitation to play an important role in the high power ultrasound domain. This work serves as an introduction to high power ultrasound applications involving cavitation activity. The application of high power ultrasound is based on the exploitation of high pressure and energy, and a series of secondary effects such as acoustic cavitation and mechanical rupture.

2.3.1 Ultrasonic cleaning

Ultrasonic cleaning is perhaps the oldest industrial application of ultrasonic power, which has been in use for more than 50 years. The cleaning technology is widely used in many industries such as the production of semiconductors, as well as the medical, aerospace, glass and optics industries. Ultrasonic cleaning employ operational frequencies in the range from 20kHz to 3MHz [35]. The use of ultrasonic cleaning can be divided into two groups. The first group is ultrasonic cleaning operated at low frequency ranges of 20kHz to 100kHz. This application is normally used for cleaning the less critical machinery within industry. Cleaning at low ultrasonic frequencies produces extreme acoustic pressure fields, and associated cavitation implosion, and can cause damage to delicate parts of the object. However, it is suggested that high frequency ultrasonic cleaning, or "Megasonic cleaning", should be used for this purpose to avoid inflicting damage to the object. Megasonic cleaning technology operates in high frequency ranges of 0.8MHz to 1.2MHz [36]. It is effective at removing surface contaminants without inflicting surface damage. Megasonic cleaning is widely used for cleaning delicate objects such as photomasks and wafers in the semiconductor industry [37]. During the cleaning process, the

cleaning action is provided by acoustic cavitation and bubbles and both ultrasonic cleaning categories have the ability to remove contaminates very effectively.

The ultrasound cleaning process works by producing sound waves in a fluid medium. When ultrasound waves are transmitted through water, the high pressure waves create cavitation. Both cleaning processes use the benefits of wave propagation, mechanical dynamics and cavitation. Hence, it is believed that the main mechanism of the cleaning process, based on expanding and collapsing bubbles in a load medium, causes contaminants to loosen on the surface of objects. The cavitation, which is the most extensively used tool in ultrasonic cleaning, is generated by ultrasonic transducers. The basic components of an ultrasonic cleaning system consist of a bank of ultrasonic transducers, an electrical generator and a cleaning bath filled with water, as depicted in Figure 2.4.

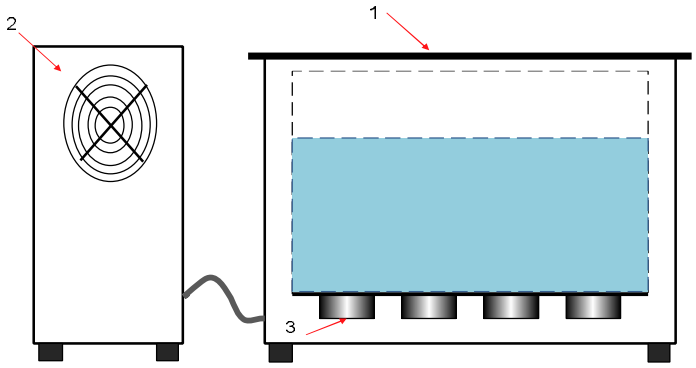

Figure 2.4 Schematic diagram of basic ultrasonic cleaning components; 1. Cleaning bath, 2. Electrical driving system (power amplifier) and 3. Ultrasonic transducers.

The cleaning process is significantly more efficient than other methods due to the effects of cavitation. Cavitation generates effects such as micro-bubbles and acoustic streaming which are capable of reaching normally inaccessible places in complex internal cavities that would otherwise be difficult to clean. It is noted that ultrasonic

cleaning on solid, rigid materials such as metals, glass, ceramics and plastics, is more effective than on soft materials due to the greater reflection properties of hard materials. Furthermore, the cleaning ability of ultrasonic waves may relate to power densities due to higher levels of cavitation formation. As mentioned in [38], the cleaning ability of an ultrasonic wave of low frequency and high power, 25kHz, is greater than that of a 40kHz wave. However, cleaning operations at high power accompanied by cavitation can cause damage to delicate parts of the objects such as semiconductor materials [39].

Although ultrasonic cleaning technology has been in use for over 50 years, it has obtained no standard method for the evaluation of the effects of cavitation. The high power and cavitation involved in the cleaning process may cause damage to objects. In order to achieve a high level of performance from the cleaning system and avoid damage to objects, the ultrasonic transducers generating the bubbles and cavitation are required to control and optimize their efficiency by design. Although no direct technique of measuring the efficiency of an ultrasonic cleaner exists, the numerical modelling technique, which is a strategy of design and understanding of the behaviour occurring as a result of the physical system implementation, can help to optimise the system design as well as predict spatial cavitation variation and acoustic intensities within the cleaning bath. For example, the employment of the numerical modelling approach, involving finite element analysis (FEA) can predict and visualize the acoustic pressure and cavitation regions. Several researchers have used this technique to predict the behaviour of their designed system [40],[41].

Currently, some researchers suggest that using an ultrasonic sensor, such as a hydrophone, to investigate cavitation activity in cleaning baths, is the best method of optimising the cleaning process. However, difficulties in taking the experimental measurements arise as the ultrasonic sensor suffers from shock waves, cavitation and micro-bubble jets. These factors can cause significant damage to the sensors. Therefore, the measurement of cavitation in a high power field requires a robust

measurement method and sensors that are durable enough to withstand acoustic cavitation [41].

2.3.2 Sonochemistry

Sonochemistry is the act of accelerating chemical and physical reactions using ultrasonic energy at high power levels. As discussed previously, the oscillation of gas bubbles and their subsequent violent collapse can produce high temperatures and intense pressures. These extreme conditions of the occurring phenomenon can lead to the acceleration of chemical reactions, as a direct result of cavitational effects. In the process of sonochemistry, the chemical products of the reaction are dispersed into a liquid medium. While the gas bubbles are in the process of violent collapse, the occurring cavitation can prompt a chemical reaction, causing the rest of the cavitation bubbles to be stimulated and emit light by a chemical reaction process known as sonoluminesence [5], which is described in Section 2.4.3. The term sonochemistry is often used to define the effect of ultrasonic sound waves on a chemical reaction.

As the term sonochemisty refers to chemical and sonochemical reactions, the results of driving high power ultrasound within a liquid medium may induce cavitation effects which enhance the reaction rate in a variety of reacting systems. The rate of increasing the reaction in chemical and electrochemical systems is linked to operational efficiency and can produce an improved yield. High power ultrasound is widely used in laboratories to accelerate the rate of the chemical reactions. As sonochemistry is a chemical enhancing method, it is a promising alternative for high-value chemicals and pharmaceuticals [28]. There are several references available which provide background knowledge of sonochemistry and chemical reactions through cavitation bubble dynamics. The equation of cavitation bubble dynamics is referred by the Rayleigh-Plesset equation which describes the oscillation and collapse of bubbles [32]. This equation assumes that the dynamics of a bubble in its spherical shape before collapse causes the sonochemisty process [23]. The outcome

of the cavitational process may produce sonochemical effects, which are diverse and include extreme improvements in both sonochemistry and sonocatalysis (an acceleration of a chemical reaction in liquid-solid system by ultrasound) [42]. It has been found that sonochemistry involves cavitation effects in two main categories: the homogeneous sonochemistry (related to bond braking and radical formation) and the heterogeneous sonochemistry (correlated with the reactions of solid and liquid states). The applications of high power ultrasound in sonochemistry are included in polymer chemistry and synthesis [43]. Nevertheless, it has been found that there are differences in application between polymer chemistry and synthesis, such as material science (catalytic materials, improved extraction of metals and plants) [44], biotechnology (used in the food industry, modification of enzyme and cell activities) [17], and environmental protection (both chemical and biological application e.g. water and sewage treatment) [45].

It acknowledged that high power ultrasound obtains several of its benefits from the effects of cavitation. While cavitation dynamics refer to mechanical and chemical effects when considering the success of sonochemistry, it is beneficial to maximize these effects in applications by limiting the ultrasound energy and the frequency range. Chemical effects related to sonochemistry normally employ frequencies below 50kHz due to their use with common laboratory equipment. However, there is also the prospect of using sonochemistry at higher frequencies, such as the oxidation process in food processing [46].

The application of sonochemistry involves high power ultrasound and the effects of cavitation. To optimize the process, measuring cavitation and predicting its location are required for implementation. In the past, cavitation activity has been demonstrated through pressure field distribution measurement. The method provides poor accuracy and cannot determine the intensity of cavitation activity. Therefore, this Thesis will attempt to develop a reliable measurement technique for monitoring acoustic cavitation, which could be used in sonochemistry applications.

2.3.3 Medical application

The role of high intensity ultrasound in therapeutic treatment has grown enormously in the last decade due to the success of high power ultrasound in areas such as ultrasonic shock waves in the treatment of kidney stones [47] and high power ultrasound in bone pathology [48], allowing the acceleration of the healing process [48]. Recently, there has been an interesting development in the use of high intensity focused ultrasound (HIFU) in disease treatment such as cancer therapy [49], tumour surgery [49] and metastatic disease [49]. HIFU has gained attention as a tool for disease treatment by applying high intensity ultrasound as a non-invasive treatment. The well documented use of HIFU as a medical treatment is reviewed in references [48],[49],[50].

HIFU is used to treat various conditions and abnormalities, and has been a subject of interest for medical research. The physics of HIFU has made it an attractive non-invasive therapy for soft-tissue tumours. HIFU techniques have been used in clinical applications for the treatment of tumours including breast cancer, and is potentially applicable to non-invasive surgery of diseased tissue [50]. Moreover, HIFU is also used for local ablation therapy for many types of tumours. The main mechanisms involved in the treatment are thermal effects, caused by ultrasound absorption, and mechanical effects involving the thermal effects induced by acoustic cavitation. At the focal point, the acoustic energy causes a rapid, intense increase in temperature to destroy malignant tissue. It is believed that cavitation may help improve treatment efficiency. The HIFU treatment for tumours is widely used in many countries such as China, Japan, Korea, the United States and a number of European countries [51]. The HIFU device is well suited to the application as rapid temperature increases are induced (approximately above 56^{o}C) within a small focal region. The HIFU technique is extensively used in various treatments including liver tumours, renal tumours, breast cancer and pancreatic cancer [51].

It is noted that the HIFU device can produce high intensity energy levels (usually in the range of 1,000 to 10,000W/cm^2) at the focused point, and can induce high temperatures in tissue [18]. It also has a very small focal spot in the range of millimetres or even sub-millimetres. Basically, it is noted that HIFU is a non-invasive surgical technique for the ablation of the regions of the target tissue. The highly focused beam of the HIFU produces high acoustic energy into a focal area. The dimensions of the focal area are dependent on the source geometry and operating frequency. A simple depiction of HIFU operation is illustrated in Figure 2.5. Although HIFU generates high intensity energy in a small focused location for disease treatment, it can generate acoustic cavitation and causes damage through two mechanisms; the conversion of mechanical energy into heat via the absorption by the tissue, and cavitation due to gases within the tissue. As the cavitation is often unpredictable, the amount of cavitation activity caused by HIFU can lead to several effects, both thermal and physical. The cavitation caused by the operation of HIFU was reported by Rabkin *et al.* [52]. The characteristics of the HIFU device can be determined through the produced HIFU field, which is essential in optimising malignant tissue ablation via cavitation. However, the characterization approach to obtain the HIFU field in general is challenging because of the high pressure field and associated acoustic cavitation, making the surrounding environment hostile to the detection device.

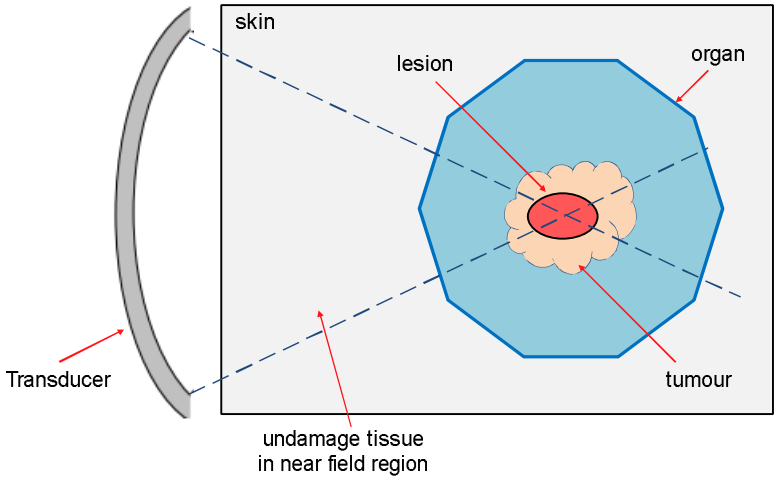

Figure 2.5 The schematic operation of HIFU device generating a focal region.

he field of high power ultrasound has been continually developed because of its non-invasive advantages. There have been many publications on the cavitation effects of high power ultrasound in mechanical, biological, and chemical areas [28], [53],[54]. Collapsing bubbles have the potential to cause significant damage in medical ultrasound applications such as therapeutics and surgery, which should be a major concern. Therefore, determining acoustic cavitation activity is proposed for safety and system limitation reasons. The likelihood of cavitation occurring is determined through intensity quantities such as the spatial peak pulse average intensity and the spatial peak intensity averaged over the largest half-cycle. They were used to provide a measurement of the potential of cavitation activity based on bio-effects due to a high intensity acoustic field. The intensity of cavitation-based bio-effects can be indicated through the mechanical index (MI) [55]. This output displays a standard for cavitation-related bioeffects developed by the Food and Drug Administration (FDA) [55]. The mechanical index can be used in reference to cavitation activity. This is important to control cavitation activity and limit cavitation effects. The evaluation of the MI is of interest when considering alternative amplitude and time and frequency dependency [55].

2.4 Cavitation Detection

Some of the difficulties in measuring cavitation occur as the measurement is being taken: damage to sensing equipment in high power ultrasonic fields, large transient signals, hostile environmental conditions and unpredictability. Cavitation can affect the local pressure within a field of bubbles which causes the non-linearity of the system and can promote several effects. Observations of cavitation activity can be investigated through bubble development to evaluate these occurring effects. Therefore, to achieve the development of a new cavitation monitoring system, a number of reliable detection approaches that have been used to investigate cavitation are briefly reviewed in this section

2.4.1 Detection through erosive effect

Measuring erosive effects is a widely used technique for monitoring cavitation activity. The effects of cavitation produce damage to objects, in this instance such as a pump impeller [56] and aluminium foil [57], under high power acoustic field conditions. This damage can be used to monitor cavitation. Over the duration of the test, cavitation bubble clouds are likely to migrate under the high power field, which will bring them adjacent to the tested sample surface. The erosion of the tested sample surface illustrates the effects of the mechanisms of the occurring cavitation. This phenomenon can potentially alter the property of materials [58] and may produce damage to the surface of objects. For instance, the erosion effect of the thin aluminium foil which is used to monitor cavitation activity in the cleaning bath provided in articles [59] is depicted in Figure 2.6.

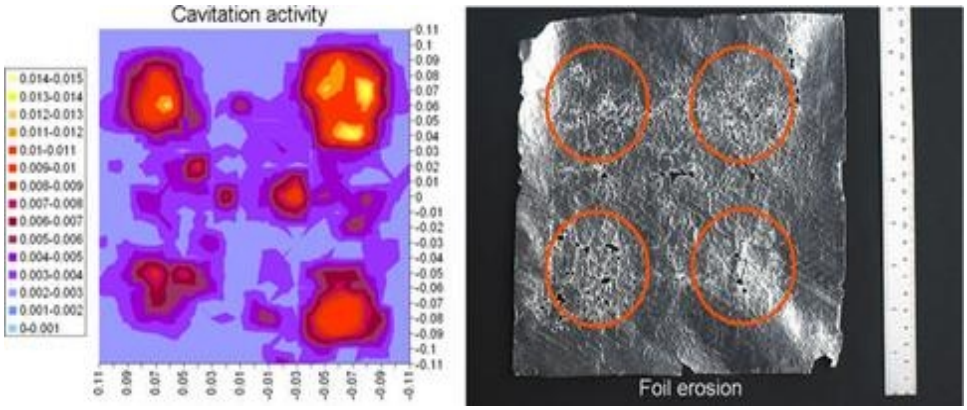

Figure 2.6 The erosion technique of thin aluminium foil used to characterize the cavitation within cleaning bath [59].

It is known that the degradation of the objects is caused by the mechanisms of cavitation as micro-bubble jets and bubble motion, induced by radiation acoustic forces under high ultrasound pressure fields. The capability of this phenomenon can be used to examine cavitation activity in cleaning baths [59]. The erosion effect technique can be used to monitor only the regions of the cavitation and it is not a real-time detection method. Moreover, the exploitation of erosion as a method of

characterizing cavitation is not simple and requires specific conditions. The most erosive effects on test objects rely on the intensity of acoustic cavitation and the resistance of materials. Monitoring acoustic cavitation using detection of the erosive effect requires extreme conditions such as high pressure sufficient enough to produce high cavitation activity capable of producing damage to test objects.

2.4.2 Detection through acoustic scattering

The scattering of acoustic signals from bubbles is a detection approach that can be used to investigate transient cavitation. This method is expected to take advantage of the large scattering cross-section of the cavitation bubbles. An excellent review of acoustic scattering from bubbles can be found in Leighton's comprehensive book [4]. The acoustic scattering cross-section, Ω_b^{scat}, is described by the ratio of the time average power scattered by bubbles from a plane wave to the intensity of that plane wave. The acoustic scatter cross-section of a single bubble assumed to be a nonlinear oscillator and is described by Leighton [4] as;

$$\Omega_b^{scat} = \frac{4\pi R_0^2}{((\omega_0/\omega_1)^2-1)^2+(2B_{tot}/\omega_1)^2}) \qquad 2.7$$

Where R_o is bubble radius, ω_0 and ω_1 are the radial frequency of bubble resonance and insonating frequency, respectively. B_{tot} is a parameter associated with the damping of bubbles. The scattering of resonance bubbles is a result of strong coupling with the incident wave. When the ultrasonic field is strong enough to impact the bubble oscillation, the scattering of bubbles is sufficient to generate a measurable signal-to-noise ratio.

Studies of acoustic scattering which have exploited the enhanced scattering of the bubbles include high frequency ultrasonic scattering in biomedicine. The scattering technique was used by Insana to investigate the acoustic backscatters from anisotropic biological tissues, which is employed to determine the scattering

coefficient of kidney tissue [59]. Fairbank *et al.* investigate the emission scattering signal from bubbles; they assumed that acoustic resonance can be subject to a broadband ultrasound signal and proposed this technique as a means of measuring the variation of blood pressure [60]. The success of the scattering technique in measuring bubble activity suggests that this approach can also be used to measure cavitation activity. Chen *et al.* measured the signals of the light scattering technique which can be related to bubble activity, especially for inertial cavitation [61]. Nevertheless, there are several articles in which the scattering technique was used to investigate the contrast between bubbles and cavitation [62],[63]. The Rayleigh-Plesset equation [28] can be used to explain acoustic cavitation through the bubble radius and the collapse of bubbles.

2.4.3 Detection through sonoluminescence

Sonoluminescence (SL) can be defined as the process by which ultrasonic waves, with sufficient intensity, are transmitted through a liquid medium, and cause bubbles to oscillate, grow and collapse. An active bubble interacting with an intense sound wave can create extreme conditions and highly non-linear situations. The high ultrasound propagation of a liquid medium which contains an intense cavitation field can produce bursts of light in picoseconds, from which, sonoluminescence originates.

It is known that sonoluminescence is driven by acoustic cavitation. Moreover, this approach is capable of monitoring acoustic cavitation. There are two separate forms of sonoluminescence employed in the investigation of cavitation: single-bubble sonoluminescence (SBSL) and multi-bubble sonoluminescence (MBSL) [62]. For example, the sonoluminecence method was used to observe cavitation in water produced by the 20kHz ultrasonic horns used by Crum [64]. When high local acoustic pressure achieves the cavitation threshold, a high pressure zone is created in which cavitation is activated and is sufficiently intense to produce light emission. The regions of intense acoustic stress of multi-bubble sonoluminescence, including

cavitation and sonoluminescence, are detected through light emission, as seen in Figure 2.7.

Sonoluminescence provides a useful probe of the conditions created by the high cavitating field. The occurrence of sonoluminesence indicates the presence of active acoustic bubbles which are sufficient to generate light emission. The presence of light highlights the regions of extreme cavitation conditions. The sonoluminescence phenomenon is a comprehensive approach as it is associated with cavitation through the intense sound waves, which are able to produce sufficient numbers of acoustic bubbles and cavitation to emit light [64].

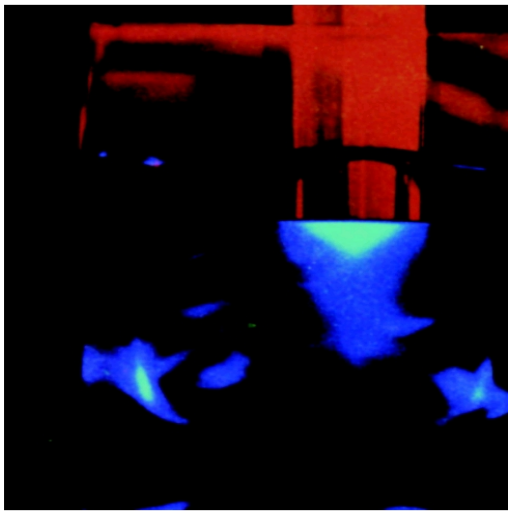

Figure 2.7 Multi-bubble sonoluminescence produced by an ultrasonic transducer [64].

2.4.4 Detection through acoustic emission

An acoustic emission technique has the potential to monitor acoustic cavitation through the detection of the acoustic signals generated by both oscillating and collapsing bubbles. The spectrum detected contains a wealth of information about the

dynamics of the cavitation process. When cavitation forms and collapses under the influence of a high ultrasound field in a liquid medium, acoustic emission signals are produced and the cavitation bubbles become a secondary source of sound to produce a broadband acoustic emission signal. The acoustic emission signal generated by cavitation can be detected using sensors such as the hydrophone [8] and the fibre-optic hydrophone [8],[65]. An example of a broadband acoustic emission spectrum generated by cavitation bubbles and detected by the B&K 8103 hydrophone produced by a 40kHz transducer is shown in Figure 2.8.

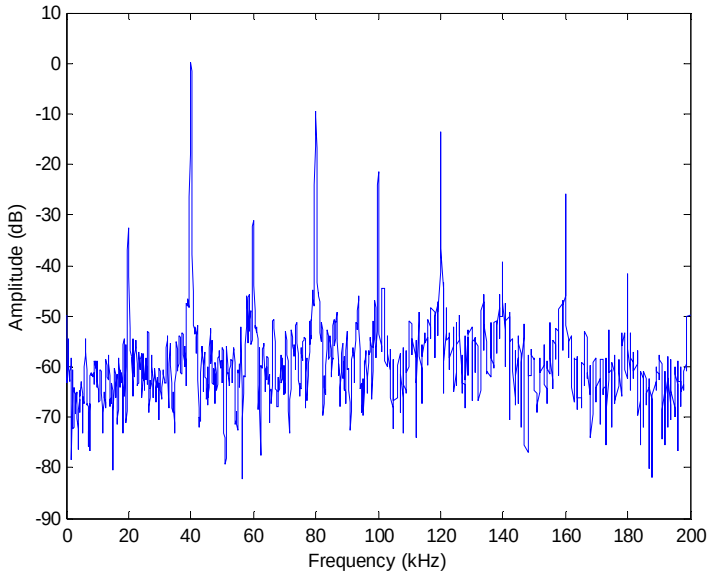

Figure 2.8 Acoustic emission (AE) spectrum measured by the B&K 8103 hydrophone. The AE signal is produced by a 40kHz transducer at 40kHz and power input of 30W.

It is known that the acoustic spectrum produced by cavitation bubbles contains various frequencies including the fundamental or driving frequency (f_o). The acoustic cavitation spectrum is also composed of sub-harmonic $(f_o/2)$, ultra-harmonics ($nf_o/2$, where n = 2, 3, ...), and harmonics (nf_o, where n = 2, 3, ...).

Moreover, the acoustic emission spectrum contains the broadband noise signal produced by shock waves from collapsing bubbles. These components contain information of the occurring cavitation events.

There are many articles that describe the acoustic emission technique as a means of monitoring and analyzing cavitation activity [57],[66],[67],[68]. An acoustic emission approach has the potential to investigate cavitation occurring in hydraulic turbines as cavitation is a source of damage to and degradation of the machine. Vibrations and pressure are induced in order to identify and analyse the cavitation activity. Wolff *et al.* [67] investigated the collapse of cavitation bubbles which generate acoustic emission signals. It was noted that the acoustic emission signal generated is linked with the high amplitude pressure pulse of the hydroturbine system. Moreover, it is believed this process will allow monitoring the intensity of cavitation. Their work shows increasing rms voltage levels of acoustic emission with increasing pressure and cavitation.

The NP10-3 Dapco hydrophone is used by the National Physical Laboratory (NPL) to measure the acoustic emission caused by cavitation events occurring in high power ultrasound fields produced by a physiotherapy transducer [66]. The NP10-3 Dapco hydrophone was designed to detect the onset of cavitation in terms of the acoustic emission spectrum. The acoustic emission generated by the ultrasonic transducer can be detected by ultrasonic sensors such as the hydrophone. The characteristics of acoustic emission signals associated with bubble cavitation activity are explained in Galat's article [68]. The cavitation activity, in terms of the acoustic emission spectrum, acquired by hydrophone detection provides broadband noise signal revealing the high frequency range of the emission spectrum. The intensity of cavitation activity determined by broadband integrated energy (BIE) from the acoustic emission spectrum was presented in Hodnett's publication [66]. The author illustrates the cavitation activity through the correlation between acoustic emissions and broadband integrated energy in the frequency ranges of 1-5MHz with increasing

ultrasound input power. Furthermore, the acoustic emission approach can assess the investigation of a spatial distribution of cavitation activity generated within the reactor vessel through, specifically, the rms voltage levels of the frequency band of 1-7MHz of the acoustic spectrum. This process will reveal the map points associated with low and high cavitation regions in a vessel [57]. The intensity of the cavitation activity is calculated by the integration of frequency-dependent spectrum magnitudes obtained from the acoustic emission [57].

2.5 Detection sensor used for cavitation measurement

The measurement of cavitation activity has been a troublesome process. Cavitation generated in the high intensity field has the possibility of damaging objects and sensing equipment under critical conditions such as a large transient signal, hostile environmental conditions and the non-uniformity of cavitation. Furthermore, the lack of proper detection devices and available standardising methods results in greater difficulty when investigating cavitation. However, some available sensors which can be used for monitoring cavitation are reviewed in this Section.

A general hydrophone, B&K 8103 hydrophone manufactured by Bruel&Kjaer, Denmark, is shown in Figure 2.9 (a) [69]. The B&K 8103 hydrophone can be used to monitor acoustic cavitation. Hydrophone measurements of cavitation may be sensitive to electrical pick up. The B&K 8103 hydrophone, which was designed for high-frequency underwater measurements, has an element size of 8mm and a piezoelectric cylinder of 6.35 mm in diameter. This hydrophone can be used to monitor acoustic parameters such as acoustic pressure, cavitation noise and shock waves. However, The B&K 8103 hydrophone is designed to operate in the frequency range of 0.1Hz to 180kHz (+2.5dB and -12.5dB) and in the temperature range of both the short term (-40 to +120 ^{O}C) and continuous (-40 to +80 ^{O}C). Importantly, the device is limited by the conditions of acoustic pressure and a shock wave of 40MPa [70]. The B&K 8103 hydrophone has been widely used for monitoring acoustic cavitation by Jenderka [8], Koch [71], and Hodnett [72] through acoustic

emission within the high pressure field. However, although this sensor can be used to monitor acoustic cavitation, it can potentially be damaged by many conditions of the high pressure field such as pressure limitation, the high impulse of shock waves and intense cavitation.

The measurement method of using light to detect and quantify a high pressure acoustic field is not a new one. The light interaction approach using a fibre-optic hydrophone as a detection probe is shown in Figure 2.9 (b) [71]. The optical-fibre hydrophone can offer minimal disturbance of the acoustic field through the reduced element size (several microns) limited by the optical fibre diameter. The device is comprised of light from a laser diode coupled into a glass optical fibre of 50 micrometers, with the end positioned in the load medium. Various models of the fibre-optic devices can be used for monitoring high acoustic pressures of up to 500MPa. The measurements of ultrasonic fields or cavitation activity have the potential to overcome some of the problems associated with hydrophones. However, the employment of optical-fibre hydrophones to measure cavitation is limited by the linear broadband frequency response, and susceptibility to the intense ultrasound field and hostile environments. Although the small tip of the device is damaged from high pressure and the cavitation field, it is possible to renovate the device by removing the end of the damaged fibre tip [8]. In general, a fibre-optic hydrophone has been used for acoustic pressure measurements in high pressure fields during cavitation creation, but it has the potential to be used as a monitor of cavitation activity. The optical-fibre hydrophone, which is used for characterising ultrasonic cleaning baths using the acoustic emission technique [8],[71], providing information on the occurring cavitation. A similar device, which is resistant to the effects of bubble collapse and cavitation close to the active element, is used to measure acoustic shock waves [73]. This technique assumed no physical interaction with the acoustic beam. Nevertheless, applying a fibre-optic hydrophone to reverberating high power fields may cause damage due to cavitation and acoustic streaming. Moreover, the results may be erroneous because of the rest of the optical fibre in the system interacting with the high power field and bubble phenomenon.

The measurement of acoustic cavitation activity using the acoustic emission technique can be achieved through the development of a specific cavitation sensor i.e. the NPL cavitation sensor. A prototype of the cavitation sensor was developed by scientists at the National Physics Laboratory (NPL) to monitor cavitation [74]. The cavitation sensor structures include a hollow cylinder block of 30mm composed of three layers; 4mm-thick polyurethane as the cavitation shield, 110μm PVDF film as a piezo-electrically active membrane, used for sensing, and 0.4mm-thick polyurethane rubber formulation, used for a matching layer and a protective layer. The construction of this sensor is shown in Figure 2.9(c) [75]. This sensor is resistant to high power ultrasound and cavitation, and operates by monitoring high frequency acoustic emissions (given an acoustic emission beyond 1MHz) [75]. The sensor has been designed for quantifying the intensity of cavitational activity occurring in high power applications such as an ultrasonic cleaning system. The typical frequency at which the sensor operates is 20 to 50kHz. The NPL cavitation sensor with a diameter of 30mm for a PVDF membrane hollow cylinder provides low spatial resolution. Nevertheless, this sensor has been used for characterizing ultrasonic cleansing vessels [73] and it has the ability to detect cavitation with a small transmitting transducer, such as a sonochemical horn, by placing a small transmitting transducer inside the sensor [75]. The cavitation activity obtained from the measurement can be displayed by a signal processing unit (designed by the same company), and can be calculated by using the broadband integrated energy across the frequency range of interest. The excellent documents of theory and experiment for the NPL cavitation sensor are provided [9],[10].

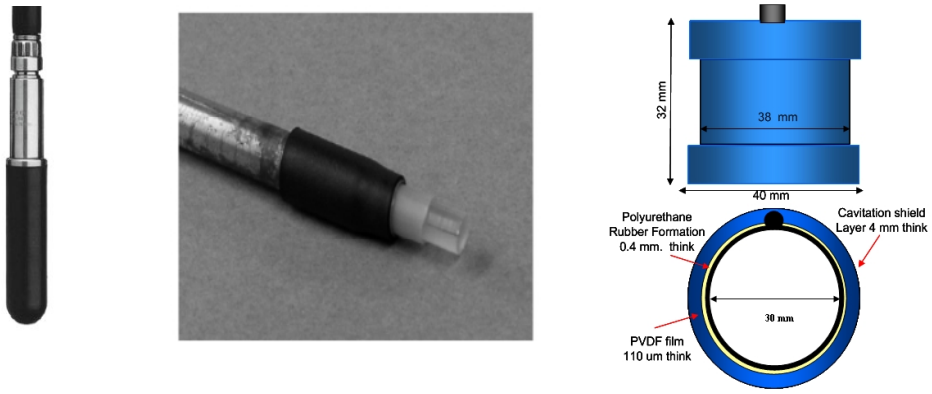

(a) (b) (c)

Figure 2.9 The detection sensor which is used to monitor cavitation; (a) the B&K 8103 hydrophone [69] (b) the fibre optic hydrophone [71] (c) the NPL cavitation sensor [75].

2.6 Summary

This Chapter has outlined the evolution of high power ultrasonics. Brief descriptions of high power ultrasound applications in several areas, for example, cleaning, sonochemistry and medical implications are introduced. The applications of high power ultrasound in a liquid medium can produce acoustic bubbles and cause acoustic cavitation. The cavitation phenomenon, including the cavitation inception and the distinction of two cavitation thresholds, both stable and inertial, has been presented. The process of bubble oscillation and collapse can produce cavitation effects which can have mechanical, biological and chemical impacts. Furthermore, available contemporary methods of cavitation detection have been discussed. However, measuring cavitation still requires precise sensors to produce accurate results and a review of contemporary sensors is presented. Importantly, the comprehensive literature review in this Chapter provides background knowledge of acoustic cavitation and gives rise to the idea of developing a cavitation measurement system.

CHAPTER 3

Development of a non-invasive optical measurement technique to monitor acoustic cavitation

3.1 Introduction

Typically, measuring high power levels and acoustic cavitation involves the insertion of a probe into the load medium. Unfortunately, probes can be damaged by the high pressure fields and cavitation activity. To avoid this, the optical measurement technique, based on Laser Doppler Velocimetry (LDV), is an attractive proposition. The removal of the hydrophone from the load medium would enable measurement of the acoustic field distribution without disturbance, as well as avoiding damage to the probe from high pressure, cavitation and micro-bubble jets. Assessing the suitability of a sensor for a particular task is important when characterising the system. For example, the interaction of an acoustic field and light provides a unique means to quantify an acoustic field in a fluid medium without altering the system dynamics

during the measurement process. The intensity of the cavitation activity can be determined by the broadband integrated energy (BIE) calculation of the acoustic spectrum in the high frequency range of interest.

Acoustic cavitation in general has been monitored using several approaches such as the aluminium foil erosive test [76], sonoluminescence [77] and conventional hydrophone detection [78]. However, many hydrophone probes are invasive to the high power ultrasound field and are susceptible to damage by high-intensity pressure and the effects of cavitation. A measurement of acoustic cavitation by the acousto-optic technique, based on light deflection, using a laser as a non-invasive probe is an attractive method as the potential of sustaining damage cause by cavitation is avoided.

The deflection of light by ultrasound has been studied extensively and employed as a method of visualizing the interaction between light and sound since the 1930s. The theoretically and experimentally extensive study of acousto-optic interaction, noted when a light beam traverses an acoustic field was introduced by Raman *et al.* [79]. Then, Light Diffraction Tomography, also known as optical diffraction tomography (ODT), was applied to demonstrate the 10MHz ultrasonic near-field pressure profile by combining a non-invasive optical technique with optical diffraction tomography [80]. Light diffraction tomography profiles a cross section of the acoustic field in a liquid medium at 10MHz can be reconstructed by implementing algorithms which are based around a specific tomography. The amplitude and phase profiles can be reconstructed though specifically chosen algorithms. The authors also proceed to compare the pressure amplitude field and the amplitude of the 10MHz ultrasonic near-field with the modelling results and a hydrophone probe. Interestingly, this paper also reported that the optical techniques demonstrate increased spatial resolution over the transitional hydrophone approach.

More recently, however, the optical diffraction tomography (OTD) method has been combined with the light intensity measurement technique to characterize airborne ultrasound in Holm and Persson's publications [81],[82], in which the light intensity measurement data contained information on sound pressure. Again using the tomography reconstruction technique, a sectional image of the airborne ultrasound pressure field, is produced. Erikson *et al.* [80] adapted this method for the study of the near field from a 10MHz device. This would be subject to several undesirable aspects associated with hydrophone use, with a lack of resolution being the primary concern.

The acousto-optic technique is generally proposed as a means of determining acoustic pressure, characterizing the ultrasound field through the merits of a non-invasive, high spatial resolution, and resolving the complex pattern of an ultrasound field. In addition, the technique has the ability to take measurements very close to the transducer surface. Quantifying the ultrasonic pressure in a medium using this approach is investigated by X. Jia *et al*. [83],[84],[85]. The author proposed the use of optical heterodyne interferometers to investigate acoustic pressure.

The combination of tomography and interferometry was proposed to characterize beam characteristics of ultrasonic transducers. Matar *et al.* investigated the use of optical heterodyne detection for the purpose of characterizing airborne transducers, with operating frequencies between 200kHz and several MHz [86],[87]. The optical interferometry method has been used to examine ultrasonic fields generated by a 33kHz Tonpilz transducer in fluid-loaded cylindrical test cells [41]. The optical interferometry technique has the potential to map acoustic pressure fields, producing 2D and 3D spatial images of pressure created by ultrasonic transducers.

For this work, it is believed that the optical interferometry technique would be capable of detecting acoustic cavitation by detecting the acoustic pressure and

presenting the signal in terms of the acoustic emission spectrum generated by the bubble dynamics.

This Chapter will describe the fundamentals of the acousto-optic effect and the principles of laser interferometry. The tomography reconstruction algorithm is then discussed. Next, the application of the optical measurement techniques, using Laser Doppler Velocimetry (LDV) to monitor acoustic cavitation activity within a Perspex reactor vessel, will be described. The evaluation of the cavitation activity detected by the broadband integrated energy of the acoustic emission spectrum is proposed. Finally, the laser vibrometry scanning routine, used to specifically map cavitation activity within a reactor vessel, will be implemented.

3.2 Acousto-optic effect

The acousto-optic effect is also known as acousto-optic interaction or the diffraction of light by sound waves. Sound waves can be used to modulate the amplitude and phase of light by deflecting it, focussing it, or shifting its frequency [88]. The acousto-optic effect has been used to characterize ultrasound waves in a liquid medium [89]. The interaction between optical beam and sound waves provides the foundation for an investigation into the visualisation of acoustic fields. Sound waves propagate through the medium producing regions of compression and rarefaction by wave radiation and this effect provides changes in the refractive index of the medium. Changes in the index of rarefaction of the medium will cause an optical beam within it to be deflected and modulated, changing the beam's amplitude, phase and frequency. The diffraction of light by high frequency sound has been reported [88],[89],[90]. Furthermore, light diffraction by ultrasonic waves has been extensively studied by Raman and Nath and published in a series of papers which outline the theory of the diffraction of light by high frequency sound waves [91],[92],[93]. These papers present the effect of sound on light in theoretical and experimental work. Light diffraction caused by ultrasonic waves is introduced within

a transparent, homogeneous medium [94]. However, Gamalath *et al.* [95] propose the idea of the acousto-optic interaction in liquids by providing the equation for the diffraction of light intensity obtained in terms of the Klein Cook parameter. This equation is widely used to describe the basis of the acousto-optic effect.The acousto-optic effect can be used for ultrasonic beam mapping. Jia *et al.* and Matar *el al.* proposed a measurement method based on an optical technique, by which the change in the reflective index of the medium caused by the propagation of acoustic waves is detected, to characterize the sound field of ultrasonic transducer [84],[86].

The development of the optical measurement technique is based on the properties of the acousto-optic effect laser used. The optical technique, relying on the acousto-optic effect, has been used more recently to characterize the various types of ultrasonic transducers and to visualize sound fields, as outlined in Section 3.3. Then, an introduction to the development of the coherent heterodyne detection technique forms the basis of the heterodyne interferometric devices discussed in Section 3.3.2. The optical measurement technique also has the potential to be applied to monitor the cavitation activity and its field. This is the focus of this Chapter.

3.3 Theoretical considerations

The optical detection technique relies on the acousto-optic effect [96], which occurs in all optical media when an acoustic wave and a laser beam are present in the medium. A harmonic sound wave can be described as longitudinal wave, $u(\mathrm{z}, t)$, as it moves through the medium. A progressive sound wave involves the displacement of fluid particles along the axis in the same direction of the wave. The elementary equation of a harmonic wave [96] is presented in Equation 3.1.

$$u(\mathrm{z}, t) = A\, sin\left[\omega\left(t - \frac{z}{c}\right) + \varphi\right] \qquad 3.1$$

where $A =$ amplitude

$\omega =$ angular frequency, $2\pi f$

φ = phase angle at $t = 0$

c = phase velocity of the wave in the load medium

f = wave frequency

As the wave propagates through the medium, it can produce a series of compressions and rarefactions at distinct regions along the wave's structure. The basic concept of the peak regions corresponding to compression and rarefaction is depicted in Figure 3.1. Regions of compressed phase correspond to points of high pressure, whilst rarefactional phases correspond with the points of low pressure and a low density of particles.

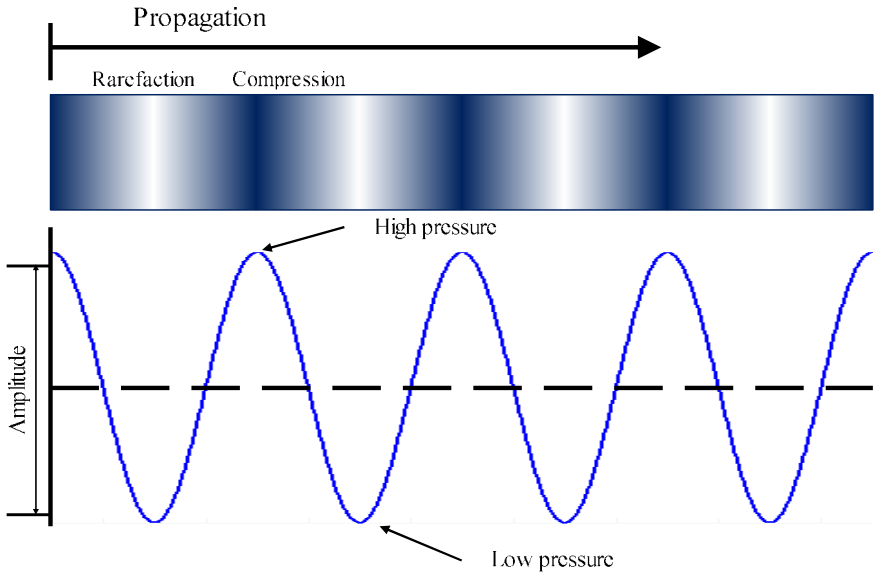

Figure 3.1 The model system of a propagating longitudinal sound wave in the load medium.

3.3.1 The Piezo-optic Coefficient

The propagation of a longitudinal sound wave within a load medium will cause a change in the density of medium properties at low and high levels [96]. The change of medium properties is a result of the relative index of the medium. As a result of the modification to the medium parameters as a consequence of the propagating sound wave, a refractive index wave is generated in direct response to changes in the density of the medium. The refractive index of the medium permittivity [96] is represented in Equation 3.2.

$$n = \sqrt{\epsilon_r} \qquad 3.2$$

where n = refractive index of medium

ϵ_r = relative permittivity of medium

The propagating sound wave causes change in pressure to the medium's refractive index. This relationship can be represented by a piezo-optical coefficient;

$$\mu_{op} = \frac{\delta n}{\delta p} \qquad 3.3$$

Where δn = variation in the ambient refractive index

δp = variation in the ambient pressure

Intuitively, the increase in density is due to an increase in pressure caused by the propagation of acoustic waves. Therefore, it may be reasonable to state that the sound wave may cause the change in the medium's refractive index. When considering a plane wave with a varying refractive index, $n(r)$, the angular plane wave will cause a small phase change in the ambient refractive index of the medium. The variation in the refractive index of n_0 results from the change in the relative

phase delay at that point. The refractive index obtained from the relative phase delay with the local refractive index [96] is represented in Equation 3.4.

$$n(r) = n_0 + \delta n \qquad 3.4$$

Where $n(r)$ = refractive index obtained from the relative phase delay

n_0 = ambient refractive index of the medium

Furthermore, the piezo-optic coefficient in the case of the plane wave is considered under the conditions that the transducer is stationary at time zero and the optical path length of a light beam has zero phase delay, the refractive index [96] in the plane wave is represented in Equation 3.5.

$$n_p(r) = n_1 \, sin\left[\omega\left(t - \frac{z}{c}\right)\right] \qquad 3.5$$

Where $n_p(r)$ = refractive index in plane wave

n_1 = maximum change in refractive index

The refractive index is obtained by the variation of density in an ambient medium due to rarefaction and compression caused by sound propagation. The change of path length and the refractive index result creates phase grating induced by Doppler-shifts in the optical frequency. This can be used to modulate or filter the optical beam. The effect of light diffraction on the inhomogeneities of the refraction index, known as the acoustic effect, has been applied to characterize the sound field produced by an ultrasonic transducer [97]. The interaction between the variation of the medium's refractive index and the light beam induces a phase delay. Quantifying this phase delay provides a non-invasive method of measuring the average pressure through laser interferometry [84].

3.3.2 Laser interferometry

The basic principle of interferometry is based on two light waves interacting with each other. When the output laser is reflected by an object, there will be an optical path difference between the original beam and the reflected beam. Two coherent light beams are made to coincide onto a photo detector. The detector sees the resulting interaction of two light waves. The two light waves will be out of phase and will create an interferometric pattern. The frequency and optical phase ($\delta\varphi$) difference between the reference beam (φ_0) and the reflected beam, (φ_{Ref}) are used as a Doppler phase shift, associated with the instantaneous displacement of a moving object. The difference between the reference beam and the reflected beam can be detected using interferometry. Evidently, this technology is a potential measurement tool in quantifying phase variations altered by sound wave produced by ultrasonic transducer. There are two different interferometric systems: homodyne and heterodyne interferometers.

3.3.2.1 Homodyne interferometer detection

Laser interferometers [96],[98] have been widely used in displacement measuring systems with sub-nanometer resolution. This technique detects the optical phase difference between the two laser beams associated with the displacement variations of moving objects and can be used for sound pressure detection. Figure 3.2 illustrates the schematic diagram of a homodyne interferometer. The optical interferometer detects variation in displacement by exploiting the relationship between the output of an interferometer and the difference between optical path lengths traversed by its beams.

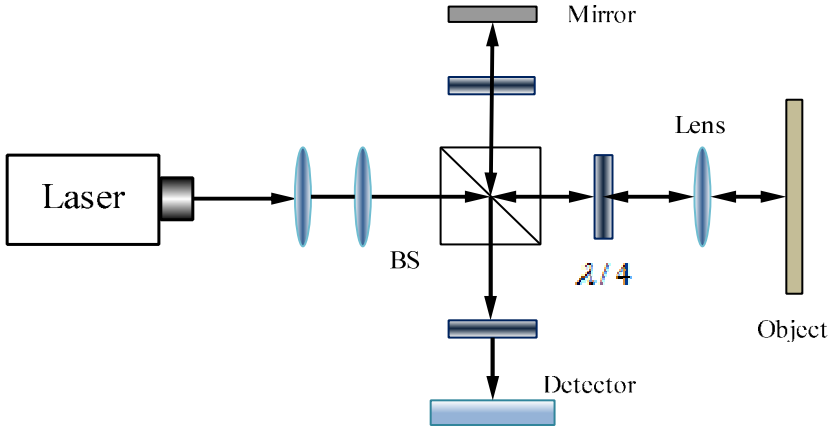

Figure 3.2 A simple schematic diagram of the homodyne laser interferometer.

The amplitude of the reference signal (A_o) and reflected beams (A_{Ref}) are detected at the photodetector as the beam is split by the beam splitter, (BS), and can be given [98] as;

$$A_0 = \frac{A_L}{2} e^{j(\omega t - \varphi_0)} \quad 3.6$$

$$A_{Ref} = \frac{A_L}{2} e^{j(\omega t - \varphi_{Ref})} \quad 3.7$$

Where φ_0 = reference phase

φ_{Ref} = reflected phase

A_L = amplitude of optical source

The phase shift (φ) can be related to the optical paths (L_i) travelled by the laser beam [98] as follows;

$$\varphi_i = \frac{2\pi L_i}{\lambda} \quad 3.8$$

Where φ_i = phase shift in optical path (L_i)

λ = wavelength of laser emission

The total amplitude of the laser beam detected at the photodetector, a combination of the amplitude of A_0 and A_{Ref}, is described [98] as;

$$A_{tot} = A_0 + A_{Ref} \quad 3.9$$

In case of light intensity detection, the amplitude of detected light intensity (I_L) at the detector [98] can be calculated from its amplitude by a multiplication with its complex conjugate A^*_{tot}, hence

$$I_L = A_{tot} \cdot A^*_{tot} \quad 3.10$$

The light intensity (I) at the detector can therefore be determined [98] through a substitution of Equation 3.9 into 3.10 and is given as;

$$I = \frac{I_L[1+\cos(\varphi_{Ref}-\varphi_0)]}{2} \quad 3.11$$

As the two optical light beams interact, the optical phase will shift. The optical phase difference carries information on the variation of the optical path length of the interferometer. The phase difference between the two light beams refers to the displacement of the vibrating object and can be described [98] as;

$$\delta\varphi = \varphi_{Ref} - \varphi_0 = \frac{4\pi D}{\lambda} \quad 3.12$$

Where D = displacement of object

$\delta\varphi$ = phase difference

The phase variation between the two light beams, according Equation 3.12, represents the optical path difference, which is dependent on the displacement measurement. The phase displacement is a result of a change in the constant velocity (c) in its position versus time [98], expressed as;

$$D(t) = c \cdot t \qquad 3.13$$

Where $D(t)$ = displacement at a given time

c = constant velocity

Then, the phase difference becomes time dependent [98], as Equation 3.14 shows:

$$\delta\varphi = \frac{2\pi\ 2c\ t}{\lambda} = 2\pi f_D t \qquad 3.14$$

Where f_D = Doppler frequency induced by a moving object

According to Equation 3.14, the displacement of the object under investigation is the same as the phase shift calculated by detecting the phase of interference signals. The Doppler shift from the displacement measurement is proportional to the modulus of the object's velocity [98], shown as;

$$f_D = \frac{2|c|}{\lambda} \qquad 3.15$$

Combining Equation 3.14 with Equation 3.11 provides the light intensity contained in the Doppler frequency [98] as;

$$I = \frac{I_L[1+cos(2\pi f_D t)]}{2} \qquad 3.16$$

The homodyne interferometer operates a frequency detecting method based on the phase of two reflected beams interfering with each other and causing displacement. The phase information will not provide directional information. This problem can be solved by adding a Bragg cell modulator [98].

3.3.2.2 Heterodyne interferometer

A heterodyne laser interferometer [96],[98] contains two light sources, as shown in Figure 3.3. This method places a Bragg cell modulator into a reference arm of the interferometer. A Bragg cell is an optical modulator which shifts the frequency of the traversing beam and produces an RF signal. The frequency of one arm of the laser beam is shifted by an offset Bragg cell modulator. The modulated frequency relates the offset frequencies f_B with a velocity. The modulation frequency, f_{out} at the detector can be described [98] as;

$$f_{out} = f_B + f_D = f_B + \frac{2c}{\lambda} \qquad 3.17$$

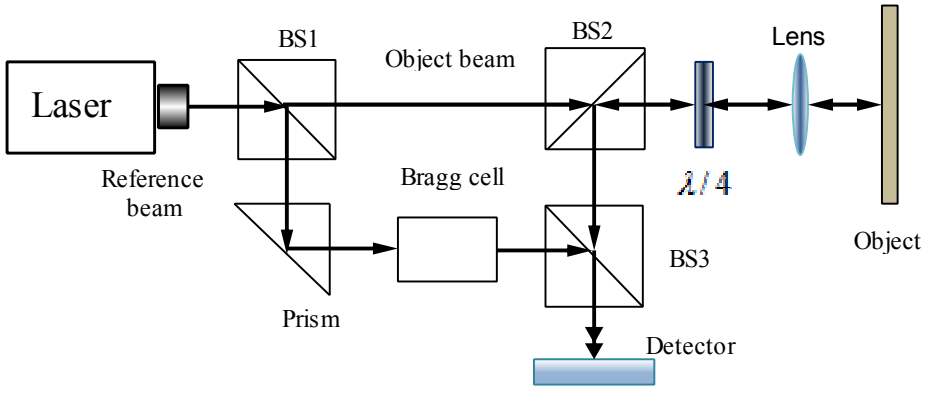

Figure 3.3 A schematic diagram of heterodyne laser interferometer with the Bragg cell.

The beam intensity of the heterodyne laser interferometer with the Bragg cell is given [96],[98] as;

$$I = \frac{I_L[1+cos[2\pi(f_B+f_D)t]]}{2} \qquad 3.18$$

Any movement of the object produces a Doppler frequency in the heterodyne interferometer. This is a direction dependant deviation of f_{out} from the offset frequency (f_B) at the Bragg cell modulator. The Bragg cell modulator modulates an RF signal. Thus, the detected frequency signal is modulated by a offset frequency (f_B) and frequency deviation (f_D). The modulated signal processes the time of the object velocity as a modulation signal. The RF signal of a Bragg cell modulation for the (Polytec OFV-303) laser interferometer used for the optical measurement is 40MHz [98].

(a) Velocity decoder

The frequency and phase modulated RF signals contain measurement information on the vibration velocity and displacement. A RF signal with a 40MHz carrier frequency is fed to the decoder. Both vibration velocity and displacement are variable in the interferometer [98]. After demodulating the FM signal, the vibration velocity is recovered by the velocity decoder. The evaluation of the velocity data allows the analysis of velocity proportional to the motion of the moving object and produces a velocity output voltage. The decoder relies on the demodulator used in the interferometry to decode the velocity data. However, there is a problem with decoding short transient signals such as ultrasonic echoes and impulse responses due to the limitation of the physical characteristics of frequency demodulation. Nevertheless, this method of signal processing covers the low vibration frequency range.

(b) Displacement decoder

The phase shift of the interferometer output signal contains the displacement information. The displacement decoder [98] can be used for processing the signals produced by the interferometer. The displacement recording process compares the phase discrimination between the RF drive signal for the Bragg cell and the modulated signal at the detector. A displacement of the object by $\pm\lambda/2$ produces a full demodulation period in phase difference at the photo detector. The maximum displacement of the Polytec HeNe laser is limited to 316.4 nm $(\lambda/2)$ for the phase difference of two signals [98]. Figure 3.4 illustrates the different signals available from the Polytec interferometer, in which the velocity and displacement decoders are available for the signal restoration of the interferometer.

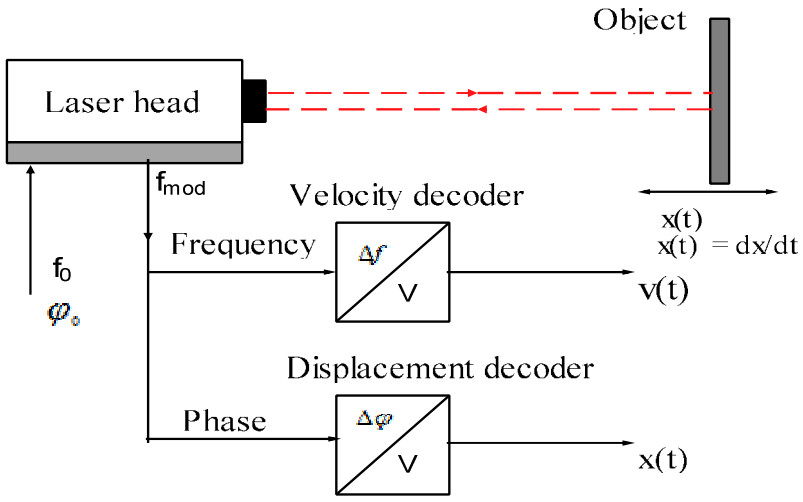

Figure 3.4 Schematic diagrams showing the signal variable for the Polytec OFV 303 interferometer [98].

3.4 Quantifying phase using Laser Doppler Vibrometry

Laser Doppler velocimetry is widely used to detect ultrasonic pressure [41],[96],[97]. A diagram of the Mach-Zehnder heterodyne interferometer [97] is presented in Figure 3.3. Using such an interferometer, the laser beam will be shifted in frequency as it crosses a transparent medium because of the acousto-optic effect, as illustrated in Figure 3.5.

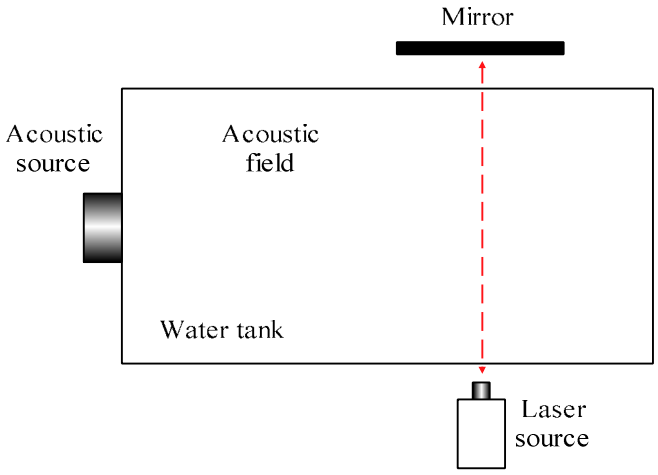

Figure 3.5 Schematic diagram of the LDV measurement taken directly from the acoustic field.

Figure 3.5 depicts a schematic diagram of the LDV measurement approach. The dynamic pressure field causes optical path length variations, which typically are small in amplitude. The acoustic pressure field is obtained by considering the dynamic pressure variation in the overall optical paths of the scan.

The pressure amplitude of the Doppler shift in the frequency of light from the vibrating object detected by the photodetector is described [41] as;

$$\delta_P(t) = p(x,t)sin(\omega t+\emptyset_c) \qquad 3.19$$

Where $\delta_p(t)$= change in ambient pressure

$\emptyset_c$ = constant phase

$p(x,t)$= sound pressure in the x-direction

Accordingly, the phase change induced by the pressure variation due to the piezo optical coefficient of the plane wave approximation in optical path (L) is represented [97] as;

$$\varphi_u(t) = \frac{2\pi\mu_{op}\delta_p(t)L}{\lambda_L} \quad 3.20$$

As the light beam crosses the sound field in the x-direction in Figure 3.5, the phase change induced will be referred to as the average pressure along the optical path length. Equation 3.20 contains the phase change combined with the pressure along the optical path [97]. This is represented as;

$$\varphi_u(t) = \frac{4\pi\mu}{\lambda}\left(\int_0^L p(x,t)\,dx\right) \quad 3.21$$

Assuming constant pressure in the plane wave, the optical phase change induced in the x- direction is represented [97] as;

$$\varphi_u(x) = \frac{4\pi\mu}{\lambda}\left[\int_0^L p(x,t)\,sin(\omega t + \emptyset_c)\,dx\right] \quad 3.22$$

By letting

$$\varphi_u(x) = \frac{4\pi\mu}{\lambda}\left[\int_0^L p(x)\,dx\right] \quad 3.23$$

It can be stated that

$$\varphi_u(t) = \varphi_u(x)\sin(\omega t + \emptyset_c) \quad 3.24$$

The optical phase change is induced by the pressure variation and plane wave approximation in the optical path. Therefore, the phase change caused by sound pressure in the medium will cause the light intensity upon the photo diode detector to be proportional to the pressure. Accordingly, Equation 3.11 can be modified [97] to

$$I = \frac{I_L[1+cos(\varphi(t)+\varphi_{Ref}-\varphi_0)]}{2} \qquad 3.25$$

According to Equation 3.25, the modulated light intensity corresponding to variations in pressure are detected by the photo detector. This intensity is demodulated by either the velocity decoder or the displacement decoder. The decoded output will be a function of phase variation due to pressure.

3.5 Tomography and Reconstruction

Tomography and reconstruction [96],[99] contribute to recovering the image of the cross section of an object from the projection data. The projections provide a set of measurements of the values of some parameters of the object. The combination of a basic tomography scan and reconstruction algorithms provides the opportunity to create images of pressure from the interference phase data. The ray-integral concept is used as the basis for the reconstruction algorithms.

The application of Fourier slice theorem provides the simplest form of the reconstruction algorithm, which is obtained by parallel beam projections in along a one- dimensional (1D) distribution. The model, as a two-dimensional distribution is typically under investigation, refers to the parallel beam projection in a two-dimensional (2D) function, $f(x,y)$, and represents a cross section of the acoustic field. The integral of $f(x,y)$ presents the a ray in the x-direction to the x-y plane. A parallel projection of optical paths creates a number of ray integrals. The projection of the object $f(x,y)$ has been defined by the line integral [96],[99].

$$P_\theta(t) = \int_{(\theta,t)line} f(x,y)ds \qquad 3.26$$

A projection of $P_\theta(t)$ is performed by a set of parallel ray integrals at the angle θ to the x axis. The projection is described in Equation 3.26 and forms the basis of the Fourier slice theory. The 1D Fourier transform of a parallel projection, $P_\theta(t)$ of the ray integrals, $f(x,y)$ taken at an angle, θ, provides a slice of 2D Fourier transform , $F(H,G)$, subtending an angle, θ, with the H-axis. When the 2D Fourier transform is applied to $F(H,G)$ function, the reconstruction of the (x,y) can be achieved [96],[99], as shown in Figure 3.6 and Equation 3.27.

$$f(x,y) = \int_{-\alpha}^{\alpha}\int_{-\alpha}^{\alpha} F(H,G)e^{j2\pi(Hx+Gy)}dHdG \qquad 3.27$$

However, the projection of the Fourier slice theorem is a finite function that can be variable in practice. $F(H,G)$ is known as a limited number of points along a scanned line. Therefore, the reconstruction of $f(x,y)$ requires an interpolation technique.

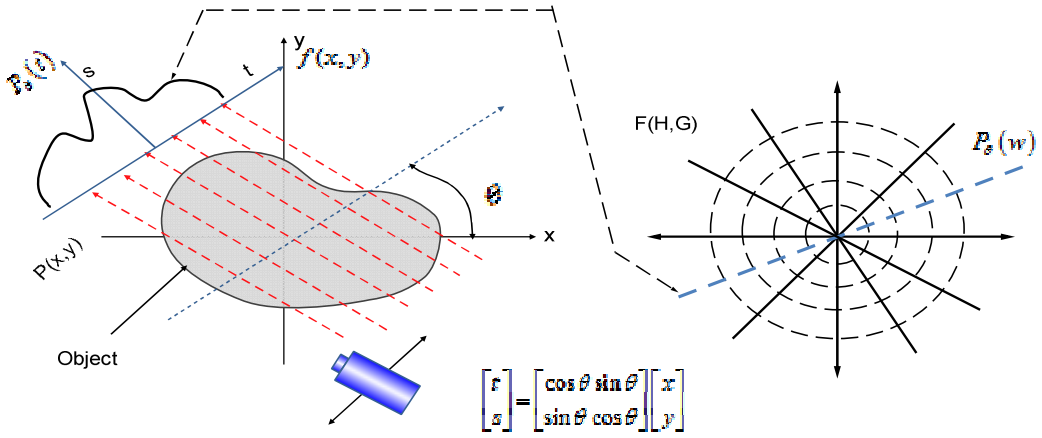

Figure 3.6 A schematic diagram of the transferred function of parallel projection between $f(\mathrm{x},\mathrm{y})$ function and $F(H,G)$ function using Fourier slice theorem.

A filtered back projection algorithm is a combination of the Fourier transform and the weighting of each projection in the frequency domain. The Fourier transform of the projection provides the proper place in the object's location in the two-dimensional domain. The reconstruction of the algorithm can be performed by taking the two-dimensional inverse Fourier transform along the paths. A simple weighting was inserted to visualize the path difference of each projection. The process of the filtered back projection algorithm is composed of two sections: the filtering section and the back projection section.

The filtering section multiplies a simple weighting in the frequency domain to each projection. This is to estimate a pie-shaped wedge of the object's Fourier transform. The simple weighting is used to multiply the Fourier function of *f(x,y)* and can be illustrated [96] as;

$$W = \frac{2\pi|w|}{K} \qquad 3.28$$

Where K= the weighting angles, θ, between 0 and 180^0

The transfer function of the Fourier transform of *f(x,y)* multiplied by the weighting, used in Equation 3.28, can be represented [96] as;

$$f(x,y) = \int_0^{\pi}\left[\int_{-\alpha}^{\alpha} F(w,\theta)|w|e^{j2\pi wt}\,dw\right]d\theta \qquad 3.29$$

Where the $F(w,\theta)$ represents the Fourier transform of *f(x,y)*, and the weighted projection provides the changes in the pie-shaped wedge between 0 and 180^0.

The back-projection section adds the two-dimensional inverse Fourier transform of each weight projection to provide the values of the Fourier transform along a single

path. The estimation of *f(x,y)* from Equation 3.29, given the transformed projection data $s_\theta(w)$, has a simple form and it can be presented as a filtering operation [96];

$$Q_\theta(t) = \int_{-\alpha}^{\alpha} s_\theta(w)|w|e^{j2\pi wt}dw \qquad 3.30$$

Equation 3.30 represents a filtering operation having the frequency response of a filter $|w|$, and it is noted that Equation 3.29 is a filtered projection from different angles. The reconstruction algorithm can provide an image of the object. The final reconstruction picture of *f(x,y)* can be obtained from the integral of *f(x,y)* and can be represented [96] as;

$$f(x,y) = \frac{\pi}{K}\sum_{i=1}^{K} Q_i(x\cos\theta_i + y\sin\theta_i) \qquad 3.31$$

These scanning and reconstruction techniques provide the data which, in turn, provides an image of the optical investigation of the acoustic pressure field. As the phase delay induced between an acoustic wave and the refractive index changes, it is detected by the laser beam measured through the load medium. Importantly, the image of the pressure field can be reconstructed through the parallel projection of light.

3.6 Development of a non-invasive optical measurement system

3.6.1 LDV and Tomographic Scanning Arrangement

In order to use an optical measurement technique and the properties of the acousto optic effect to monitor acoustic cavitation within a reactor vessel, a non-invasive optical measurement approach has been developed. This system has several basic requirements; tomographic scanning and LDV systems which work in cooperation. The former is composed of the laser interferometer instrument and a reflector at the far side of the medium under investigation, in addition to motion control in the

vertical and horizontal axes. The system must also have a sufficient range of motion to investigate the extended field associated with lower frequency (long wavelength) applications, which produce more cavitation. The latter is composed of the cavitation generating system, producing high power ultrasound, and the cavitation measurement system. The measurement system must have a high quality decoder suitable for the wide range of applications. The demodulated signal from the decoder can offer information on cavitation activity produced in the reactor vessel.

3.6.2 Tomographic Scanning Arrangement

The range of the tomographic scanning equipment available for the acousto-optic measurement set-up is as follows [98];

- Polytec OFV-3001: Modular controller with voltage output available from 2 BNC ports
- Polytec OVD-01: 5 range high linear velocity decoder
- Polytec OVD-02: 4 range wide bandwidth velocity decoder
- Polytec OFV-303: High sensitivity sensor head (HeNe laser source)
- Polytec OFV-310: Remote focus module

The OVD-01 and the OVD-02, are card modules that plug into the OFV-3001 Modular controller. The OVD-01 velocity decoder is available in the frequency range of 0Hz to 50kHz and is suitable for vibration measurement on buildings, bridges and low frequency applications. The OVD-01 decoder can be an excellent tool in acoustic and ultrasonic frequency applications. The OVD-02 velocity decoder is suitable for wide bandwidth and high amplitude (velocity 10m/s) operation. Again, this fits with ultrasound frequency measurements. The combination of OVD-01 and

the OVD-02 decoder services a wide bandwidth for decoding velocity of 0Hz-20MHz. For this work, the fundamental frequency of the high power ultrasound is <50kHz and the acoustic emission produced by cavitation is in the range of 1-5MHz. Therefore, this application is suitable for the OVD-01 and the OVD-02 decoder.

A diagram of this system combing LDV and tomography is shown in Figure 3.7. A scan of x-z planes is provided by a Phoenix ISL custom built tomographic scanning frame, with two co-operating motors. These are connected by an RS-232 serial port to a PC and controlled by the NINT controller code. In addition, the reflector beam of the tomographic scanning system operates using the same motor that controls the movement in the vertical position, providing excellent synchronization. The OFV-303 laser head, used as a sensor, was attached to the linear stage to provide a parallel laser beam through the object. The demodulated signal from the OFV-3001 controller is collected by a digital oscilloscope (Tiepie Handy oscilloscope with 50MHz bandwidth) for data acquisition purposes. The scanning system is controlled by a PC, where the data collection and position instructions were written. The sample position is controlled by two Physik Instrument (PI) liner positioning states with a 2mm resolution. This tomograph scanning system is provided to visualize the acoustic field and cavitation distribution. The images from LDV scanning were manipulated by Matlab, where a reconstruction algorithm was written.

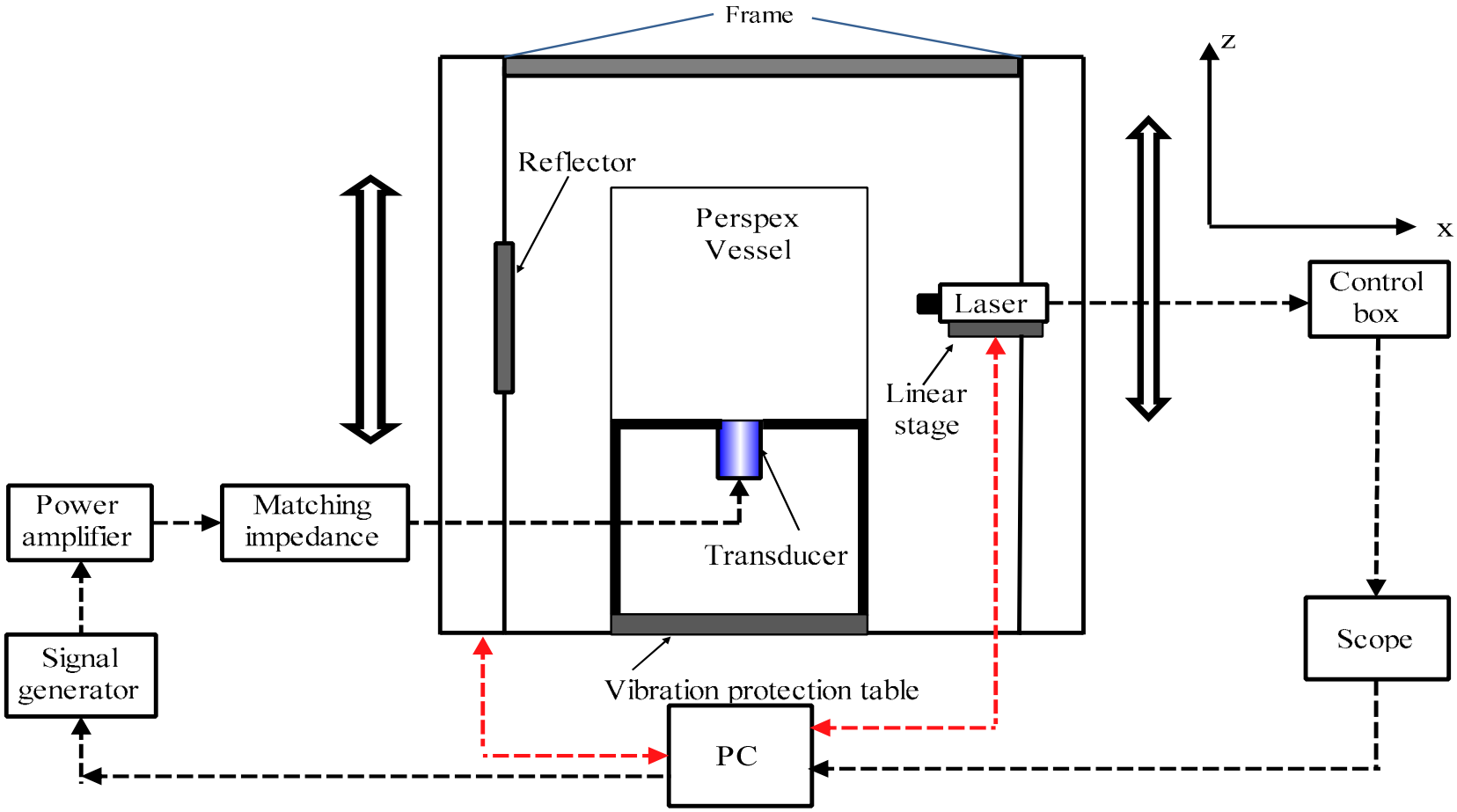

Figure 3.7 Schematic diagram of a non-invasive measurement system combining LDV and tomography techniques.

3.6.3 Tonpilz Transducer

The Tonpilz transducer is a type of low-frequency transducer and can generate high power sound emissions. The typical configuration of a Tonpilz transducer is shown in Figure 3.8. A transducer comprises the piston head, piezoceramic ring stack (pzt) and a tail [96]. These transducers are known as 'mass spring type' transducers, as they are analogous to the movement of a mass on spring. The conventional Tonpilz transducer, as a longitudinal vibrator, has a limited bandwidth to produce high power sound waves. The Tonpilz transducer is widely used in high power applications and is the device used throughout this Thesis. In particular, a 40kHz Tonpilz transducer is chosen as a device in order to generate the acoustic cavitation due to availability within the laboratories at Strathclyde. As illustrated in Figure 3.7, a function generator is used to produce a continuous 40kHz sine wave, which is then passed through an amplifier (50dB) before being used to drive the Tonpilz transducer. To ensure efficient energy transfer, an electrical matching circuit has been used to match the electrical impedance of the power amplifier (50Ω) to the 40kHz transducer electrical impedance (~500Ω). This arrangement is used throughout the Thesis to generate a high power, cavitating field. The Tonpilz transducer is widely used in high power applications and is the device used throughout this Thesis. In particular, a 40kHz Tonpilz transducer is chosen as a device in order to generate the acoustic cavitation due to availability within the laboratories at Strathclyde. It is expected that the device will produce a high power ultrasonic field and acoustic cavitation.

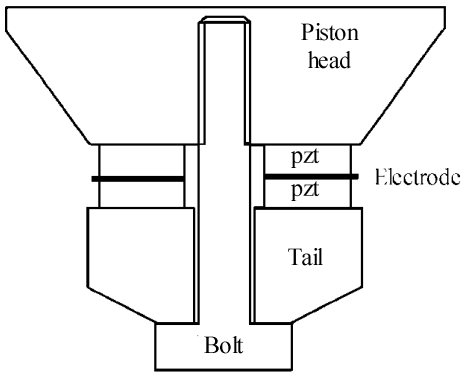

Figure 3.8 Schematic diagram of a Tonpilz transducer.

3.6.4 LDV System Arrangement

The LDV measurement system is non-invasive and the measurement setup is depicted in Figures 3.7 and 3.9. The system features a Polytec OFV-303 Helium-Neon laser used in conjunction with a Polytec OFV-3001 controller and incorporating the OVD-01 and OVD-02 decoders [98]. A Polytec OFV-303 Helium-Neon laser has an average $40\mu m$ spot size and wavelength of $633nm$ ($\lambda = 633nm$) [98]. The red He-Ne laser beam was used as the detector. The OVD-01 and OVD-02 decoders have a wide frequency bandwidth and are used to decode the velocity into an output voltage. The reactor is a Perspex walled vessel which has dimensions of 120x130x150mm and contains 1.4 litres of degassed water. A 40kHz Tonpilz transducer was integrated into the bottom of the vessel, referred to as the "0" position and used as the high power acoustic source. Importantly, vibration isolation was provided through a vibration protection table.

Cavitation is produced by a 40kHz Tonpilz transducer being excited by continuous sine waves at the fundamental operating frequency of 40kHz. The excitation signal was produced by a function generator (Agilent 33120A) and amplified using a wideband RF amplifier (155LCR, Kalmas Engineering), with a gain of 50dB. The 40kHz Tonpilz transducer is excited with input power levels corresponding to 10-

40W. The excitation signal is controlled by the magnitude of the signal generated by the function generator.

Prior to using the laser beam approach as a cavitation detector, it was calibrated using a B&K 8103 hydrophone. During the experimental phase, the cavitation activity occurring within the reactor vessel was measured using the optical laser approach through variations in acoustic pressure. The detected cavitation signals are recorded on a digital oscilloscope and transferred to a PC, where a Matlab program converts the time domain signal into the frequency domain for further analysis.

The tomographic scanning system is used to generate images of peak pressure in a load medium. The combination of tomographic scanning and cavitation measurement systems makes it possible to illustrate the distribution of the acoustic pressure field (in low and high peak pressures) and the cavitation field, in which, high amplitude, or the “hot spot”, is associated with regions of high cavitation while low amplitude, or the “cold spot”, refers to areas of low cavitation activity.

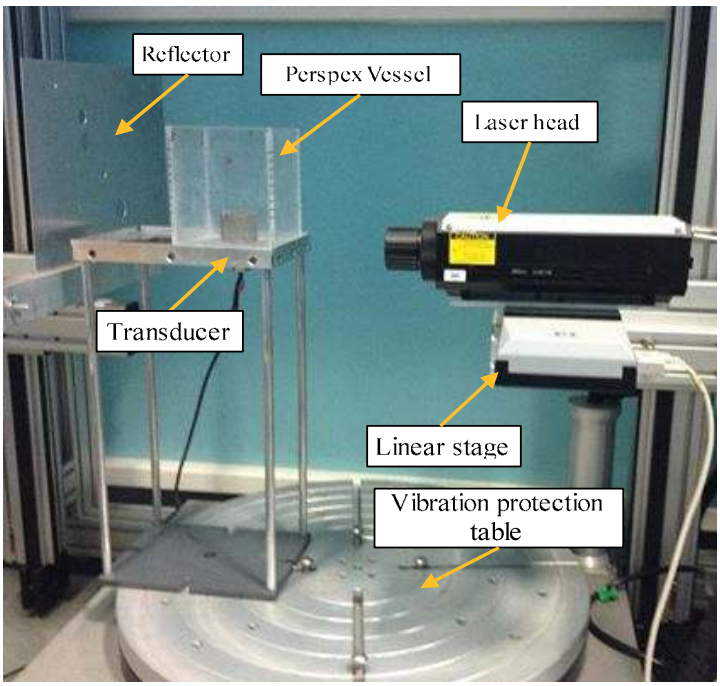

Figure 3.9 Laser Doppler Velocimetry set up: Experimental LDV measurement setup.

The OFV-303 sensor head was attached to the mechanical linear stage to allow laser samples to be taken throughout the volume of the load. The demodulated signal from the OFV-3001 controller is available from a BNC output as a voltage proportional to velocity. A scan of the LDV is conducted in the xz-plane, 80 mm in x-axis, and 70mm in z-axis with 2mm resolution, as provided by a Phoenix ISL linear stage controller.

3.6.5 Broadband Integrated Energy

The broadband integrated energy (BIE) technique has been reported as a means of estimating cavitation activity [9],[10],[22],[100], and is adopted here to evaluate the amount of cavitation activity in this work. BIE uses the energy of broadband noise produced by the collapse of cavitation bubbles. The BIE is calculated by integrating

the high-frequency components of the frequency spectra of the received signal, and is defined as;

$$BIE = \int_{f1}^{f2} v(f)\, v^*(f) df \qquad 3.32$$

Where $v(f)$ represents the frequency magnitude of the acoustic cavitation spectrum signals received by Laser Doppler velocimetry (LDV) which were then converted into the frequency domain. In this work, the frequency range limits used in integration are taken as 1MHz and 5MHz, which relates to the broadband acoustic signal generated by a 40kHz ultrasonic transducer [10].

3.7 Experiment results for cavitation monitoring

3.7.1 Acoustic pressure field

It is well known that the application of high power ultrasound produces cavitation. In order to predict acoustic cavitation activity, an investigation of the phenomenon was conducted by measuring acoustic pressure using a LDV. The experimental set-up is described in Section 3.6.3. The 40kHz Tonpilz transducer placed at the centre of the bottom of the vessel (referred to the "0" position) and produces the high power sound field. As a laser beam crosses the ultrasonic field, sound pressure signals are measured by the laser. Each LDV measurement will be referred to as the average pressure along the optical path length. The demodulated signal from the OFV-3001 controller is available from a BNC output as a voltage proportional to velocity. Figure 3.10 illustrates the spatial distribution of average acoustic pressure from the 40kHz Tonpilz transducer excited with a constant frequency of 40kHz and electrical power of 30W, as detected by the LDV. The LDV scans the xz-plane, 80mm in x-axis and 70mm in z-axis, which is parallel to the Perspex wall of the vessel. The LDV is calibrated by the B &K 8103 hydrophone using the substitution method [101] to provide measurements of acoustic pressure. Both the B &K 8103 hydrophone and the LDV are placed at the same position in the far-field of the transducer.

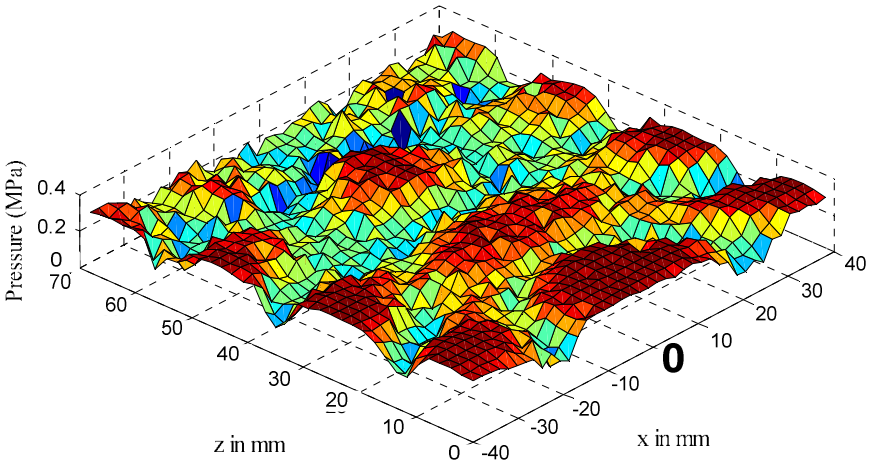

Figure 3.10 Distribution of the acoustic peak pressure detected by LDV. A 40kHz ultrasonic transducer is excited with a frequency of 40kHz and input power level of 30W.

From monitoring cavitation activity by pressure detection, it is assumed that the cavitation is produced at the points where the acoustic pressure is maximised. The cavitation obtained by this approach is poor in accuracy because it is difficult to identify the sound pressure and the cavitation, and even more difficult to evaluate its activity. Nevertheless, this method can reveal cavitation locations, assumed to be the higher peaks of pressure and can be used to monitor acoustic cavitation, as documented by Leighton [102].

3.7.2 Acoustic emission signal

Acoustic emission has been introduced as a measure of monitoring cavitation. The cavitation process may produce a range of emission frequencies, as well as the emission signal as the bubble explodes [9],[22],[65]. The acoustic emission signal can be detected by the sensors as well as the LDV approach. Figure 3.11 illustrates the typical characteristics of the acoustic spectrum signal acquired through the non-

invasive optical measurement system shown in Figure 3.8. Here, the laser beam interrogates cavitation in the parallel plane 10mm away from the transducer surface using the measured acoustic emission spectrum. The acoustic spectrum below 0.5MHz is shown in Figure 3.11 and clearly illustrates a range of acoustic components;

- The fundamental frequency component, f_0 at 40kHz; this is produced by the direct driving field, and possibly makes future contributions to the linear oscillation of bubbles.
- Harmonics of the fundamental frequency component, nf_0 at the 80kHz and 120kHz and so on; this can be produced by itself due to the harmonic signal in the electronic drive waveform, and perhaps, nonlinear propagation occurring in the medium
- Sub-harmonics of the fundamental frequency, f_0/n where n is an integer at 20kHz, the sub harmonic signal can be clearly seen at $f_0/2$. This can occur when a bubble is excited to twice the maximum radius before the bubble collapses [103].
- Ultra-harmonics of the fundamental frequency; there are signals located in a high frequency range, mf_0/p where m and p are integers and m greater than p, this produces odd integers and multiples thereof. The signals will be indicated at 60kHz, 100kHz and so on. This is produced in a similar process to that which produces sub-harmonics.
- Broadband signal at the range of 1-5MHz from a sound source of 40kHz [9]; this is the noise of all frequencies and it is believed to be generated by the shock wave emitted by bubble explosion and by collapsing bubbles of many sizes.

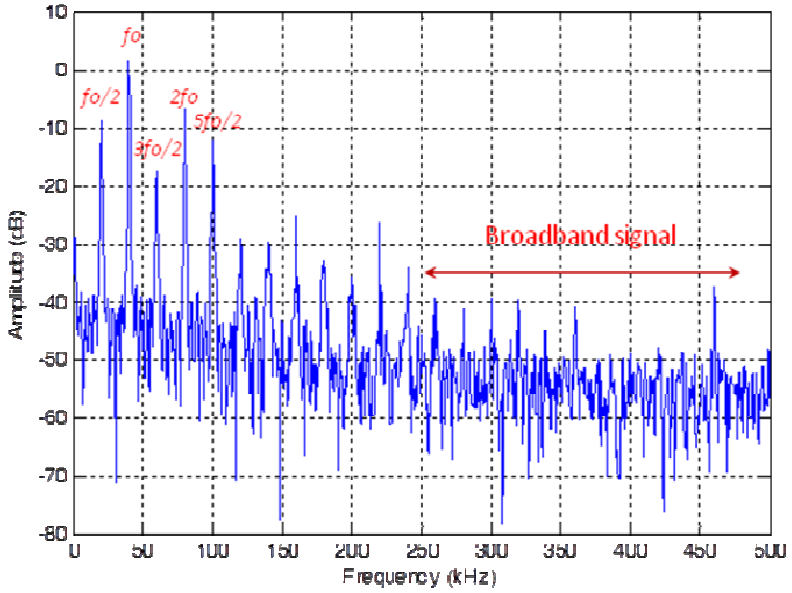

Figure 3.11 Acoustic spectra detected by LDV up to 0.5MHz. The ultrasonic transducer is excited with frequency of 40kHz and input power level of 30W. The spectrum also shows acoustic components: sub- and ultra-harmonic and broadband signal in high frequency.

All of these components can be used to provide information on the cavitation process occurring. The principle features of the spectra produced have been modelled extensively and rely upon sufficient knowledge of the behaviour of the bubbles within a cavitation region. It is suggested by Neppiras that broadband signal can be used to monitor cavitation activity [104]. These have been considered as appropriate for an investigation into analyzing cavitation activity [9],[22],[100].

It is well known that cavitation is a secondary source of sound producing high frequency acoustic emission from the bubble collapse process and the ultrasonic source generating sound waves in the kHz frequency range would produce broadband signals well into the MHz region [9]. LDV investigation is able to detect acoustic spectrum signals up to 10MHz. Figure 3.12 shows the acoustic spectrum measured by LDV and the NPL cavitation sensor. The ultrasonic source is excited by

the frequency of 40kHz and input power of 30W. The dB-offset reference on oscilloscope is set at 50 dB.

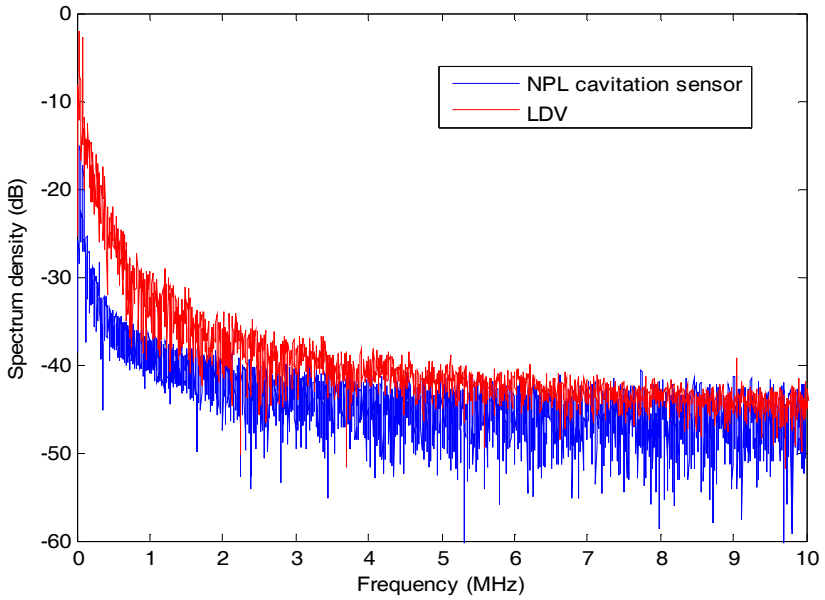

Figure 3.12 The acoustic spectrum of 0-10MHz measured by the NPL cavitation sensor and LVD at the driving power level of 30W. The acoustic spectrum was generated using a 40kHz excitation.

The laser beam and the NPL cavitation sensor, developed by the National Physical Laboratory, were again positioned 10mm away (to the bottom of the NPL sensor) from the transducer surface to monitor the acoustic spectrum signals. The signals detected follow reasonably similar trends, as illustrated in Figure 3.12, but the amplitude of the acoustic spectrum signal detected by LDV is higher than that detected by the NPL cavitation sensor due to the high sensitivity of LDV. These signals within the band of 10MHz contain all of the acoustic components as shown in Figure 3.11, but resolution of the displayed data is lower. Nevertheless, it is possible for these signals to be used to monitor cavitation in the ranges of the 1-5MHz.

The acoustic spectrum, derived from a number of drive settings of a reactor, covering the range of 10 to 40W (electrical input power) was acquired. The high frequency spectra for different input power levels obtained using LDV are shown in Figure 3.13. The laser beam was again positioned 10mm away from the transducer surface to monitor the relationship of input power and acoustic spectrum signals. The dB-offset reference on the oscilloscope is set at 50dB. In Figure 3.13, only four drive levels of 10, 20, 30 and 40W and the background noise of the system (0W) are shown. These results indicate that changing the acoustic pressure of the fluid medium due to the input power levels inside the reactor will change the intensity of cavitation activity produced. The detected acoustic emission signals rely on occurrence of sound pressure and cavitation. The acoustic emission signal for 30W power level in Figure 3.13 is higher than that of 40W due to local variation cavitation field dynamics. Therefore, it is considered that using this relationship will enable the laser measurements to be used to qualify, not quantify, the intensity of acoustic cavitation activity within the reactor.

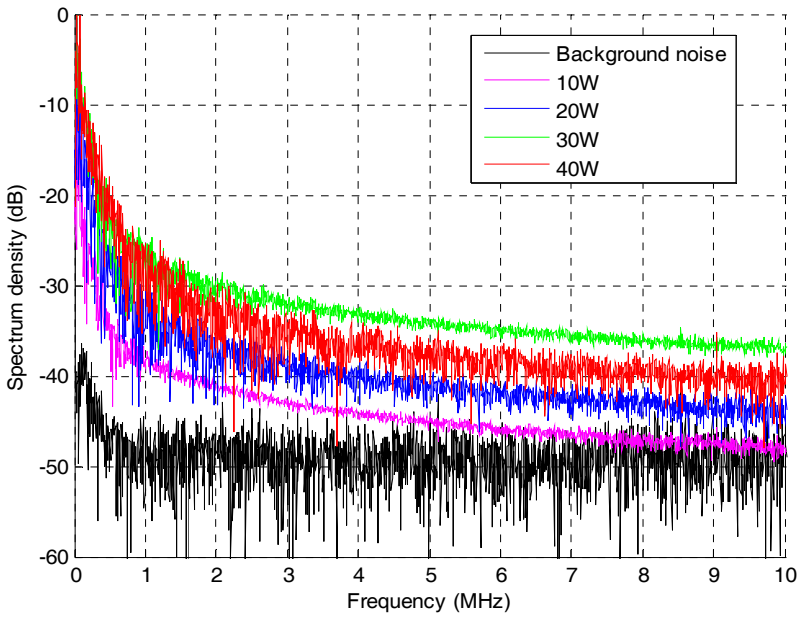

Figure 3.13 The acoustic spectrum characteristics acquired by LDV within the band of 10MHz for different power input power levels of 10, 20, 30 and 40W, generated using a 40kHz excitation.

3.7.3 Cavitation activity

It is considered that measuring cavitation using acoustic emission and BIE calculations is more accurate than detecting sound pressure. Cavitation activity is analyzed by using the BIE relationship, described in Equation 3.32, and calculated from the high-frequency components in the spectrum. Each LDV measurement, at power levels between 0-40W, characterizes a single parameter value from the acoustic spectrum across the frequency range between 1MHz and 5MHz. Hence, the relationship between input power and cavitation activity in degassed water was measured. The measurement was repeated three-times. The normalised BIE and the variation of measurements obtained through the standard deviations of the three measurements are shown. The result for a single point in the central axis of the transducer located at 1, 5, 10, 15 and 20mm from the front face is shown in Figure 3.14. When the input power was increased, BIE clearly indicates the intensity of cavitation activity due to a change of input power. It was noted that the BIE for all measurements increases with input power levels. The BIE increases higher with the input power of 20W at a distance of 1mm and for 30W at 5, 10, 15 and 20mm locations.

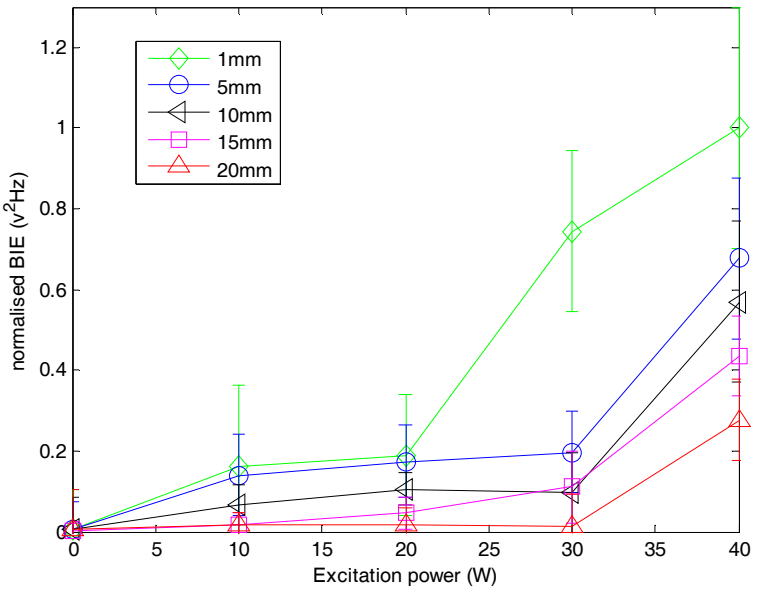

Figure 3.14 Empirical relationships of the BIE and the input power produced by the 40kHz transducer. The BIE is calculated in the frequency range of 1-5MHz. The deviation of measurements is illustrated.

At each measurement position, the required power was varied between 10-40W. This is to monitor cavitation at different distances in the central axis of the transducer surface along sound field at the position 0-70mm as shown in Figure 3.15. The graph illustrates that high cavitation is produced at distances close to the source and decreases when moved further away from the source. This suggests that there is a relatively high cavitation cloud close to the source, which might be considered as the main source of the broadband emissions. Furthermore, Figure 3.15 illustrates the relative positions of low and high cavitation activity. The BIE of 30W and 40W is generally higher than that of 20W, although the BIE for 20W is slightly higher that of 30W between 40-50mm. It is difficult to fully explain this result, but it is hypothesized that the non-linear behavior of the cavitation will produce local variations in the dynamics of the field, can result in localized spikes in the acoustic emission spectra.

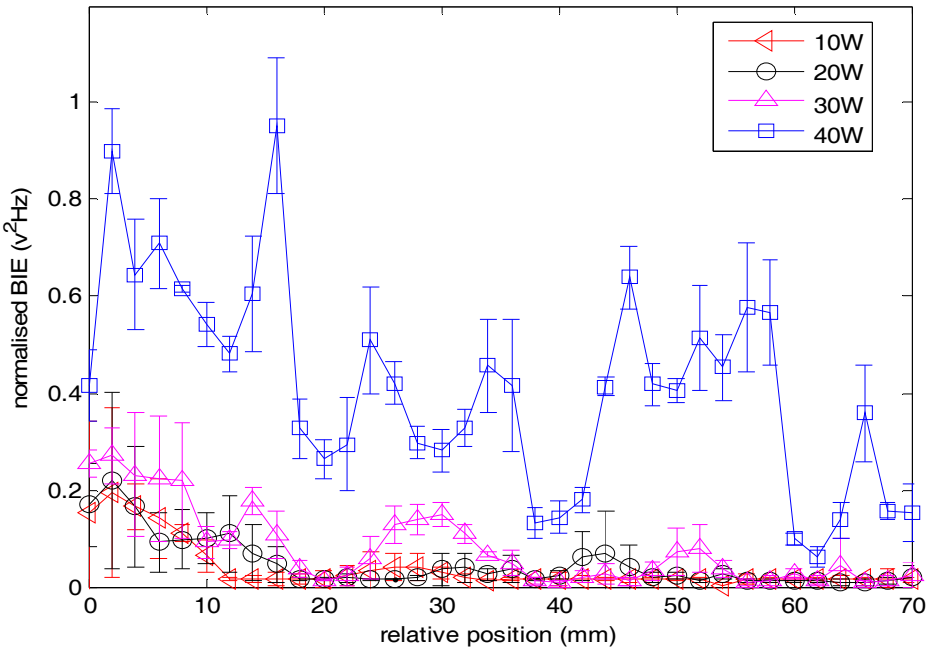

Figure 3.15 The variation of the BIE as a function of vertical position in the central axis of the transducer surface along sound field at the position 0-70mm.

3.7.4 Distribution of cavitation activity

The spatial distribution of sound pressure was measured at the excitation frequency and presented in Figure 3.10. However, it is difficult to classify regions of cavitation using this method. It is well known that cavitation is a secondary sound source whose emission spectrum contains a substantial amount of information relating to the cavitation process. It was considered appropriate to investigate the extent of the emission spectrum to identify regions in the load where cavitation could be occurring. Here, the use of BIE has been selected and calculated for different frequency ranges. Hence, a scan of the LVD in the xz-plane can provide the spatial distribution of the cavitation field, which can be plotted at different frequency bands. The cavitation regions within the vessel can then be illustrated by identifying 'hot spot' and 'cold spot' locations.

Figure 3.16 shows the two-dimensional distribution of selected parameters in a scanning plane parallel to the Perspex wall of the vessel (xz-plane). For this experiment, the input power level was 20W. Each pixel in these images corresponds to the BIE (for different frequency regimes) at a single position in the xz-plane. The four images correspond to the spatial distribution of these frequency regimes: sub-harmonic, ultra-harmonic, fundamental and high frequency The BIE is considered in frequency ranges of 19-21kHz for sub-harmonics, 39-41kHz for fundamental frequency, 59-61kHz for ultra-harmonics and 1-5MHz for cavitation. A different scale is used to illustrate the spatial distribution of each frequency regime. These BIE results are indicative of the acoustic field distribution in the reactor vessel. The correlation between the magnitude of the fundamental frequency component estimated in the acoustic spectra of the acoustic pressure and cavitation is shown in the right hand column of Figure 3.16. There is a reasonable correlation between these field distributions, although the magnitudes are quite different. Cavitation is highest close to the transducer surface and decreases with distance. As a result, the cavitation refers to broadband noise signals produced in a high frequency of the acoustic spectrum. Investigating the cavitation behaviour through the acoustic spectrum components can provide understanding of the effects of each acoustic component of cavitation. The spatial distribution measurements were repeated three times and the results follow a similar trend.

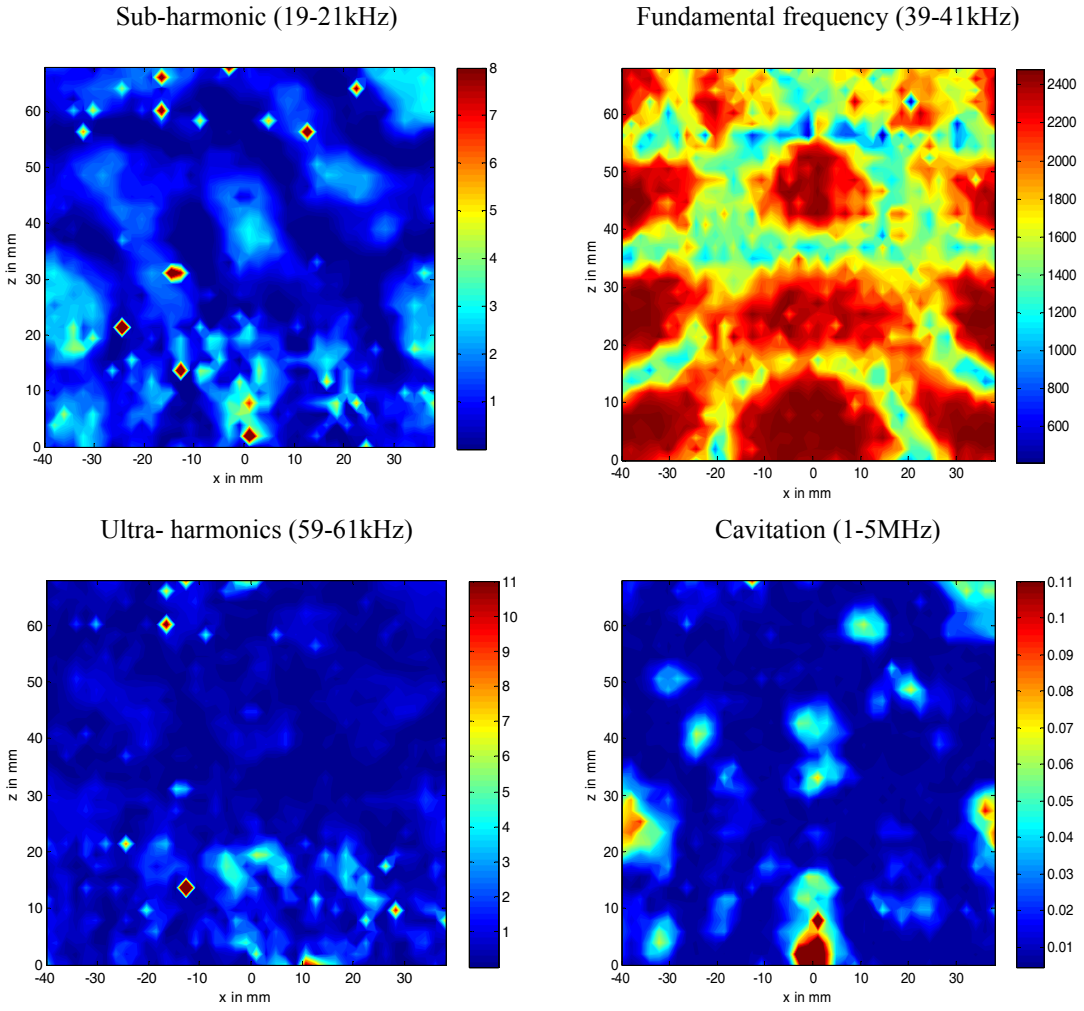

Figure 3.16 The relationship of acoustic parameters in each component of the acoustic spectrum of 40kHz. The figure shows the spatial distribution of components within reactor vessel.

LDV can provide the spatial distribution of sound pressure in high spatial resolution, as shown in Figure 3.16, and can be used to monitor the spatial distribution of cavitation activity within the vessel. Next, by focussing on the AE between 1-5MHz, four further images are presented in Figure 3.17 and correspond to the spatial distribution of cavitation. These results are indicative of the cavitation distribution within the reactor vessel at the input powers of 10, 20, 30 and 40W. The results

indicate that the number of hotspot locations increases with increased power levels. The cavitation distribution measurements were repeated three times. The results follow a similar trend and the 'hot-spot' locations are slightly different due to the variation of cavitation occurrence. This provides knowledge of cavitation initiation and cavitation locations and may be beneficial to ultrasound industry applications such as sonochemistry or cleaning processes. It is interesting to compare the cavitation fields in Figure 3.16 (Cavitation 1-5MHz) and 3.17 (20W 1-5MHz) as they are measurements from the same experimental conditions. Although, they are not identical there are indications of high intensity cavitational fields in both figures at similar locations, albeit with different intensities. Hence, it can be concluded that the field mapping is repeatable in terms of location, but varies in terms of intensity.

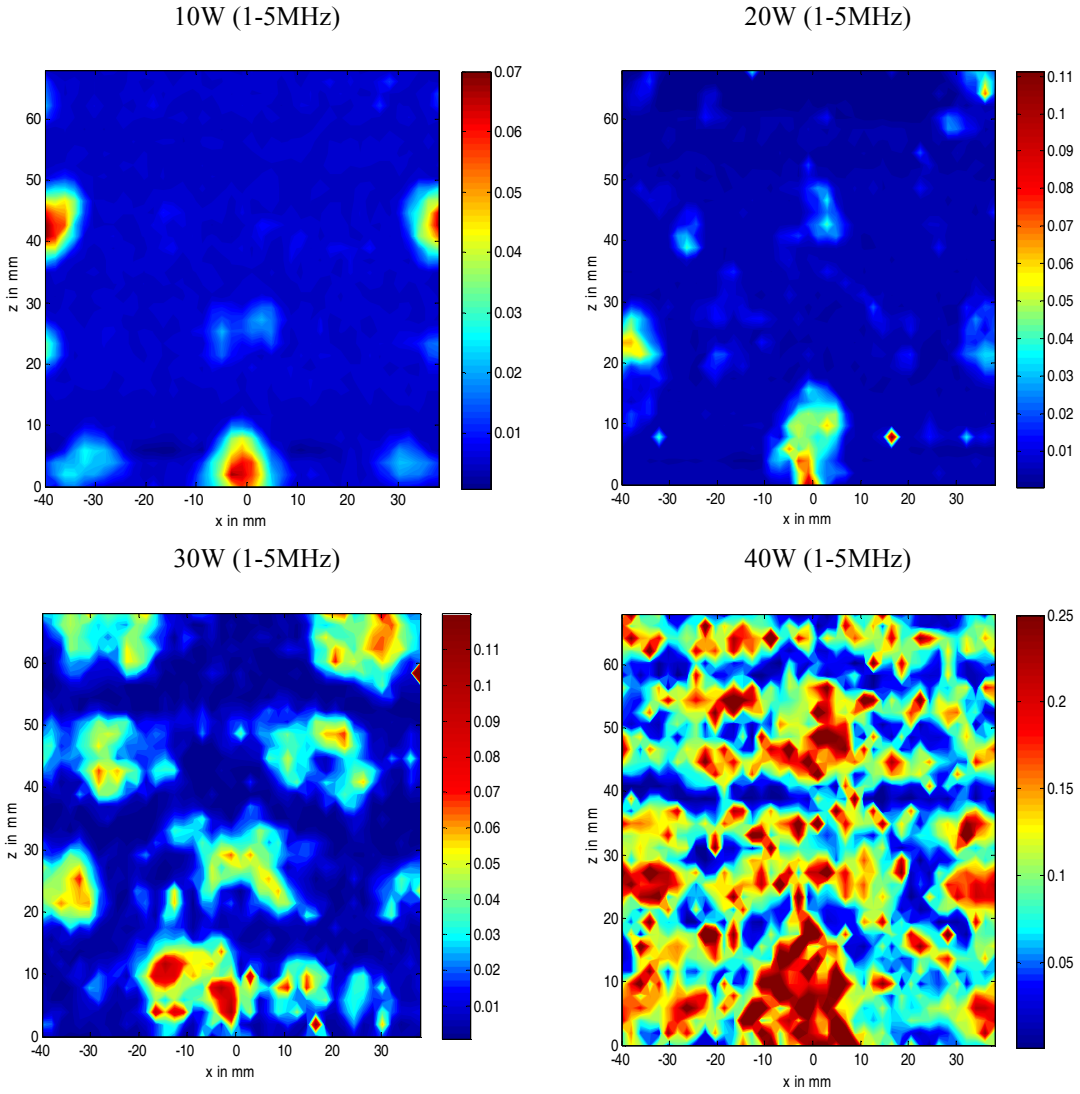

Figure 3.17 The distribution of BIE in two-dimensions calculated by broadband noise in the frequency range of 1-5MHz at 40kHz at the power inputs of 10-40W.

The measured results in Figure 3.16 and Figure 3.17 clearly illustrate 'hot-spots' and 'cold-spots' associated with the high and low regions of cavitation. Therefore, LDV is an effective technique for the identification of an acoustic cavitation field within the reactor vessel. For each position in the xz-plane, the cavitation activity (BIE in the frequency range of 1-5MHz) has been calculated and the distribution is shown in Figure 3.16 (in the right hand column) and Figure 3.17. Here, the colour shading

indicates higher cavitation activity and this can be seen to be concentrated directly in front of the device.

3.8 Foil erosion analysis

A conventional aluminium foil erosion test was used to indicate regions of cavitation. Thin aluminium foil (a thickness less than 0.2 millimeters), 120mm wide and 120mm long, were positioned in the vessel at distances of 5, 10, 15 and 20mm from the 40kHz transducer surface. The transducer located in the bottom of the vessel is referred to as the "0" position. During the experimental phase, the 40kHz Tonpilz transducer is excited with power levels of 40W to produce the cavitation. An aluminium foil is placed in high power ultrasound fields for 20 minutes, after which the aluminium foil was removed from the reactor vessel. High resolution images of these aluminium foil sheets were obtained and the images were manipulated in Matlab to quantify the aluminium foil damage through image processing. The experiment indicates a localized pattern of erosion on the aluminium foil and using these results, the regions of degradation on the aluminium foils can be used to map the distribution of the acoustic field and therefore, the cavitation activity.

The cavitation activity was also monitored through the observation of aluminium foil erosion which was accomplished under the conditions of 40kHz and 40W. The cavitation regions measured by LDV correlated with the aluminium foil erosion tests. The cavitation distribution of BIE, obtained by LDV, is shown in Figure 3.18. The damage to the aluminium foil at 5, 10, 15 and 20mm positions is shown in Figure 3.19. The aluminium foil sustains significant damage at 5mm, but this decreases as the position moves away from the transducer. To quantify the agreement between the LDV in Figure 3.18 and the aluminium results, the foil results have been processed to provide an integrated figure of merit associated with the erosion quantity in the same plane (at 5mm from transducer surface) as the LDV results. The LDV results and the aluminium results were manipulated by Matlab. These are presented in

Figure 3.20 and good correlation directly in front of the transducer can be seen. It is noted that LDV and the aluminium foil erosion test can indicate cavitation occurring in a similar region.

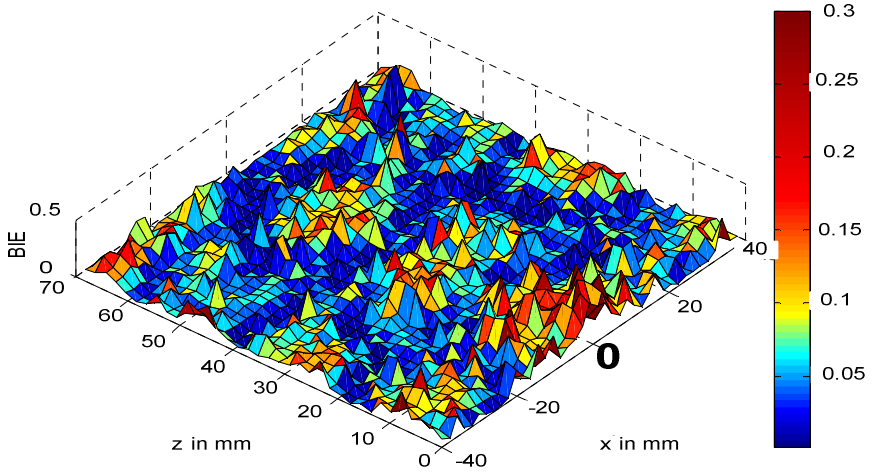

Figure 3.18 The distribution of BIE in three-dimensions calculated by broadband noise in the frequency range of 1-5MHz at 40kHz and 40W input power.

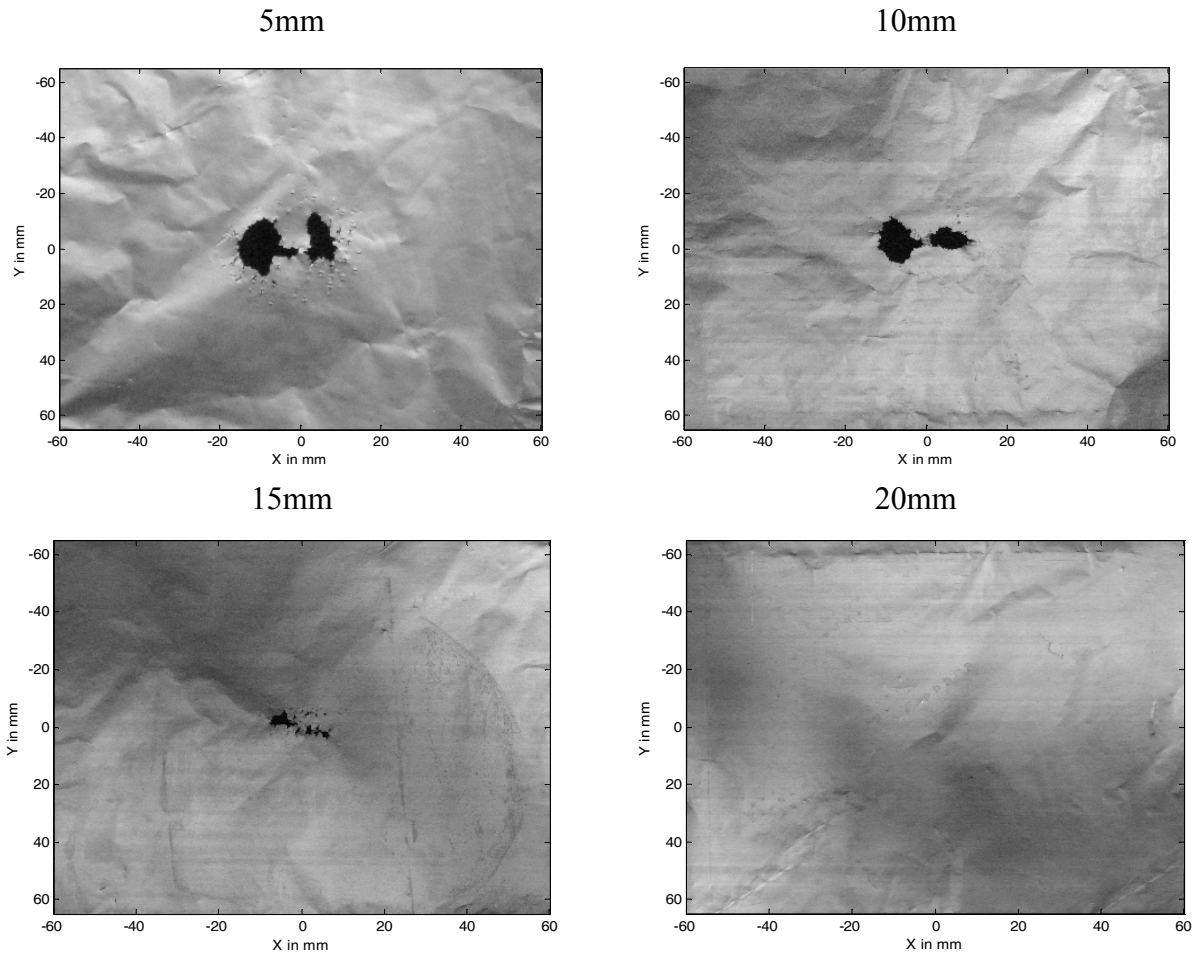

Figure 3.19 The damage to thin aluminium foil when positioned at 5, 10, 15 and 20 mm from surface of 40kHz Tonpilz device, generating the frequency of 40kHz and 40W.

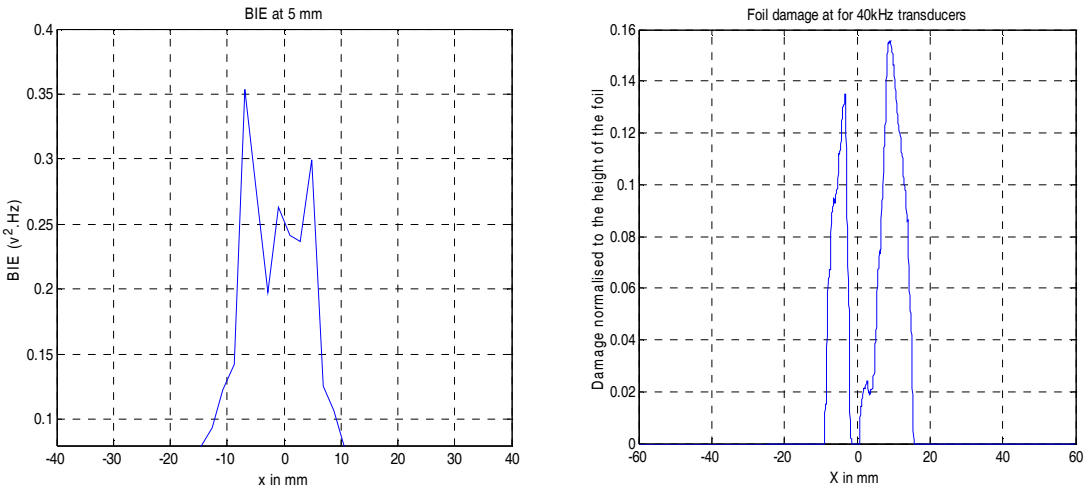

Figure 3.20 The correlation of BIE acquired by LDV approach (left) and the damage to thin aluminium foil (right) when positioned at 5mm from the 40kHz transducer surface. A 40kHz transducer operates at 40kHz and 40W.

3.9 Linearity of cavitation activity

The monitoring of the acoustic cavitation generated by the 40kHz Tonpilz transducer is presented in Section 3.6.1. This Section describes an investigation of acoustic cavitation activity produced by a series of transducers within the Perspex reactor vessel. The cavitation is produced by a series of four 40kHz Tonpilz transducers. The experiment set-up is similar to the LDV measurement system in Section 3.6.3.

The measurement system contains a Polytec OFV-303 Helium-Neon laser used in conjunction with a Polytec OFV-3001 controller incorporating the combination of the OVD-01 and OVD-02 decoders. The laser beam of the OFV-303 laser head was used as the detector. The OVD-01 and OVD-02 decoders were set at the velocity range (125mm/s/V) to decode the velocity into output voltage. The reactor is a Perspex walled vessel which has dimensions of 120x180x150mm and contains 2.8 litres of degassed water. The series of four 40kHz transducers were integrated into the bottom of the vessel and used as the high power acoustic source. Importantly,

vibration isolation was provided through a vibration protection table. The schematic measurement system setup is shown in Figure 3.21.

Cavitation is produced by a series of four ultrasonic transducers excited by continuous sine waves at a frequency of 40kHz. The excitation signal was produced by a system composed of 12 high power supply units (comprised of an FPGA controlling unit and 12 high power output units) [105]. The ultrasonic transducers were excited with voltage input levels of 0-80V.

For this investigation, the laser beam was located 10mm away from the transducer surface. The cavitation signal was measured using the optical laser. The demodulated signal from the OFV-3001 controller is collected and recorded by digital oscilloscope. The measured signal is transferred to a PC to calculate the BIE (or cavitation activity). During the experimental process, the number of the ultrasonic transducers excited was varied. These represent the occurrence of cavitation caused by the series of transducers.

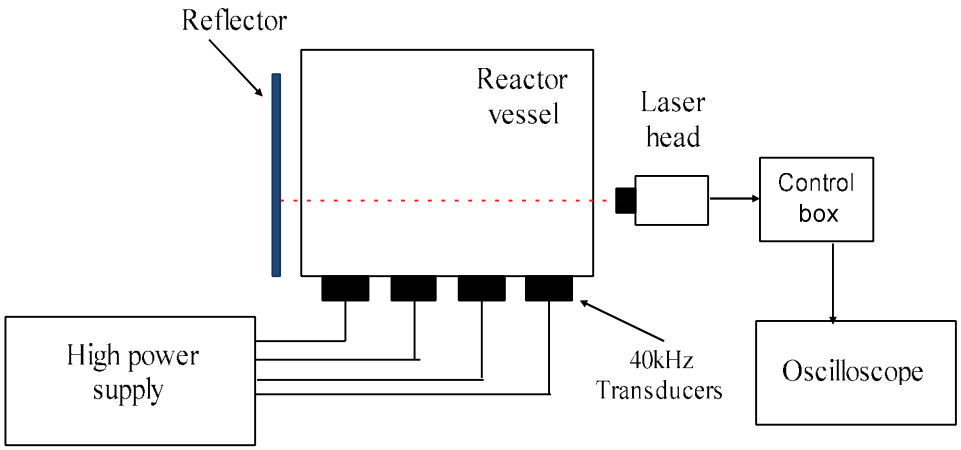

Figure 3.21 Schematic diagram of a series of four 40kHz transducer measurement system.

Cavitation is present in different regions of the reactor vessel, primarily directly in front of each transducer, and the laser beam is used to measure the acoustic emission signal at different times. The normalised BIE and the variation of measurements obtained by the standard deviations of the measurements are shown in Figure 3.22 for excitation of transducers 1, 2, 3, and 4. It is evident that cavitation increases with the excitation input level and each trace follows a reasonably similar trend. Figure 3.23 presents the cavitation activity at each input voltage level with various numbers of driving transducers, in which each individual result has been normalised. It is noted that BIE increases with the number of driving transducers. Although, it may be considered that as the number of operational transducers increases that the scattering of light passing through the extended cavitational field would increase and ultimately, result in no light being detected by the LDV. It should be noted that the LDV only requires 2% of the emitted light to be returned to determine the phase path difference and hence, this system is relatively robust to highly scattering media [96].

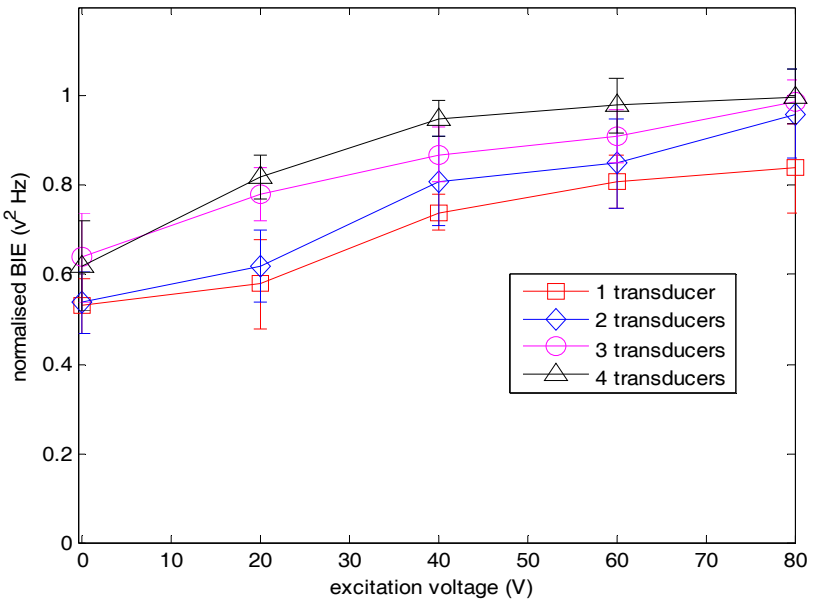

Figure 3.22 Variation in normalised BIE derived using LDV determined over the excitation voltage range of 0-80V. A single transducer and a series of four 40kHz Tonpilz transducers are used to generate the cavitation. The LDV is positioned 10mm from 40kHz Tonpilz transducers surface to measure acoustic emission signal.

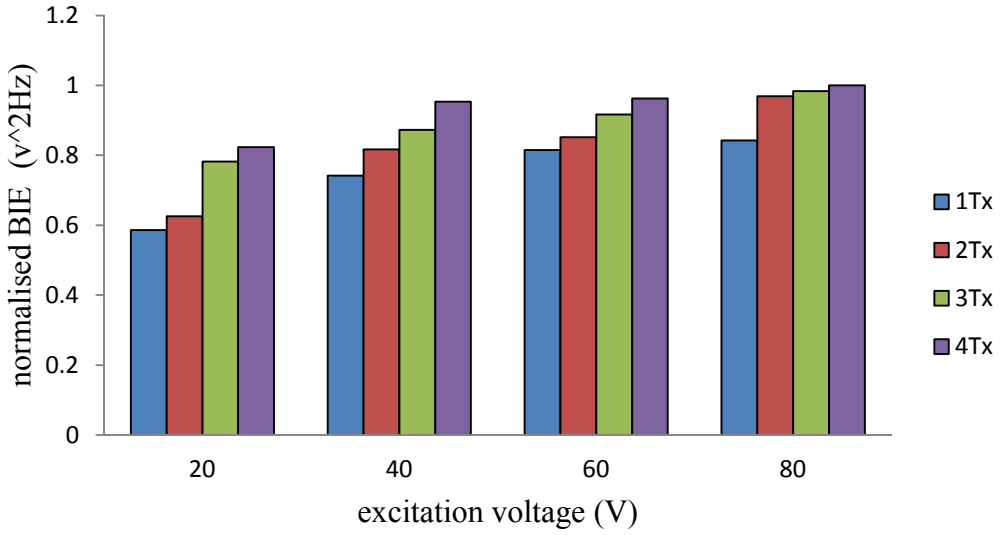

Figure 3.23 The relationship between the normalised BIE and excitation voltage of 20-80V acquired from the series of four 40kHz Tonpilz devices. The laser beam is positioned 10mm away from 40kHz Tonpilz transducer surface to detect the acoustic emission signal.

3.10 Limitations of the measurement system

There are some inherent limitations associated with using LDV for monitoring cavitation. Generally, LDV is designed to measure the acoustic sound pressure and the OVD-30 decoder provides an output in terms of voltage. However, monitoring cavitation requires an acoustic spectrum signal output in the frequency domain. Thus, the output data is collected in the time domain before being converted to the frequency domain.

Importantly, the LDV probe may sometimes detect a false signal i.e. a transient signal generating itself. The false signal provides a higher spatial distribution of cavitation (only one point) than other areas. The LDV system also requires a transparent medium and vessel i.e. glass or Perspex. Additionally, it is important to note that the probe and other measurement techniques may also struggle to operate in

regions close to the cell walls due to sensor manipulation difficulties, but it is not a major limitation of this system.

The development of the optical technique is challenging due to the complexity of the necessary equipment and sensitivity of the laser within an industrial environment because of factors such as vibration, noise in the system, and the size of the system. Installation is complex, the scanned areas within the vessel are limited by scanning devices and the measurement is not achieved in real-time. Additionally, the LDV may struggle to detect the high-amplitude signals due to the transient nature of cavitation.

3.11 Summary

This Chapter has described the development of a non-invasive optical measurement system using Laser Doppler Velocimetry (LDV) as a probe to monitor acoustic cavitation within a Perspex reactor vessel. The measurement approach is based on the acoustic emission technique by monitoring broadband acoustic signals caused by cavitation. Extensive experimental investigations of cavitation through the acoustic spectrum, with the broadband acoustic signal and the broadband integrated energy (BIE) approach, have been completed for a 40kHz Tonpilz device. The broadband acoustic signal is generated by the oscillation and the collapse of bubbles undergoing acoustic cavitation. The BIE in frequency ranges of 1MHz to 5MHz has been calculated to quantify the amount of acoustic cavitation activity present in a reactor. A scan of the LDV illustrates the spatial distribution associated with high and low cavitation regions within the reactor vessel. These results have been confirmed by the degradation of thin aluminium foil. Furthermore, the LDV is used to monitor acoustic cavitation within the vessel, using a series of four 40kHz Tonpilz transducers to generate cavitation. The non-invasive optical measurement system using Laser Doppler Velocimetry has the potential to indentify the presence of

cavitation and the measurement system is ideally suited to single-point measurements, where the onset (location) of cavitation is known.

CHAPTER 4

Modelling the effects of the reactor vessel

4.1 Introduction

Cavitation is induced by the application of high power ultrasound in a liquid medium. A measurement of the output levels of high power ultrasound and cavitation activity can be taken by inserting a transducer sensor directly into the high pressure fields. However, this may cause damage to the device. In order to avoid damage to the transducer, a non-invasive optical measurement technique, using Laser Doppler Vibrometer (LDV) to monitor acoustic cavitation, was implemented, as described in Chapter 3. However, there are some inherent limitations with using LDV for monitoring cavitation such as the required transparent vessel and medium, the size of the system and the complexity of the installation. Hence, the development of an ultrasonic transducer probe for the non-invasive measurement of cavitation would be more convenient for deployment.

It is necessary to produce an ultrasonic transducer that is appropriate for monitoring acoustic cavitation. The design process of a transducer requires a simulation software tool capable of analyzing the design of a bespoke transducer and the suitability of the transducer design specifications for a particular application. Finite element (FE) analysis is a powerful tool in the research and design of ultrasonic devices and systems for disciplines such as non-destructive testing, SONAR and biomedical applications [106]. The FE technique has the ability to simulate full ultrasonic systems, including wave propagation and interaction with complex shaped structures. FE analysis, employing the PZFlex code [106], enables the development of a comprehensive model of both the active device and its surroundings, providing the functionality to model a variety of cell structures and transmission loads, in conjunction with a selection of high power transducer technologies.

This Chapter will describe the development of an FE model which will be used to investigate the wave propagation from the acoustic emission (AE) of the broadband acoustic waves associated with the signal of acoustic cavitation interacting with the wall of the reactor. Modelling the sound wave propagation with the use of the wall of the reactor vessel leads to the understanding of the frequency range required for a non-invasive monitoring system. The FE analysis code PZFlex enables the development of a comprehensive model of the reactor vessel with a variety of wall materials, sound sources and transmission loads. The sound source associated with a cavitation field is comprised of high acoustic pressure and broadband frequency ranges. In particular, the acoustic emission signal is in the high frequency range and can be simulated using the functionality of a linear chirp signal. The modelling results will provide the basis of the transducer design specification for the development of a non-invasive measurement system with which to monitor acoustic cavitation.

4.2 Modelling of the reactor vessel

In order to study the interactions of mechanical structures, FE modelling is preferred due to the complexity of the physical system. The method of FE analysis is a numerical process and has been used for solving the complex problems encountered in a variety of applications. The finite element package used in this work is PZFlex, developed by Weidlinger Associates [107]. The code has been applied to a wide range of problems including geotechnical, seismic wave propagation [108], transient wave propagation in elastic wave guides [109],[110] and ballistic structure interaction [111]. The finite element software is capable of modelling nonlinear systems such as nonlinear propagation [112] caused by higher power applications, although for this Thesis, the modelling in undertaken in the linear domain [112]. PZFlex is tailored for piezoelectric, ultrasonic and bioengineering wave propagation problems.

The FE model can be used in simulation of high ultrasonic pressure [113],[114]. In this work, the simulation model based on PZFlex code remains too idealized for application to more complicated problems involving the generation of high power ultrasonic field associated with cavitation events in the reactor vessel. The concept used here is similar to acoustic emission and analogous to process monitoring, as seen in references [115],[116],[117]. All aspects of the modelling reactor vessel process are required to predict the AE signal in the vessel. A number of important modelling results will be presented which will be used to establish a bespoke transducer design to be employed for detecting cavitation.

4.2.1 A linear chirp signal

It is reported that cavitation is a sound source over the frequency range of 1-10MHz [9]. It is difficult to generate cavitation through the imploding bubbles in the PZFlex environment. Therefore, the simulation will model a sound source similar to a source of cavitation and a linear chirp signal, composed of broadband frequencies, is used to generate this source of cavitation. A linear chirp signal is a sinusoid in which the frequency increases or decreases linearly with time over a defined time window [118].

In This work, a 40 Tonpilz transducer will be used to generate a high power ultrasonic field. Hodnett *el al.* [10] have calculated the BIE over the frequency range of 1-5MHz for operation at 40kHz. Hence, for the modelling of the transmission source, excitation of the model is achieved by using acoustic pressure loading, using a linear chirp with a frequency range of 1-7MHz, as this contains the required frequency range to be used to calculate the BIE for this work. Figure 4.1 illustrates a linear chirp signal in the time and frequency domain generated at the frequency range of 1-7MHz. The sound pressure excitation is simply adjusted by applying the pressure amplitude.

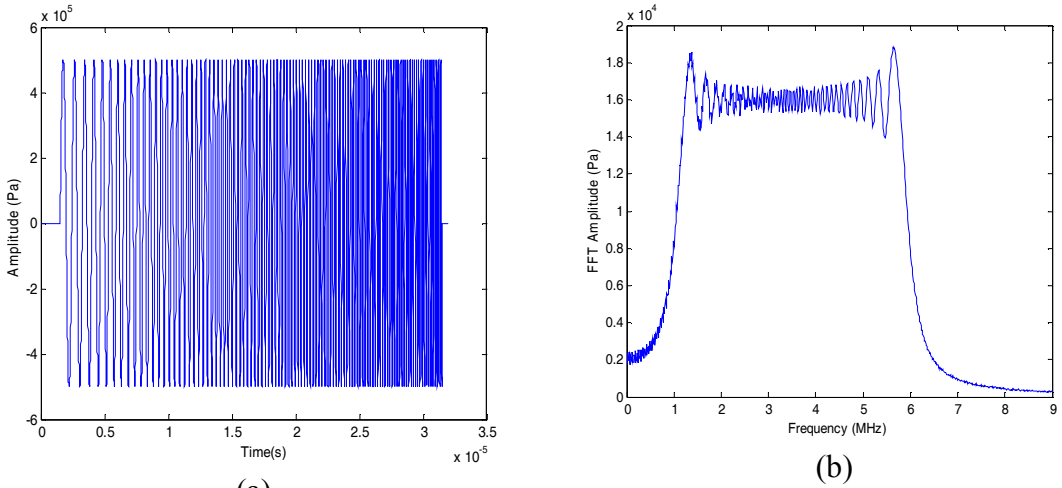

(a) (b)

Figure 4.1 A linear chirp signal (a) time-domain (b) frequency-domain.

4.2.2 Simulation model

A numerical method, such as FE modelling, is preferred when studying cavitation events within a reactor vessel. Figure 4.2 shows the two dimensional (2D) representation of a reactor vessel system. The dimensions of the reactor vessel used in the model are presented in Figure 4.2 and match the experiment apparatus. The reactor vessel container, with a width of 120mm and a height of 30mm, comprises the water load medium and the vessel wall which is 10mm thick, which is similar to the manufactured Perspex vessel in Chapter 3. The inner vessel contains the water medium, and the external wall of the vessel is surrounded by air. The dipole transmission sources (S1, S2, S3, S4, S5, S6 and S7), which generate sound pressure waves associated with the source of the cavitation using the function of a linear chirp signal, are located on the grid line within the vessel. The reception points (R1, R2, R3, R5, R6 and R7) are located on the external wall of the reactor vessel. The relative position between the transmission source and reception point in the model is approximately 40mm and represents cavitation events within the load medium. The physical properties of materials used in the FE modelling programme are shown in Table 4.1. These material properties (density, longitudinal velocity, shear velocity and acoustic attenuation) are obtained by the Centre for Ultrasonic Engineering (CUE) laboratories [119] and National Physical Laboratory (NPL) [120].

The acoustic and physical properties of Perspex were characterised at the frequency of 5MHz in the CUE Laboratories [119]. The acoustic and physical properties of glass and steel were characterised at the frequency of 10MHz by the NPL Laboratory [120]. This data is appropriately used in the modelling to suggest that materials transmit broadband signals and stimulate acoustic emission events associated with cavitation. The PZFlex FE model suite will match loss across a broad range of frequencies. The loss in a material as a function of frequency is matched at the frequency of 5MHz, which is well suited to the modelling.

The purpose of the FE model is to provide information about the effects of varying the number of the transmission sources, the pressure amplitude of the transmission sources, the distances of the transmission and the receipt points, wall materials and the thickness of the reactor vessel wall. The changes in the AE signal caused by these variations in parameters are investigated on the external wall of the reactor vessel.

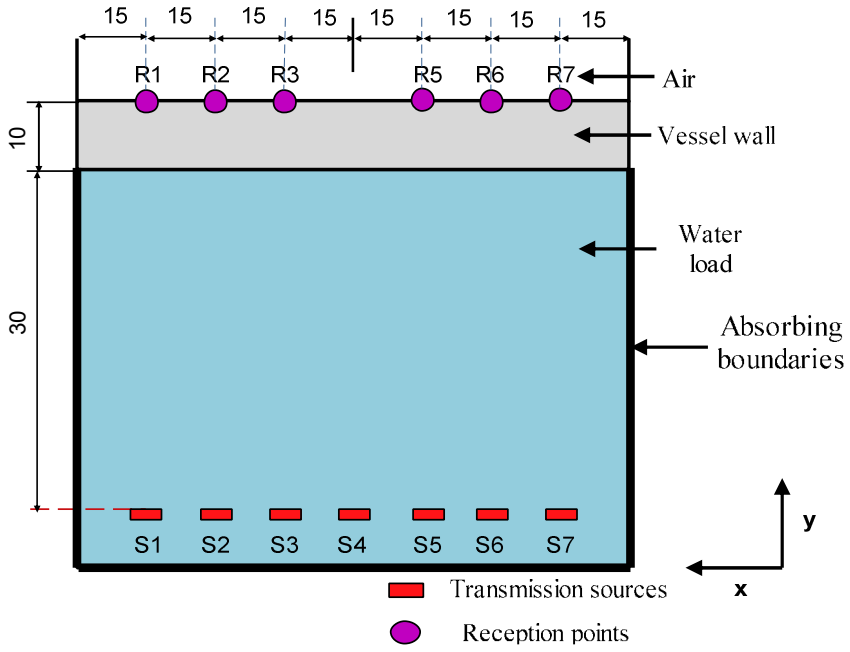

Figure 4.2 Schematic diagram of modelling the effects of the reactor vessel.

The excitation of the model corresponds to an acoustic pressure loading within the reactor vessel at the transmission positions (S1, S2, S3, S4, S5, S6 and S7) using a linear chirp signal, as discussed in Section 4.2.1, with an associated high ultrasound pressure. A high ultrasonic power application in the pressure range of 10kPa-100MPa [35] can produce acoustic cavitation. The dipole transmission source has a dimension of a 60 micron bubble close to the bubble radius produced by a 40kHz ultrasonic transducer [84],[121] and a range of pressures between 0.25 and 6MPa have been used. Acoustic emission events caused by cavitation and the interaction of the acoustic wave front with the walls of a vessel are investigated. The ultrasonic wave propagates through the reactor vessel wall to detection points (R1, R2, R3, R5, R6 and R7). Acoustic emission in pulse sound waves is generated by cavitation sources represented as S1, S2, S3, S4, S5, S6 and S7. The detected AE signal is

investigated at the reception points R1, R2, R3, R5, R6 and R7. The model output was selected as the displacement on the external vessel wall at the desired reception points chosen to be located at the position where the piezoelectric transducer would be positioned. The Fast Fourier Transform (FFT) of the signal output in the time domain was then used to compute the AE spectrum.

In order to avoid interference from the acoustic wave reflection from the edges of the model, absorbing boundaries were incorporated into the model, as shown in Figure 4.2. This avoids further wave reflections from the edges of the model interfering with the wave propagation of interest in the model. The simulation model is used to consider the ultrasonic wave propagation within the wall of the reactor vessel and the ultrasonic transducer is positioned in these regions to detect the appropriate AE signals.

Table 4.1 Material properties: Perspex, glass, steel and water used for FE model [119],[120].

Material	**Density**	**Long Vel.**	**Shear Vel.**	**Long. attenuation**	**Thickness**
	[kg/m^3]	[m/s]	[m/s]	[dB/m]	[mm]
Perspex	1183.5	2774.6	1395.4	347	10.0
Glass	2240	5100	3420	17.39	10.0
Steel	7900	5900	3200	42.95	10.0
water	1000	1496	N/A	0.002	30.0

Note: Perspex and water are characterised at 5MHz and 1MHz [119] respectively. Perspex. Glass and steel are characterised at 10MHz [120].

4.3 Simulation Results

A number of parameters were selected to provide an insight into the acoustic emission associated with the propagation of a sound wave into the external wall of the reactor vessel. The aim of the modelling work was to ascertain if the conceptual model prediction of the system output would define the feasibility of the non-invasive monitoring system and to provide a prediction of the AE signal at the external wall of the reactor vessel, on which the sensor is placed.

4.3.1 Prediction of ultrasonic wave propagation

An investigation to simulate the propagation of ultrasonic waves through the reactor vessel system of the FE model was carried out. The transmission source generates a high pressure wave with a broadband frequency range, which is referred to as the signal generated by the cavitation field.

An example of wave propagation from such a source is given in Figure 4.3. The propagation of the ultrasonic waves can be observed in the Figure as a top-down view of the ultrasonic wave through the reactor vessel and is presented as a series of frame shots from a movie generated using PZFlex.

The images presented in Figure 4.3 show the simulated ultrasound wave propagation, including interaction with the reactor wall. This sound wave propagation can produce a complex acoustic wave system within the vessel wall. The snapshots show the evolution of the ultrasound wave as it propagates within the wall of the vessel. A portion of the sound wave is reflected on encountering the Perspex wall of the reactor vessel. The rest of the sound wave propagates into the wall and spreads through the thickness and lateral dimensions of the wall of vessel. The acoustic emission propagates from the internal surface to external surface. Thus, the AE signal detected by a transducer, at the reception points indicated in the model, are a combination of wave propagation due to longitudinal and shear waves, as shown in

Figure 4.4. These signals are acquired on the external wall of the reactor vessel at each of the reception points. Longitudinal waves occur in the direction of wave propagation and the energy travels directly to the external wall of the vessel. Shear waves are relatively weak when compared to longitudinal waves and are usually generated through mode conversion at the material interfaces in the model. Interestingly, the mode conversion can be analysed and will be modelled with PZFlex by using Snell's Law [122]. The six y-displacement signals in the time-domain acquired in the reception positions R1, R2, R3, R5, R6 and R7 are shown Figure 4.4.

In Figure 4.4, the predicted y-displacement signal amplitudes acquired, in the time domain, on the outer wall of the reactor vessel associated with a simulated cavitation event in the liquid load medium are illustrated. Importantly, the acoustic source was S4, which is directly in the centre for the model. The amplitude of the modelled sound signals at the reception points R2/R6 and R3/R5 is high due to the high-energy transfer of the AE signal and low reflection and attenuation when compared to the reception points R1/R7. The amplitude of the sound signal decreases with an increase between the distances of the transmission source and the reception points. The initiation of AE signal is delayed because of the increased distances to the detection points R2/R6 and R1/R7, which are located furthest from the transmission source, as shown in Figure 4.2. The predicted signal in Figure 4.4 is converted to the AE spectrum which is shown in Figure 4.5, where this AE signal is considered for the detection of cavitation. In this Figure, the influence of beam spread and mode conversion at the water/Perspex interface has resulted in an effective low pass filtering effect as the receive position increase from the direct axial path.

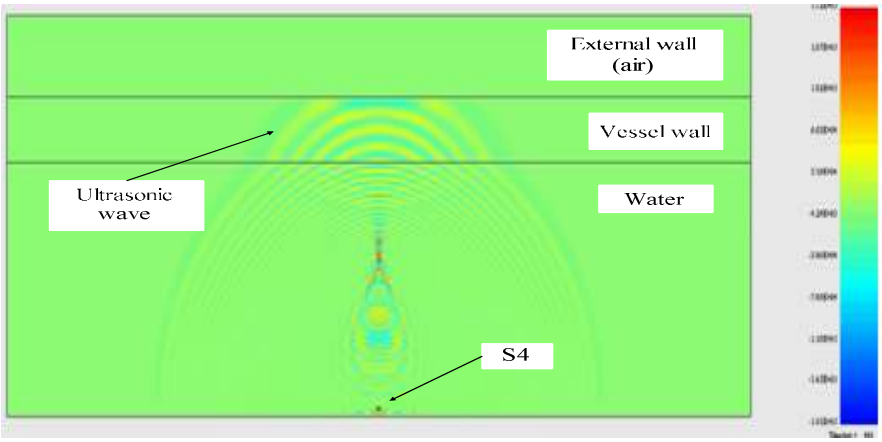

a) 2.60μs

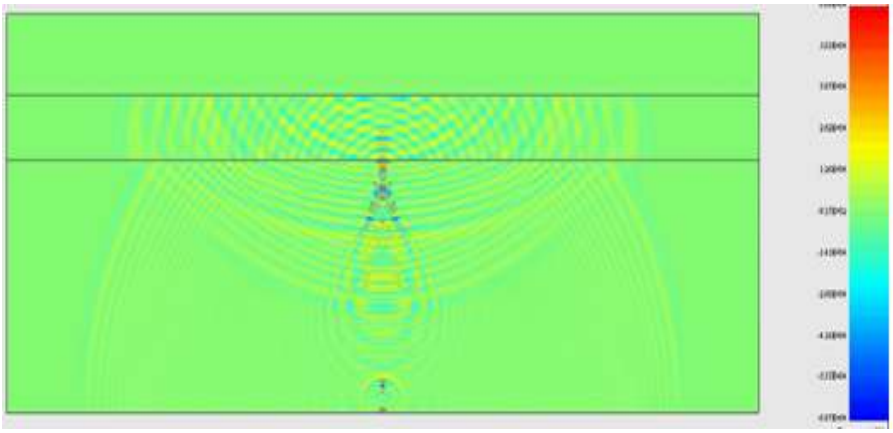

b) 3.40μs

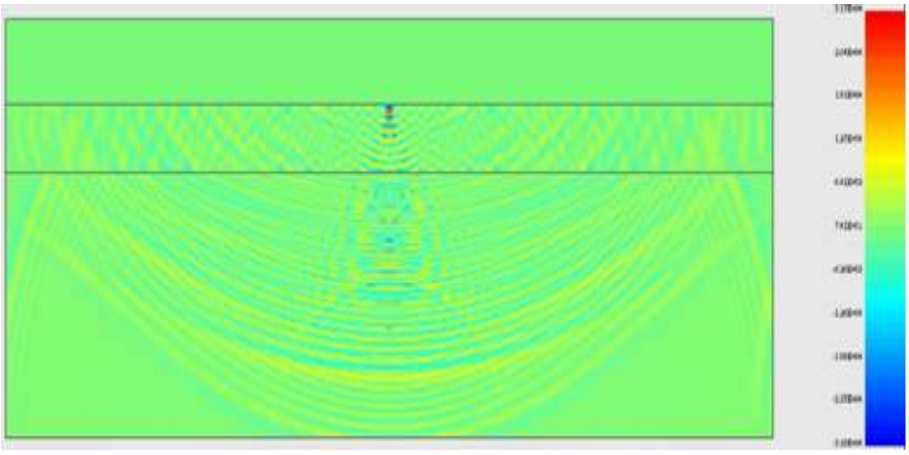

c) 4.50μs

Figure 4.3 Propagation of the ultrasonic wave for Perspex vessel, lateral view, time steps: a) 2.60μs, b) 3.40μs, c) 4.50μs.

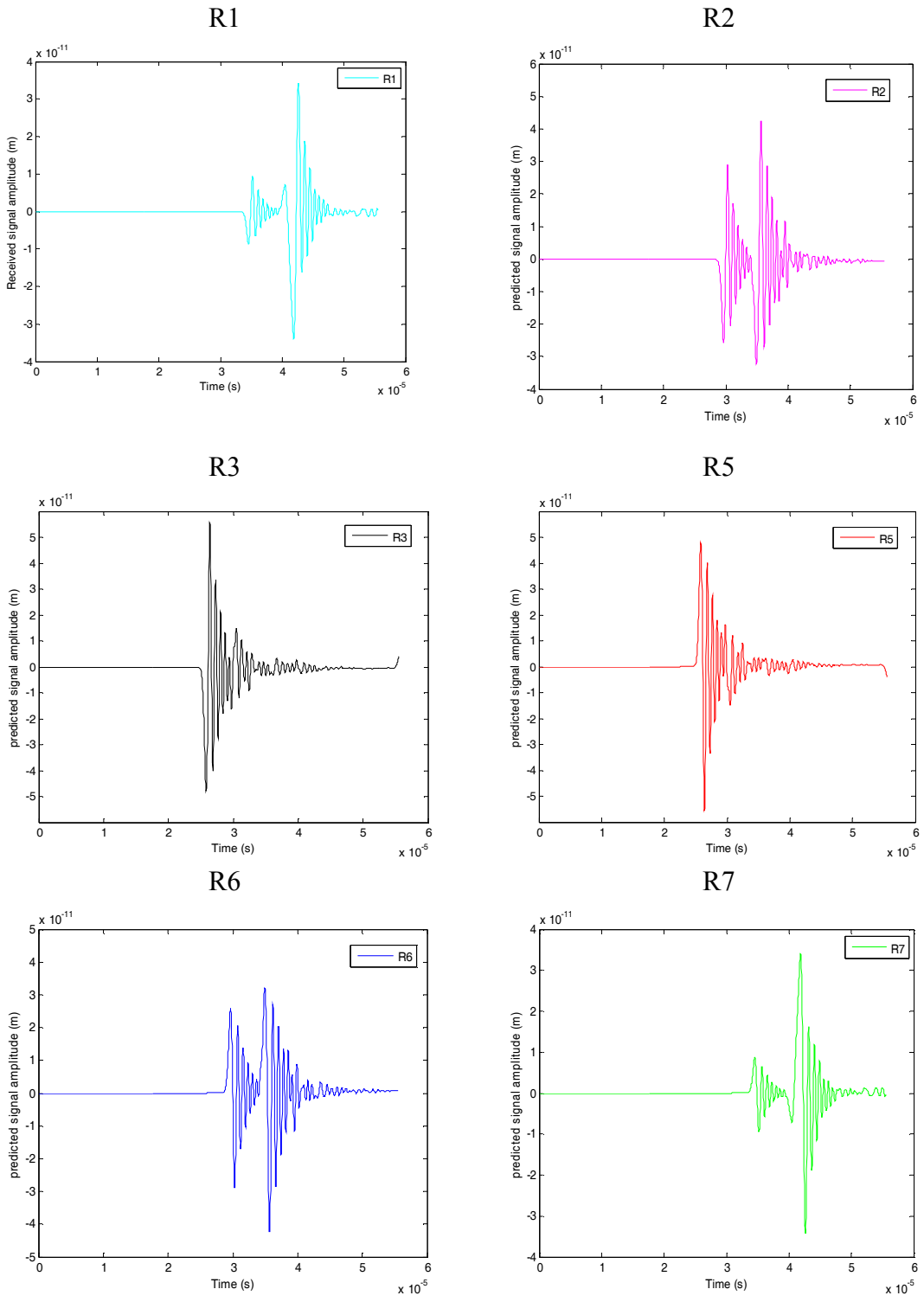

Figure 4.4 The FE derived y-displacement signal amplitude of Perspex vessel in time-domain at the reception positions of R1, R2, R3, R5, R6 and R7 for Perspex vessel. Sound wave is generated at the transmission source S4 with a linear chirp signal of 1-7MHz and sound pressure of 3MPa.

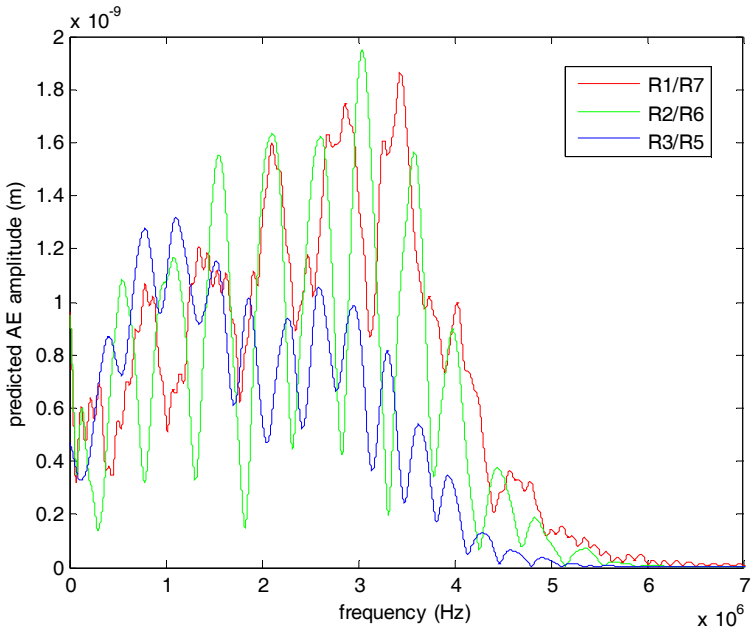

Figure 4.5 The FE derived AE signal in a Perspex vessel acquired at the reception points of R1/R7, R2/R6 and R3/R5. The acoustic emission containing the sound pressure of 3MPa and a linear chirp signal of 1-7MHz is generated at the transmission source S4.

4.3.2 Effects of the reception position

From Section 4.3.1, it is noted in Figure 4.5 that the frequency range of the AE signal is dependent on the reception position. Interestingly, although the AE is generated with a linear chirp signal of 1-7MHz, the predicted AE signal is restricted to a frequency range below 6MHz due to the filtering effects of the reactor vessel material [122]. According to the modelling results, the received AE amplitude of R3/R5 is higher than that of R1/R7 and R2/R6 due primarily to the propagating distance and the low mode conversion to shear wave modes, in this case. The frequency range of received acoustic emission signal is related to the reception point position and frequency dependent attenuation in the solid wall material. Moreover, the simulation model can be used to confirm that the sensor attached to the external wall at these reception points can detect the AE signal. Moreover, the simulation is

significant when the position of the attachment of the ultrasonic transducer is considered.

4.3.3 Effects of transmission sources

The computer models were produced by generating at the transmission sources (S1, S2, S3, S4, S5, S6 and S7) in relation to a number of sources of cavitation occurring within the Perspex reactor vessel. It is reported that the pressure range of above10kPa can produce acoustic cavitation [35], with the sound pressure range of 1MPa is used in this model. The transmission sources were excited at different positions via the application of sound pressure loadings, as described previously, and a linear chirp signal was chosen as an input stimulus. This Section will investigate the AE signal through the effects of single transmission and multi-transmission sources.

4.3.3.1 Single transmission source

A single transmission source is used to consider the effects of the external wall of the Perspex reactor vessel on the detection of the AE signal. The transmission source S4 produces an ultrasound wave containing a sound pressure amplitude of 1MPa. The acoustic signal on the external wall of the vessel caused by the sound propagation was detected at the reception points of R1/R7, R2/R6 and R3/R5. As expected, due to symmetry, the emission signal obtained at positions R1/R7, R2/R6 and R3/R5 produced identical results and the resultant output spectra are depicted in Figure 4.6.

It is noted that in Figure 4.6 the reception points R2/R6 and R3/R5 detect higher acoustic amplitude closest to the transmission point because they receive the high energy transfer. The predicted AE signal at reception points R1/R7 decreases, as the reception points get further away from the transmission source. Hence, the detected AE spectra vary with reception position and importantly, the bandwidth of the acoustic spectrum is dependent on the reception position. The predicted peak

amplitude of the AE spectrum is indicated in the high frequency range of 1-4MHz. In addition, the bandwidth frequency of the emission spectrum is higher closer to the transmission source than at the reception points positioned further away. Furthermore, the predicted acoustic spectrum is restricted to the frequency range of 0-6MHz.

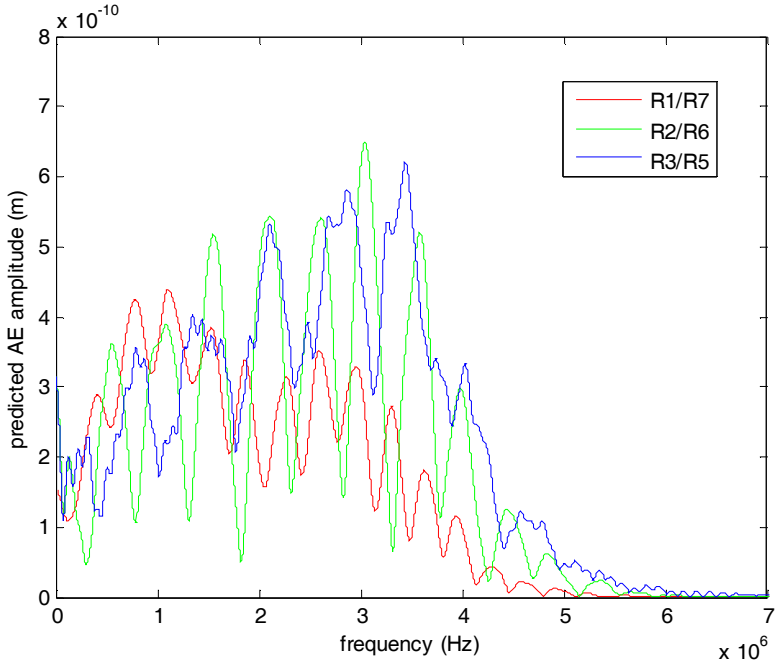

Figure 4.6 The FE derived AE signal in a Perspex vessel at the reception points of R1/R7, R2/R6 and R3/R5, acquired by FE model. The acoustic emission containing the sound pressure of 1MPa and a linear chirp signal of 1-7MHz is generated at the transmission source S4.

4.3.3.2 Multi-transmission sources

This Section considers the cavitation activity occurring at multi-transmission sources in the reactor vessel. To study the influences of multi-transmission sources, a number of transmission sources, as shown in Figure 4.2, operating together were modelled. In this example, the sound wave, containing the sound pressure of 1MPa and a linear chirp signal of 1-7MHz, is generated at the transmission sources of S3, S4 and S5.

The multi sound sources of the wave propagations make the physical system more complex. The model output in terms of AE signal is investigated at the reception points of R1/R7, R2/R6 and R3/R5.

Figure 4.7 illustrates the predicted AE signals in the frequency domain. The results show the differences of the AE spectra obtained at positions R1/R7, R2/R6 and R3/R5, with each combination producing identical results due identical propagation paths in this symmetrical model. Their frequency range is dependent of the reception positions and the detected acoustic emission is again restricted to the frequency range of 0- 6MHz. All of the acoustic emission profiles are strongly dependent on an increase in the number of transmission sources. As the number of transmission sources is increased, the high peak amplitude of the AE spectrum increases as a result of the more complex acoustic propagation. The peak amplitude of the AE spectrum is dependent on the events and the reception positions and is highest in the frequency range of 1-3.8MHz. It is expected that the AE signal produced on the vessel wall will be detectable by an ultrasonic transducer.

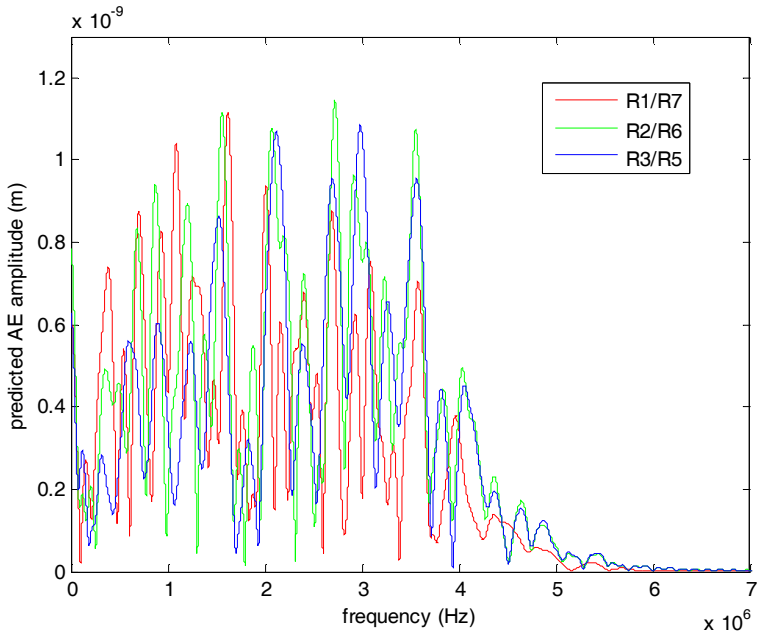

Figure 4.7 The FE derived AE signal in a Perspex vessel obtained using different input positions acquired from the reception points of R1/R7, R2/R6 and R3/R5. The transmission sources of S3, S4 and S5 were used to generate sound waves containing 1MPa.

The vessel wall acts as a carrier for the propagation of the sound wave. The ultrasonic energy levels of the sound wave propagating to the outside of the vessel wall depend on the positions of the detectors. The simulation results presented highlight that the AE signals propagating through the reactor vessel wall can be collected, over the broadband frequency range of 0-6MHz and can be used to consider the acoustic cavitation activity for the Perspex reactor vessel.

4.3.4 Effects of the sound pressure

This Section describes the analysis of the effects of sound pressure. The investigation into the effects of the sound pressure inputs was simulated by varying the sound pressure levels to generate cavitation events within the reactor vessel. The sound pressure range of 0.25 to 2MPa was simulated, for a linear chirp signal of 1 to 7MHz

at the transmission source S4. The AE signals are detected at the reception points R1/R7, R2/R6 and R3/R5. The pressure variation predicted at the external wall was converted into the AE spectrum and considered as the output of the system.

An example of the predicted AE spectra from the sound pressure of 0.25, 0.5, 1, 1.5 and 2MPa is shown in Figure 4.8. The AE signal is detected at the reception point R5 on the external vessel wall. The changes in the AE spectra are in the frequency range of 0 to 6MHz. The shape of the predicted frequency spectra at each sound pressure level show similar trends and are not influenced by the detection of the transducer. An increase in the pressure levels of the transmitting source corresponds to an increase in the AE signal output and results in an overall increase of AE spectra with increased pressure amplitude input. An increase in the pressure levels is associated with high power ultrasonic wave operation, which can produce cavitation.

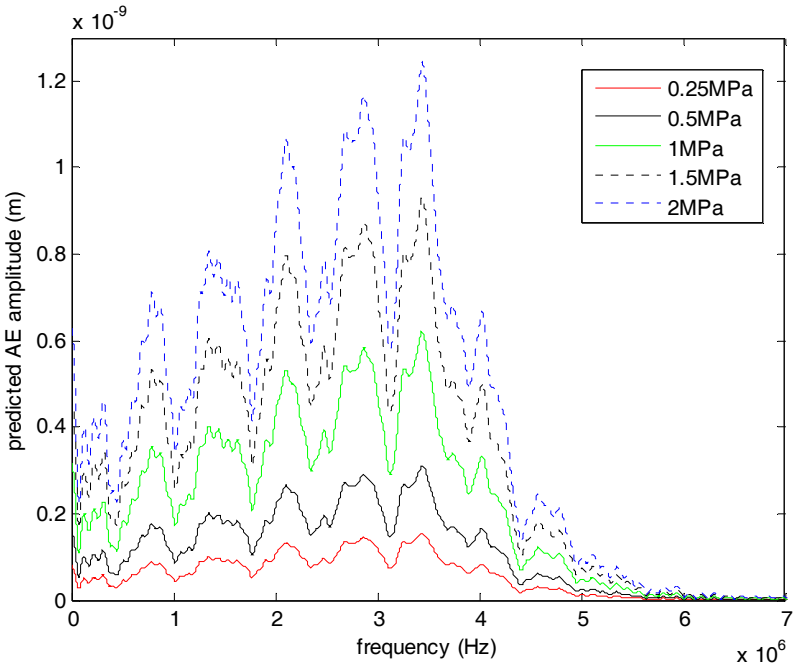

Figure 4.8 The FE derived AE signal in a Perspex vessel obtained by the pressure inputs from 0.25MPa to 2MPa. The acoustic emission is generated at transmission source S4 and is detected in the reception position R5.

The variation of the input sound pressure affects the amplitude of the AE signal. This increase in the AE signal allows the level of broadband integrated energy (BIE) to be calculated, as described in Section 3.6.5. The intensity of cavitation activity obtained by the BIE approach at the sound pressures of 0.25, 0.5, 1, 1.5 and 2MPa is shown in Figure 4.9. It is noted that increasing the AE spectrum by manipulating sound pressure causes an increase in the intensity of BIE. The feasibility study of the sound pressure reactions is similar to that of the force impact reaction [122],[123].

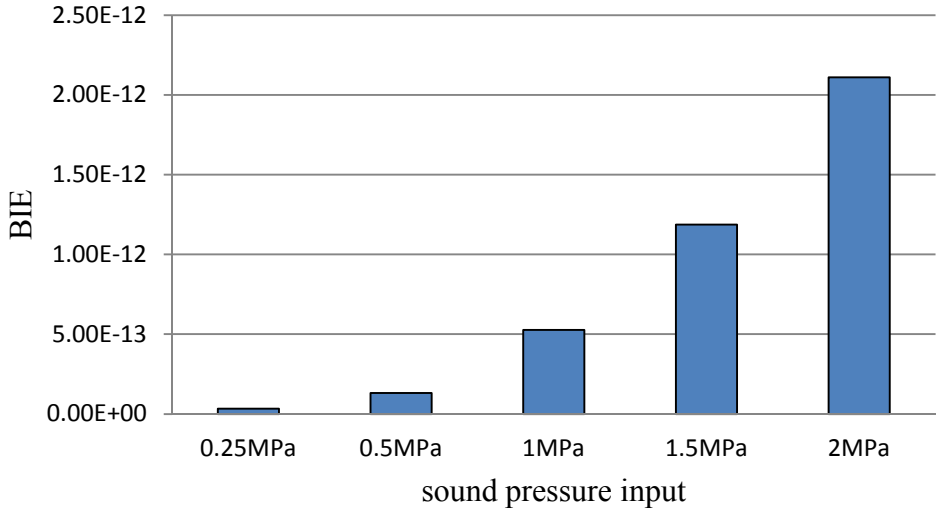

Figure 4.9 The intensity of cavitation activity obtained by BIE calculation in the frequency range of 1-5MHz and the sound pressure range of 0.25 to 2MPa.

4.3.5 Effects of distance between transmission source and reception point

The effects of the transmission source and the reception points are analysed in this Section. The interval between the two positions was set at 20, 40, 60, 80 and 100mm. The acoustic emission containing the sound pressure of 1MPa and a linear chirp signal of 1-7MHz is produced at the transmission source S4 and the signal output was detected at reception points R1, R2, R3, R5, R6 and R7. The resultant signals predicted at R5 only, profiled in terms of the frequency spectra, are plotted in Figure 4.10. The frequency range of each spectrum depends on the detected signal, from

which high energy detection produces the frequency bandwidth. The detected AE signal from the input pressure of 20mm is in the frequency range of 0-6MHz, but the upper frequency limit in the detected signal reduces with an increase in distance. It is noted that an increase in the separation distance results in a decrease in the AE signal amplitude due to the attenuation of the sound wave in the load medium, which is clearly shown in Figure 4.11.

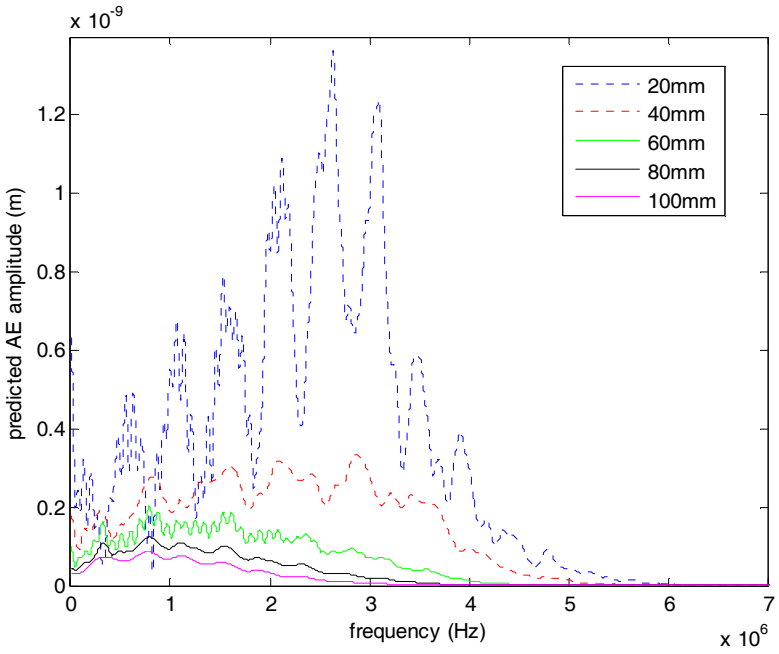

Figure 4.10 The FE derived AE signal in a Perspex vessel obtained by varying the distances between transmission sources and reception points of 20mm to 100mm. The acoustic emission is generated at transmission source S4 with the pressure of 1MPa and detected in the reception position R5.

In order to predict the effects between the two positions, the BIE approach, as described in Section 3.6.5, was computed in the frequency range of 1-5MHz. Figure 4.11 shows the intensity of cavitation activity at each distance. It is noted that BIE is high at the distance of 20mm and decreases with the increasing interval between the transmission sources and reception points. It is possible to note that the intensity of

BIE, the energy of the acoustic spectrum at the frequency range of interest, increases with decreasing distances between the transmission sources and reception points.

The AE spectrum profiles strongly depend on the pressure input and the distances between two positions. Changes in the AE frequency content as a function of distance could be an important index for analysis of the transducer receiving signal.

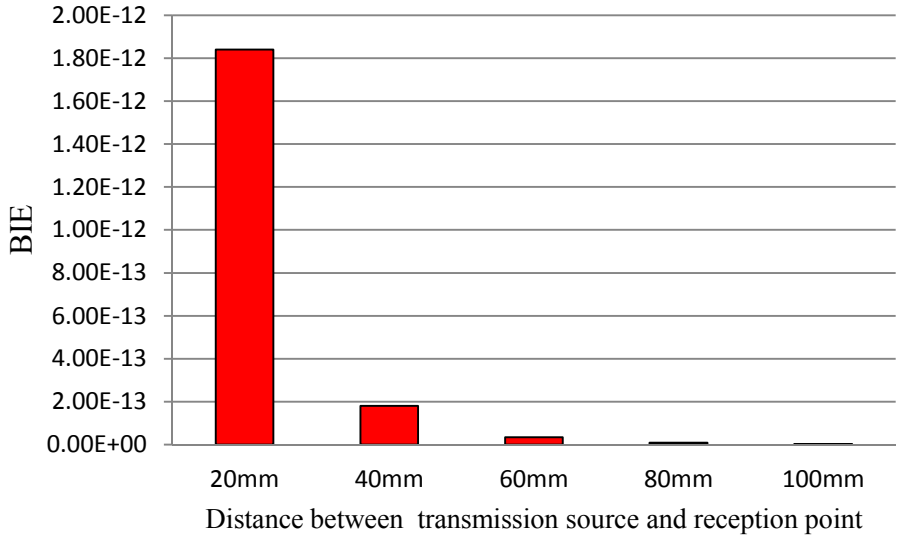

Figure 4.11 The intensity of cavitation activity obtained by BIE calculation in the frequency range of 1-5MHz at the reception point R5 and distances of 20, 40, 60, 80 and 100mm. The acoustic emission is generated at transmission source S4.

4.3.6 Influence of wall Material

The prediction of the effects of the wall material is discussed in this Section. Within the FE model, as shown in Figure 4.2, there is provision to change the properties of the wall material. To ensure a realistic operation of the model, different practical wall materials are selected to investigate the influence of the properties of the wall material. Many materials are used as the reactor vessel wall such as steel [105] and glass [115] and in this work, three materials Perspex, glass and steel, are employed in

the model. Table 4.1 reports the acoustic material properties: density, longitudinal velocity, shear velocity and acoustic attenuation of each material. These parameters are subsequently utilized in the FE modelling program. The thickness of the material wall used in the simulation is 10mm to be consistent with the thickness of the Perspex vessel in Chapter 3.

Figure 4.12 illustrates the predicted output frequency spectrum at the reception point R5, when acoustic emission is generated at transmission source S4 with the sound pressure of 1MPa and the system is subjected to the different wall materials of the reactor vessel. The plots show the effects in the AE spectra of complex wave propagation on the wall of the reactor vessel. The AE signal of the Perspex material produces a frequency range of 0-6MHz and a high amplitude signal. The upper frequency limit of the AE signal for glass and steel is about 5MHz. Interestingly, the AE amplitude of Perspex is higher than that of glass and steel. The amplitude of the AE spectrum relies on the reflection and transmission of sound waves in the materials and the energy transfer [122] and hence, the lower acoustic impedance of the Perspex material produces a higher signal level at the reception points. It is noted that the frequency ranges of the AE signal observed is dependent on the material properties and transfer function of the model. The predicted AE signal has been modified by the frequency transfer function and by the filtering effects of materials which can be used as the vessel walls [122]. The frequency range of the predicted AE signal can be used to consider the bandwidth of an ultrasonic transducer to be designed for monitoring of cavitation.

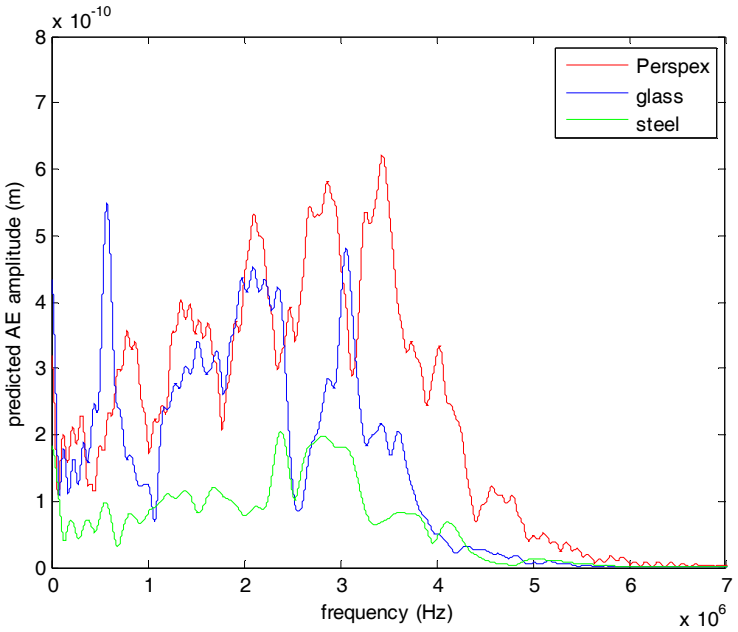

Figure 4.12 The FE derived AE signals of different materials at reception point R5, Perspex, glass and steel, as obtained by FE model. The acoustic emission is produced at transmission source S4 with the sound pressure of 1MPa and is detected in the reception position R5.

4.3.7 Effects of vessel wall thickness

In order to predict the effects of the thickness of the reactor vessel wall on the detection of AE signal, a range of thicknesses for a Perspex wall were analysed. The thickness of the Perspex container was selected to be 2, 4, 6, 8 and 10mm. The specific properties of Perspex used in simulation are shown in Table 4.1. The sound pressures associated with the power input of 10-40W (see Table 4.2) and a linear chirp signal of 1-7MHz are applied to the model to generate the acoustic emission. The AE is produced at the transmission source S4 and is detected at the reception point R5. The BIE approach is used to evaluate the intensity of the cavitation activity in each wall thickness. The results of the simulations of the wall thickness are displayed in Figure 4.13. The BIE is highest at the thickness of 2mm and decreases as the thickness increases. From this result, it is clear that the BIE decreases as the wall thickness increases primarily due to the attenuation of the sound wave in the Perspex material.

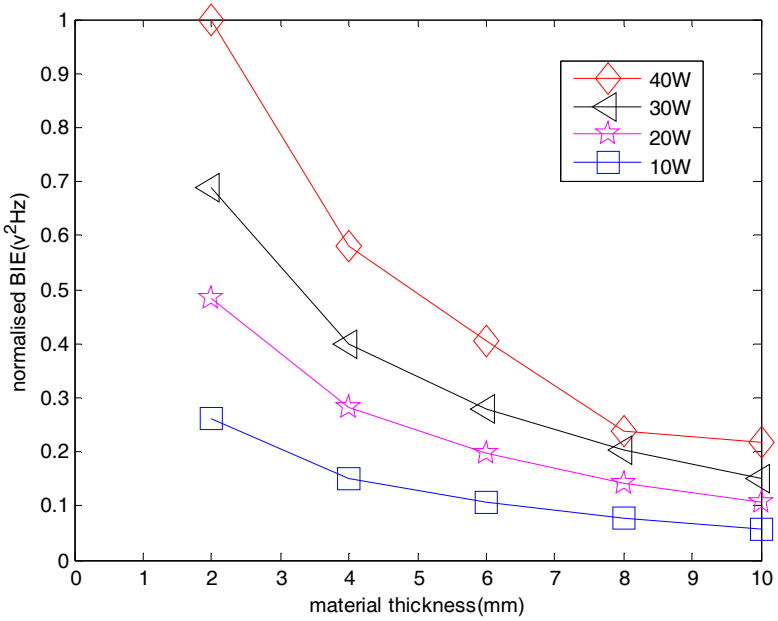

Figure 4.13 The relationship of BIE in the frequency range of 1-5MHz and Perspex wall thickness with the power input of 10-40W. The acoustic emission is produced at the transmission source S4 and is detected at reception points R5.

4.4 Narrow band analysis

The bandwidth of the ultrasonic transducer is related to its properties and those of the materials used. Hence, the ultrasonic transducer typically operates over a narrow bandwidth. In order to obtain the ultrasonic transducer for monitoring cavitation activity, it is necessary to evaluate a frequency range that provides high signal amplitude. The predicted bandwidth can be determined by analyzing the BIE approach, as described in Section 3.6.5, which determines the energy distribution and the transfer function of the signal. In order to obtain the bandwidth of an ultrasonic transducer which is suitable for monitoring cavitation activity in the Perspex reactor vessel developed in Chapter 3, BIE analysis of the FE model output at reception point R5, which is selected as it is not in the direct path from the source, is calculated in the bandwidth ranges of 1-2MHz, 1-3MHz, 1-4MHz and 1-5MHz. The predicted BIE from the FE model calculated in different bandwidths is compared to experimental results measured by the NPL cavitation sensor (as described in Section

4.5.), in which cavitation is primarily measured within its internal volume. In the experiment, the BIE is calculated in the frequency range of 1-5MHz. The BIE of different bandwidths, obtained by the FE model and the NPL cavitation sensor measurement, is shown in Figure 4.14. It is noted that the frequency bandwidths of 1-3MHz, 1-4MHz and 1-5MHz provide high energy distribution. The BIE of 1-3MHz, 1-4MHz and 1-5MHz obtained from the FE modelling and the measured results of the NPL cavitation sensor are comparable. It is noted that the bandwidth corresponding to 1-3MHz provides a similar performance to the BIE results from the NPL cavitation sensor measurement. Hence, it is considered that the design of an ultrasonic transducer could have to frequency bandwidth between 1-3MHz to be used to monitor acoustic cavitation activity.

The same methodology was conducted for both glass and steel walls and is shown in Figure 4.15 and 4.16, respectively. All results indicated that an ultrasonic transducer located on the outer wall of the reactor vessel, with an operating bandwidth between 1-3MHz would produce a similar trend to the intensity of the NPL cavitation sensor.

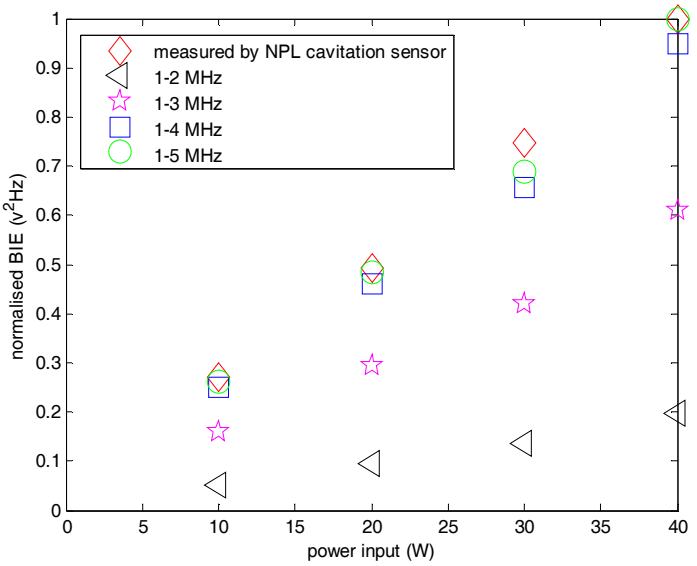

Figure 4.14 The BIE obtained by Perspex wall at the reception point R5 and by the NPL cavitation sensor measurement. The BIE of FE modelling is calculated in the different frequency bandwidth of 1-2MHz, 1-3MHz, 1-4MHz and 1-5MHz and of the NPL cavitation sensor measurement is calculated in the frequency range of 1-5MHz.

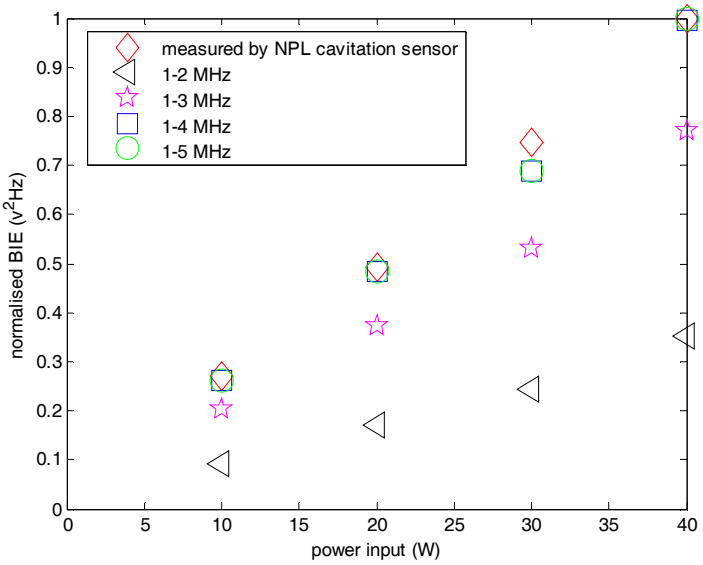

Figure 4.15 The BIE obtained from the glass wall at the reception point R5 and by the NPL cavitation sensor measurement. The BIE of FE modelling is calculated in the different frequency bandwidths of 1-2MHz, 1-3MHz, 1-4MHz and 1-5MHz and of the NPL cavitation sensor measurement, which is calculated in the frequency range of 1-5MHz.

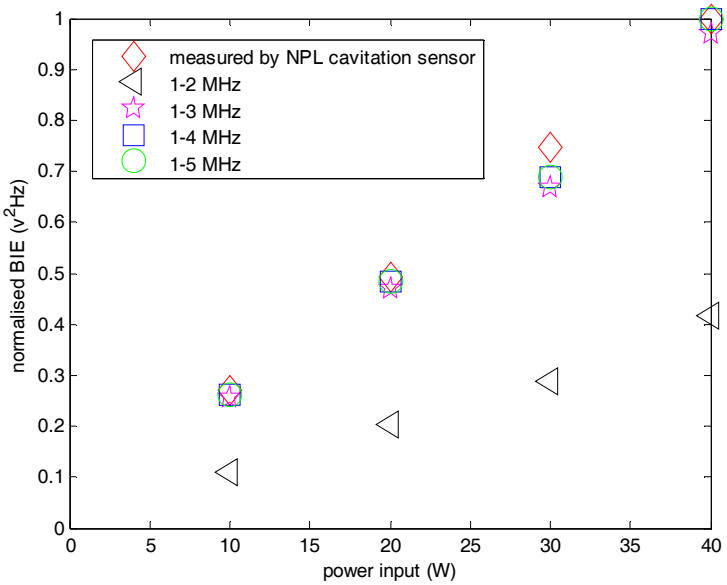

Figure 4.16 The BIE obtained from the steel wall at the reception point R5 and by the NPL cavitation sensor measurement. The BIE of FE modelling is calculated in the different frequency bandwidths of 1-2MHz, 1-3MHz, 1-4MHz and 1-5MHz and of the NPL cavitation sensor measurement, which is calculated in the frequency range of 1-5MHz.

4.5 Relationship between experiment and simulation

4.5.1 Arrangement for experimental measurement and simulation

The BIE approach was used to analyse cavitation activity and it was expected that BIE obtained by FE analysis would show a similar trend to the hydrophone measurement. The transfer process between experiment and simulation is conducted in two different stages.

4.5.1.1 The NPL cavitation sensor and the 8103 hydrophone measurement

To attain the acoustic pressure, the B&K 8103 hydrophone measurement system was developed and is represented in Figure 4.17. The reactor vessel, with dimensions of 120x130x150mm, was manufactured and contains 1.4 litres of degassed water.

During the experiments, two hydrophone transducers are utilised: the B&K 8103 hydrophone [70] and the NPL cavitation sensor [75], as described in Section 2.5. The hydrophones are positioned at 30mm from the ultrasonic high power transmitter and in the centre of the reactor vessel. Again, a 40kHz Tonpilz transducer was employed as an ultrasonic transmitter and integrated into the bottom of the vessel.

Cavitation was produced by driving the 40kHz Tonpilz transducer under continuous wave conditions. The excited signal was produced using a function generator (Agilent 33120A) and amplified using a wideband RF amplifier (155LCR, Kamas Engineering), with a gain of 50dB. The ultrasound transducer is excited by power levels corresponding to 10-40W and is controlled by the signal level generated by the function generator (Agilent 33120A). The AE spectra, containing both the fundamental frequency and broadband acoustic emission, once detected, were transferred to a digital oscilloscope (Agilent 54642A) for data acquisition purposes.

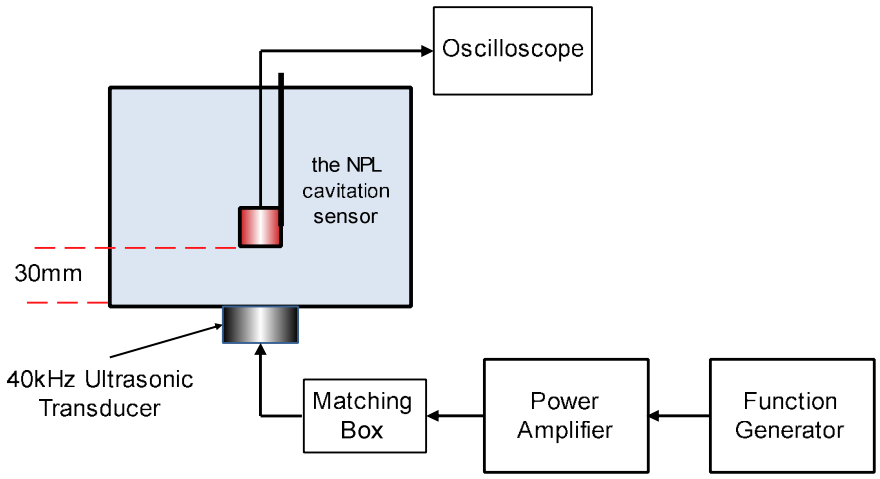

Figure 4.17 Schematic diagram of the NPL cavitation sensor and the B&K 8103 hydrophone measurement setup.

The power input (driving the ultrasonic transmitter), output peak-to-peak voltages detected by the B&K 8103 hydrophone measurement and equivalent sound pressure

are illustrated in Table 4.2. The output pressure acquired by the hydrophone measurement was then employed as an excitation signal input for the simulation model in the second stage of the transfer process (Section 4.5.1.2).

The measured output voltage of the B&K 8103 hydrophone was converted to acoustic sound pressure via the pressure calibration method [101] with the sensitivity of -215 dB ($17.782\mu V/Pa$) at 40 kHz [70]. In the measurement process, the sensors are placed in the same location within the reactor vessel to detect the AE signal. The acoustic spectrum detected by the NPL cavitation sensor, which has a frequency range of 0-10MHz, for variations in the input power of 10-40W level, is shown in Figure 4.18. These spectra were used to evaluate the BIE performance from the simulation.

Table 4.2 Relationship of the power input, the calculated sound pressure and the measured voltages acquired by the B&K 8103 hydrophone.

Power input	**Output voltage**	**Sound pressure**
Watts	Volts (peak-to-peak)	kPa (peak-to-peak)
10	2.63	147.92
20	3.57	200.79
30	4.26	239.60
40	5.13	288.53

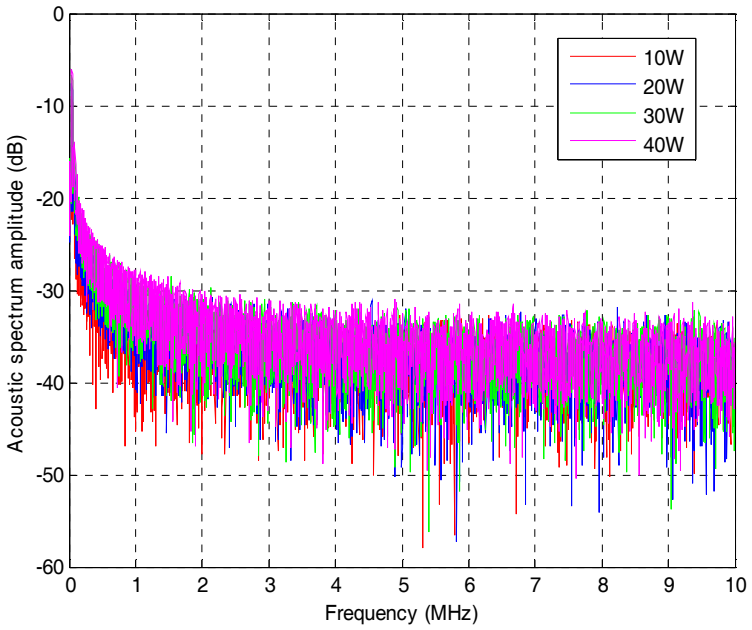

Figure 4.18 The AE spectra detected by the NPL cavitation sensor at the frequency of 40kHz, across the power input of 10-40W when located at the centre of the reactor vessel.

4.5.1.2 Finite Element Modelling

The FE model, shown in Figure 4.2, was constructed to analyse the effects of the reactor vessel. A rectangular reactor vessel with 10mm thick walls and dimensions of 120x40mm was modelled and loaded with water. During the simulation process, acoustic emissions rely on the influences of the distribution of acoustic pressure and the Perspex wall of the reactor vessel. To simplify the modelling process, the output pressure in Table 4.2, which is associated with the input power of 10-40W, was employed as the signal input for the FE model. The transmission source S4 generates acoustic pressure using the sound pressure measured during the first stages.

The transmission source S4 generates sound pressure at the levels of 10-40W with a linear chirp signal of 1-7MHz. Then, the AE signal is detected by reception points

R5, R6 and R7. The AE spectrum of the frequency range of 0-6MHz acquired by the simulation model at reception point R5 is represented in Figure 4.19. It is clear that the AE spectrum increases with the levels of the input power signal, which is caused by the higher amplitude AE signal within the vessel wall. These signals were employed in the BIE calculation to examine the cavitation activity (as described in Section 3.6.5) in the frequency range of 1-5MHz from the predicted AE spectrum. The relationship between the power input and the intensity of normalized BIE, produced at different levels and received at points R5, R6 and R7, is illustrated in Table 4.3.

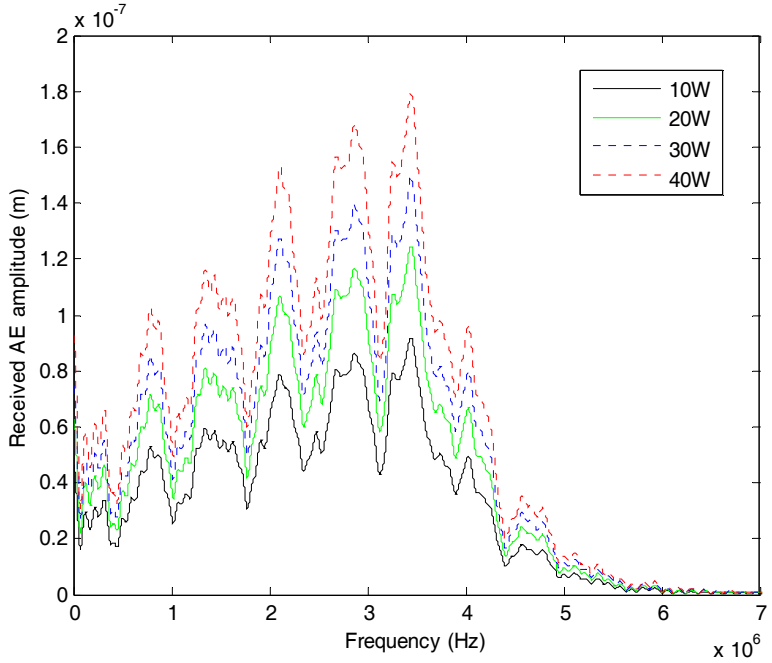

Figure 4.19 The FE derived AE signal in a Perspex vessel obtained by FE model with input power of 10-40W. The acoustic emission is generated at transmission source S4 and is detected at reception point R5.

Table 4.3 The relationship of power input levels, sound pressure and cavitation activity obtained by BIE calculation in the frequency range of 1-5MHz at reception points R5, R6 and R7.

Power input	Sound Pressure	BIE (V^2 Hz)		
		R5	R6	R7
Watts	kPa	Normalized	Normalized	Normalized
10	147.92	0.263	0.218	0.107
20	200.79	0.484	0.402	0.197
30	239.60	0.690	0.573	0.281
40	288.53	1.000	0.831	0.728

4.5.1.3 Relationship between acoustic emission and cavitation activity

The AE spectra obtained experimentally using the NPL cavitation sensor, the B&K 8103 hydrophone measured in the centre of reactor vessel and the FE modelling at reception point R5, are represented in Figures 4.18 and 4.19. To assess the correlation between experiment and simulation, the intensity of cavitation activity at both stages is calculated by BIE in the frequency range of 1-5MHz, and is compared. Figure 4.20 shows the cavitation activity obtained through the normalised BIE from the NPL cavitation sensor in which cavitation was measured in a limited cylinder along a transducer's axis, the B&K 8103 hydrophone and FE modelling. The B&K 8103 hydrophone measurement and the FE model collects the AE signal from a cavitation sources throughout the vessel. The graph illustrates a tendency for BIE to increase linearly with power input. Moreover, it is noted that the cavitation activity shows a similar trend in the experiment and the FE modelling.

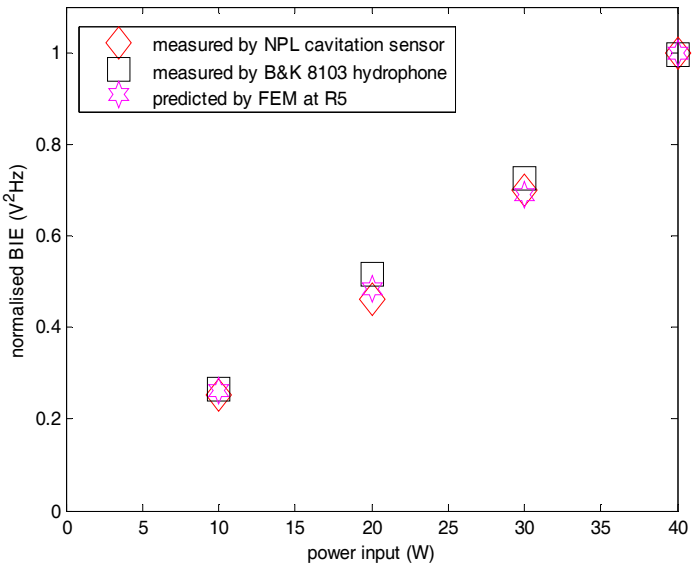

Figure 4.20 The normalised BIE calculated in the frequency between 1-5MHz, obtained by the NPL cavitation sensor, the B&K 8103 hydrophone measurement and the FE modelling. The acoustic emission is generated at transmission source S4 and is detected at reception point R5.

The graph in Figure 4.21 also illustrates a trend in the cavitation activity obtained by the BIE approach in the frequency range of 1-5MHz, when predicted by reception points R5, R6 and R7. The intensity of cavitation activity is different due to the detected AE signal in different regions. The BIE at reception point R7 is lower because this reception point is far from the transmission source and the effect of attenuation in the load medium and the reactor wall. Nevertheless, the BIE of these positions are comparable. The model shows excellent correlation with the response from the experiments by the NPL cavitation sensor measurement. It is noted that the AE signals detected on the wall of the vessel represent what could be detected by the ultrasonic transducer.

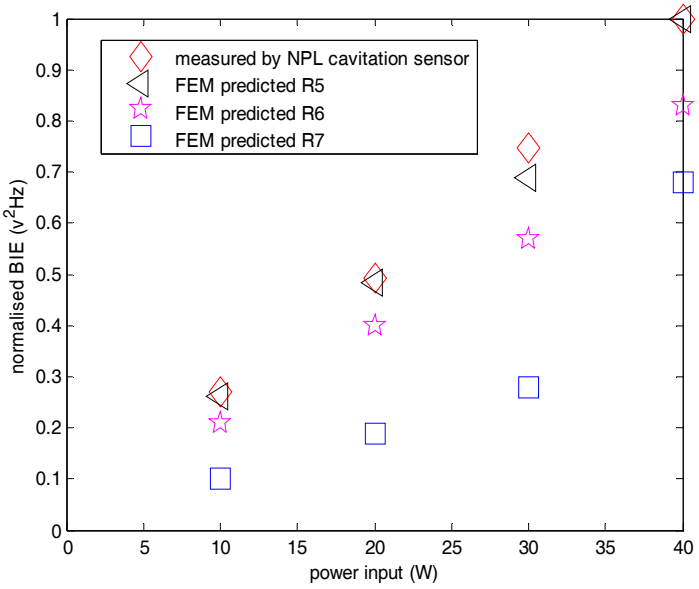

Figure 4.21 The BIE of FE model at the reception points of R5, R6, R7 and of the NPL cavitation sensor measurement with the input power of 10-40W. The cavitation activity is calculated by the BIE approach in the frequency range of 1-5MHz.

4.6 Discussion

This Chapter is very important for the design of an ultrasonic transducer with which to monitor cavitation when located on the outer wall of the reactor vessel. Before designing any system it is necessary to ensure the requirements of the transducer will be fulfilled. In this work, FE modelling has been used to enhance understanding of the underlying dynamics of the complex system of wave propagation caused by the cavitation events in a reactor vessel. The source of cavitation comprises of high pressure and broadband frequencies, which have been simulated using a linear chirp signal.

The major contributions of this Chapter to the design of a non-invasive cavitation monitoring system using an ultrasonic transducer are listed below;

- The sound wave generated by the source of cavitation propagates through the external wall of the reactor vessel and produces a detectable signal which is effectively a channel (reactor wall) modulated AE signal.

- The simulation programme has indicated that the upper frequency present is the AE signal arriving at the transducer location is reduced due to the material properties of the wall. This upper frequency is 5MHz for glass and steel and 6MHz for Perspex. Importantly, this frequency range is used to consider the bandwidth of an appropriate ultrasonic transducer for monitoring the cavitation.

- The amplitude of the AE signal increases with an increase of sound pressure levels and the number of the transmission sources.

- An increase in the distance between the transmission sources and reception points leads to a decrease of the AE amplitude due to a combination of sound wave attenuation in the load medium, mode conversion of the interface and the directivity profile of the acoustic sources used in the model.

- The AE signal is attenuated by the thickness of the reactor vessel wall and hence, attention will have to be paid to the sensitivity of the ultrasonic transducer.

- A narrow bandwidth ultrasound transducer is capable of monitoring acoustic cavitation activity. The narrow bandwidth of 1-3MHz has been demonstrated to provide a similar trend to the NPL cavitation sensor measurement.

The results presented so far offer an approach to designing a non-invasive cavitation monitoring system, in which FEA can be used to model the behaviour of a reactor vessel. Predicting the AE signal and its frequency bandwidth is fundamental to designing a suitable sensor for monitoring acoustic cavitation activity. Moreover, confidence in the simulated results was enhanced by using the sound pressure obtained by hydrophone measurements directly in the FE model. Through this technique, it is feasible to provide a good correspondence between simulation and experimental results. Subsequently, the analysis of the simulation outputs was used

to inform the design specification for an ultrasonic cavitation monitoring transducer, which will be used non-invasively from the outer wall of the reactor vessel.

4.7 Summary

This Chapter has presented a simulation approach to generate information on the behaviour of cavitating field in a reactor vessel and analyse the outputs to provide a transducer specification. An FE model, employing PZFlex code, is used to analyse the complex interactions between sound wave propagation caused by cavitation events and the wall of the reactor vessel. This is key to understanding how the original AE signal is modified by these propagation channels before being detected by an ultrasonic transducer positioned on the outer wall. As the FE software cannot model a cavitation event, a simulated transmission source was used which comprised a linear chirp signal in the range 1-7MHz with different pressure levels to simulate a high power field. These simulations have provided information about the effects of varying the position of the reception points, the distances between the transmission sources and the reception points, the sound pressure of sources and the influence of wall material. The FE modelling has predicted that the AE signal can be adequately acquired on the external wall of the reactor vessel. Therefore, it is possible for an ultrasonic transducer placed there accordingly. The modelling results also provide the basis of the transducer design specifications for a non-invasive measurement system with which to monitor acoustic cavitation. The main transducer specification information is that the operational bandwidth of the transducer should ideally span 1-3MHz and that the acoustic impedance of the device is well matched acoustically to the wall material to provide high energy transfer.

CHAPTER 5

Broadband ultrasonic transducer: Design and Characterisation

5.1 Introduction

Ultrasonic transducers are used in many ultrasound applications. Typically, the application will govern the transducers specification – there is often scope for tailoring the transducer design to the specific task. The design of an ultrasonic transducer requires a simulation software tool capable of analyzing the transducer design.

In order to develop an ultrasonic transducer suited to monitoring acoustic cavitation, the finite element modelling code, PZFlex, is used to analyse the proposed transducer. The finite element simulation facilitates rapid analysis of the cause and effect relationships within a design. This technique is also capable of being used to analyse the effects of the reactor vessel, which presents complex problems such as

the interaction between cavitation activity and the itself vessel. More information on this was presented in Chapter 4, which provides an understanding of the behaviour of the reactor vessel wall when used in a non-invasive measurement system. The results of this study provide the basis for the transducer design specifications which will be applied to the monitoring of acoustic cavitation through a non-invasive monitoring system.

This Chapter focuses on the design and the development of a broadband ultrasonic transducer for monitoring cavitation activity. The design of the ultrasonic transducer relies on the transducer design specifications obtained from Chapter 4. The ultrasonic transducer, a piezoelectric composite transducer, is modelled to determine and optimise its performance. Parameters such as the ceramic pillar aspect ratio, the electromechanical coupling coefficient, and the matching layer are analysed. Moreover, the piezoelectric composite transducer is designed to match the impedance of the reactor vessel wall in order to obtain a high energy transfer function. The results of this experimental phase are presented in Chapter 6.

5.2 Piezoelectric ceramic composites

The piezoelectric composite material has been developed to improve transducer performance in ultrasound applications such as ultrasound imaging and underwater applications [124]. The piezoelectric composite transducer typically comprises two constituent phases: the active piezoceramic elements and a passive polymer material, to yield enhanced piezoelectric properties. Determination of the acoustic impedance of the transducer is achieved by varying the relative percentages of the piezoelectric ceramic and the passive polymer phase to form the piezoelectric composite structure [125]. There are a number of piezoelectric composite structures, with a 1-3 composite configuration commonly used as it gives improved transducer efficiency due to such as low acoustic impedance (ranging of 5-30MRayls), high coupling efficient factor ($k_t \rightarrow 0.75$) [126] due to the decrease of lateral modes in the

composite structure when the device is constructed using long, tall, thin ceramic pillars [127]. The decrease in lateral modes makes the piezoelectric composite structure a preferential choice for many transducer applications.

Typically, transducers made from piezoelectric composite material provide superior efficiency when compared to a piezoelectric ceramic transducer. The design of the composite transducer enables optimization of the electrical and mechanical force for particular applications by maximizing the input and output response of the electromechanical transducer system. The configuration of a typical 1-3 piezoelectric composite is depicted in Figure 5.1. The simple geometric structure can be developed by a dice and fill process and subsequently filled with a polymer material such as an epoxy resin [122].

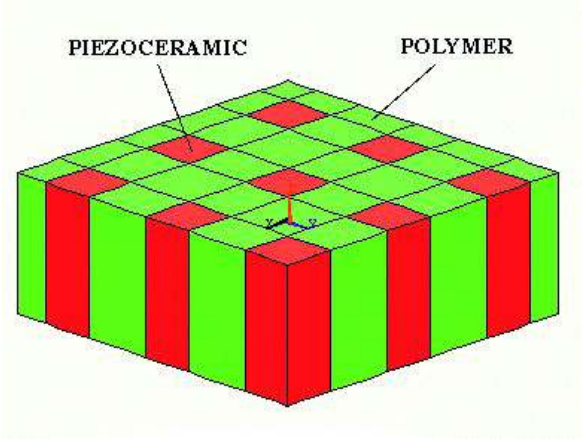

Figure 5.1 A schematic drawing of the 1-3 piezoelectric composite structure.

5.3 Design of ultrasonic transducer

In Chapter 4, a non-invasive measurement system for monitoring cavitation activity was studied via a finite element (FE) model of cavitation within a reactor vessel. The FE considered the acoustic emission signal caused by the cavitation activity, and its characteristic bandwidth. Piezoelectric composite material is chosen due to excellent

material properties [126]. The combination of the piezoelectric ceramic and the passive polymer phase can create devices of low acoustic impedance, similar to that of the reactor vessel wall (for example, 3.2 MRayls of the acoustic impedance of Perspex [119]). The piezoelectric composite configuration offers further advantages to enhanced electromechanical coupling efficiency and a reduction of unwanted lateral resonance [128]. Owing to the merits of the piezoelectric composite properties, a large amount of published research has been directed toward the development and improvement of these devices through the influence of microstructure geometry and material parameters of their operation [129],[130],[131],[132].

Although a large variety of ultrasound transducers are available on the market, none are able to fully satisfy these requirements. This is why a bespoke transducer was created. The transducer design specification is detailed in Table 5.1 and matches the requirements which emerged from the simulation task described in Chapter 4.

Table 5.1 Target parameters for a broadband piezoelectric composite transducer.

Operating at the resonance frequency of 2 MHz with flat frequency bandwidth of 1-3 MHz
Electrical impedance : matched to 3.2 MRayls for Perspex wall
Maximized electromechanical coupling factor

5.3.1 Theoretical consideration of the electrochemical coupling coefficient

The development of a finite element model with which to investigate transducer behaviour in piezoceramic composite structures has been reported in many articles [130],[131],[132]. Constructive matrix equations have been employed to describe an FEA model with mechanical and electrical quantities occurring in piezoelectric

composite transducers, which are used to predict the transducer performance. An investigation into the behaviour of a 1-3 composite structure, investigated through transducer theory and finite element analysis, is presented [133]. Importantly, the performance of a transducer relies on its composite microstructure, as illustrated in Figure 5.1. The FE modelling approach can be used to analyse the thickness mode operation of the piezoelectric composite structure. The resonance frequencies of the piezoelectric composite structure are related to the effective electrochemical coupling coefficient (k_t)- k_t is calculated using the electrical resonance frequency (f_m) and mechanical resonance frequency (f_n) of the fundamental resonance mode. The electrochemical coupling coefficient of a piezoelectric composite structure can be evaluated as follows [133];

$$k_t^2 = \frac{\pi f_m}{2 f_n} / tan\left(\frac{\pi}{2}\frac{f_m}{f_n}\right) \qquad 5.1$$

This approach is used to determine the coupling coefficient of the 1-3 composite transducers simulated in this study.

5.4 Broadband transducer development: design and characterisation

As discussed previously, the broadband piezoelectric composite transducer will be attached to the outer wall of the reactor vessel and used to acquire acoustic emission signals caused by the cavitation activity within the reactor vessel.

The design process of the piezoelectric composite transducer, specified in Table 5.1, involved the following considerations;

- Piezoelectric composite structure selection
- Constituent material selection, both active and passive phases

- Parameter choices such as aspect ratio (AR), ceramic volume fraction (CVF) and electromechanical coupling factor (k_t).
- Matching layer design
- Backing layer design (if required)

5.4.1 Piezoelectric composite structure selection and material selection

A 1-3 connectivity device was designed, to operate at a fundamental thickness mode of 2MHz. The PZT-5H (Ferromprem, Denmark) was selected for the design because this material provides a very high permittivity, coupling coefficient, and piezoelectric constant. The PZT-5H material also provides low dielectric and mechanical loss, which is an important factor for assessing a material's suitability for acting as a receiver. The piezoelectric ceramic composite (PZT-5H) incorporates a hard-setting polymer (Vantico HY1300/CY1301), which is selected for manufacturability and thickness mode sensitivity performance. Prior to using the simulation package, it is necessary to determine the basic piezoelectric composite parameters to promote good performance and, importantly, ensure the manufacturability of the device. To achieve this aim, a CUE design program has been developed based on the equivalent parameter model developed by Smith and Auld [126]. The 'CompD' program uses the active and passive material selection, along with the desired operating frequency and the saw blade width to be used in the fabrication process to determine both the fabrication parameters and a fundamental understanding of the piezoelectric properties of the device. It is important to note that this is a 1-D modelling approach and hence, PZFlex is required to fully examine the behaviour and performance of the piezoelectric composite for the desired application.

The selection of piezoelectric composite lateral dimensions was primarily based on material availability in the CUE lab. For this work, the device will have a diameter of 30mm, which is considered appropriate for the size of vessel (120x130x150mm).

CompD was then used to determine the active layer thickness of 0.95mm for a mechanical resonant frequency of 2MHz. Using a saw width of 0.12mm results in a saw pitch of 0.2mm for a 40% ceramic volume fraction device. The importance of these parameters will be explained in Section 5.4.2.1. Figure 5.2 illustrates the structure and configuration of the 1-3 piezoelectric composite transducer in two-dimensions, as obtained from the FE modelling code, PZFlex. A summary of the main parameters used in the simulation of the transducer is illustrated in Table 5.2 and the material properties used in the FE modelling can be found in Tables 4.1 and 5.3.

After selecting this suitable transducer configuration, the finite element model is used to analyse the characteristics of the transducer. This helps the transducer to achieve high levels of performance and analysis of the parameter choices is provided in the following Section.

Table 5.2 The main design parameters of the piezoelectric composite transducer.

Frequency	Thickness	Diameter	Pitch width	Saw width
2.0MHz	0.95mm	30 mm	0.20 mm	0.12 mm

Figure 5.2 The geometry of the simulated 1-3 piezoelectric ceramic composites in a 2D FE model, which composes the PZT-5H embedded with hard-set polymer material.

5.4.2 Parameter choice analysis

This Section provides an overview of the piezoelectric composite thickness mode parameters that are used to define the transducer microstructure prior to a detailed evaluation using PZFlex. The results presented here have been generated by CompD and have been used to guide the initial design phase for the piezoelectric composite transducer.

5.4.2.1 Aspect ratio

Prior to analyzing the complete composite structure, it was necessary to consider the vibrational and electromechanical characteristics of isolated pillars in the 1-3 connectivity composite structure. Importantly, the pillars' behaviour in a composite structure may be related to the influence of the passive polymer phase. A comprehensive study of composite pillar geometries in square, circular and triangular elements is introduced by Hayward *et al*. [129],[132]. There is a requirement to quantify the influence of the pillar aspect ratio on composite performance. The pillar aspect ratio can be defined as the ratio of the width to the height of the ceramic pillars [134],[135], as seen in Equation 5.2. This equation can be used to calculate the aspect ratio of a 1-3 piezoelectric composite structure.

$$AR = \frac{w}{h} = \frac{Pillar\ width}{height} \qquad 5.2$$

The relationship between the aspect ratio (AR) and the ceramic volume fraction specified for a suite of PZT-5H/hardset polymer composite structures, using a constant saw width of 0.12mm, is shown Figure 5.3. It is clear that the AR increases with ceramic volume fraction. The AR of a composite structure provides information of an upper limit, above which lateral mode activity is detrimental to thickness mode operation. Importantly, the ceramic pillar aspect ratio must be sufficiently low to minimize the influence of the inter-pillar resonance and promote homogeneous operation at the thickness mode [136]. This has led to the concept of maximum pillar aspect ratio (MPAR) which specifies the maximum value for a configuration of piezocomposites for a given volume fraction [129],[134].

For the proposed design, the pitch width and the saw width are 0.20mm and 0.12mm, which results in an aspect ratio (AR) of 0.085 for the 40% ceramic volume fraction device. This AR is significantly lower than the MPAR for a 40% CVF device and has been selected to minimise unwanted lateral resonances in the frequency band of interest (1-3MHz).

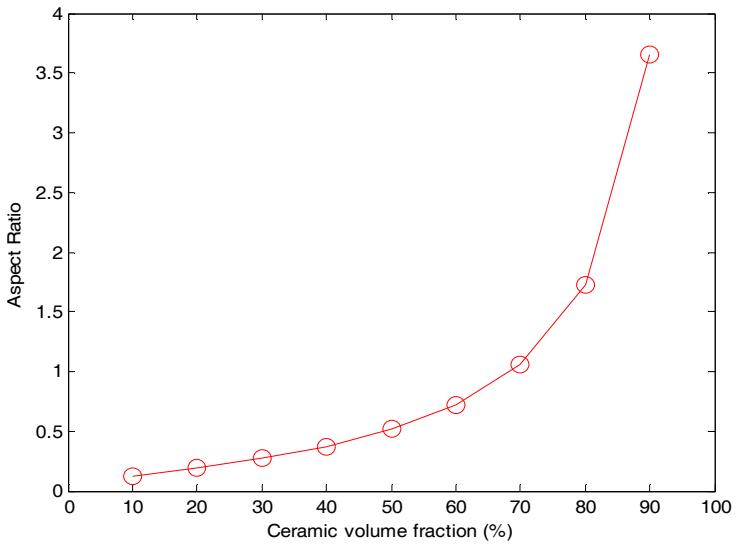

Figure 5.3 The relationship between aspect ratio and ceramic volume fraction, for constant saw width.

5.4.2.2 Electromechanical coupling coefficient

The electromechanical coupling coefficient [142] can be used to describe the efficiency of the energy transfer function of a transducer. The electromechanical coupling coefficient, k_t, is determined by using Equation 5.1. The coupling coefficient factor has been studied by Hayward for a 1-3 piezoelectric composite transducer [131]. The developed transducer is intended as a cavitation monitoring device which also provides a high electromechanical coupling coefficient. Therefore, this Section will provide predictions for various volume fractions of the coupling coefficients for a 1-3 piezoelectric composite transducer. The PZT-5H/hardset polymer composite is modelled with a saw width of 0.12mm and varying ceramic volume fractions of between 10% and 90%.

Figure 5.4 illustrates the electromechanical coupling coefficient factor of the PZT-5H/hardset polymer composite with ceramic volume fractions of 10-90%, obtained using CompD. In terms of the thickness-mode coupling constant, the composite is

superior in the ceramic volume fraction range between 40%-70%. The result in Figure 5.4 indicates that the highest theoretical volume fraction factor is approximately 0.7, which matches the general theory of piezoelectric composites [126]. Therefore, a volume fraction of 40-70% would be the most appropriate choice for use in the design of the transducer because it provides the maximum electromechanical coupling efficiency.

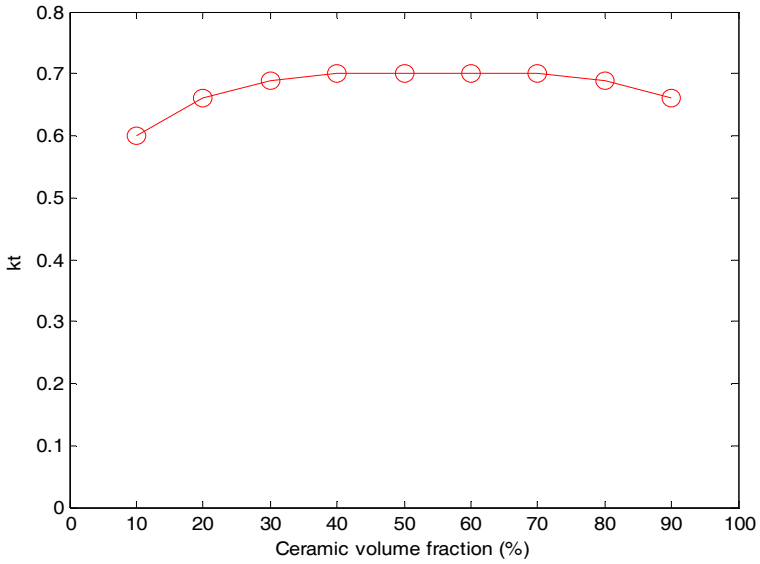

Figure 5.4 The electromechanical coupling coefficient as a function of the ceramic volume faction.

5.4.2.3 Velocity factor

Next, variation in thickness mode velocity for piezoelectric composite designs with ceramic volume fractions between 15-100% is predicted. Again, the saw width is kept constant at 0.12mm. Figure 5.5 shows the equivalent longitudinal wave sound speed in the thickness direction as a function of variations in ceramic volume fraction. The acoustic velocity of a PZT-5H/hardset polymer composite in the designed transducer increases relatively linearly between ceramic volume fractions of 40-80%. The velocity at the high end, about 90-100%, sweeps up due to the

stiffening of the ceramic pillar caused by lateral forces from the polymer [126]. The longitudinal wave speed determines both the operating thickness and acoustic impedance of the composite, in combination with the density of the material.

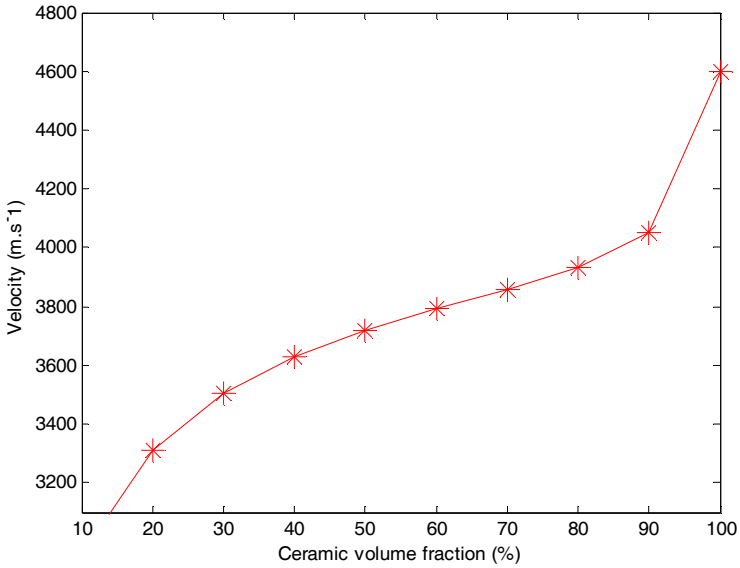

Figure 5.5 The wave velocity as a function of ceramic volume fraction.

5.4.2.4 Acoustic impedance factor

The final basic transducer parameter considered was the acoustic impedance of a piezoelectric composite [127]. Again, the ceramic volume fraction is varied from 10-100%, with a constant saw width of 0.12mm, and Figure 5.6 shows the behaviour of the composite acoustic impedance (Z) compared to variations in CVF from Figure 5.6. It is clear that the impedance variation and volume fraction increase linearly, except at the high end of 90-100%, where the clamping of the pillars causes it to sweep up at a faster rate. It is clear that the impedance of the piezoelectric composite is low when compared to a piezoelectric ceramic component (30 to 36MRayls) [137]. The particular piezoelectric composite impedance, which is a result of the variation of the ceramic volume fraction, is a significant factor in acoustic matching to the load medium. The acoustic impedance property of the 40% volume fraction, which is

selected for use in the transducer design, is approximately 13.4MRayls, and is far away from the specific acoustic impedance of Perspex, 3.2MRayls [119]. Therefore, the inclusion of a matching layer will be necessary to allow good energy transfer.

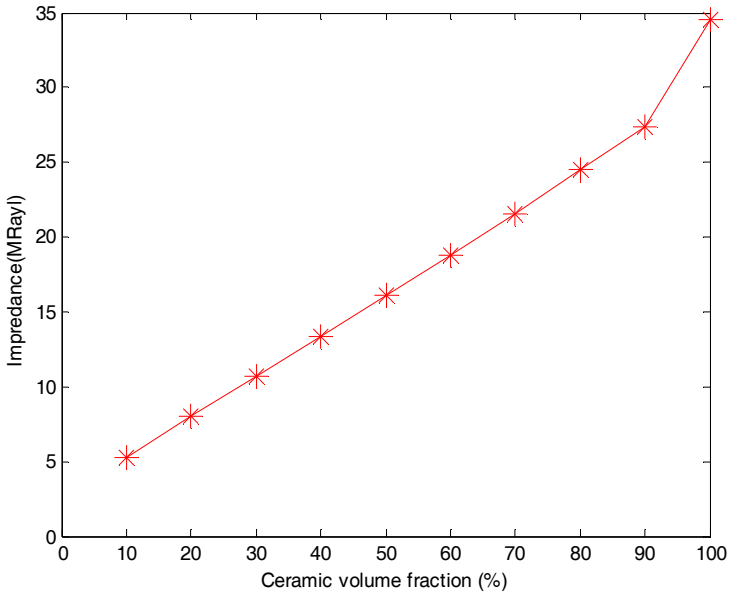

Figure 5.6 The acoustic impedance factor as a function of the ceramic volume fraction.

5.4.2.5 Summary of parameter choice results

Collating these thickness mode analysis results used to identify a suitable transducer configuration into Table 5.3, provides a useful overview of the key design metrics for the PZT-5H/hardset polymer composite. The results, such as the transducer aspect ratio, the thickness mode coupling coefficient and the acoustic impedance factor, are provided for the volume fraction range of 10% to 90% from the Table. However, this is only valid for the particular hard setting filler material and piezocermic design under consideration. The predicted variations in these parameters (AR, k_t, and Z) are directly related to the ceramic volume fraction. The CVF of 40% selected for use in this piezoelectric composite transducer is highlighted in Table 5.3.

Table 5.3 The properties of the piezoelectric composite material (AR, k_t, and Z) for different piezoceramic volume fractions.

CVF	Height (mm)	AR	k_t	Z (MRayls)
10%	0.73	0.10	0.62	5.276
20%	0.82	0.15	0.66	8.012
30%	0.87	0.22	0.69	10.06
40%	0.90	0.30	0.70	13.39
50%	0.93	0.41	0.70	16.08
60%	0.95	0.57	0.70	18.81
70%	0.96	0.84	0.70	21.58
80%	0.98	1.37	0.69	24.49
90%	1.01	2.92	0.66	27.81

Note: The piezoelectric composite properties of the different ceramic volume fractions for the PZT-5H/hardset polymer composites

5.4.3 Matching layer and backing block options

5.4.3.1 Overview of PZFlex Simulation model

This Section describes the adopted approach of FE modelling employed with a view towards evaluating the transducer constituent components. The model comprises the PZT-5H/hardset polymer composite, the quarter wavelength matching layer and an attenuative backing material. The 40% CVF PZT5H/hard set piezoelectric composite configuration, parameters shown in Table 5.2, is initially simulated to produce the electrical impedance characteristic without the addition of a matching layer or backing material. Details of all material properties are given in Tables 4.1 and 5.4, as used in FE modelling. The loss in materials is defined as a function of frequency and

defined at the frequency of 5MHz. It is assumed that FE modelling provides the perfect acoustic coupling between the piezoelectric composite transducer and the reactor wall and therefore, the ultrasonic coupling gel layer is ignored.

In Figure 5.7, the blue dashed line illustrates the predicted electrical impedance characteristic for the piezoelectric composite layer in isolation (i.e. no matching layer). It is clear that this piezoelectric material is unimodal and that the mechanical resonance frequency is at 2MHz. Moreover, the electromechanical coupling coefficient has been calculated to be 0.64 which is slightly less than the CompD predicted thickness mode k_t detailed in table 5.3. This is to be expected as CompD predicts the maximum theoretical value without taking the complex interaction between the active and passive phases into account. Please note that the additional results in Figure 5.7 will be discussed in next Section.

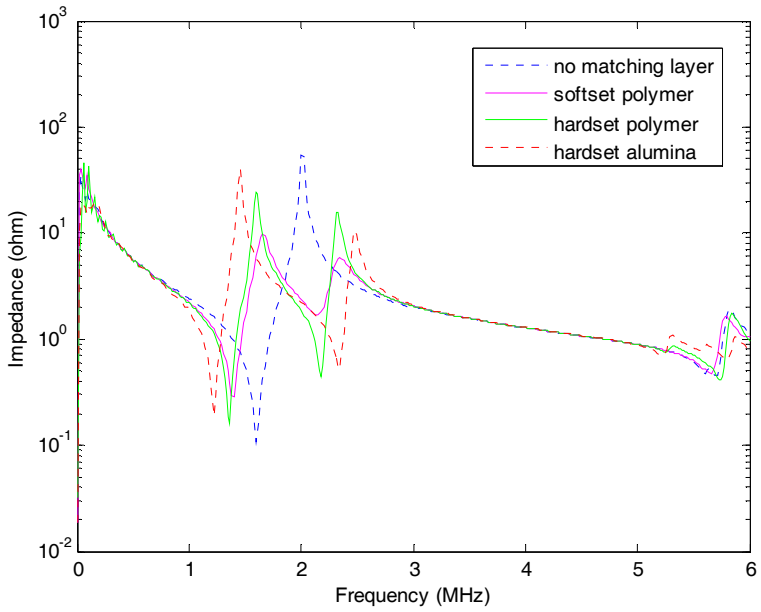

Figure 5.7 The impedance amplitude of the piezoelectric composite with the various matching materials – plotted on a logarithmic scale.

Table 5.4 The properties of materials used in the FE model [119],[120],[138].

Nemonic	Material	Longitudinal velocity	Impedance	Thickness
		m/s	MRayls	mm
Softset polymer	Vantico HY956/CY208	1989	2.32	0.249
Hardset polymer	Vantico HY1300/CY1301	2536	2.91	0.317
Hardset-alumina	Vantico HY1300/CY1301 +70% by weight Alumina	2999	6.92	0.375
PZT-5H/hardset polymer composite	PZT-5H/Vantico CY1301-HY1300 hardset piezocomposite	3629.5	13.39	0.95
Tungsten loaded epoxy	tungsten loaded (CY1301-HY1300) epoxy 25% volume fraction	1750	10.00	30.00
Titanium	Titanium	6100	27.33	0.763

Note: Perspex [119], steel and glass [120]. Softset polymer, Hardset polymer, Hardset-alumina, Tungsten loaded epoxy and Titanium [138].

(a) Matching layer

In order to improve transducer efficiency, it is usual to incorporate a matching layer between the active piezoelectric material and the load medium. In this case, the introduction of a matching layer between the reactor vessel wall and the front face of the 1-3 piezoelectric composite transducer was investigated. Traditionally, a quarter-wave matching layer of materials with an acoustic impedance calculated as the geometric mean between the transducer and load material is selected. For operation in a Perspex load, the geometric mean is calculated [122],[139] using Equation 5.5.

$$Z_m = \sqrt{Z_1 * Z_2} = 6.54 \quad \text{MRayls} \qquad 5.5$$

Where Z_1 is acoustic impedance of the first medium (the Perspex vessel wall = 3.2MRayls) and Z_2 is the acoustic impedance of the second medium (the piezoelectric composite transducer, 13.39MRayls from Table 5.3 at 40% CVF).

From the CUE materials database [119], hard-set alumina (Vantico CY1301-HY1300 + 70% by weight Alumina) has an acoustic impedance of 6.92MRayls [138]. This is the material with the acoustic impedance closest to the geometric mean value and is therefore used as the matching layer material. The thickness is determined using the quarter-wavelength (λ/4) acoustic matching layer technique. Details of the layer geometry, for operation at 2MHz, and acoustic properties are detailed in Table 5.4.

PZFlex was used to evaluate the electrical impedance for three matching layer conditions: Vantico HY956/CY208 (softest); Vantico HY1300/CY1301 (hardset) and hard-set alumina (Vantico CY1301-HY1300 + 70% by weight Alumina). These material properties and the λ/4 layer thicknesses used in the modelling are presented in Table 5.4. These three materials were selected as two of the standard polymeric materials used in CUE and the closest match to the theoretical geometric mean condition. Figure 5.7 shows the electrical impedance magnitude profiles for these different matching materials, along with the unmatched case. In each of the impedance profiles when the piezoelectric composite structure is combined with the matching layer, two distinct frequency resonance modes are observed. These modes are a result of the individual resonances of the piezoelectric layer and passive matching layer and are symmetrical around the centre point of the unmatched case.

(b) Backing layer

A backing layer is a damping block connected to the rear face of a piezoelectric transducer to reduce reverberation and hence, increase the device operational bandwidth. Ideally, the backing block should have an acoustic impedance matched to that of the piezoelectric layer and an ability to attenuate ultrasonic waves within the structure of the backing material. Thus, all the energy at the rear face of the piezoelectric layer will propagate into the backing material and nature of the backing material composition will attenuate all of this acoustic energy. Unfortunately, the addition of a backing layer will reduce the transducer sensitivity as energy is dissipated in the backing material. Hence, a lower acoustic impedance backing material is usually used as a compromise between sensitivity and bandwidth. It is, therefore, necessary to model the device with an applied backing layer in order to evaluate the predicted bandwidth improvement, noting that the objective of this work is to design a piezoelectric composite transducer with a 100% bandwidth centred around 2MHz.

The CUE materials database was used again and tungsten loaded epoxy (25% volume fraction) with the acoustic impedance of 10MRayls [138] was selected as it is close to the impedance of the PZT-5H/hardset polymer composite (13.39MRayls). Now, FE modelling was used to consider the performance of the backing layer when attached to the piezoelectric composite material using a pulse-echo response configuration: note that this is also used in the experimental evaluation in Section 5.5.2. In this operational scenario, the transducer is used to generate the ultrasonic pulse and the reflected signal, from the back-wall of a Perspex load material, is received by the same device. Moreover, the matching layer configuration discussed in the previous Section, $\lambda/4$ hard-set alumina layer, is included in the model. Again, the properties of the tungsten loaded epoxy in given in Table 5.4.

Figure 5.8 presents the simulated received spectral characteristics of the piezoelectric composite transducer both with and without a backing layer. The results shown in

this Figure have been normalised in order to illustrate the improvement in bandwidth characteristics for the transducer as predicted by PZFlex. The trace without a backing layer has two amplitude peaks due to the resonances in the transducer and matching layer. This is because the matching layer was designed to maximise performance when the device is acting as a receiver and in this simulation, the transducer operates in pulse-echo mode. The peak amplitude decreases when the backing layer is added, but the bandwidth of the transducer increases significantly. The centre frequency of the spectral response when the backing layer is included is around 1.5MHz, which has reduced from the expected 2MHz due to the complex interaction between the constituent materials in the transducer. Nevertheless, the -6dB bandwidth extends from 0.8-2.4MHz, which equates to an operational bandwidth in excess of 100%. Thus, it is concluded that this matching layer and backing material combination is appropriate for use in the cavitation monitoring transducer.

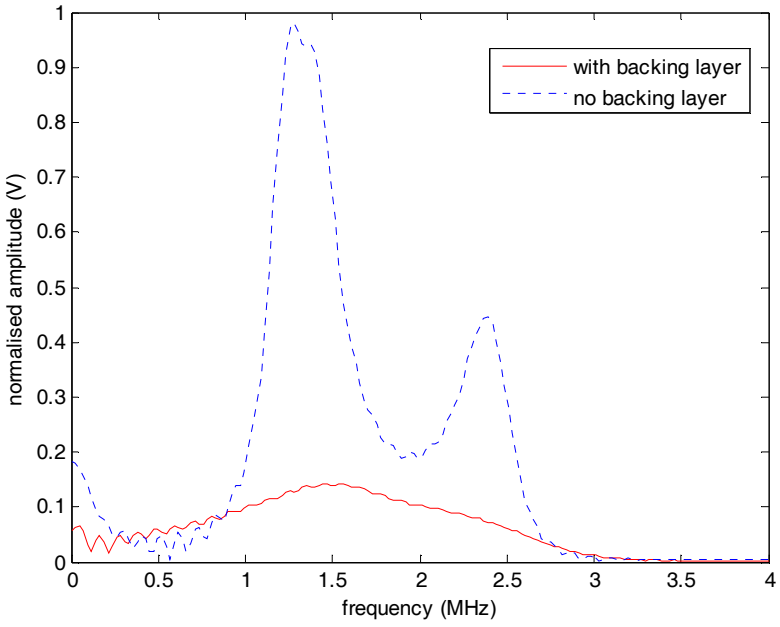

Figure 5.8 The FE derived spectral amplitude of the piezoelectric composite transducer with backing layer and no backing layer.

5.4.4 Transmission-Reception analysis

The fundamental behaviour of the piezoelectric composite transducer is described by different performance parameters, AR, k_t, v, and Z, described in Section 5.4.2. However, it is possible for a general ultrasonic transducer to operate in two modes: transmission and reception. It is vital to evaluate the effectiveness of the transducer operating under both the reception and transmission conditions to ensure optimal performance for the desired application [139]. Under the transmission or reception mode conditions, the relationship between the complex input voltage of the transducer $\hat{V}_{in}(\omega)$ and the average output pressure $\hat{P}_{out}(\omega)$ generated across the front face of the ultrasonic transducer produces transmission sensitivity, $S_{TX}(\omega)$, [139] which is given as;

$$S_{TX}(\omega) = \left|\frac{\hat{P}_{out}(\omega)}{\hat{V}_{in}(\omega)}\right| \qquad 5.3$$

The reception sensitivity under reception conditions, $S_{RX}(\omega)$, has a similar condition, written [139] as;

$$S_{RX}(\omega) = \left|\frac{\hat{V}_{out}(\omega)}{\hat{P}_{in}(\omega)}\right| \qquad 5.4$$

Where the complex pressure incident on the whole front transducer surface is defined by $\hat{P}_{in}(\omega)$, the complex output voltage generated by this complex pressure is defined by $\hat{V}_{out}(\omega)$.

In order to predict and optimize the performance of the transducer in transmission and reception modes, the finite element analysis code PZFlex is employed to simulate the transducer's behaviour under typical operating conditions. The relative performance of the piezoelectric composite transducer was investigated across the ceramic volume fraction range and high peaks in sensitivity at specific volume

fractions are anticipated. However, the transducer is designed to be a receiver and thus, the received performance of the device is of primary interest.

5.4.4.1 Simulation model of Transmission-Reception analysis

This Section describes the adopted approach of FE modelling employed with a view towards verifying the FE code PZFlex for more practical arrangements. The performance of the broadband transducer was examined under its transmission and reception modes of operation [139]. The simulation model used for transmission-reception analysis, including the piezoelectric composite transducer and the reactor wall, is depicted in Figure 5.9. The modelling diagram comprises the PZT-5H/hardset polymer composite, the quarter wavelength of hardset alumina material (Vantico HY1300/CY1301 +70% by weight Alumina with the acoustic impedance of 6.96MRayls) as the matching layer, tungsten loaded epoxy as the backing material. The load was a water filled reactor vessel comprising 10mm thick Perspex walls. Initially, the model is used to analyse the effect of Perspex used as the wall material, which is then extended to glass and steel, materials commonly used in practical reactor vessels [105],[115]. The performance of the various ceramic volume fractions in the range of 15%-90% were investigated to confirm the choice of 40% CVF used in this design. The loss in materials is defined as a function of frequency and defined at the frequency of 5MHz. It is assumed that FE modelling provides the perfect acoustic coupling between the piezoelectric composite transducer and the reactor wall and therefore, the ultrasonic coupling gel layer is ignored.

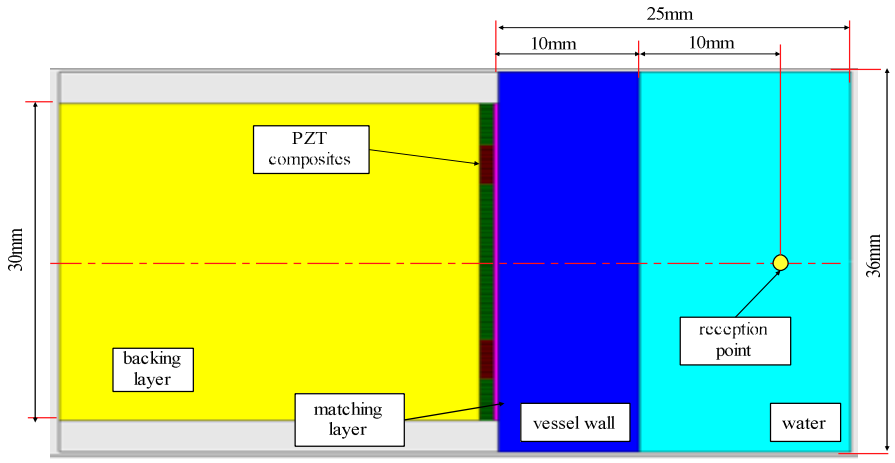

Figure 5.9 The schematic simulation model of the finite element analysis for analysing PZT-5H/hardset polymer composite transducer.

The application of a piezoelectric composite transmitter in generating an approximate planar pressure impulse on the front face of the load medium is considered. The acoustic wave generated by the transducer propagates through the reactor vessel wall and into the load medium. The sound pressure generated by the piezoelectric composite transducer is detected at the reception point at a distance of 10mm away from the inner surface of the reactor wall. The system model, depicted in Figure 5.9, is used to investigate the transmission performance of the piezoelectric composite transducer.

The reception mode of the transducer [139],[140], which is the more important operational mode for this work, is considered by detecting the pressure pulse wave generated by a virtual source. A diagram of the simulation model using reception mode is shown in Figure 5.9, expect the reception point is replaced in the model by a line source. In this case, a series of pressure loading points are located in a line 10mm from the inner wall of the reactor. Each source is driven in phase using the standard 1-7MHz linear chirp described in Chapter 4. During the simulation process, the reactor wall material was changed from Perspex to glass and steel in order to study the influence of the wall material.

The piezoelectric composite parameters shown in Table 5.2, and details of all material properties given in Tables 4.1 and 5.4, are used in FE modelling. Moreover, the transducer configurations used to model the system under different wall material conditions are given in Table 5.5.

Table 5.5 Combination of transducer materials used in FE model.

Wall material	Piezoelectric composite material	Matching material	Backing material
Perspex	PZT-5H/hardset polymer composite	Hardset-alumina	Tungsten loaded epoxy
Steel	PZT-5H/hardset polymer composite	Titanium	Tungsten loaded epoxy
Glass	PZT-5H/hardset polymer composite	N/A	Tungsten loaded epoxy

5.4.4.2 Transmission-reception simulation results

Normalized transmit pressure levels, measured at the reception point in Figure 5.9, for the designed piezoelectric composite transducers (i.e. incorporating both matching and backing layers) are shown in Figure 5.10. Variation in the peak transmission output as a function of the ceramic volume fraction may be observed. The correlation of transmission operation between theory and experiment was observed by Hayward *et al.* [131],[136]. In general, it is often assumed that piezoelectric composite devices represent the optimal configuration due to their combination of a high coupling coefficient factor and good acoustic matching to a load medium. From Figure 5.10, it is evident that ceramic volume fraction of 40% to 60% possess the best driving performance as a result of the compromise between the coupling coefficient, electrical permittivity and acoustic matching to the reactor wall. Hence, the PZT-5H/hardset polymer composite transducer will operates most efficiently at the electrical resonance due to minimum impedance. A high volume

fraction would give rise to an improved transmission output. Nevertheless, the ceramic volume fraction of 10-30% gives low peak transmission due to the influence of the high ceramic volume fraction.

Figure 5.11 illustrates the variation in the reception impulse response for the piezoelectric composite transducer. It is clear that for all three wall materials modelled, the maximum receive sensitivity occurs at a 40% ceramic volume fraction. As stated previously, this is an important result as the transducer is to be deployed as a receiver in a cavitation monitoring system. Hence, the designed transducer which uses a 40% CVF piezoelectric composite active layer is appropriate for use across a wide range of reactor wall materials. This result confirms the validity of the piezoelectric composite design developed in this Chapter. For clarity, the relative reception performance for a 40% CVF has been extracted and illustrated in Figure 5.12. The evaluation phase for the designed transducer once fabricated will use a Perspex vessel. Nevertheless, the same device could be used in either a glass or steel walled reactor with reductions in sensitivity of 24% and 40%, respectively.

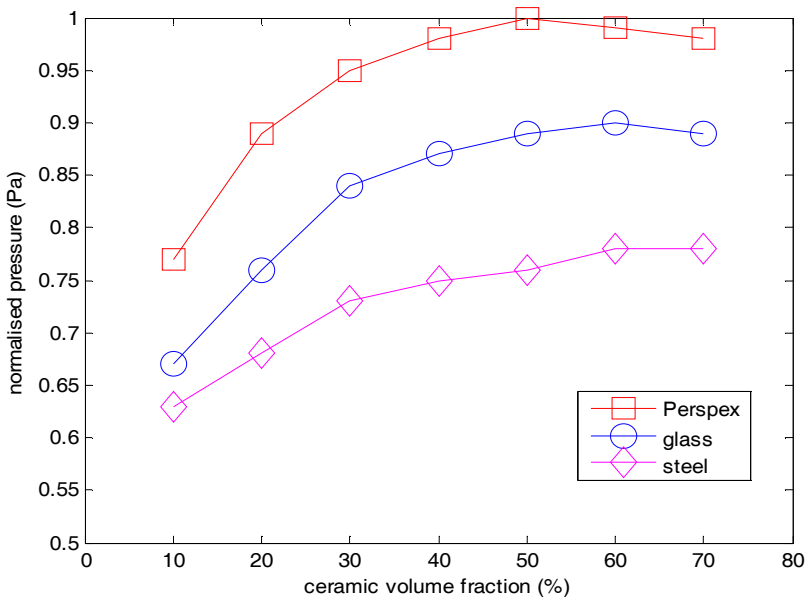

Figure 5.10 The derived FE relationship between transmission pressure and CVF from different wall materials: glass, Perspex and steel.

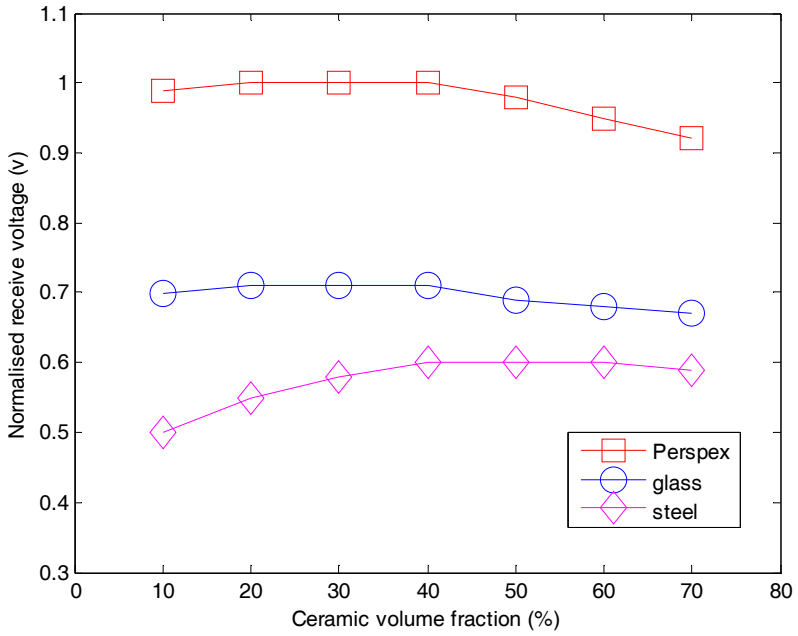

Figure 5.11 The derived FE relationship between received voltages of the PZT-5H/hardset polymer composite transducer and CVF from the different wall materials: glass, Perspex and steel.

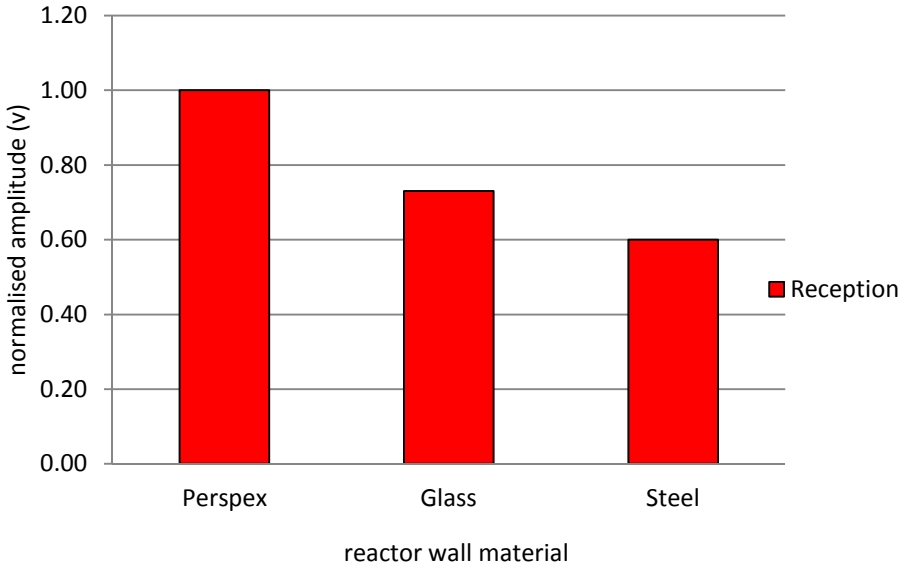

Figure 5.12 PZFlex derived reception performance for a 40% ceramic volume fraction of PZT-5H/hardset polymer composite under reception conditions.

5.5 Transducer manufacturing

The 1-3 connectivity piezoelectric composite transducer used in this work was manufactured using the information gained from FE modelling, as discussed in Section 5.4. The ceramic volume fraction of 40% was selected to provide the maximum energy transfer as a reception device, using a mechanical 0.20mm pitch width, and 0.12mm saw width. The ceramic block was lapped to a thickness of 0.95mm in order to produce the desired frequency of operation for the composite of 2MHz. The piezoelectric composite incorporates a combination of PZT-5H and a hard-set polymer phase (Vantico HY1300/CY1301). Evaporated gold electrodes were applied to both faces. An alumina loaded hardset epoxy layer (Vantico HY1300/CY1301 + 70 % by weight Alumina) of thickness 0.375mm was added directly onto the front face of the active layer and a 30mm thick tungsten loaded epoxy (25% volume fraction material) was added as a backing layer onto the rear of the device. The piezoelectric composite block was placed in the holder case and external electrical connections made using coaxial cable soldered to the transducer surfaces. The exit hole for the coaxial cable at the rear of the holder was sealed using

5-minute epoxy and a BNC male connector incorporated into the end of the cable to facilitate connection to appropriate instrumentation. Photographs of the fabricated piezoelectric composite layer and the finished transducer are depicted in Figure 5.13. It should be noted that in Figure 5.1.3 (a) a failure area at the centre of front surface in the fabricated piezoelectric composite block is evident. This represents an effective loss in thickness due to the lapping stage of the manufacturing process. This will degrade the overall performance of the transducer, but due to time constraints it was decided to continue with the characterisation and experimental evaluation using this device.

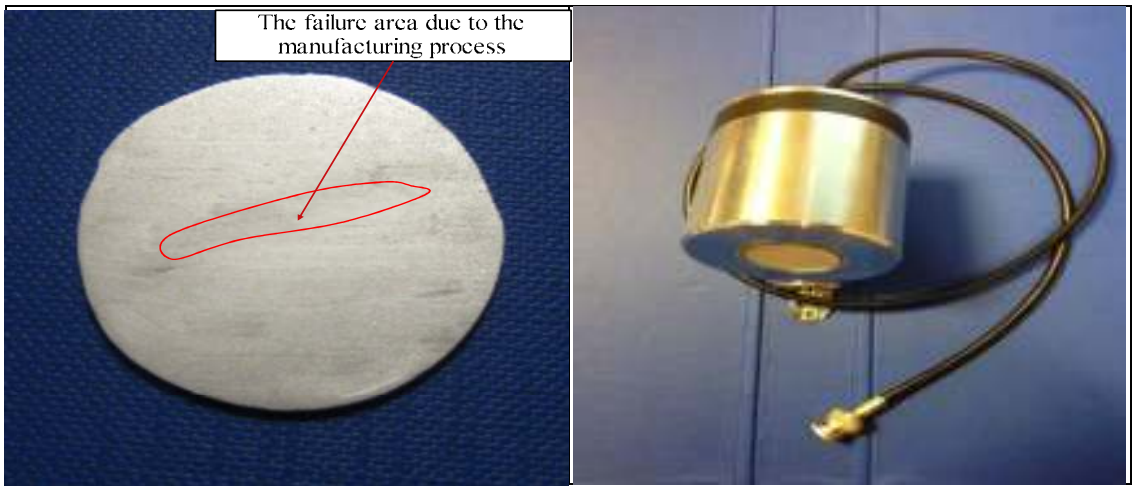

(a) (b)

Figure 5.13 The piezoelectric composite prototype transducer: (a) fabricated piezoelectric composite block (b) the finished transducer.

To characterise the transducer, the electrical impedance and surface displacement profile (SPD) measurement have been taken using an HP-4194A electrical impedance analyser and OFV-056 Scanning Vibrometer system, respectively. In addition, the pulse-echo response of the transducer is experimentally measured to evaluate the sensitivity and bandwidth of the device.

5.5.1 Resonance analysis

The nature of the designed transducer's resonance modes is identified using electrical impedance measurements. The measured modulus of impedance and phase profile of the transducer's electrical impedance was acquired for the piezoelectric composite layer only, i.e. without a matching layer, and is illustrated in Figure 5.14. In addition, the PZFlex predicted electrical impedance is also presented in this Figure.

Importantly, the transducer was designed to operate in reception at the frequency of 2MHz. With reference to Figure 5.14(a), this is identified as the peak in the electrical impedance mode and is clearly defined in the simulated result. Moreover, the minimum impedance of this mode is the electrical resonance mode, where the transducer would operate most efficiently as a transmitter. From Figure 5.14, it is clear that the manufactured piezoelectric composite is sub-optimal. Importantly, the mechanical resonance frequency is matched in both simulation and experimental datasets, although the actual electrical impedance is lower in the manufactured device. This could reduce the transducer efficiency when operated as a receiver, but will depend on the input impedance of the pre-amplifier stage connected to the device. Although this necessarily does not have a negative influence on the ability of this transducer to perform adequately for the proposed cavitation monitoring application, there are three issues with the measured data from the fabricated piezoelectric composite layer.

- The electrical impedance magnitudes for the electrical and mechanical frequencies do not match the simulated values and will have an impact on the transmission and reception performance of the transducer.
- The shift in the electrical resonance frequency from the predicted 1.45MHz to 1.6MHz will result in a lower electromechanical coupling coefficient (0.51 for the manufactured device).
- The slope of the electrical impedance profile for the fabricated device indicates that the damping between the simulated and manufactured device is significantly different. It is considered that this will be due to inconsistencies

in the manufacturing process rather than incorrect modelling data, as the PZFlex material data files have been extensively researched over many years [126],[127],[128],[129],[130].

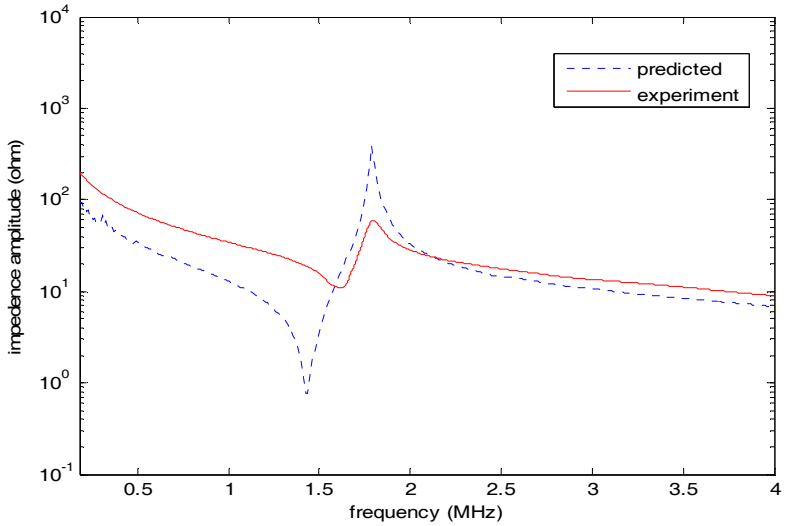

(a) Electrical impedance

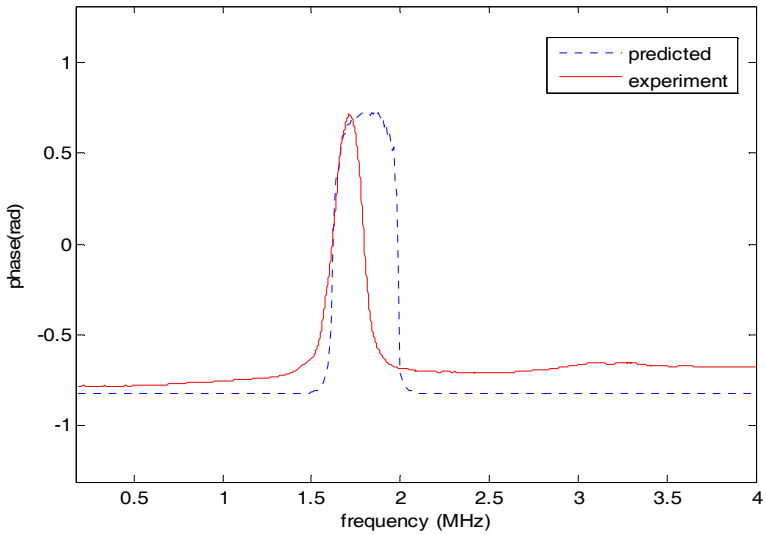

(b) Phase

Figure 5.14 Electrical impedance profile of the fabricated piezoelectric composite transducer from experiment and PZFlex modelling – plotted on on a logarithmic scale.

The next stage of the transducer characterisation process involves measuring the surface displacement properties of the material at its thickness resonance mode. Importantly, the design process for the piezoelectric composite material selected a low aspect ratio configuration to ensure that any inter-pillar resonances occur far away from the fundamental thickness mode and consequently will have little impact on the transducer's performance [128]. To check this, consideration of composite displacement is necessary in the characterisation of the transducer. The surface displacement profile (SDP) is obtained by driving the transducer at the electrical resonance frequency, identified on the electrical impedance profile shown in Figure 5.14. The OFV-056 Scanning Vibrometer system is used in the experiment to evaluate the surface displacement profiles and the uniformity of the transducer displacement.

The SDP is acquired by driving the fabricated piezoelectric composite layer only, with a 1.6MHz continuous sine wave. The laser vibrometer is used to detect the surface vibration, as described in Section 3.3. Figure 5.15 shows the SDP magnitude and phase measured from the designed piezoelectric composite transducer at the electrical resonance frequency of 1.6MHz. From the Figure, it is clear that the piezoelectric composite material has been damaged, as shown earlier in Figure 5.13. There is an inactive band through the centre of the material and this will impact on the performance of the device. Even though the transducer is designed to operate in reception mode, its behaviour when acting as the transmitter was tested to assure that the transducer displacement is uniform and unimodal in the thickness resonance mode. In the phase measurements, shown in Figure 5.15(b), the uniform movement of the transducer surface is a clear indication of the efficient operation of the transducer. This statement has ignored the inactive band within the device, but indicates that the transducer has potential to operate as an effective transducer.

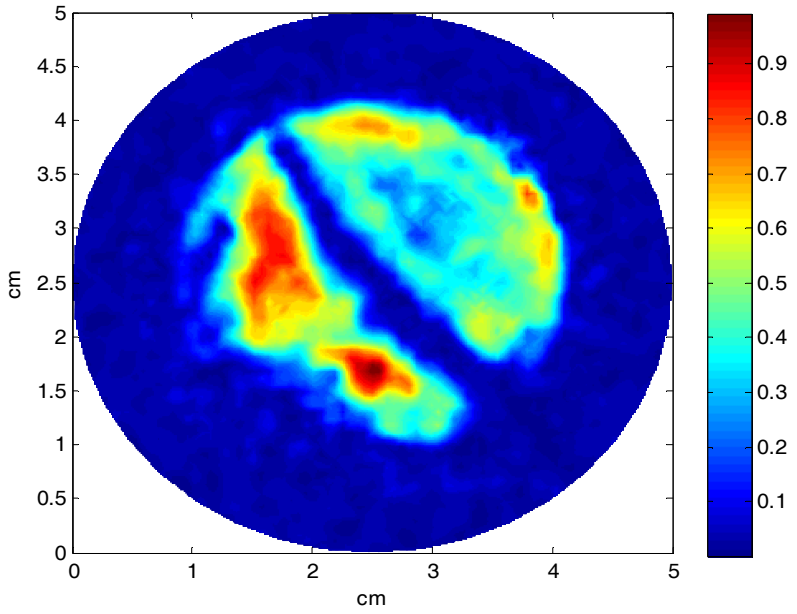

(a) Measured surface displacement

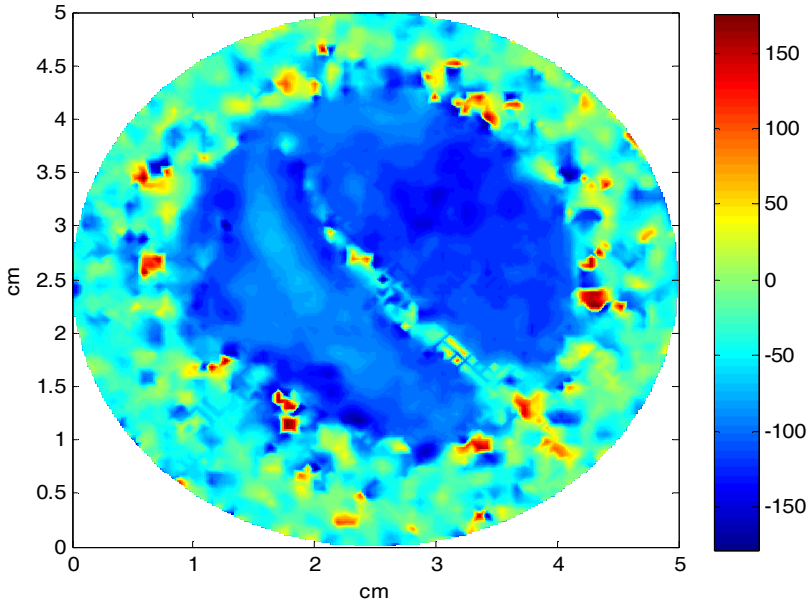

(b) Measured phase of the surface displacement

Figure 5.15 Experimental surface displacement profile of the fabricated piezoelectric composite transducer.

5.5.2 Sensitivity and bandwidth analysis

It is vital to investigate the sensitivity of the sensor as this indicates the ability of the transducer to operate effectively in the proposed monitoring system. Even through the transducer will be operated in reception mode, measurement of the pulse-echo response [141] is relatively straight-forward to measure experimentally. The transducer was placed into a water bath and a glass block positioned 60mm. The transducer both generates the ultrasonic propagating wave and detects the echo from the test block. A UT340 (Utex, USA) was used to drive the transducer with a wideband pulse and receive the echo with the gain setting set to 0dB. The time domain signal acquired in this test is shown in Figure 5.16. Also, presented in this Figure is the simulated echo using PZFlex. Reasonable agreement is observed in the main pulse shown in Figure 5.16, although the tail of the signal extends further in time for the experimental measurement. Figure 5.17 presents the corresponding frequency spectrum for each time domain trace in Figure 5.16. It is clear that the extended time domain signal associated with the experimental transducer has reduced the expected bandwidth of the transducer. In fact, instead of the single broad spectral characteristic predicted by modelling, the measured pulse-echo response has three distinct peaks at frequencies of 0.75MHz, 1.6MHz and 2.8MHz. Obviously, the operational bandwidth is significantly reduced, but this measured result demonstrates that the fabricated transducer will acquire spectral components across the intended frequency range of 1-3MHz. So, although it is clear that the manufacturing was not successful with regard to 100% bandwidth between 1-3MHz, the transducer is able to be deployed as a cavitational monitoring device over this frequency band. The main issue will be in the relative weighting of spectral components across the frequency band, but this may not adversely influence the operation of the device as the accumulative power in the frequency band associated with the cavitational acoustic emission will be used to quantify the extend of the cavitational field.

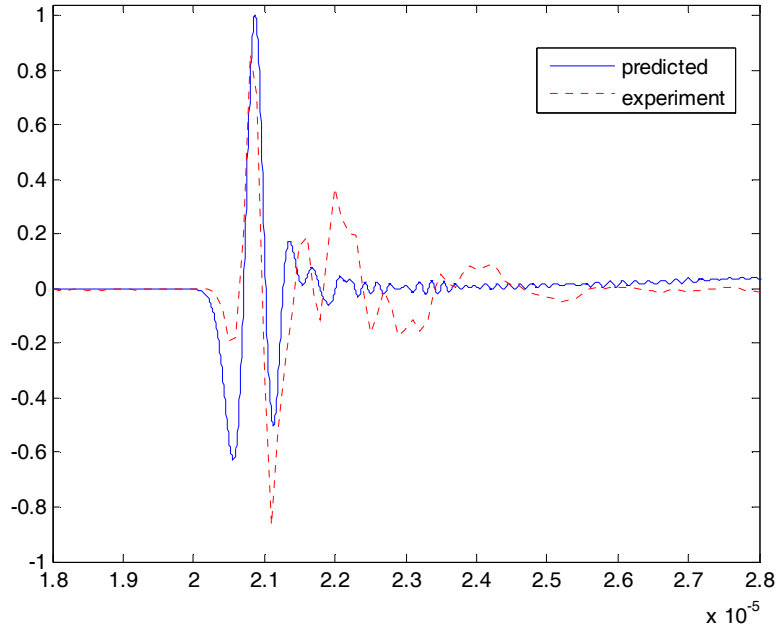

Figure 5.16 Comparison of experimentally measured and PZFlex derived reception response from a glass reflector immersed in water.

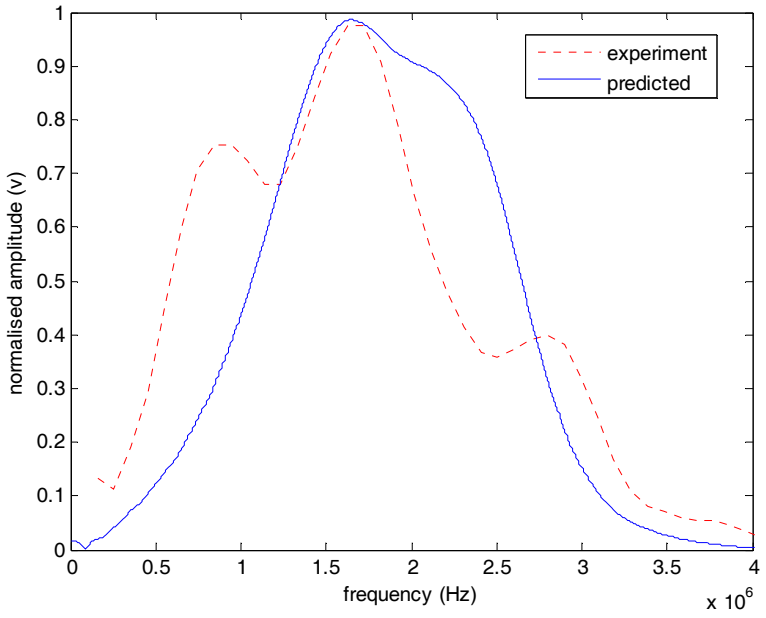

Figure 5.17 Normalised amplitude obtained by experiment and the PZFlex model.

5.6 Summary

Using the results from the model-based approach to investigate the ability to measure cavitation activity within a reactor vessel, as described in Chapter 4, were used to design an ultrasonic receiver for use in such a cavitation monitoring system. The finite element modelling platform, PZFlex, was used in the design process to check the transducer operation, especially when matching and backing layers were included and when the transducer is configured to operate when attached to the outer wall of a reactor vessel.

A 1-3 connectivity piezoelectric composite transducer was designed to operate at 2MHz with an operational bandwidth of 100%. The piezoelectric composite microstructure (40% CVF) was demonstrated to be applicable to a range of wall materials. Moreover, both matching and backing materials were identified and simulated to analyse their influence on the performance of the transducer. The complete transducer design was fabricated in the CUE workshop, but the characterisation process highlighted manufacturing faults with the device. Nevertheless, it is considered that the transducer will have sufficient sensitivity across the frequency range 1-3MHz to be used in the subsequent experimental evaluation of the cavitation monitoring system approach. Consequently, the use of the fabricated piezoelectric composite transducer on a Perspex walled high power ultrasonic reactor will be described in Chapter 6.

CHAPTER 6

Development of a broadband non-invasive transducer measurement system to monitor acoustic cavitation

6.1 Introduction

As has been described in the previous chapters, a liquid medium is influenced by high intensity ultrasound, acoustic cavitation generally occurs. During the cavitation process, the collapse of bubbles produces intense local temperatures and high pressures. This leads to mechanical and chemical phenomena [25]. The cavitation events, including bubble jetting and shock wave generation, can cause substantial surface damage and high surface temperatures to components with the cavitating field. Moreover, the cavitation process produces cavitation effects such as erosion [1], sonoluminescence [62] and sonochemical and biological effects [20]. There is

much research concerned with cavitation measurements in order to evaluate the influence of the effects of cavitation [8], [72]. It is believed that the measurement of cavitation activity will provide a guide for the improvement of process control and safety conditions.

Measurement methods for cavitation activity and acoustic pressure output generally insert the sensor within the high pressure field associated with cavitation events [8], [59]. The measurement methods are often inadequate, due to the effects of cavitation. The measurement device can be damaged by the high acoustic pressures associated with the occurring cavitation [41]. Therefore, a non-invasive technique is an attractive proposition.

The employment of a non-invasive measurement technique, based on acoustic emission, to monitor industrial processes using particle interaction within a reactor vessel using the finite element (FE) technique has been reported [117]. This modelling approach provides a better understanding of the frequency range for the acoustic emission monitoring of the heterogeneous system under investigation. Importantly, an acoustic monitoring technique is desirable for more effective process control. Hence, a non-invasive monitoring system is an attractive measurement technique to monitor acoustic cavitation activity within the reactor vessel. Significantly, modelling the influence of the cavitation on the reactor vessel was successful and is discussed in Chapter 4.

The acoustic emission technique is based on the detection and conversion of high frequency elastic waves, generated by the system itself, to electrical signals through the piezoelectric effect associated with the ultrasonic transducer. A development of the acoustic emission system for heterogeneous process monitoring is presented by Besenyei *et al.* [123]. The acoustic emission can be measured by a passive technique and yield information on the physical properties of a sample such as viscosity,

particle size, density or displacement [123]. Acoustic emission approaches, based on a non-invasive technique, are useful for process monitoring and control as the sensor is not in direct contact with the sample. The acoustic emission methods in some cases rely on the employment of a waveguide [123]. Acoustic emission measurements relying on non-invasive methods are of particular interest in process analysis as, in principle; the acoustic sensor is attached to the outside of the reactor vessel and does not influence or impact on the reaction itself. .

The information that can be derived from acoustic emission signals is dependent on the frequency range of the transducer and the way in which the signal is acquired. The information content, acquired across a wide frequency range is collected using a transducer to measure variations in both emission frequency and amplitude. The use broadband acoustic emission in the study of chemical reactions was conducted by Nordon [116] for the monitoring of particulate system and has also been used in the study of acoustic cavitation [9],[10],[20].

These examples illustrate the potential for the acoustic emission approach to be used to monitor cavitation activity occurring inside a reactor vessel. The broadband acoustic spectrum signal detected can be analysed to provide information on the cavitation activity [10],[68],[142].

This Chapter describes the implementation of a non-invasive measurement system to monitor cavitation, using a broadband transducer attached to the outer wall of the reactor vessel. In particular, the transducer is designed to acquire the acoustic emission signals generated by the cavitation activity over a wide frequency range. The cavitation activity has been investigated, with particular attention paid to the information content of the broadband acoustic measurement. Hence, the potential usefulness of the measurement technique for process monitoring and control has been evaluated. The first Section of this Chapter provides a simulation of the

measurement system using finite element analysis to predict whether the acoustic emission signal produced by the acoustic cavitation can be detected by the piezoelectric composite transducer designed in Chapter 5. The last Section describes the experimental evaluation of the developed non-invasive monitoring system and the cavitation activity analysis, which is calculated by broadband integrated energy (BIE) in the frequency range of 1-5MHz. A comparison of cavitation measurement techniques is obtained for the non-invasive optical measurement system, the NPL cavitation sensor and the non-invasive transducer measurement system. Overall, the acoustic emission presents a good approach for monitoring cavitation and the successful application of the developed non-invasive measurement system is presented.

6.2 Finite element modelling of the cavitation measurement system

This Section provides the simulation model for the developed non-invasive measurement system described in Chapters 4 and 5, with PZFlex used to predict the operation of the cavitation monitoring system. A full FE model is utilised, including the components of the piezoelectric composite transducer employed as the cavitation sensor. Here, the aims of the FE modelling are to predict that the non-invasive measurement system would operate as expected and to evaluate the performance of the designed piezoelectric composite transducer. A 2-D simulation model was developed to reduce the complexity of the cavitation monitoring system. Figure 6.1 depicts a schematic of the simulation model used to model the non-invasive measurement system, reactor vessel and source of cavitation in the liquid load medium.

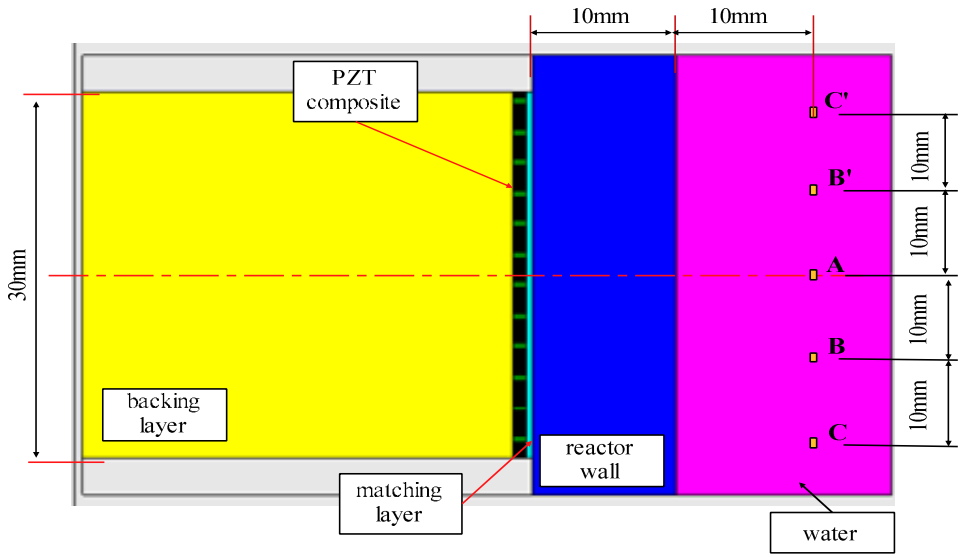

Figure 6.1 Schematic of the FE simulation model for the developed non-invasive measurement system.

The simulation model is established in 2-D and hence is equivalent to a rectangular reactor vessel. Initially, the reactor vessel wall is made from Perspex, but glass and steel materials are also simulated to provide information on more practical materials for use in an industrial application. The properties of the materials used are shown in Tables 4.1 and 5.4, and in all cases the wall thickness is 10mm. The reactor vessel is filled with water and five dipole transmission sources A, B, B', C and C' are positioned 10mm away from the vessel wall to simulate individual acoustic emission events associated with cavitation. As described previously in Chapter 4, the AE signal has been simulated using a linear chirp signal, over the frequency range 1-7MHz. Moreover, the lateral distance between dipole sources is 10mm. The piezoelectric composite transducer is modelled as the piezoelectric composite layer, backing layer and matching layer, as described in Section 5.4, and is attached to the external wall of the reactor vessel. It should be noted that the matching layer configuration is changed, in accordance with Table 5.5, when a different reactor wall material was modelled. The ultrasonic gel in FE modelling is ignored due to the perfect acoustic coupling between the piezoelectric composite transducer and reactor wall. The model investigated sound pressure variation of the transmission sources,

over the input power range of 10-40W. The output of the model is the converted voltage signal from the piezoelectric composite transducer. The PZFlex FE model suite will match loss across a broad range of frequencies and the material loss parameters are set in the material file at the frequency of 5MHz. The material properties in the modelling can be found in Tables 4.1 and 5.4.

Figure 6.2 shows a snapshot of the simulated ultrasonic wave propagation in the model for single and multiple source excitation schemes. The sound wave is emitted from the source and incident on the wall of the reactor vessel before the complex wave structure in the solid wall material is detected by the piezoelectric composite transducer. It is shown that the sound wave from a single transmission source is a spherical sound wave and when all five transmission sources are active the field profile is more complex in the water load. The acoustic spectra obtained will vary with input position and in accordance with the horizontal symmetry of the model. The spectra obtained at the positions B-B' and C-C' produced identical results. Thus, the results of AE signal are shown for positions A, B and C only. Moreover, the most challenging case, in terms of sensitivity, was considered to be the single source scenario and this has been used in the remaining simulations in this Section.

The following Figures illustrate the simulation results for the predicted AE spectrum obtained for the three different wall materials of interest: Perspex (Figures 6.3 and 6.4), glass (Figures 6.5 and 6.6) and steel (Figures 6.7 and 6.8). The Figures are presented in pairs and represent the model output for each material when the input power and number of cavitation sources are varied. The AE signal observed in each Figure has been modified by the transfer function of the vessel wall and of the piezoelectric composite transducer. It can be observed that the predicted acoustic emission is in the frequency range of 0.5-4.0MHz. In Figures 6.3, 6.5 and 6.7 the single transmission source has produced acoustic spectra at the receiver, at power input levels of 10, 20, 30 and 40W. The predicted AE amplitude of Perspex and glass is higher than that of steel due to the lower acoustic impedance and attenuation of

these materials. Interestingly, the amplitude of the predicted acoustic emission is directly related to the sensitivity of the piezoelectric composite transducer in each scenario. Figures 6.4, 6.6 and 6.8 depict the AE spectrum with the wall materials of Perspex, glass and steel, respectively, when multiple transmission sources are excited. The peak of the acoustic emission is each simulation scenario shows a similar trend.

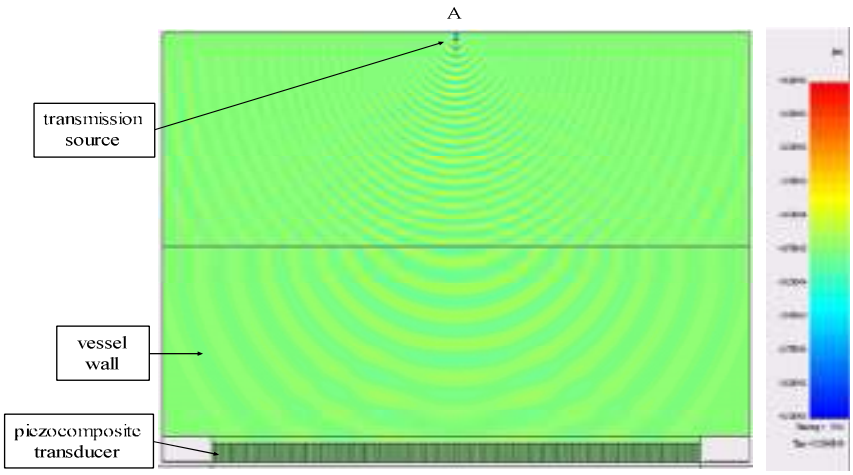

a) Generated by a single transmission source, A.

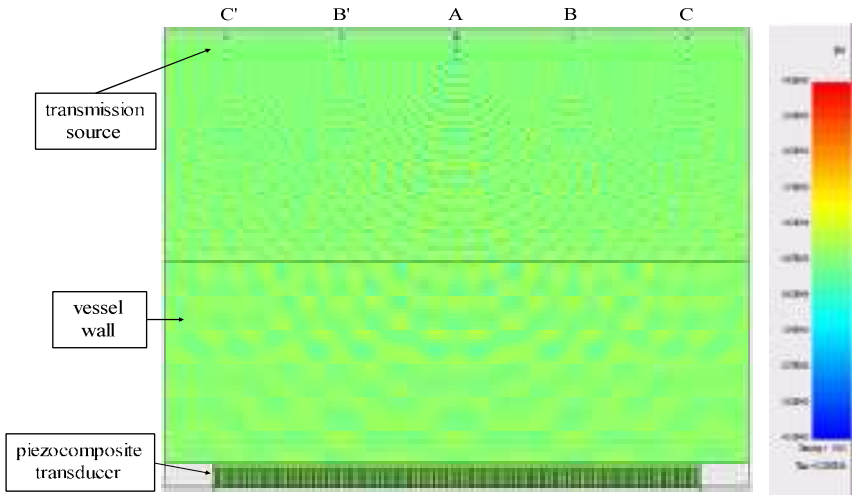

b) Generated by transmission sources: A, B, B', C and C'.

Figure 6.2 Propagation of the ultrasonic wave generated by (a) one transmission source and (b) all transmission sources of cavitation.

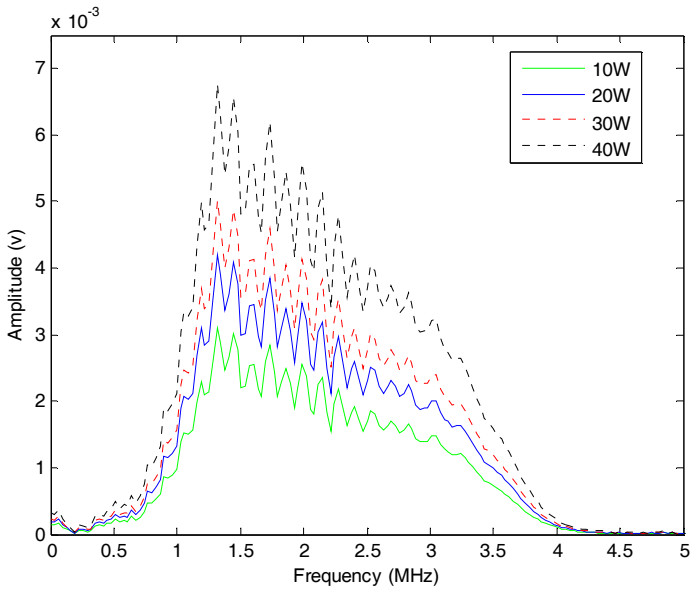

Figure 6.3 The FE derived AE spectrum obtained by the simulated piezoelectric composite transducer from FE model. The AE produced at the transmission source A with the various power inputs of 10-40W propagates through the Perspex wall of the reactor vessel and is detected by the piezoelectric composite transducer.

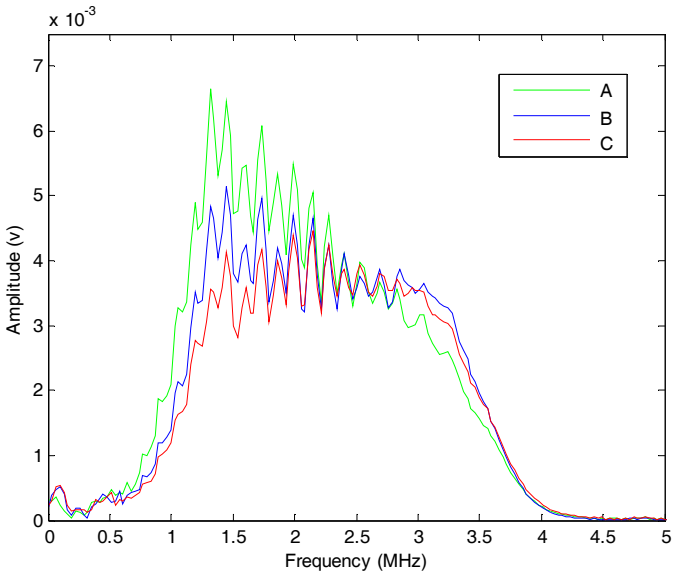

Figure 6.4 The FE derived AE spectrum detected by the simulated piezoelectric composite transducer, The AE is generated at transmission sources A, B and C propagating through the Perspex wall and is detected by the piezoelectric composite transducer.

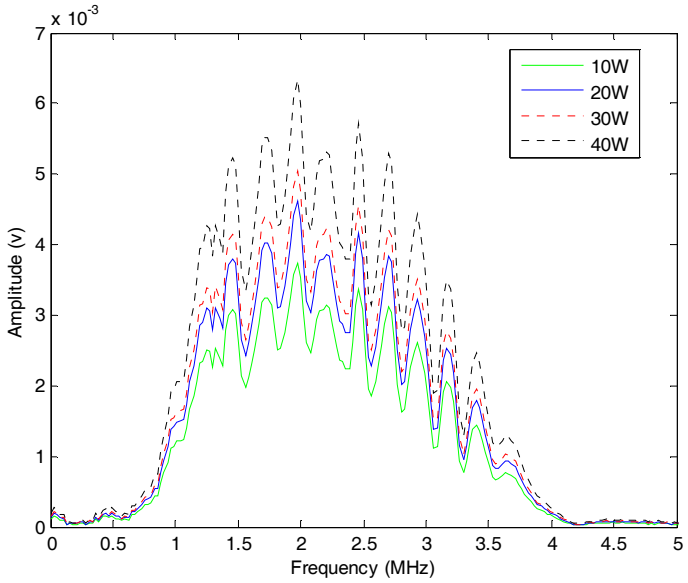

Figure 6.5 The FE derived AE spectrum obtained by the simulated piezoelectric composite transducer from FE model. The AE produced at the transmission source A with the various power inputs of 10-40W propagates through the glass wall of the reactor vessel and is detected by the piezoelectric composite transducer.

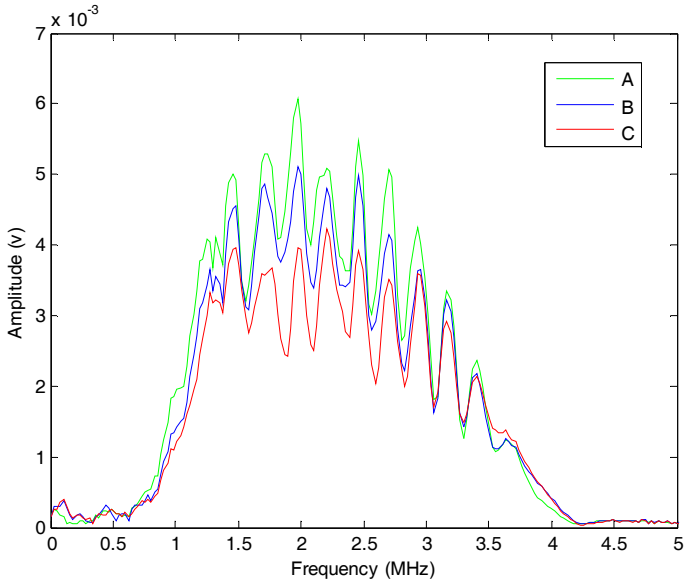

Figure 6.6 The FE derived AE spectrum obtained by the simulated piezoelectric composite transducer. The AE is generated at transmission sources A, B and C propagating through the glass wall and is detected by the piezoelectric composite transducer.

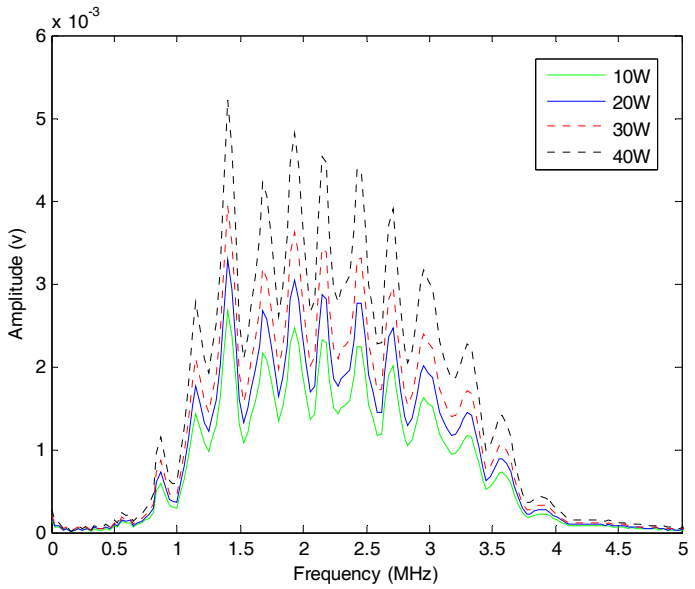

Figure 6.7 The FE derived AE spectrum obtained by the simulated piezoelectric composite transducer from FE model. The AE produced at the transmission source A with the various power inputs of 10-40W propagates through the steel wall of the reactor vessel and is detected by the piezoelectric composite transducer.

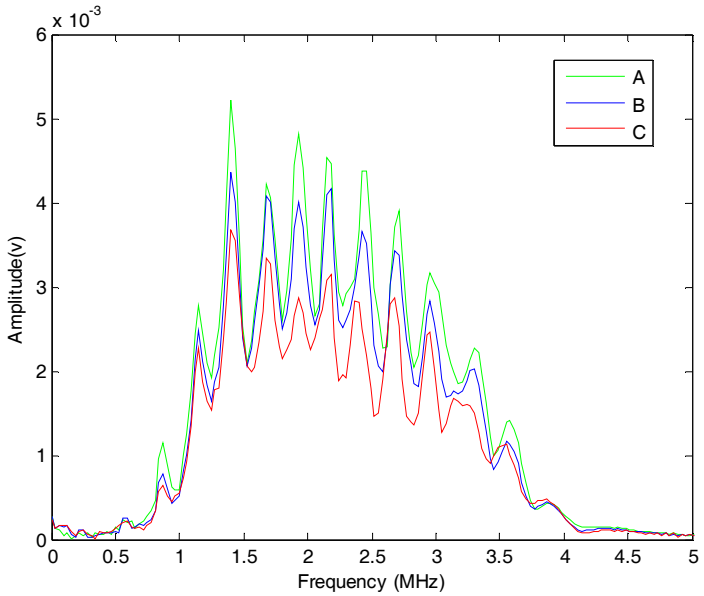

Figure 6.8 The FE derived AE spectrum obtained by the simulated piezoelectric composite transducer. The AE is generated at transmission sources A, B and C propagating through the steel wall and is detected by the piezoelectric composite transducer.

Simulation of the full ultrasonic monitoring system has demonstrated that the piezoelectric composite transducer offers more sensitivity when the reactor wall is constructed from a lower acoustic impedance material. This will not be the case in an industrial scenario, but the modelling results indicate that the transducer will acquire data over a similar frequency range independent of the wall material, albeit with a lower sensitivity for higher acoustic impedance materials. Thus, to evaluate this monitoring approach the manufactured piezoelectric composite transducer will be evaluated using a Perspex tank in which a high power transducer will be used to generate cavitation.

6.3 Development of a non-invasive transducer measurement system

6.3.1 Development of a non-invasive measurement system

Figure 6.9 illustrates a schematic of the non-invasive cavitation measurement system using the developed broadband transducer. The physical experiment setup is displayed in Figure 6.10. The reactor is a 10mm Perspex walled vessel which has dimensions of 120x130x150mm and contains 1.4 litres of degassed water. A 40kHz Tonpilz single-transducer was integrated into the bottom of the vessel and used as the high power acoustic source. The piezoelectric composite transducer is attached to the wall of the Perspex reactor vessel to investigate acoustic emission signal generated by the cavitation activity. Ultrasonic gel is applied to the surface of the piezoelectric composite transducer in order to effectively couple the acoustic signal into the Perspex wall.

Cavitation is produced by the Tonpilz single-transducer when excited by a continuous sine wave at a frequency of 40kHz, delivered at a high excitation voltage. The excitation signal is produced by a function generator (Agilent 33120A) and amplified using a wideband RF amplifier (155LCR, Kalmas Engineering), with a gain of 50dB. The ultrasonic transducer is excited with power levels corresponding

to 10, 20, 30 and 40W at the amplifier and is controlled by the magnitude of the signal generated by the function generator.

During the experimental phase, the acoustic emission signal is collected by the fabricated piezoelectric composite transducer. The NPL cavitation sensor, as described in Section 2.5, is also used in the measurement process. The detected signals are recorded on a digital oscilloscope. The Matlab program is used to determine the intensity of cavitation from the detected acoustic emission spectrum.

The main difference between experiment non-invasive transducer measurement system, depicted in Figure 6.9, and the arrangement modelled by FE, in Figure 6.1, is the location of the cavitational field. In the simulation, the acoustic emission events are located 10mm from the inner surface of the Perspex wall, whereas in the experimental setup this distance cannot be controlled and in fact, it is anticipated that many cavitation events will be distributed randomly within the volume (albeit with a preference direct in front of the Tonpilz transducer). It is also obvious that the FE model has only considered a 2D section of the setup.

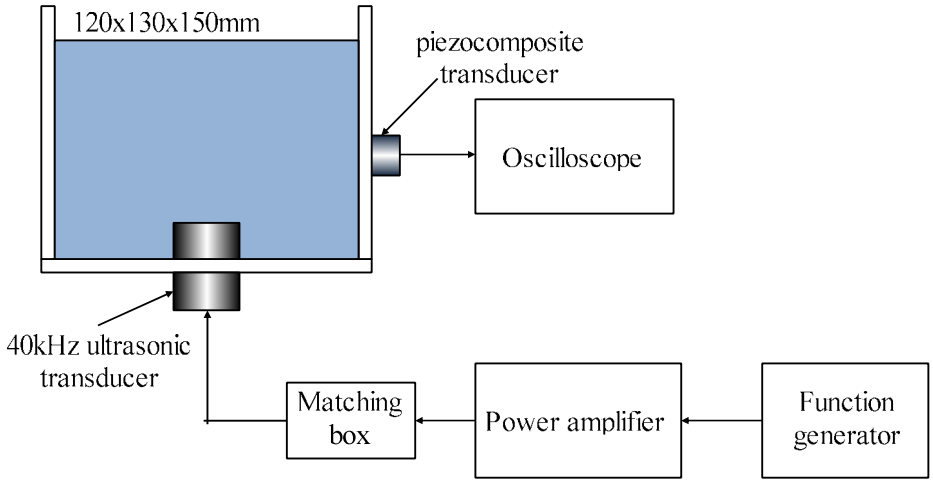

Figure 6.9 Schematic diagram of the broadband non-invasive transducer measurement system to monitor acoustic cavitation.

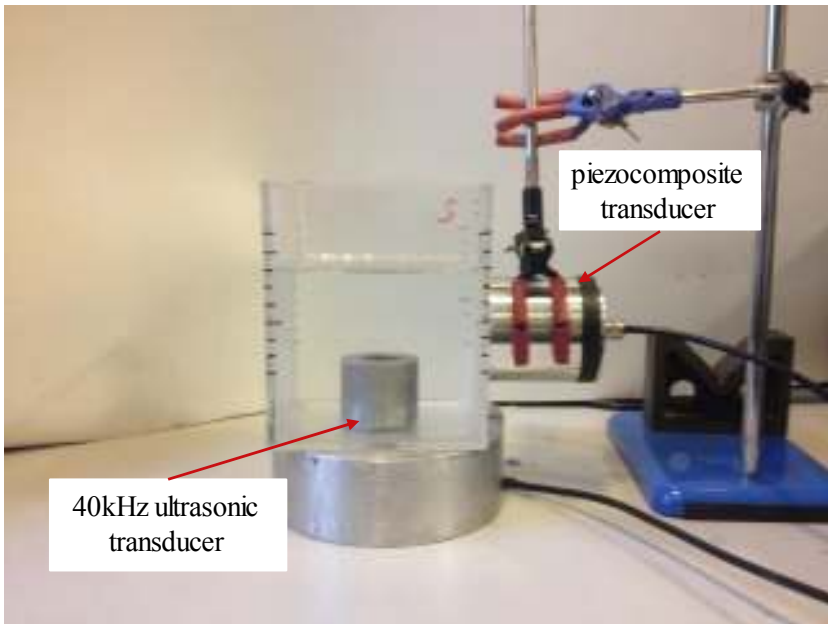

Figure 6.10 The non-invasive cavitation monitoring system set up.

6.3.2 Evaluation of the piezoelectric composite transducer's performance

6.3.2.1 Evaluation of frequency response for the developed piezoelectric composite transducer

The non-invasive monitoring system is used to monitor cavitation in the frequency domain. The characteristics of the ultrasonic transducer, in terms of frequency response, dominate when the frequency response of the total system is examined. Hence, it is important to initially understand the frequency response of the whole ultrasonic system. Moreover, this type of experimental arrangement can also be used to evaluate the sensitivity performance of the fabricated piezoelectric composite transducer.

Figure 6.11 illustrates the equipment used in the frequency response experiment arrangement. There are three scenarios that will be evaluated: the use of a calibrated commercial hydrophone; and the fabricated piezoelectric composite transducer assessed both directly in the water load and attached to the outer wall of the Perspex reactor. In this work, low power Panametrics ultrasonic transducers [143], with

operating frequencies of 0.5, 1, 2 and 5MHz, are used as transmission sources to produce the acoustic sound waves at these distinct frequencies. The excitation signal was produced by a function generator (Agilent 33120A), with a single cycle sinusoid at the transducer centre frequency subsequently amplified using a wideband RF amplifier (155LCR, Kalmas Engineering) with a gain of 50dB. The transmission transducers are excited with power levels corresponding to 5W and controlled by the magnitude of the signal generated by the function generator. A B&K 8103 hydrophone was used initially to provide a calibrated response to the incident ultrasonic energy. This was placed at a distance of 50mm from the transmission transducer. Once this set of ultrasonic signals were collected, the B&K hydrophone was replaced by the fabricated transducer and the experimental steps repeated. In both cases, the detected acoustic signal is recorded using a standard digital oscilloscope, before being converted into the frequency domain using Matlab. The final stage is when the fabricated piezoelectric composite transducer is attached to the outer wall of the Perspex reactor vessel, with the transmission transducer positioned 50mm away from the reactor wall onto which the transducer has been coupled. Again, the measured signals are converted into the frequency domain and then used to estimate the bandwidth of the transducer. The detected acoustic spectrum signals are shown in Figures 6.12, 6.13 and 6.14, for all 4 transmission transducer cases.

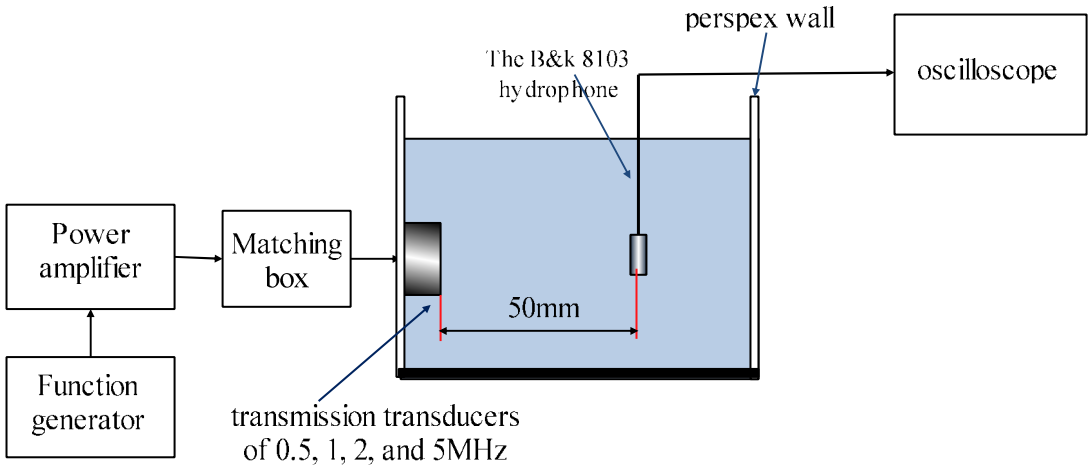

(a) The B&K 8103 hydrophone measurement

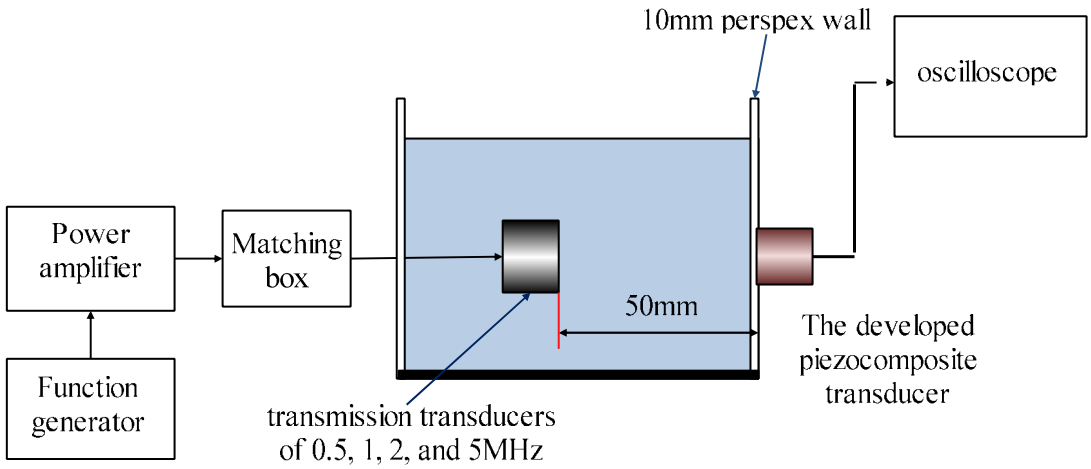

(b) The developed piezoelectric composite transducer measurement

Figure 6.11 Schematic diagram of the experiment system to evaluative frequency response of the developed piezoelectric composite transducer (a) The B&K 8103 hydrophone measurement (b) The developed piezoelectric composite transducer measurement.

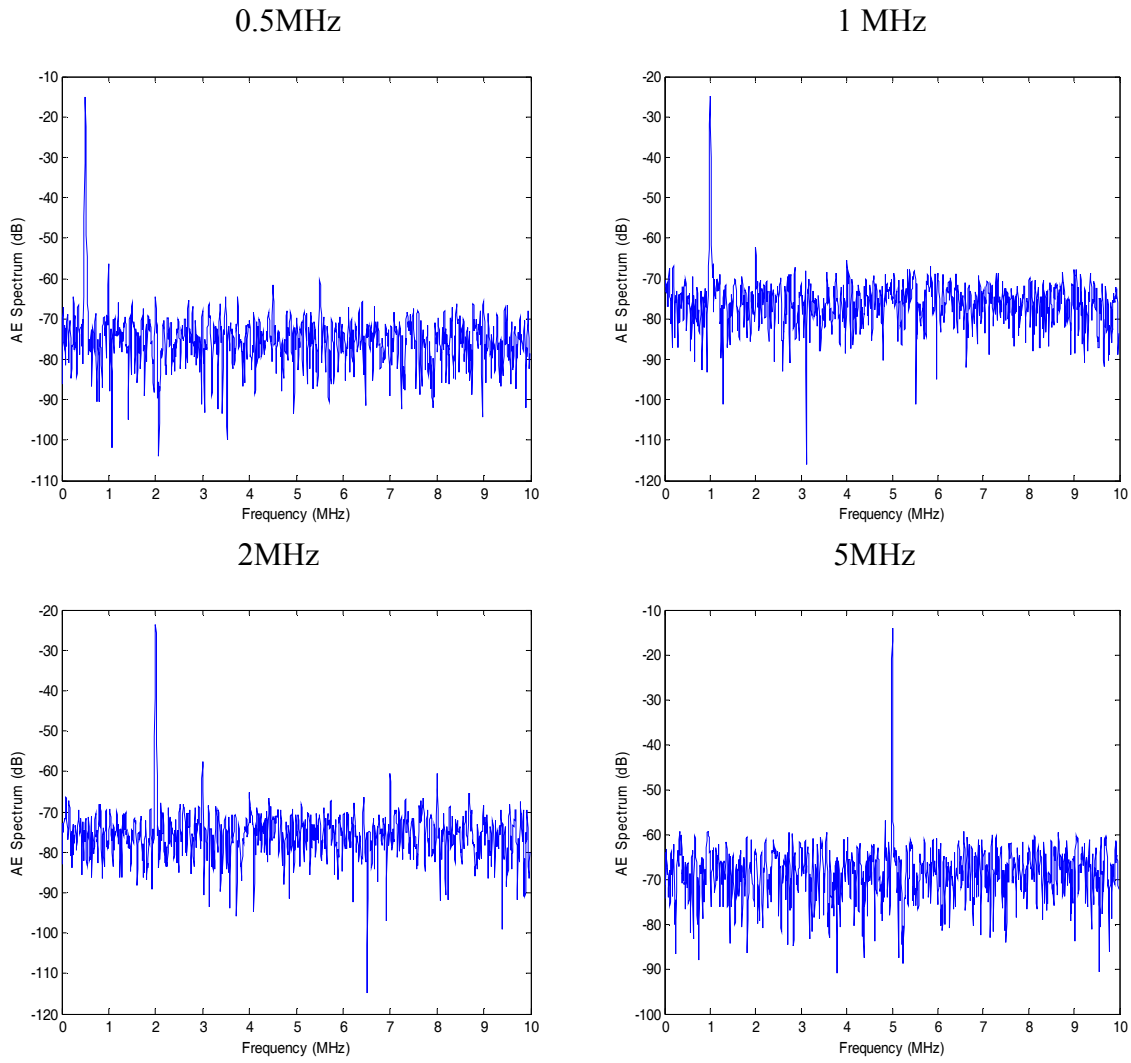

Figure 6.12 The detected acoustic emission profile obtained by the B&K 8103 hydrophone with various frequency excitations of 0.5, 1, 2 and 5MHz. The acoustic emission is generated by Panametrics ultrasonic transducers of 0.5, 1, 2 and 5MHz with input power of 5W. The B&K 8103 hydrophone is positioned at 50mm from transmission transducer in water to collect the signal.

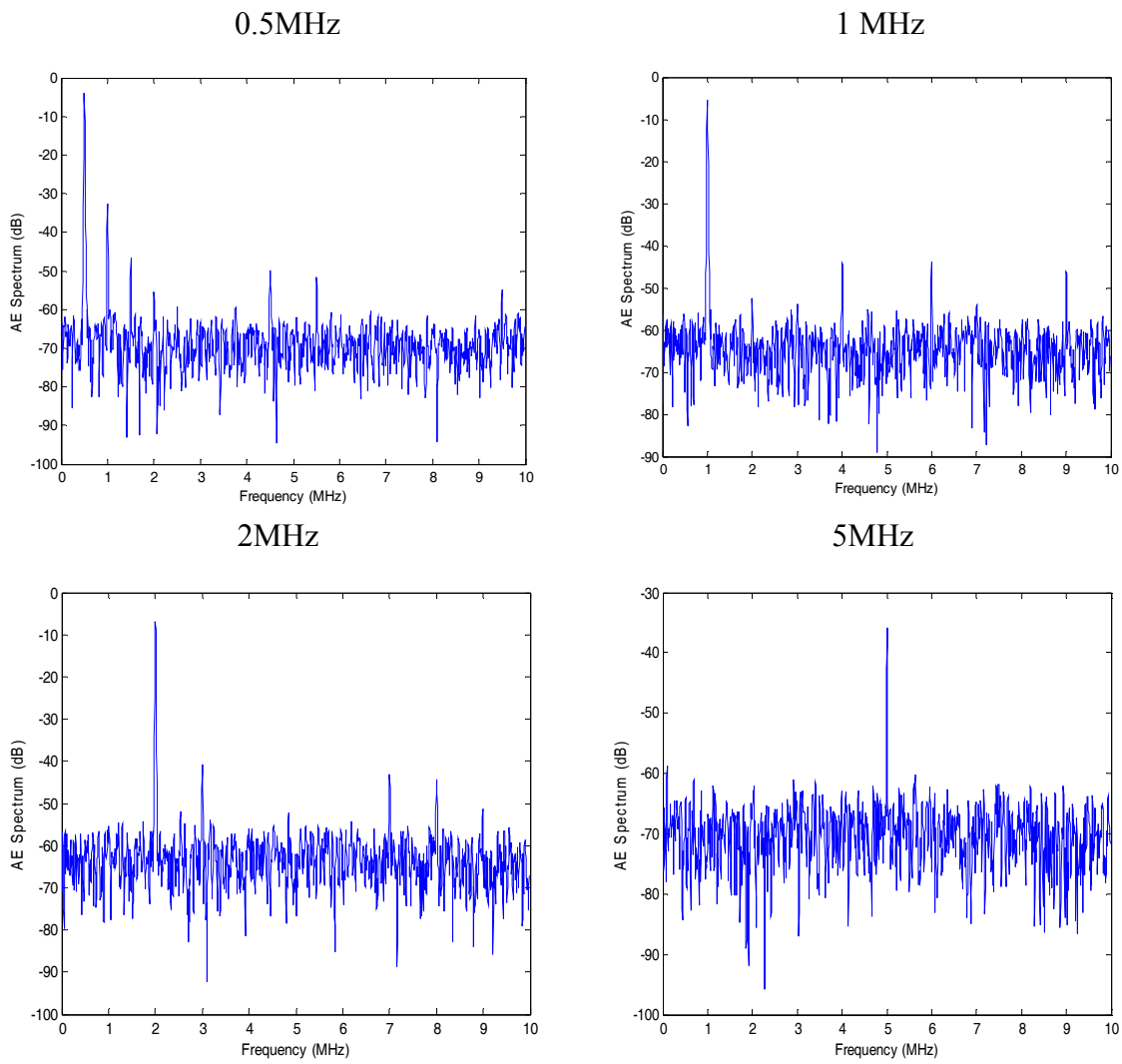

Figure 6.13 The detected acoustic emission profiles obtained by the designed piezoelectric composite transducer with various frequency excitations of 0.5, 1, 2 and 5MHz. The acoustic emission is generated by Panametrics ultrasonic transducers of 0.5, 1, 2 and 5MHz with input power of 5W. The designed piezoelectric composite transducer is positioned at 50mm from transmission transducer in water to collect the signal.

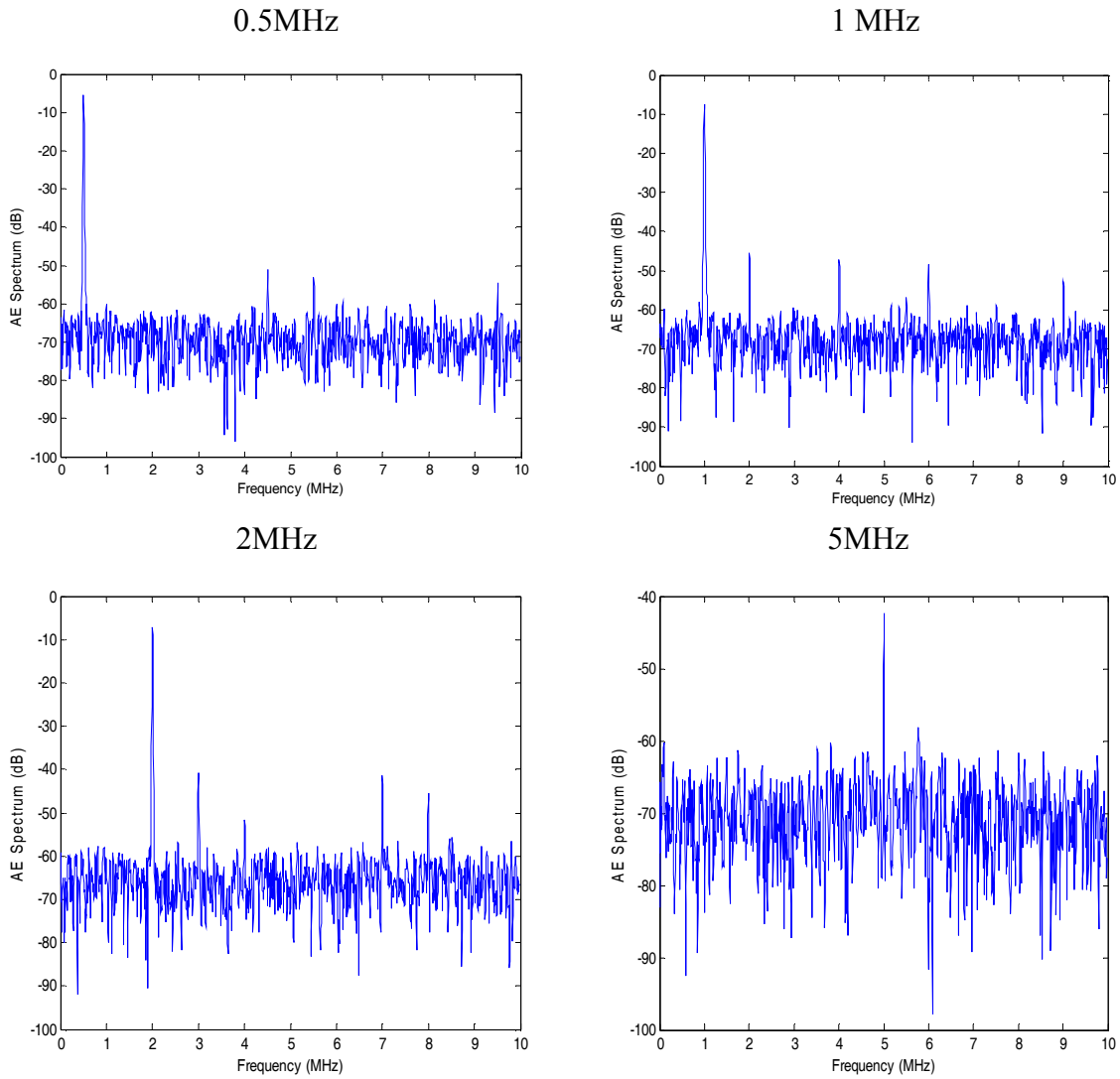

Figure 6.14 The detected acoustic emission profiles obtained by the designed piezoelectric composite transducer of various frequency excitations of 0.5, 1, 2 and 5MHz. The acoustic emission is generated by Panametrics ultrasonic transducers of 0.5, 1, 2 and 5MHz with input power of 5W. The piezoelectric composite transducer is attached to the external wall of the Perspex reactor vessel at 50mm from transmission transducer to collect the signal.

Figures 6.12, 6.13 and 6.14 present the frequency response acquired by the B&K 8103 hydrophone and the designed piezoelectric composite transducer positioned in the liquid medium and attached to the wall of the Perspex reactor vessel, in distinct

frequency bands. It is clear from each spectrum that the fundamental frequency has been measured and hence that each reception scenario provides an accurate representation of the different ultrasonic signals. Figure 6.15 has been produced by extracting the maximum amplitude from the received spectra for both the B&K 8103 hydrophone and the piezoelectric composite transducer cases. The amplitudes of the signals collected by the B&K 8103 hydrophone are lower than that of the developed piezoelectric composite transducer due to the sensitivity differences between the devices. The fabricated piezoelectric composite transducer acquires greater amplitudes at the frequencies of 0.5, 1 and 2MHz, and detects very weak signal at 5MHz. The result at 5MHz was not unexpected as the measured pulse-echo response of the transducer, in Section 5.5, demonstrated that the upper frequency limit for the device was around 3MHz. Nevertheless, there is spectral information obtained by this transducer up to 5MHz and consequently, it was considered appropriate to maintain the BIE frequency range at 1-5MHz for the work in this Chapter. Interestingly, the sensitivity of the fabricated transducer is still high when used in a non-invasive arrangement, i.e. coupled to the outer surface of the reactor wall. This is extremely encouraging for use in the intended cavitation monitoring system.

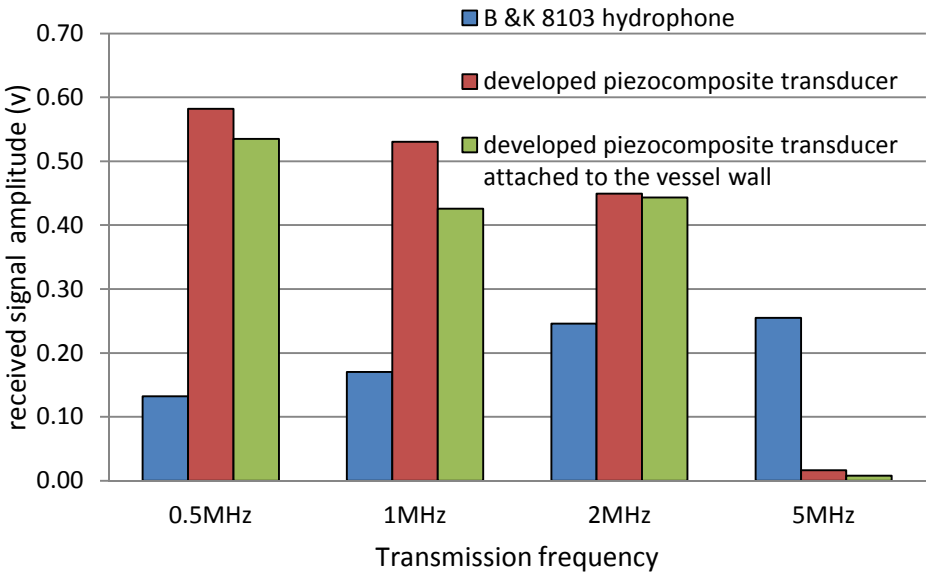

Figure 6.15 The received amplitude of the fundamental frequency obtained experimentally by the designed piezoelectric composite transducer and the B&K 8103. The acoustic emission is generated by Panametrics ultrasonic transducers of 0.5, 1, 2 and 5MHz with input power of 5W.

6.3.2.2. Acoustic emission spectrum detection

In order to evaluate the acoustic emission spectrum detection, the basic cavitation measurement system in Figure 6.9 is used and adapted slightly to locate the receiving transducer from a location within in the liquid load medium. Cavitation is generated by the 40kHz Tonpilz single-transducer being excited with a power level corresponding to 10W, in order to investigate the acoustic emission signal arising from the cavitation. For this work, the NPL cavitation sensor and the developed piezoelectric composite transducer are placed at a location 30mm axially aligned away from the front face of the Tonpilz transducer. It is anticipated that both transducers are exposed to similar acoustic emission conditions. i.e. the main cavitation activity is located in front of the Tonpilz device and is consistent between experiment.

Figure 6.16 shows the acoustic emission spectrum detected by the developed piezoelectric composite transducer and the NPL cavitation sensor at the input power of 10W. It is clear that both receivers have measured a similar spectral content and importantly, that the piezoelectric composite transducer offers superior sensitivity at frequencies above 300kHz. Moreover, the acoustic components of the fundamental frequency, harmonics, super-harmonics and the broadband frequency are evident in the acoustic emission spectrum and are indicative of cavitation activity in the liquid load medium [4],[8],[22],[144].

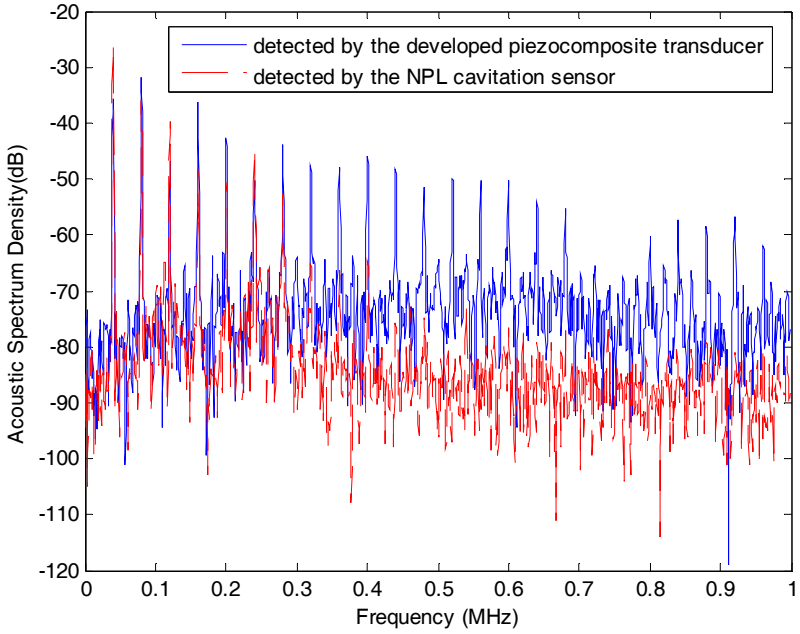

Figure 6.16 The acoustic emission profile detected by the piezoelectric composite transducer and the NPL cavitation sensor at the power input of 10W. The ultrasound transducer is excited by the fundamental frequency of 40kHz. The piezoelectric composite transducer and the NPL cavitation sensor are positioned at 30mm away from the 40kHz Tonpilz transducer to collect the signal.

6.3.2.3. Cavitation detection performance

The next phase in the evaluation of the proposed non-invasive monitoring system is to compare the operating performance of the developed transducer when attached to the reactor wall with the water-loaded configuration discussed in the previous sub-Section. Similar excitation conditions were adopted, the only difference being the excitation level used was 20W, and the NPL sensor and fabricated transducer located at the same position in the water load, i.e. 30mm from the front face of the Tonpilz device. For the non-invasive configuration, the piezoelectric composite transducer was coupled to the outer surface of the Perspex wall and held in place using a mechanical clamp stand. Importantly, the position of the transducer was maintained at 30mm above the surface of the Tonpilz device, with the transducer orientation 90^{o} relative to the propagating ultrasonic wave.

As the application of the transducer is to measure acoustic emission in the frequency range 1-3MHz, the data presented in Figure 6.17 illustrates the acoustic emission spectrum in the range 0-10MHz. The acoustic emission signals detected follow reasonably similar trends, but the spectrum signal detected by the developed piezoelectric composite transducer is higher than that that detected by the NPL cavitation sensor, when both are water loaded, due to the high sensitivity of the developed piezoelectric composite transducer in the range 1-3MHz. Interestingly, the spectrum signal detected by the developed piezoelectric composite transducer attached to the reactor vessel wall is comparable to the output from the NPL cavitation sensor. It should be noted that the detected spectrum signal contains all of the acoustic spectrum components, as shown in Figure 6.16, but resolution of the spectral data is lower.

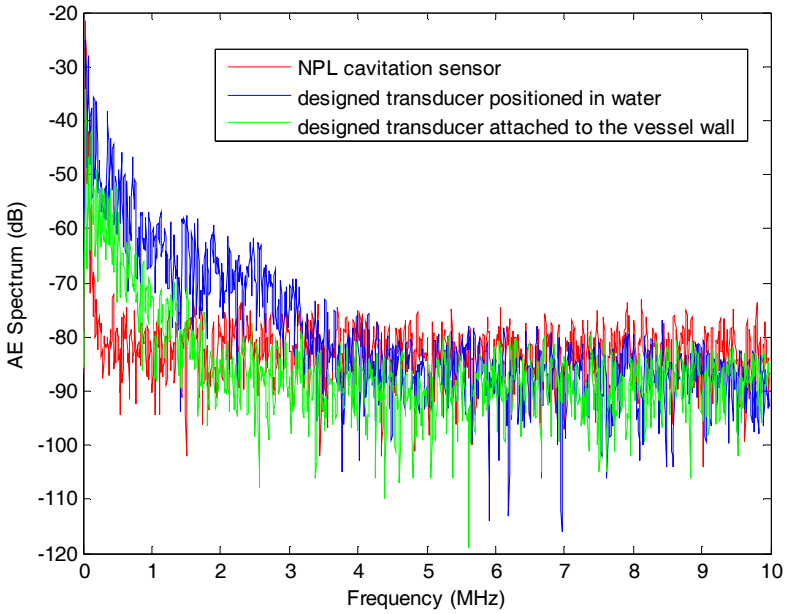

Figure 6.17 The acoustic emission spectrum obtained by the NPL cavitation sensor and the piezoelectric composite transducer positioned in the liquid medium 30mm away from the transmission transducer and attached to the wall of the Perspex reactor vessel approximately 30mm away from the transmission transducer with the input power of 20W.

This experimental arrangement was extended to cover the range of excitation levels from 10W to 40W. Figure 6.18 shows the calculated cavitation activity of the power inputs of 10-40W obtained by the NPL cavitation sensor and the developed piezoelectric composite transducer when positioned in the liquid medium and attached to the wall of the reactor vessel. These measurements equate to the BIE calculated in the frequency range 1-5MHz. The repeatability, determined using standard deviation, of the measurements is shown on the Figure. Moreover, these results have been tabulated and are shown in Table 6.1. As expected, the BIE of the piezoelectric composite transducer positioned in the liquid medium is higher than that of the NPL cavitation sensor and the same piezoelectric composite transducer attached to the wall of the reactor vessel. The trends of the cavitation occurring in each investigation approach are similar and increase linearly with input power level.

Interestingly, the non-invasive piezoelectric composite transducer measurement shows excellent correlation with the response from the NPL cavitation sensor experiment.

Table 6.1 Cavitation activity obtained by BIE calculation from the NPL cavitation sensor and the piezoelectric composite transducer measurement at 30mm from the 40kHz Tonpliz transducer.

Power input	BIE (V^2 Hz)		
watt	NPL cavitation sensor	Piezoelectric composite transducer attracted to the vessel wall	Piezoelectric composite transducer positioned in water
10	1.833E-3	3.020E-4	5.367E-3
20	2.567E-3	8.595E-4	1.307E-2
30	2.933E-3	9.588E-4	2.010E-2
40	4.000E-3	2.150E-3	2.843E-2

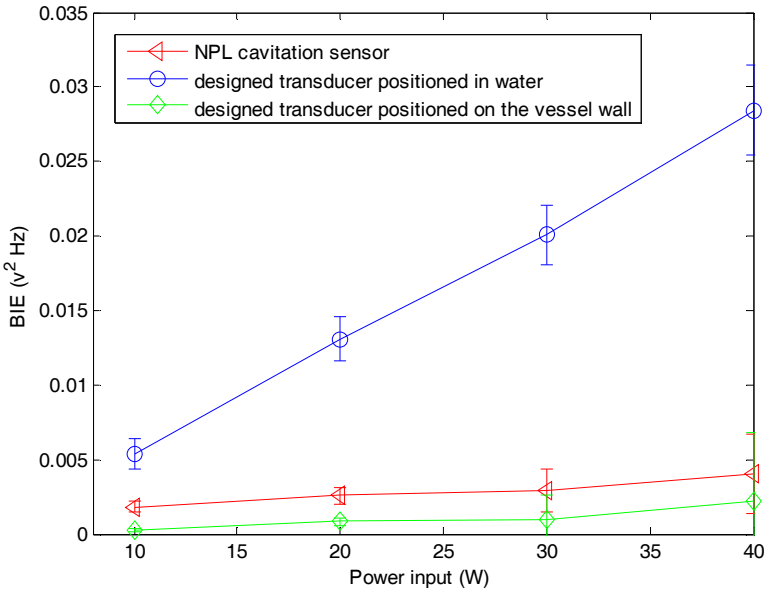

Figure 6.18 The BIE of 10-40W obtained by various measurements, the NPL cavitation sensor and the developed piezoelectric composite transducer positioned in the liquid medium at 30mm away from the 40kHz Tonpilz transducer and attached to the wall of the Perspex reactor vessel 30mm away from the transmission transducer.

6.4 Experiment results for cavitation monitoring

The final evaluation of the designed transducer uses the same experimental arrangement as described in Section 6.3, with the piezoelectric composite transducer attached to the outer wall of the reactor vessel, as depicted in Figure 6.10. The experimental measurements will first evaluate the measured frequency spectrum at different excitation power levels and in different frequency bands, with the transducer positioned at a height of 30mm from the Tonpilz transducer front face. Next, the BIE is calculated for a variety of transducer positions on the outer wall and this information is used to provide a map of cavitational activity generated by the 40kHz Tonpilz transducer, within the vessel.

6.4.1 Acoustic spectrum evaluation

Figure 6.19 shows a series of acoustic spectra covering the frequency range up to 200kHz and acquired at power drive levels of 10, 20 and 40W, with a sampling frequency of 50MHz. This reduced frequency range has been chosen to enhance the y-axis resolution in order to better illustrate the systematic increase in the acoustic emission signal occurring in the harmonics of the acoustic emission spectrum as the applied power is increased. There are a number of other interesting features of Figure 6.19. The graph clearly illustrates that the AE spectra comprises the fundamental frequency (f_0: 40kHz), subharmonic frequency (f_s: 20kHz) and harmonic frequencies (f_h: 60, 80, 100, 120 ... kHz). The sharp peaks of the fundamental, harmonic and sub-harmonic frequencies are shown clearly in this frequency range of 0-200kHz. It has been suggested that the acoustic spectrum components, including harmonics, sub-harmonics and ultra-harmonics, can be used to identify the presence of (both stable and inertial) cavitation. The features of the acoustic emission caused by the cavitation have been well documented [9],[10],[32] and represent nonlinear oscillations generated by cavitational bubbles.

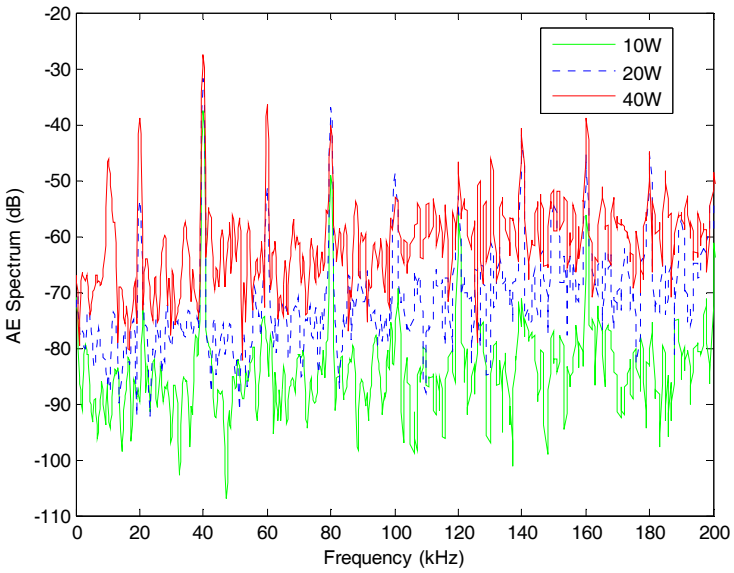

Figure 6.19 Acoustic spectra determined over the frequency range of 0-200kHz, acquired using the developed piezoelectric composite transducer. The acoustic emission spectra have been acquired at the power drive levels of 10, 20 and 40W of the 40kHz Tonpilz transducer. Measurements were made by attaching the developed piezoelectric composite transducer to the wall of the reactor vessel.

Figure 6.20 shows the expanded acoustic emission spectra over the frequency range of 0-5MHz and again the input power levels of 0W to 40W. The acoustic spectrum signals detected follow reasonably similar trends, with a general increase in received amplitude across the entire frequency range as the power level increases. Again, these spectral signals contain all of the acoustic spectrum components, as shown in Figure 6.19, but the resolution of the spectral data is lower. These spectra results indicate that changing the acoustic pressure of the liquid medium inside the reactor will change the intensity of cavitation activity produced. In progressing the input power levels of 10, 20, 30 and 40W, the magnitude of the 1MHz component increases by almost 20dB. Importantly, the energy associated with cavitation that resides in the acoustic spectrum in the MHz range has been detected by the developed piezoelectric composite transducer and can be used to determine the intensity of cavitation activity occurring within the reactor.

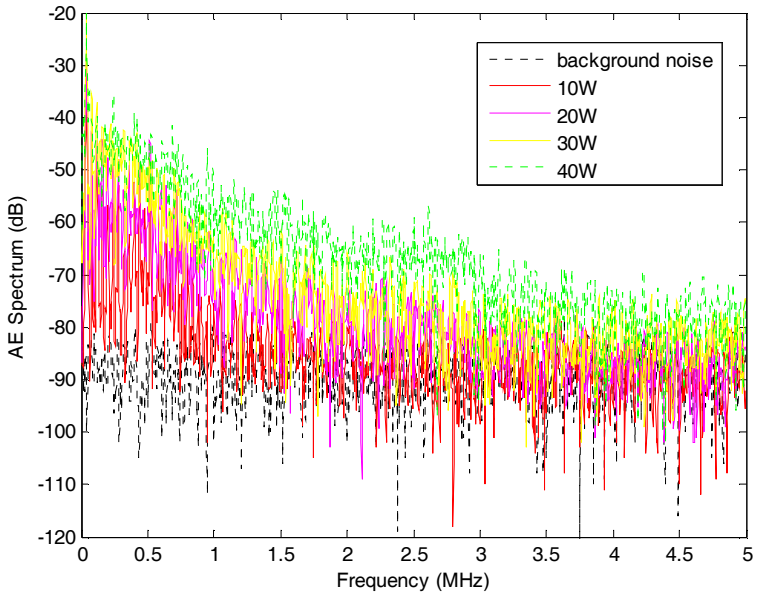

Figure 6.20 High-frequency spectrum obtained by the prototype piezoelectric composite transducer at the power inputs of 10-40W which is produced by the 40kHz Tonpilz transducer. Measurements were made by attaching the transducer to the wall of the reactor vessel. The results represent a typical "ascending" measurement with spectra increasing as the delivered power is increased.

6.4.2 Cavitation activity monitoring

As described in Section 3.6.5, cavitation activity can be analyzed using the BIE relationship, in which an integration of the high-frequency components in the acoustic emission spectrum provides a quantification of the cavitation intensity. From the measurements in Section 6.4.1, the BIE of each measurement, corresponding to power levels between 0-40W, is calculated in the frequency range of 1MHz to 5MHz. Thus, the relationship between input power level and cavitation activity in degassed water within the reactor vessel was determined. Now, the developed piezoelectric composite transducer is attached to the wall of the Perspex reactor vessel at locations corresponding to a height of 15, 25, 40 and 60mm from the front face of the Tonpilz transducer. The BIE results for each single point along the vertical central axis are shown in Table 6.2 and Figure 6.21. The repeatability of the measurements is obtained by the standard deviation calculation and illustrated in the

Figure 6.21. As the input power is increased, the BIE clearly indicates a change in acoustic energy levels due to the extent of the cavitation activity and follows a reasonably similar trend for each power level. Moreover, it is noted that the BIE increases with the input power.

Table 6.2 Cavitation obtained by BIE calculation at the positions of 15, 25, 40 and 60mm.

Power input (W)	BIE (V^2 Hz)			
	15mm	25mm	40mm	60mm
10	0.00056	0.00030	0.00023	0.00022
20	0.00122	0.00086	0.00037	0.00036
30	0.00203	0.00096	0.00072	0.00027
40	0.00597	0.00215	0.00163	0.00082

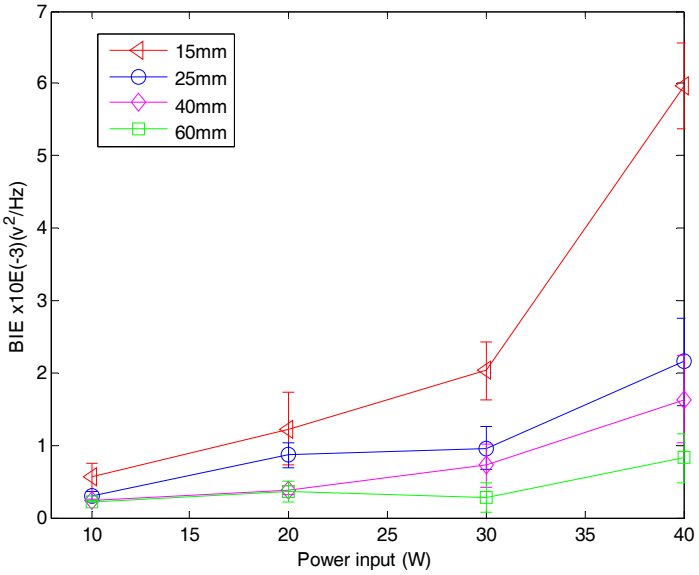

Figure 6.21 Empirical relationships of the cavitation activity obtained by BIE calculation in the frequency range of 1-5MH and the input power of 10, 20, 30 and 40W. The cavitation is detected at the positions of 15, 25, 40 and 60mm away from the 40kHz Tonpilz transducer.

6.4.3 Influence of power delivery to the monitoring cavitation approach

The trend of cavitation measurement with the prototype piezoelectric composite transducer is extended to consider both an increase and decrease in input power levels. This is conducted to determine if there are any measurement artefacts in the system that may be problematic in a practical application. Again, the NPL cavitation sensor is as a comparison for the developed piezoelectric composite transducer and the sensor/transducer position is 30mm from the front face of the 40kHz Tonpilz transducer. The high power transducer is excited across the input power levels of 5-40W and cavitation spectra acquired over the frequency range of 1MHz to 5MHz. This constitutes an “ascending” measurement. Following this set, the "descending" measurements run at the same powers, starting at 40W and ending at 5W. The experiment was repeated seven times.

The cavitation activity obtained from the BIE calculation can be used to indicate the threshold between the non-cavitating state and the cavitating state. The BIE calculations, corresponding to cavitation intensity measurements, are given in Figures 6.22 and 6.23, for the NPL and piezoelectric composite receivers, respectively. It should be noted that the NPL sensor is within the liquid load medium and the piezoelectric composite transducer attached to the external face of the vessel. These results are interesting as it is clear that the designed transducer, operating in a non-invasive mode, demonstrates an enhanced consistency (reduced variation between ascending and descending trends) when compared to the NPL sensor. The measured output from the piezoelectric composite transducer offers good repeatability when the power levels are stepped up/down. Hence, there is a high level of confidence that the device is suitable for deployment in the non-invasive cavitation monitoring scheme.

It is clear from Figure 6.23 that the developed piezoelectric composite transducer provides a more stable value of broadband integrated energy (BIE) from these sets of measurements, although the descending values of cavitation activity appear systematically higher. This result acquired by the NPL sensor in this work is similar to that observed by Zeqiri *et al.* [10]. Overall, the results of the NPL cavitation sensor measurement show higher levels of variation than the developed piezoelectric composite transducer measurement. Interestingly, the repeatability of the developed piezoelectric composite transducer measurement at the input power of 40W is $\pm 25\%$.

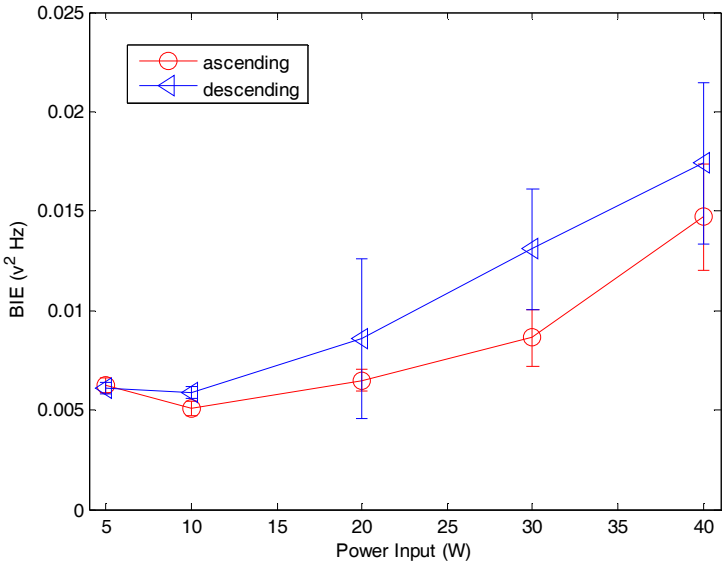

Figure 6.22 Variation in cavitation activity obtained by BIE approach derived using the NPL cavitation sensor determined over the range 5 to 40W of the developed reactor vessel. Measurements shown are both "ascending" and " descending". The repeatability obtained by the standard deviations of the measurements is illustrated.

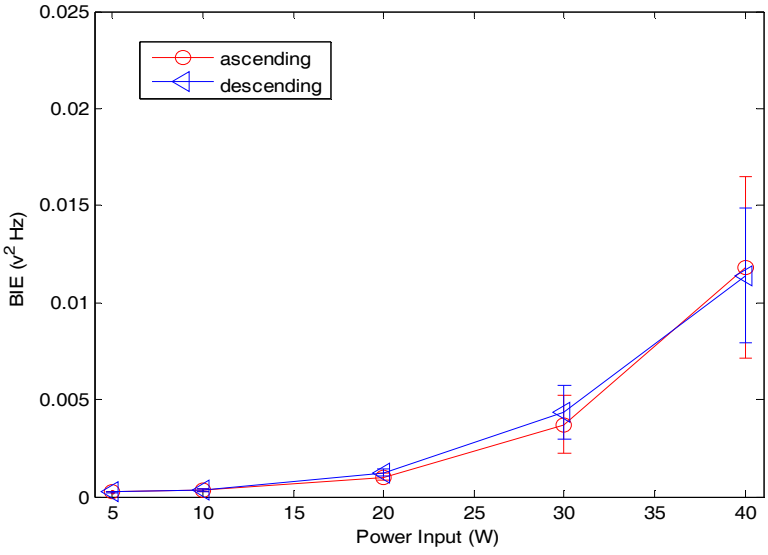

Figure 6.23 Variation in cavitation activity obtained by BIE approach derived using the developed transducer, determined over the range 5 to 40Wof the developed reactor vessel. Measurements shown are both "ascending" and "descending". The repeatability obtained by the standard deviations of the measurements is illustrated.

6.4.4 Mapping the cavitation activity within the reactor vessel

The ability of the non-invasive monitoring approach to map acoustic cavitation activity within the vessel volume was investigated by moving the piezoelectric composite transducer to specific locations on the outer wall and acquiring experimental measurements at different power levels. Figure 6.24 illustrates the nine locations used, which are not intended to produce a comprehensive coverage map of the vessel rather to illustrate the potential of the technique. In Figure 6.24, there are three lateral and vertical positions identified and these are clearly denoted as {x, z} coordinates. At each location, BIE has been calculated across the input power range 10W – 40W and the results are presented in Table 6.3. Moreover, the BIE values have been included in Figure 6.24 for the 30W input power level case.

Table 6.3 Cavitation activity obtained by the BIE calculation at the specific positions with the input power of: 10, 20, 30 and 40W.

Detection position	BIE $x10^{-3}$ (V^2 Hz) measured at power levels of			
	10W	20W	30W	40W
{35,15}	0.15	0.32	0.61	0.64
{70,15}	0.27	3.13	4.70	5.43
{100,15}	0.42	1.43	2.50	2.70
{35,40}	0.10	0.02	0.46	0.86
{70,40}	0.14	0.45	0.62	0.86
{100,40}	0.13	0.30	0.70	0.72
{35,60}	0.16	0.27	0.53	0.57
{70,60}	0.12	0.40	0.61	0.81
{100,60}	0.17	0.27	0.71	0.79

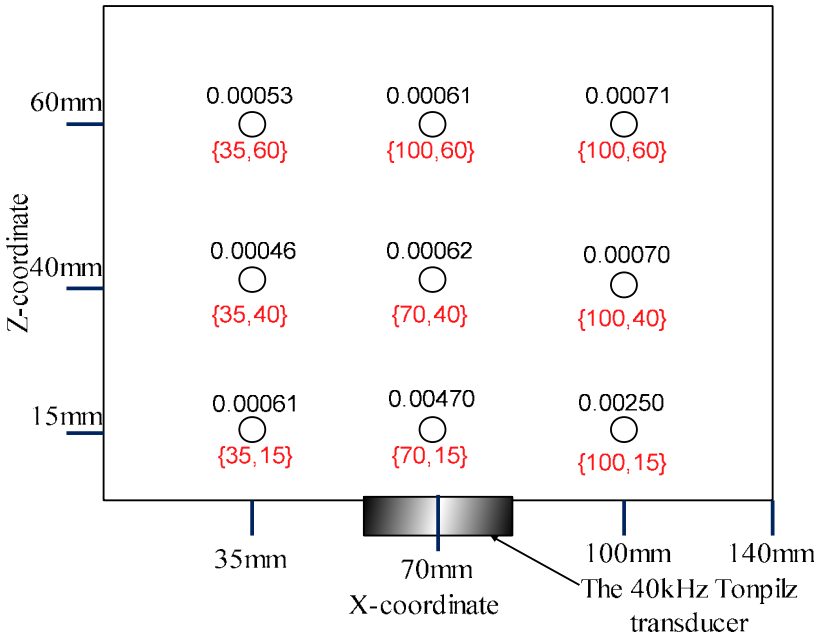

Figure 6.24 XZ-view of the reactor vessel showing the cavitation activity at the specific locations. The 40kHz Tonpilz transducer is excited by the input power of 30W.

The main conclusion to be reached from the data presented in Table 6.3 is that the location directly in front of the transducer experiences a significant rise in BIE when the input power level increases beyond 10W, i.e. from 20W – 40W. This is indicative of the cavitation threshold being exceeded and cavitation activity resulting in acoustic emission events being detected by the transducer. Interestingly, the location to the right of the high power transducer location, see Figure 6.24, also indicates a cavitating region which is not shown in the corresponding measurement to the left of the transducer. This asymmetry was not expected and serves to illustrate the volatility in the establishment of a cavitation field, where measurement unpredictability constitutes a major barrier to use in industrial applications.

6.5 Cavitation measurement techniques comparison

There are many approaches with which to monitor cavitation. This Thesis has introduced an optical cavitation measurement technique, based on laser Doppler vibrometry (LDV), and a non-invasive measurement system using the broadband piezoelectric transducer. In addition, the NPL cavitation sensor has been used throughout the Thesis as the state-of-the-art sensor technology and used for comparison with the developed techniques. Hence, it was considered appropriate to illustrate the performance of each measurement approach using the reactor vessel depicted in Figure 6.10.

Figure 6.25 presents the BIE for each technique, at a position 30mm from the 40kHz Tonpilz transducer, calculated in the frequency range 1-5MHz. The standard deviations of the measurements for each method are included in the Figure 6.25. From the Figure 6.25, it can be inferred that the sensitivity of the LDV method is highest and the non-invasive piezoelectric composite transducer the lowest. This reasoning is considered too simplistic. The most important aspect is that each technique follows a similar trend as the input power level increases. Thus, it is more appropriate to state that each approach offers a viable technique to monitor acoustic cavitation and that the choice of method will depend on the practical system configuration in which the measurements are intended to be made. Obviously, an opaque material or metallic wall surface would exclude the use of optical techniques and in some of these situations, the insertion of a sensor into the load medium may be prohibitive. Overall, the non-invasive transducer monitoring approach offers potential to be implemented across a great many vessel types and importantly, is considered to have sufficient sensitivity for operation in vessels comprised of material ranging from Perspex to steel, which effectively covers the range of solid materials used in both research and industry.

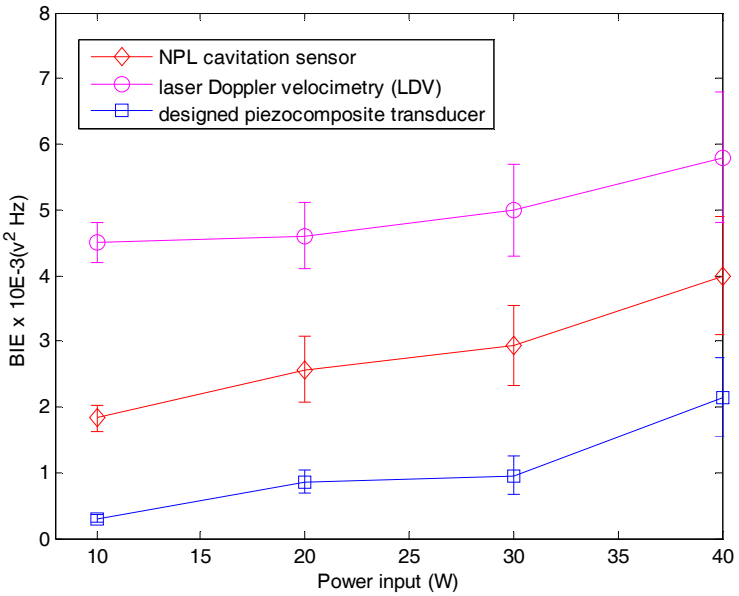

Figure 6.25 The BIE obtained by various measurement approaches: the NPL cavitation sensor, the LDV optical measurement technique and the piezoelectric composite transducer attached to the reactor vessel wall. The measurement sensors were positioned 30mm from the 40kHz Tonpilz transducer.

6.6 Limitations of the measurement approach

Monitoring cavitation is challenging due to the unpredictability of cavitation occurrence, as well as the potential damage to a sensor located close to the cavitating field. Although measurements of cavitation have been demonstrated using a non-invasive measurement system, there are some inherent limitations associated with the transducer manufactured for this work and monitoring approach itself.

Monitoring of cavitation activity requires a broadband transducer, operating in the megahertz region. Simulation predicted that a piezoelectric composite transducer could be designed to operate efficiently with a bandwidth transducer of 1-3MHz, centred around 2MHz. However, the bandwidth of the manufactured piezoelectric composite transducer was limited due to fabrication issues. This may has resulted in a reduction in the measured BIE, as the frequency spectrum contained nulls in the

desired operational bandwidth as shown in Figure 5.17. Hence, it is clear that improvements in both sensitivity and bandwidth could be produced if the manufacturing stages can be improved.

The reactor vessel was developed with a 10mm thick Perspex wall and a 40kHz Tonpilz transducer. The reactor is limited by the driving power input of 40W due to the performance of the 40kHz Tonpilz transducer and the wall material is non-standard for industrial applications. Nevertheless, the use of Perspex is convenient for laboratory based experimentation and simulation has been used to predict the operation of the transducer system on both glass and steel walled reactors. Moreover, the lateral dimension of the developed piezoelectric composite transducer (active area of 30mm) provides low spatial resolution. Hence, this technique is not considered appropriate to be used as a mapping tool. It is more suited to being located on the vessel close to where the cavitational field is expected to exist and in this situation, offers the potential to monitor in real-time fluctuations in the cavitational field which may be useful in terms of the efficiency or performance of the ultrasonic reactor.

6.7 Summary

This Chapter has presented the development of a non-invasive measurement system through which monitoring of acoustic cavitation within the reactor vessel using a broadband transducer approach can be performed. The transducer design and fabrication was the subject of Chapter 5 and therefore, the application of the device and experimental measurements of cavitation were the focus of this Chapter. Initially, PZFlex was used to model the implementation of this non-invasive measurement system and confirm that this approach is suitable for use across a range of reactor wall materials. For ease of implementation, for both the piezoelectric transducer and optical approaches, Perspex was used in this work, which interestingly was also predicted to offer the highest sensitivity due to its low acoustic

impedance – affording enhanced acoustic coupling to the water load in the experimentation presented. Then, the performance of the fabricated piezoelectric composite transducer was evaluated, including ensuring the transducer's ability to measure across the desired 1-3MHz range. Overall, the transducer is shown to be appropriate for use in this technique and it was noted that the approach has scope for improvement, in both sensitivity and bandwidth, due to the manufacturing faults that inhibited the performance of the fabricated piezoelectric composite device.

An interesting comparison was conducted to conclude the Thesis, in which three cavitation monitoring techniques were compared: the two non-invasive techniques developed through this Thesis and the contact, immersion NPL caviation sensor. Overall, the cavitation activity for all measurement approaches follows similar trends; the cavitation activity increases with the power input. Hence, the results demonstrate that a non-invasive measurement system is capable of being used for monitoring acoustic cavitation. Moreover, the use of a broadband piezoelectric transducer when deployed in a non-invasive mode, has the potential for use across a wide range of industrial reactor types.

CHAPTER 7

Conclusions and Future work

7.1 Conclusions

7.1.1 General overview

High power ultrasound has become an integral component in many application areas such as industrial processing and medicine. The application of high power ultrasound in a liquid medium can cause acoustic cavitation. The unique and dramatic effects of both the stable and inertial stages of cavitation activity, generated at high pressure regions, often serve as the primary mechanism for accelerating chemical reactions and removing contaminants from the surfaces of cleaning implements, which conventionally is difficult due to their complex shape. Moreover, high power ultrasound, especially HIFU, is now being considered as a viable means for healing processes and the treatment of cancers via a non-invasive surgery [49].

However, when cavitation occurs in high power fields and extreme conditions, this can cause damage to system components and any sensor equipment used in the

monitoring process. Many measurement techniques were developed to predict the intensity of cavitation activity and the regions in which it was likely to occur. Unfortunately, due to the extreme conditions of high power ultrasound applications, coupled with the adverse conditions presented by cavitation, the contemporary cavitation measurement technique using a conventional hydrophone can suffer from cavitational erosion, which can cause irreparable damage to the device. Typically, the physicality of the hydrophone probe is not resistant to high power ultrasound fields and the conditions within an occurring cavitation event. Recently, NPL developed a robust cavitation sensor to measure cavitational intensity and map the distribution of cavitation, in 3D. This has an upper operational limit of 50kHz (in terms of the driving frequency associated with the high power transducer). Therefore, non-invasive measurement systems to monitor cavitation activity were investigated in this Thesis. In non-invasive measurement systems, the sensor is removed from the high power ultrasound and cavitating field. This means the device does not suffer the effects of the cavitational bubbles and does not disturb the acoustic field. The cavitation measurement is obtained through the analysis of acoustic emission signals caused by the cavitation activity. The cavitation activity occurring in an experiment can be measured by the Broadband Integrated Energy (BIE) calculation, which integrates all the frequency components associated with the acoustic emission from cavitational events – this is typically 1-10MHz.

This Thesis has presented the implementation of two non-invasive measurement systems using both optical and piezoelectric measurement techniques as a means of monitoring cavitation activity. The results of the experimental programmes illustrate that the non-invasive measurement system developed is applicable to monitoring acoustic cavitation activity. Albeit, scanning or mapping of the cavitational field is not considered practical using these techniques.

Throughout the Thesis, simulation models have been developed using PZFlex of the reactor vessel and transducer, to support the design and optimisation of a broadband

piezoelectric transducer. Using this as a form of virtual prototyping, a design specification for the broadband transducer was selected and the application of a piezoelectric composite active material was explored. It is clear that the use of advances simulation tool offers significant advantages in the design of ultrasonic systems and importantly, can be extended to high power ultrasonic reactors.

7.1.2 Non-invasive optical measurement technique

A non-invasive measurement technique using Laser Doppler Velocimetry (LDV) was developed to address the issues caused by the use of conventional probes, such as hydrophones, in the direct measurement of cavitation activity. The developed technique is based on acoustic emission measurements acquired through modifications to the phase of the light passing through the liquid load medium. BIE calculations, in the frequency range of interest 1-5MHz, were performed on the experimentally measured acoustic emission spectra.

The optical cavitation measurement technique was successfully demonstrated on a high power test cell, in which a 40 kHz Tonpilz transducer was excited at input power levels between 10W – 40W to generate acoustic cavitation. The measured phase information, which is modified through interaction with the sound field, is converted to the acoustic emission spectrum using the FFT. The detected acoustic emission signal is demonstrated to contain a substantial amount of information relating to the cavitation process. These signals were analysed in different frequency bands corresponding to sub-harmonic, fundamental, harmonic and high frequency AE. Good correlation was achieved in matching the regions of high BIE from the broadband AE spectral band to cavitation activity measured using a standard aluminium foil test.

The laser monitoring approach was implemented in a scanning mode to determine its capacity to map the regions of cavitation within a reactor. This demonstrated some

potential, but the dynamic nature of the cavitating field, coupled with the small active area of the laser beam and the time to scan this beam throughout the vessel are considered barriers to successful implementation of such a scanning system. Moreover, this technique is only applicable for use with transparent materials, or if an optical window is introduced a reactor.

7.1.3 Simulation of high power ultrasonic reactor operation

Finite element analysis (FEA) has been used to solve complex problems in both scientific and engineering fields, but the FEA approach cannot directly simulate acoustic cavitation. In this work, the FEA package PZFlex has been used throughout. However, this modelling method is capable of simplifying complicated systems and this Thesis has proposed a methodology to simulate cavitation events to support the development of a non-invasive monitoring system. Individual bubble implosion events are simulated using a linear chirp, from 1-7MHz, to represent the broadband acoustic emission associated with the cavitating field. This can be incorporated into the model as a pressure loading function and it is possible to utilise multiple excitation events, as found with cavitation.

Using the cavitation AE simulation model, this Thesis analysed the wave propagation within a reactor vessel and determined a frequency specification appropriate for a piezoelectric transducer attached to the external wall of the vessel. In was demonstrated that a externally mounted transducer with a centre frequency of 2MHz and a 100% bandwidth was suitable for use as a broadband transducer to measure AE signals associated with cavitation events. This information was then utilised in another FEA model specifically developed to analyse the performance and behaviour of a 1-3 connectivity piezoelectric composite transducer. By incorporating both matching and backing layers, the full transducer operation for the non-invasive monitoring application was demonstrated.

The finite element analysis package allows the in depth analysis of parameter variation and their subsequent influence on the performance of the transducer and the overall system. Furthermore, finite element analysis can offer the opportunity to model the acoustic propagation and gain an insight into the acoustic emission events associated with cavitation. This was used in the modelling of the whole non-invasive measurement approach, to ensure that in practice the developed measurement system is suitable for implementation.

7.1.4 Implementations of a non-invasive cavitation monitoring system

As discussed in Chapter 5, FEA was utilised to design a broadband piezoelectric composite transducer for use in a non-invasive cavitation monitoring system. During characterisation of the manufactured device, it was shown that the performance of the device was sub-optimal and importantly, the specified 100% bandwidth centre around 2MHz was not achieved. Nevertheless, further investigation indicated that the transducer performance warranted a full evaluation as a cavitation sensor. A series of experimental measurements were conducted to demonstrate that the developed piezoelectric composite transducer was capable of detecting acoustic emission events and importantly, provide qualitative information on the cavitation intensity. Interestingly, the performance was comparable to the use of the NPL cavitation sensor, which operated in direct contact with the water load medium.

7.1.5 Main finding of this Thesis

- A non-invasive optical measurement technique using Laser Doppler Velocimetry (LDV) has been developed to monitor acoustic cavitation. The acoustic cavitation activity is monitored using the acoustic emission technique. The acoustic emission signal contains a substantial amount of information relating to the cavitation process. Changes in the amplitude of the acoustic emission signal are a result of a change in acoustic energy due to the extent of cavitation activity.

- An experimental approach combining LDV and tomography has been implemented to predict the acoustic field and cavitation regions. A scan of the LVD in the acoustic field indicates 'hot spot' and 'cold spot' locations associated with high and low regions of cavitation activity.

- The aluminium foil erosion test has been developed to indicate the cavitating regions, which correlated well with the cavitation regions measured by the LDV.

- Finite element analysis has been used to model the wave propagation associated with acoustic emission events in a cavitating field. The FE simulation is used to predict the detection capability of a transducer located on the outer wall of the reactor vessel. Cavitation bubbles are simulated using a linear chirp. This modelling approach was used to specify the frequency characteristic for the transducer to be used in the non-invasive cavitation monitoring system.

- FEA was also used to design a broadband (1-3MHz) 1-3 connectivity piezoelectric composite transducer matched to the reactor wall material. Unfortunately, the manufactured transducer did not match the predicted performance characteristics, but it was considered adequate to be used to evaluate the potential of the non-invasive cavitation monitoring system.

- A non-invasive measurement technique using the broadband piezoelectric composite transducer, when attached to the outer all of the reactor, was demonstrated to be capable of measuring the acoustic emission cavitation events.

- The intensity of the cavitation activity has been evaluated using the broadband energy calculation (BIE) method, in which the spectral components in a defined frequency range, 1-5MHz was typically used in the Thesis, were integrated to provide a figure that is directly related to the extent of cavitation.

- A comparison of three different cavitation monitoring approaches: LDV, NPL cavitation sensor and broadband piezoelectric composite transducer was conducted. Overall, all three techniques show similar operational characteristics and the choice of technique will be determined by the type of industrial system to be monitored.

7.2 Suggestions for future work

It is noted that the work presented in this Thesis has contributed to the development of non-invasive measurement approaches to monitor acoustic cavitation. It is hoped that it will provide a useful method for the investigation of cavitation in many applications. For future work, this could be extended in several ways.

7.2.1 Using cavitation activity for the scale-up of applications

The application of high power ultrasound deals with cavitation activity, which provides different advantages and disadvantage, depending on the application areas. Understanding cavitation helps to scale the cavitation and its effects in each application**.** However, for most applications, the necessary level of cavitation activity measurement has always been a limiting factor. The degree of cavitation activity indicates the application's efficiency and can be used to maximise the system performance and to consider the safety of the application.

The measurements of cavitation activity can be used to scale-up an application such as the sonochemical reactor, which is important in optimising and controlling chemical processing, and indicating the performance of the reactor vessel. The scale-up of the sonochemical reactor can save energy and time in chemical processes. This also reduces the number of samples. The scale-up of the sonochemical reactor using cavitation is an interesting possibility within the context of this work as the results would be directly applicable to industrial processes. Furthermore, by understanding cavitation, it becomes possible to apply this phenomenon to control systems and industrial processes.

Moreover, it is possible to use cavitation measurements when considering safety. Cavitation activity causes damage not only to the sensor but also soft tissues. Measuring cavitation would provide information in order to consider safety reasons

and the avoidance of damage to objects. Additionally, the cavitation measurement is a powerful tool in optimising, controlling and scaling up processes. Thus, the measurement of cavitation would allow for safety considerations and system optimisation and provide process monitoring when applied to a system.

7.2.2 The power amplifier and real-time monitoring

The non-invasive measurement technique based on acoustic emission has the potential to monitor acoustic cavitation. Changes in the frequency distribution of the acoustic emission and its amplitude could be a useful index for monitoring changes in the cavitation activity within the reactor vessel. This is provided by attaching the sensor to a wall of the reactor vessel. However, it is believed that cavitation is the secondary source of high frequency sound generated in the form of an acoustic emission spectrum by individual cavitation bubbles imploding. In this Thesis, a piezoelectric composite transducer is used to collect this low amplitude acoustic emission signal. Hence, the inclusion of a pre-amplifier would be required to amplify the signal. The designed pre-amplifier requires a low noise, high power gain and wide frequency bandwidth.

The measurement of cavitation in both Chapter 3 and Chapter 6 is not real-time monitoring. Therefore, another potential future work could be conducted as a real-time measurement. The optical measurement requires a DSP board to process the data. The non-invasive measurement using the piezoelectric composite transducer requires combining the device with the low noise preamplifier and a DSP board in a single integrated unit. Optimum system real-time monitoring could therefore be constructed. The data is collected by combining hardware and software written in the Labview programme for off-line data analysis with data acquisition and analysis. The monitoring system would identify the amount of cavitation activity from the spectral features of the acquired signals.

7.2.3 Influence of constituent materials for reactor vessel.

Analysing the influence of sound on the reactor vessel wall, as detailed in Chapter 4, focussed on the use of Perspex as the wall material. There are a number of advantages to this: the vessel was developed and used in the optical cavitation measurement, which requires transparent cell walls; the material is easily sourced; and fabrication of a test cell was relatively straight-forward. This will not generally be the case for use in an industrial application and the non-invasive monitoring system will typically be retro-fitted onto the industrial reactor vessel. Thus, it will be necessary to refine the transducer design depending on the application. In this Thesis, finite element analysis was successfully used to conduct investigations into other wall materials such as glass and steel. This approach could be extended using the methodology described in Chapter 5 to design new transducer configurations as required.

7.2.4 Hybrid optical and broadband transducer measurement

There are some inherent limitations associated with non-invasive measurement approaches using LDV and the broadband transducer for monitoring acoustic cavitation activity, which are noted throughout this Thesis. The combination of the optical measurement and the broadband transducer in a hybrid measurement can reduce the limitations of each technique in monitoring acoustic cavitation activity. The optical measurement technique provides details about the high resolution of the cavitation distribution. The small size of the laser beam provides high resolution in measurement. The broadband transducer can be used with any type of vessel wall and can be used in real-time monitoring with the integration of a DSP board. Combined investigation using optical and broadband transducer measurements could be beneficial in process monitoring applications and provide a good means of investigating cavitation activity in industrial applications such as Sonochemistry.

References

[1] ATCP Physical Engineering, "Technical report RT-ATCP-02: Ultrasonic cleaning: overview and state of the art", 2010, pp 1-2.

[2] M Lucus, A. Gachgan and A. Cardoni "Research applications and opportunities in power ultrasonics", Journal of Mechanical Engineering Science, vol. 223 (12), 2009, pp 2949-2965.

[3] B. J. O'Daly, E. Morris, G P. Gavin, J. M. O'Byrne and G. B. McGuinness "High power low frequency ultrasound: A review of tissue dissection and ablation in medicine and surgery", Journal of Materials Processing Technology, 2008, pp 38-58.

[4] T. G. Leighton, "*The Acoustic Bubble*", Academic Press Limited, 1994. ISBN0-12-441920-8.

[5] S. Baig, R. Farooq and F. Rehman "Sonochemical and its industrial applications", Journal of World Applied Sciences, vol. 10, 2010, pp 936-944.

[6] M. Dular, B. Bachert, B. Stoffel and B. Sirok "Relationship between cavitation structures and cavitation damage", Journal of Science Direct, vol. 257, 2004, pp 1176-1184.

[7] Y. T. Shah, A. B. Pandit and A. S. Moholkar, *Cavitation Reaction Engineering,* Kluwer Academic/Plenum Publishers, 1999. ISBN: 978-1-4613-7168-7.

[8] K. V. Jenderka and C. Koch "Investigation of spatial distribution of sound field parameters in ultrasound cleaning bath under the influence of cavitation", IEEE, Ultrasonics Symposium, vol.44, 2006, pp e401-e406.

[9] M. Hodnett, R. Chow and B. Zeqiri "High-frequency acoustic emissions generated by a 20kHz sonochemical horn processor detected using a novel broadband acoustic sensor: a preliminary study", Ultrasonics Sonochemistry, vol.11, 2004, pp 441-454.

[10] B. Zeqiri, N. D. Lee, M. Hodnett and P. N. Gelat "A novel sensor for monitoring acoustic cavitation. Part II: Prototype performance evaluation", IEEE, Transactions on Ultrasonics, Ferroelectrics and Frequency Control, vol.50, 2003, pp 1351-1362.

[11] M. C. Ziskin and P. A. Levin, *Ultrasonic Exposimetry*, 1993 CRC Press, Inc London Toyo, 1993. ISBN 0-8493-6436-1.

[12] W. P. Mason "Sonic and Ultrasonics: Early history and application", IEEE, Transactions on sonics and ultrasonics, vol. Su-23, 1976, pp 224-1976.

[13] C. F. Schueler and H. Lee “Fundamental of digital ultrasonic imaging”, IEEE, Transactions on Sonics and Ultrasonic, vol. su-31, 1984, pp 195-217.

[14] J. Majchrzak, M. Michalski and G. Wiczynski “Distance estimation with a long-range ultrasonic sensor system”, IEEE, Journal of Sensors, vol. 9, 2009, pp 767-773.

[15] A. Burguera, Y. Gonzalez and G. Oliver “The sNDT: A Grid-Based Likelihood Field approach to robust and Accurate sonar scan matching location”, December 5, 2007.

[16] G. R. Harris “Medical ultrasound exposure measurement: update on devices, methods, and problems”, IEEE, Ultrasonic Symposium, 1999, pp 1341-1352.

[17] Z. J. Dolatowski, J. Stadnik, D. Sasiak “Application of ultrasound in food technology”, Technologia Alimentaria, 2007, pp 89-99.

[18] V. Dogra "High intensity focused ultrasound use widens in research, practice", Interventional Radiology, Tumour Ablation, Ultrasound, 2007, pp 1-2.

[19] R. E. Apfel “Sonic effervescence: A tutorial on acoustic cavitation”, Acoustical Society of America, vol. 101, 1997, pp 1227-1237.

[20] K. S. Suslick, Y. Didenko, M. M. Fang, T. Hyeon, K. J. Kolbeck, W. B. McNamara III, M. M. Mdleleni and M. Wong "Acoustic cavitation and its chemical consequences", The Royal Society, Mathematical, Physical & Engineering Science, 1999, pp 335-353.

[21] R. E. Apfel “Acoustic cavitation prediction”, Acoustical Society of America, vol. 69, 1981, pp 1624-1632.

[22] J. Frohly, S. labouret, C. Bruneel, I. B. Baquet and R. Torguet “Ultrasonic cavitation monitoring by acoustic noise power measurement”, Acoustical Society of America, vol. 108, 2000, pp 2010-2020.

[23] B. E. Noltingk and E. A. Neppiras "Cavitation Produced by ultrasonics", Proceedings of the Physical Society. Section B, vol. 63, 1950, pp 674-685.

[24] T. J. Mason " Sonochemistry - beyond synthesis", Royal Society of Chemistry, 2009, pp1.

[25] T. G. Leighton "Bubble population phenomena in acoustic cavitation", Ultrasonic Sonochemistry, vol. 2, 1995, pp S123-S136.

[26] A. D. Maxwell, T. Wang, L. Yuan, A. P. Duryea, Z. Xu and C. A. Cain "A tissue phantom for visualization and measurement of ultrasound-induced cavitation damage", Ultrasound in Medicine and biology, vol. 36, 2010, pp 2132-2143.

[27] R. E. Apefl and C. K. Holland “Gauging the likelihood of cavitation from short-pulse, low-duty cycle diagnostic ultrasound”, Ultrasound in Medicine and Biology, vol. 17, 1991, pp 179-185.

[28] L. H. Thompson and L. K. Doraisway “Sonochemistry: Science and Engineering”, The Royal Society, Mathematical, Physical & Engineering Science, vol. 38, 1999, pp 1215-1249.

[29] L. A. Crum “Acoustic cavitation”, IEEE, Ultrasonic Symposium, 1982, pp 1-11.

[30] P. A. Lawin and L. Bjorno “Acoustically induced shear stresses in the vicinity of microbubble in tissue”, Acoustical Society of America, vol. 71, 1982, pp 728-734.

[31] W. R. Hedrick and D. L. Hykes “Biological effect of ultrasound: II interactions of ultrasound with Matter", Diagnostic Medical Sonography, 1991, pp 194-196.

[32] E. A. Neppirus “Acoustic cavitation", Physic Reports, North-Holland Publishing Company, vol. 61, 1980, pp 159-251.

[33] V. S. Moholkar, S. P. Sable and A. B. Padit "Mapping the cavitations intensity in an ultrasonic bath using the acoustic emission", An Official of Publication Institute of Chemical Engineers (AIChE), vol. 46, 2000, pp 684-694.

[34] W.R. Hedrick and D. L. Hykes “Biological effect of ultrasound: I specification of intensity", Journal of Diagnostic Medical Sonography, 1991, pp 188-193.

[35] M. Hodnett and B. Zeqiri “A strategy for the development and standardisation of measurement methods for high power/cavitating ultrasonic files: review of high power field measurement techniques”, IEEE, Ultrasonic Sonochemistry, vol. 4, 1997, pp 273-288.

[36] A. A. Busnaina and G. W. Gale “Ultrasonic and Megasonic particle Removal", Cleaning 95 proceeding, 1995, pp 347-360.

[37] Blackstone-Ney Ultrasonics “Fundamentals of Ultrasonic & Megasonic Cleaning” Process Cleaning Magazine, 2009.

[38] A. Shoh “Industrial applications of ultrasound - A review I. High power ultrasound”, IEEE, transaction on Sonic and Ultrasonic, vol. su-22, 1975, pp 60-71.

[39] C. Franklin, Y. Fan, E. Brause, and V. Nguyen "Using to extended chemical cleans for 45nm technology", The Electrochemical Society, 212th ECS meeting, ECS Transaction, vol.11, 2007, pp 190-116.

[40] J. L. Laborde, C. Bouyer, J. P. Caltagirone and A. Gerard "Acoustic cavitation field prediction at low and high frequency ultrasounds", IEEE, Ultrasonics Symposium, 1998, pp 581-587.

[41] G. Harvey and A. Gachagan, "Non-invasive field measurement of low-frequency ultrasonic transducers operating in sealed vessels", IEEE Transactions on Ultrasonics, Ferroelectrics and Frequency Control, 2006, pp 1749-1758.

[42] B. D. Storey and A. J. Szeri “A reduced model of cavitation physics for use in sonochemistry", Proceeding of Mathematical, Physical &Engineering Sciences, 2001, pp 1685-1700.

[43] T. J. Mason “Ultrasound in synthetic organic chemistry", Chemical Society Reviews, 1997, vol. 26, pp 443-451.

[44] K. S. Suslick, J. W. Goodal, P. E. Schubert and H. H. Wang “Sonochemisty and sonocatalysis of metal carbonyls”, Journal of American Society, vol. 105, 1983, pp 578-5785.

[45] U. S. Bhirud, P. R. Gogate, A. M. Wilhelm and A. B. Pandit “Ultrasonic bath with longitudinal vibrations: a novel configuration for efficient wastewater treatment”, IEEE, Ultrasonic Sonohemistry, vol. 11, 2004, pp 143-147.

[46] A. R. Jambrak, V. Lelas , T. J. Mason, Greta Kresic and M. Badanjak "Physical properties of ultrasound treated soy proteins", Journal of Food Engineering, vol. 93, 2009, pp 386-393.

[47] S. K. Shrivastava and Kailash "Stone fragmentation by ultrasound", Indian Academy of Sciences, vol. 27, 2004, pp383-385.

[48] J. H. Hwang and L. A. Crum "Current status of clinical high intensity focused ultrasound", IEEE, Ultrasound in Medicine and Biology, 2009, pp 130-133.

[49] J. Barkin "High intensity focused ultrasound (HIFU)", The Canadian journal of Urology, vol. 18, 2011, pp 5635-5643.

[50] J. G. Lynn, R. L. Zwemer, A. J. Chick and A. F. Miller "A new method for the generation and use of focused ultrasound in experimental biology", Journal of General Physiology, 1942, pp 179-193.

[51] H. Chan, V. Y. Fujimoto, D. E. Moore, R. T. Held, M. Paun, and S. Vaezy "In vivo feasibility of image-guided transvaginal focused ultrasound therapy for the treatment of intracavitary fibroids", American society for Reproductive Medicine, Fertility and Sterility, vol. 82, 2004, pp 723-730.

[52] B. A. Rabkin, V. Zderic, L. A. Crum and S. Vaezy “Biological and physical mechanisms of HIFU-induced hyperecho in ultrasound images", Ultrasound in Medicine & Biology, vol. 32, 2006, pp 1721-1729.

[53] M. E. Stratmeyer and F. L. Lizzi, Special Issue on the Biological Effects of Ultrasound”, IEEE, Transactions on Ultrasonics, Ferroelectrics, and Frequency Control, vol. 33, 1986, pp 137-138.

[54] K. S. Suslick “The Chemical Effects of Ultrasound”, Scientific American, vol. 2 1989, pp 80-86.

[55] NIH public access author manuscript "Section7-Discussion of the mechanical index and other exposure parameters", Journal of ultrasound Medicine, 2000, pp 143-168.

[56] P. Zima, M. Sedlar and F. Marsik "Bubble creation in water with dissolved gas prediction of regions endangered by cavitation erosion", Conference on the properties of water and steam in Kyoto, pp 232-235.

[57] B. Zeqiri, M. Hodnett and A. J. Carroll "Studies of novel sensor for assessing the spatial distribution of cavitation activity within ultrasonic cleaning vessels", IEEE, Ultrasonics Symposium, vol. 44, 2006, pp 73-82.

[58] A. Ebrahiminia, M. Mokhtari-Dizaji and T. Toliyat " Correction between iodide dosimetry and terephthalic acid dosimetry to evaluate the reactive radical production due to acoustic cavitations activity", Ultrasonics Shonochemistry, vol. 20. 2013, pp366-372.

[59] M. F. Insana “Modelling acoustic backscatter from kidney microstructures using an anisotropic correlation function", Acoustic Society of America, 1994, pp 649-655.

[60] W. M. Fairbank and M. O. Scully "A new non-invasive technique for cardiac pressure measurement: resonant scattering of ultrasound from bubble", IEEE Trans on Biomedical Engineering, vol. BME-24, 1977, pp 107-110.

[61] W. S. Chen, T. J. Matula and L. A. Crum "A light-scattering technique for investigating the destruction of ultrasound contrast agents", IEEE, Ultrasonics Symposium, 2001, pp 1683-1686.

[62] J. F. Guan and T. J. Matula "Using light scattering to measure the response of individual ultrasound contrast microbubble subjected to pulsed ultrasound in vito.", Acoustic Society of America, vol.116, 2004, pp 2832-2842.

[63] Y. Lida, J. Lee, T. Kozaka, K. Yasui, A. Towata and T. Tuziuti "Optical cavitation probe using light scattering from bubble clouds", IEEE, Ultrasonics Chemistry, vol. 16, 2009, pp 519-524.

[64] L. A. Crum, "Sonoluminescence: a simple mechanical system can producer light from sound. In process energy densities can increase by a factor of 1012, and 50-picosecond light pulses are synchronized to a few parts in 1011", American Institute of Physics, 1994, pp 22-29.

[65] A. Arvengas, K. Davitt and F. Caupin "Fibber optic probe hydrophone for the study of acoustic cavitations in water", Review of Scientific Instruments, vel. 82, 2011, pp 034904-1-034904-8.

[66] M. Hodnett and B. Zeqiri "A detector for monitoring the onset of cavitation during therapy-measurements of ultrasonic power", Journal of Physics: Conference Series1, 2004, pp 112-117.

[67] P. J. Wolff, R. Keith Jones and P. March "Evaluation of Results from Acoustic Emissions-Based Cavitation Monitor, Grand Coulee Unit G-24", Report of Wolff Ware Ltd., 2005, pp 1-15.

[68] P. Galat, M. Hodnett and B. Zeqiri "Establishing a reference ultrasonic cleaning vessel: Part1 supporting infrastructure and early measurement", NPL Report CMAN 55, 2000.

[69] Product data of Bruel & Kjaer hydrophone (Type 8103, 8104, 8105, 8106), Bruel&Kjaer, Denmark.

[70] Calibration certificate of Bruel & Kjaer 8103 hydrophone Sn. 2241649, Bruel & Kjaer, 2000.

[71] C. Koch and K. V. Jenderka "Measurement of sound field in cavitating media by an optical fibber-tip hydrophone", IEEE, Ultrasonic Sonochemistry, vol. 15, 2008, pp 502-509.

[72] M. Hodnett, Min J. Choi and B. Zeqiri "Toward a reference ultrasonic cavitation Vessel, Part 1: Preliminary investigation of acoustic file distribution in a 25 kHz cylindrical cell", IEEE, Ultrasonic Sonochemistry, vol. 14, 2007, pp 29-40.

[73] C. Wurster, J. Staudenraus and W. Eiesnmenger "The fibber optic hydrophone", IEEE, Ultrasonics Symposium, 1994, pp 941-944.

[74] B. Zeqiri, P. N. Gelat, M. Hodnett, and N. D. Lee “A novel sensor for monitoring acoustic cavitation. Part I: Concept, Theory, and Prototype development", IEEE, transactions on Ultrasonics, Ferroelectrics, and Frequency Control, vol. 50, 2003, pp 1342-1350.

[75] NPL cavitation sensor manual, National Physical Laboratory, London.

[76] F. J. Fuchs "Ultrasonic intensity measurement technique" http://www.ctgclean.com/tech-blog/wp-content/uploads/Ultrasonic-Intensity-Clean.

[77] H. Cao, M. Wan, Y. Oiao, S. Zhang and R. Li "Spatial distribution of sonoluminescence and sonochemiluminescence generated by cavitation bubbles in 1.2 MHz focused ultrasound field", IEEE, Ultrasonics Sonochemistry, 2012, pp 257-263.

[78] A. Petosic, B. Ivancevic and D. Svilar "Measuring derived acoustic power of an ultrasound surgical device in the linear and nonlinear operating modes", Ultrasonics, vol. 49, 2009, pp 522-531.

[79] C. V. Raman and N. S. Nath “The diffraction of light by sound waves of high frequency: part II”, Proceeding Indian Academy of Science A2, 1936, pp 431-420.

[80] R. Eriksson, A. Holm, M. Landeborg, H. W. Persson and K. Lindstrom "The 10 MHz ultrasonic near-field: calculations, hydrophone and optical diffraction tomography measurements”, Ultrasonics, vol. 31, 1993, pp 439-446.

[81] A. Holm and H. W. Persson “Measurement of airborne ultrasound with optical Diffraction tomography”, IEEE, Ultrasonics Symposium, 1991, pp 961-991.

[82] A. Holm and H. W. Persson “Optical diffraction tomography applied to airborne ultrasound”, Ultrasonics, vol. 31, 1993, pp 259-265.

[83] X. Jia, L. Adler and G. Quentin "Interferometric detection of finite amplitude ultrasound waves", IEEE, Ultrasonics Symposium, 1994, pp 833-836.

[84] X. Jia, G. Quentin and M. Lassoued “Optical heterodyne detection of pulsed ultrasonic pressure”, IEEE, Transactions on Ultrasonics, Ferroelectric, and Frequency Control, vol. 40, 1993, pp 67-69.

[85] X. Jia, M. Lassoued and G. Quentin “Quantitative measurement of ultrasonic pressures with an optical heterodyne interferometer”, IEEE, Ultrasonic Symposium, 1991, pp 1137-1140.

[86] O. B. Matar, J. P. Remenieras, S. Calle, and F. Patat, "Acoustic pressure measurement by acoustic optic tomography", IEEE, Ultrasonics Symposium, vol1, 2001, pp 505-508.

[87] O. B. Matar, L. Pizarro, S. D. Santos and F. Patat "Characterisation of air-bone transducers by optical tomography", Ultrasonics, vol. 38, 2000, pp 787-793.

[88] A. Korpel “Acousto-optics: what is behind it?”, IEEE, Ultrasonics Symposium, 1986, pp 417-422.

[89] P. Debye and W. Sears "On the scattering of light by supersonic wave", Proceedings of The national academy of Sciences, vol. 18, 1932, pp 409-414.

[90] K. N. Rao "Diffraction of light by ultrasonic waves", Proceedings Indian academy of Sciences, vol.18, 1938, pp 124-134.

[91] C. V. Raman and N. S. Nath "The diffraction of light by high frequency sound wave: parts I", Proceeding Indian Academy of Science A2, 1936, pp 406-412.

[92] C. V. Raman and N. S. Nath "The diffraction of light by high frequency sound wave: parts III", Proceeding Indian Academy of Science A2, 1936, pp 75-78.

[93] C. V. Raman and N. S. Nath "The diffraction of light by high frequency sound wave: Parts IV", Proceeding Indian Academy of Science A2, 1936, pp 119-125.

[94] R. Adler "Interaction between light and sound", IEEE, Spectrum, vol.4, 1967, pp 42-54.

[95] K. A. I. L. Wijewardena Gamalath and G. I. A. U. Jayawardena "Diffraction of light by acoustic wave in liquids", International Letters of Chemistry, Physics and Astronomy, 2012, pp 39-57.

[96] G. Harvey "An investigation into the simulation and measurement of high intensity ultrasonic system", PhD Thesis, University of Strathclyde, 2008.

[97] A. R. Harland, J. N. Petzing, J. R. Tyrer, C. J. Bickley, S.P. Robinson and R. C Preston "Application and assessment of laser Doppler velocimetry for underwater acoustic measurements", Journal of Sound and Vibration, vol. 265, 2003, pp 627-645.

[98] Polytec " User manual: laser Vibrometer OFV 303, OFV2200" 01e

[99] A. C. Kak and M. Slaney "Principles of Computerized Tomographic Imaging", Society of Industrial and applied Mathematics Philadelphia, 1998, ISBN: 0-89871-494-X.

[100] T. Uchida, S. Takeuchi, T. Kikuchi "Study of measurement of the amount of generated acoustic cavitation: relationships among broadband integrated voltage, dissolved oxygen, and sonochemical luminescence", IEEE, Ultrasonics Symposium, 2010, pp 2223-2226.

[101] G. Ludwing and K. Breadel "Calibration of hydrophone based on reciprocity and time delay spectrometry", IEEE, Transactions on Ultrasonic, Ferroelectrics, and Frequency Control, vol. 35, 1988, pp 168-174.

[102] T. G. Leighton "Strategy for the development and standardisation of Measurement methods for high power/cavitating ultrasonic fields: Review of cavitating monitoring techniques", Institute of Sound and Vibration Research (ISVR), University of Southampton, 1997.

[103] S.Yoshizawa, S.Umemura and Y. Matsumoto " Cavitation Detection with Subharmonic Emissions by Low Intensity Sustaining Ultrasound", Ultasonics Symposium, 2008, pp 772-775.

[104] E. A. Neppiras "Measurement of acoustic cavitation", IEEE, Transactions on Sonics and Ultrasonics, vol. Su -15, 1968, pp 81-88.

[105] T. Matasa, A. Gachagan, A. Nordon and R.L. O'Leary "Ultrasonic wave propagation in cylindrical vessel and implementations for ultrasonic reactor design", IEEE, Ultrasonics Symposium, 2010, pp 1470-1473.

[106] PZFlex user manual v1J9, Weidlinger Associates Inc, Applied Science Division, 399 West EI Camino Real, Mountain View, CA.

[107] www.wai.com.

[108] G. L. Wojcik, J. C. Mould and L. M. Carcione "Combined transducer and nonlinear tissue propagation simulations", Proceedings of the international Mechanical Engineering Congress & Exposition Proceedings, 1999, pp 1-10.

[109] F. Moser, L. J. Jacobs and J. Qu "Modelling elastic wave propagation in wave guides with the finite element method", NDT&E International, vol. 31, 1999, pp 225-234.

[110] F. Moser, L. J. Jacobs and J. Qu. "Application of finite element methods to study transient wave propagation in elastic wave guides", Proceeding of 24th Annual review of progress in Quantitative non-destructive Evaluation, 1988, pp161-167.

[111] M. Aare and S. Kleiven "Evaluation of head response to ballistic helmet impacts using finite element method", International Journal of Impact Engineering, vol. 34, 2007, pp 596-608.

[112] G. Harvey and A. Gachagen" Simulation and measurement of nonlinear behavior in a high power test cell", IEEE, Transactions on Ultrasonics, Ferroelectric, and Frequency Control, vol. 58, No4 2011, pp 808-819.

[113] A. Gachagan, A. McNab, R. Blindt, M. Patrick and C. Marriott "A high power ultrasonic array based test cell", Ultrasonics, vol. 42, 2004,pp57-68.

[114] A. Gachagan, D. Speirs and A. McNab "The design of a high power ultrasonic test cell using finite element modeling techniques", Ultrasonics, vol.41, 2003, pp283-288.

[115] G. Carson, A. J. Mulholland, A. Nordon, M. Tramontana, A. Gachagan and G. Hayward "Particle sizing passive ultrasonic measurement of particle-wall impact vibrations", Journal of Sound and Vibration, vol. 317, 2008, pp 142-157.

[116] A. Nordon, Y. Carella, A. Gachagan, D. Littlejohn and G. Hayward," Factors affecting broadband acoustic emission measurements of a heterogeneous reaction", The Royal Society of Chemistry, 2006, pp 323-330.

[117] M. Tramontana, A. Gachagan, G. Hayward, A. Nordon and D. Littlejohn "Ultrasonic monitoring of heterogeneous chemical reactors", IEEE, Ultrasonics Symposium, 2006, pp 906-909.

[118] P. Flandrin "Time-frequency and chirps", The International Society for Optical Engineering, Wavelet Applications VIII, vol.4391, 2001, pp 1-15.

[119] CUE materials database http://www.strath.ac.uk/media/departments/eee/cue/downloads/cue_materials_database_ver1.2_aug_2005.pdf.

[120] www.kayelady.npl.co.uk/genral_physics/2_4/2_4_1.html.

[121] B. Aldham, R. Manasseh, S. Illesinghe, K. Liffman, A. Ooi and I. D. Sutalo "Measurement of pressure on surface using acoustic resonances", Measurement Science and Technology, vol. 21, 2011, pp1-12.

[122] M. Tramontana "The application of passive and active acoustic technique in process monitoring", PhD Thesis, University of Strathclyde, 2011.

[123] A. Besenyei, L. Gershuni, I. Plans, M. Rechberger, O. Shipilova and T. Mulholland "Monitoring of a heterogeneous using broadband acoustic emission measurement", American Society for Testing and Materials, 2004, pp 1-13.

[124] W. A. Smith "The role of piezocomposites in ultrasonic transducer" IEEE, Ultrasonics Symposium,1989, pp 755-766.

[125] W. Qi and W. Coa "Finite element analysis and experimental studies on the thickness resonance of the piezocomposite transducer", Ultrasonic Imaging, vol. 18, 1996, pp1-9.

[126] W. A. Smith and B. A. Auld "Modelling 1-3 composite piezoelectric: Thickness-mode oscillation", IEEE, Transaction on Ultrasonics, Ferroelectrics and Frequency Control, vol. 38, 1991, pp 40-47.

[127] W. A. Smith "The application of 1-3 pizocomposites in acoustic transducer", IEEE, Applications of Ferroelectrics, 1990, pp 145-152.

[128] A. Gachagan and G. Hayward "Improving the bandwidth of 1-3 connectivity composite receiver using mode coupling", Acoustical Society of America, 1998, pp 103:3344-3352.

[129] G. Hayward and J. Bernnett "Assessing the influence of pillar aspect ratio on the behaviour of 1-3 connectivity composite transducers", IEEE, Transaction on Ultrasonics, Ferroelectrics and Frequency Control, vol. 43, 1996, pp 98-108.

[130] J. Bennett and G. Hayward "Design of 1-3piezocomposite hydrostatic transducers using finite element", IEEE, Ultrasonics Symposium, 1994, pp 979-982.

[131] G. Hayward and J. A. Hossack "Unidimensional modelling of 1-3composite transducers", Acoustical Society of America, 1990, pp 599-608.

[132] J. A. Hossack and G. Hayward "Assessment of different pillar geometries for 1-3 composite transducers using finite element analysis", IEEE, Ultrasonics Symposium, 1990, pp 389-392.

[133] J. Bennett, R. Hamilton and G. Hayward "Finite element modelling of 1-3 composite transducer for underwater application", IEEE, Ultrasonics Symposium, 1993, pp 1113-1116.

[134] W. A. Smith "Composite piezoelectric material for medical ultrasonic image transducers", IEEE, Ultrasonices Symposium, 1986, pp 249-256.

[135] J. T. Bennett "Finite element modelling system for piezocomposite transducers", PhD Thesis, University of Strathclyde, 1995.

[136] G. Hayward and A. Gachagan "An evaluation of 1-3connectivity composite transducers for air-coupled ultrasonic applications", Acoustical Society of America, 1996, pp 2148-2157.

[137] P. Reynolds, J. Hyslop and G. Hayward "The influence of constructional parameters on the practical performance of 1-3 piezocomposite transducers", IEEE, Ultrasonics Symposium, 1996, pp 967-970.

[138] Material property available in finite element analysis PZFlex package.

[139] A. Gachagan "An evaluation of 1-3 connectivity composite transducers for air-couple ultrasonic application", PhD Thesis, University of Strathclyde, 1996.

[140] A. Gachagan, G. Hayward, S. P. Kelly and W. Galbraith "Characterization of air-coupled transducers", IEEE, Transactions on Ultrasonics, Ferroelectrics and Frequency Control, vol. 43, No4, 1996, pp 678-689.

[141] Manual of ASTM "Standard guide for evaluating characteristics of ultrasonic search units", ASTM Designation, An American National Standard (E1065), 2007, pp 1-21.

[142] M. Lorenc, M. Szmechta, D. Zmarzly and T. Boczar "Acoustic emission spectral analysis of ultrasound induced cavitation in insulating oil", Proceeding of 2008 International symposium on Electrical Insulating Materials, 2008, pp 452-455.

[143] Panametrics ultrasonic transducers, Olympus Corporation, www.olympus-ims.com

[144] M. Ashokkumar, M. Hodnett, B. Zeqiri, F. Grieser, and G. J. Price, "Acoustic emission spectra from 515kHz cavitation in aqueous solutions containing surface active solutes", Journal of American Chemical Society, vol. 129, 2007, pp 2250-2407.